General Disclaimer

One or more of the Following Statements may affect this Document

- This document has been reproduced from the best copy furnished by the organizational source. It is being released in the interest of making available as much information as possible.

- This document may contain data, which exceeds the sheet parameters. It was furnished in this condition by the organizational source and is the best copy available.

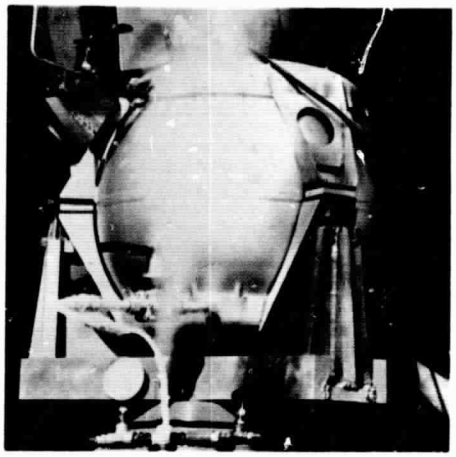
- This document may contain tone-on-tone or color graphs, charts and/or pictures, which have been reproduced in black and white.

- This document is paginated as submitted by the original source.

- Portions of this document are not fully legible due to the historical nature of some of the material. However, it is the best reproduction available from the original submission.

Produced by the NASA Center for Aerospace Information (CASI)

Final Report



Development of Supercritical Pressure Cryogenic
Storage and Supply Systems
Incorporating
The Radial Bumper — Discrete Shield Design
NASA Contract NAS9-2978

FACILITY FORM 602
N 68-24696
(ACCESSION NUMBER)
203
(PAGES)
CR-92137
(NASA CR OR TMX OR AD NUMBER)
(THRU)
1
(CODE)
33
(CATEGORY)

GPO PRICE $ _____

CFSTI PRICE(S) $ _____

Hard copy (HC) 3.00

Microfiche (MF) .65

ff 653 July 65

Bendix
Instruments &
Life Support
Division

Davenport, Iowa 52808

Bendix Instruments & Life Support Division

NASA CR 92137

FINAL REPORT

DEVELOPMENT OF SUPERCRITICAL PRESSURE CRYOGENIC STORAGE AND SUPPLY SYSTEMS INCORPORATING THE RADIAL BUMPER-DISCRETE SHIELD DESIGN

NASA CONTRACT NAS9-2978

BRUCE GERTH

ROBERT LUNDEEN

THE BENDIX CORPORATION
INSTRUMENTS & LIFE SUPPORT DIVISION
DAVENPORT, IOWA

Prepared for:

PROPULSION AND POWER DIVISION
NASA-MANNED SPACECRAFT CENTER
HOUSTON, TEXAS 77058

Publication No: 3873-67
LER 56
Date: April 11, 1968

FOREWARD

This report has been prepared by the Instruments & Life Support Division of The Bendix Corporation, Davenport, Iowa, under Contract No. NAS 9-2978. The work described herein was conducted by The Bendix Corporation under the sponsorship of the Propulsion and Power Division of the NASA Manned Spacecraft Center, Houston, Texas. Mr. Gordon Rysavy, EP5, Power Generation Branch, Propulsion and Power Division of the NASA Manned Spacecraft Center, was the technical representative.

The program was divided into two successive portions, Phase A and Phase B. Mr. Dale L. Hankins was the Bendix project leader for the Phase A portion and Mr. James A. Mientus was the Bendix project leader for the Phase B portion of the program. Other Bendix personnel contributing technical consulation to the program were Dr. Blase J. Sollami, Dr. George H. Bancroft, Mr. John T. Beher, and Mr. Robert Lundeen. Mr. Paul J. Gardner, Chief Cryogenics Engineer of The Bendix Corporation, Instruments & Life Support Division, provided technical consultation and administrative supervision. The report summarizes work begun June 1964 and concluded January 1967.

ABSTRACT

The development program described herein consisted of a two phase program directed toward the design, fabrication, testing and evaluation of supercritical cryogenic storage systems incorporating significant advancements in the state-of-the-art for thermal insulation, structural characteristics, and fabrication techniques.

The Phase A portion of the program resulted in the fabrication of a 2.5 ft^3 supercritical oxygen storage system. This early effort demonstrated the physical integrity and low thermal transfer properties associated with the Bendix-developed radial bumper inner support concept, and also revealed greater thermal barrier efficiency for a storage vessel through the use of discrete radiation shields suspended in the vacuum annulus between the pressure vessel and the outer shell.

The Phase B program, an extension of the Phase A program, was hardware oriented to produce two flight-sized self contained supercritical systems, one 4.8 ft^3 oxygen system and one 6.7 ft^3 hydrogen system. The system embodied advanced thermal and structural concepts with emphasis on design, weight optimization, processing, fabrication, and assembly. The Phase B program successfully demonstrated that large flight-type cryogenic storage systems utilizing the radial bumper support and discrete radiation shielding can be built to meet extremely low heat leak requirements necessary for future long duration space missions.

TABLE OF CONTENTS

SECTION	TITLE	PAGE
I	INTRODUCTION	1
II	TECHNICAL DISCUSSION	4
2.1	Description of Radial Bumper - Discrete Shield Design	5
2.2	Dewar Insulations	7
2.3	Insulation Summary	26
III	PHASE A PROGRAM	29
3.1	System Description and Operation	29
3.1.1	Dewar Description	29
3.1.2	System Description	35
3.1.3	System Operation	37
3.2	Program Description	38
3.2.1	Vendor Survey	39
3.2.2	Outer Shell Tests	63
3.2.3	Bumper Tests	65
3.2.4	Pressure Vessel Weld and Heat Treat Testing	70
3.2.5	Pressure Vessel Plating Tests	72
3.2.6	Fabrication and Assembly	73
3.2.7	Testing	92
3.3	Conclusions and Recommendations	100
IV	PHASE B PROGRAM	104
4.1	System Description and Operation	104
4.1.1	System Operational Concepts	104
4.1.2	System Description	110
4.2	Program Description	124
4.2.1	System Fabrication	124
4.2.2	System Performance Tests	138
4.2.3	Problem Areas and Solutions	143
4.3	Conclusions and Recommendations	150
	APPENDICES	
A	Hemisphere Buckling Tests	A-1
B	Outer Shell Analyses	B-1
C	Phase A Post-Contract Effort	C-1
D	Phase A Vapor-Cooled Unit Vibration Testing	D-1
E	Phase B Hydrogen Pressure Vessel Stretch Forming	E-1

SECTION I

INTRODUCTION AND SUMMARY

Recent and future space programs continue to increase in scope and duration necessitating greater use of stored cryogenic fluids for power generation and life support. Because of longer duration missions and weight factors, the most important functional parameter is that fluid be preserved for its required function rather than being expelled as a result of heat leak into the storage tank. For flight type storage vessels pure vacuum insulation combined with some reduction of radiant heat transfer has proven to be most efficient in terms of weight, size, heat leak consistency and static vacuum integrity.

Typically the design of a cryogenic storage vessel requires directing considerable effort toward minimizing heat transfer to the stored fluid through conduction and radiation. Bendix developed the radial bumper suspension concept to reduce conductive heat transfer from the outer shell to the pressure vessel and has used this technique for several years in small liquid oxygen systems for aircraft use.

The program performed under Contract No. NAS 9-2978 and described herein consisted of the development, fabrication and test of prototype supercritical pressure cryogenic oxygen and hydrogen storage and supply systems. The systems incorporated the Bendix radial bumper suspension concept and isothermally-mounted discrete radiation shields for minimization of heat transfer to the stored cryogens.

A two-phase program was performed. The Phase A portion of the program consisted of providing one supercritical oxygen system for evaluation of the thermal and functional characteristics of the radial bumper-discrete shield design. The 20.3 in. diameter spherical vessel is capable of storing 2.5 ft^3 of oxygen at 900 psia; two discrete radiation shields are isothermally mounted in the vacuum void. Because of its function as an evaluation article for the thermo-physical design concept, the system did not employ certain functions such as quantity sensing, dynamic destratification, and supplemental internal heating. The dewar contained a static thermal conductor for evaluation of this type of destratification device. The objectives of the Phase A portion of the program consisted of the following:

1. Development testing of dewar components for design optimization.

2. Development testing of fabricating and processing techniques.

3. Survey of current dewar shell fabrication methods and vendors.

4. Design of a supercritical oxygen storage system.

5. Fabrication of a supercritical oxygen storage system.

6. Thermal and structural testing of the system.

The Phase A storage system successfully demonstrated the basic thermal and physical characteristics of the radial bumper-discrete shield dewar design, and thus served as a source of information applied to the subsequent Phase B portion of the overall program. Atmosphere vented heat leak to the stored liquid oxygen averaged 7.25 Btu/hr; the ratio of this heat leak to the inner vessel surface area was 0.777 Btu/hr-ft^2. Similar testing performed with hydrogen resulted in a heat leak of 5.1 Btu/hr, or 0.547 Btu/hr-ft^2. The thermal quality of the dewar was not optimum, due to fairly poor silver electroplating of the pressure vessel. However, the performance of the Phase A dewar showed a significant advance in the state-of-the-art for thermal insulation of flight-type cryogenic storage vessels. Structural testing performed on the Phase A system proved the thermal-physical stability of the radial bumper-discrete radiation shield design concept.

The Phase B portion of the program consisted of providing one oxygen tankage system and one hydrogen tankage system. The storage dewar of each system approached maximum weight optimization; because of the program limits, certain system components were not weight optimized, although flight design principles were employed to the greatest extent possible. The 29.8 inch diameter spherical oxygen storage vessel is capable of storing 4.8 ft^3 of oxygen at 900 psia; two discrete shields are isothermally mounted in the vacuum void. The 32.3 inch diameter spherical hydrogen storage system stores 6.7 ft^3 of hydrogen at 290 psia, and employs four discrete shields (one shield vapor-cooled). Both systems are self contained in that each has built-in quantity measurement, internal heaters, destratification motor-fans, thermocouples, external mounting frame, and valves and electrical components.

The objectives of the Phase B portion of the program consisted of the following:

1. Design of oxygen and hydrogen supercritical cryogenic storage systems.

2. Development of techniques required for fabrication.

3. Fabrication of one oxygen and one hydrogen prototype system.

4. Thermal and structural testing of the systems.

The design and fabrication of the two storage systems demonstrated that large flight-type cryogenic storage systems utilizing the radial bumper-discrete radiation shield concept could be built to meet extremely low heat leak requirements necessary for long duration space missions. Atmosphere vented heat leak for the Phase B oxygen system was 11.7 Btu/hr for oxygen storage, 10.3 Btu/hr for nitrogen storage, and 7.9 Btu/hr for hydrogen storage. Atmosphere vented heat leak for the Phase B hydrogen system was 8.0 Btu/hr and 2.9 Btu/hr for hydrogen storage, non-vapor cooled and vapor cooled respectively, and 5.3 Btu/hr and 1.7 Btu/hr for helium storage, non-vapor cooled and vapor cooled respectively. Structural testing proved the thermal-physical stability of the design concept as applied to large tankage.

Demonstration of the feasibility of producing such systems involved considerable development work directed toward pressure vessel fabrication techniques and evaluation of new forming processes for producing large hemispherical shells. Processing and assembly techniques gained from the Phase B portion and upgraded from the Phase A portion of the program added considerably to the state-of-the-art for building large tankage.

Program results and testing as described and evaluated in this report show that the two-phase program conducted under contract No. NAS 9-2978 was highly successful in achieving the desired goals.

SECTION II

TECHNICAL DISCUSSION

The following discussion makes reference and comparison to the radial bumper-discrete shield design. This design evolved during the 1958-1960 period and has been service-tested by several qualification programs and over 2000 delivered tank systems. It was preceded by over 50 dewar designs at Instruments & Life Support Division and was developed for the specific purposes of improving the thermal conductivity heat transfer and structural integrity of the annular suspension mechanism. It has proven to be a versatile and compatible design for fabrication reproducibility and supplemental insulation for reduced heat transfer, when applied to smaller type tankage. The NAS 9-2978 program described in this report consisted of the application of the design concept to larger flight-type tankage.

Included in this discussion is a description of the design, a review of various approaches to dewar insulation, and a review of developmental testing performed by I & L S Division in improving dewar insulation methods.

2.1 Description of Radial Bumper-Discrete Shield Design

The basic design is described in Figure 2-1. A minimum of six olive-shaped bumpers, equally positioned on the annular fill and vent lines, maintain the annular space relation. Sub-figures 4 and 5 show the segmented improvement to further reduce the conductivity heat transfer.

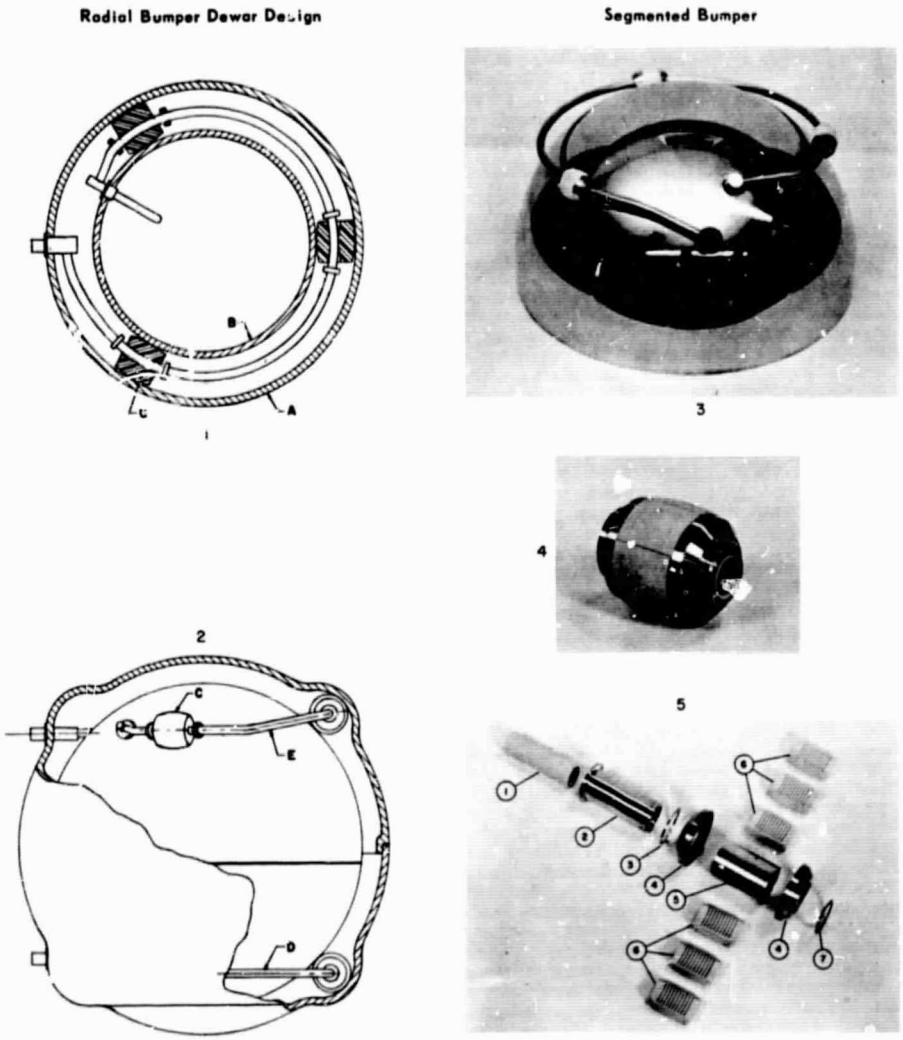


Fig. 2-1

Radial Bumper Design

Figures 2-2 and 2-3 show the addition of isothermally mounted discrete shields which are attached by low conductivity devices to the annular tubes. The design is simple, purely mechanical, complies with theory, is readily reproducible, and is consistent with established vacuum vessel practices.

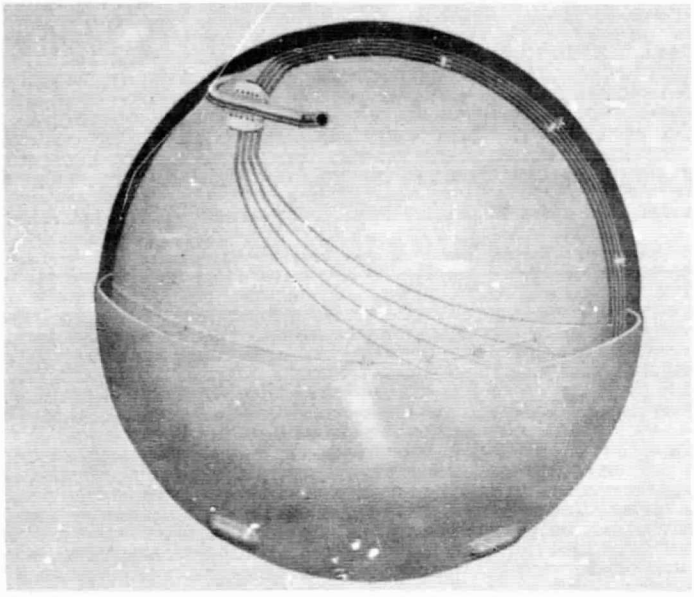


Fig. 2-2

Discrete Shield-Radial Bumper Design

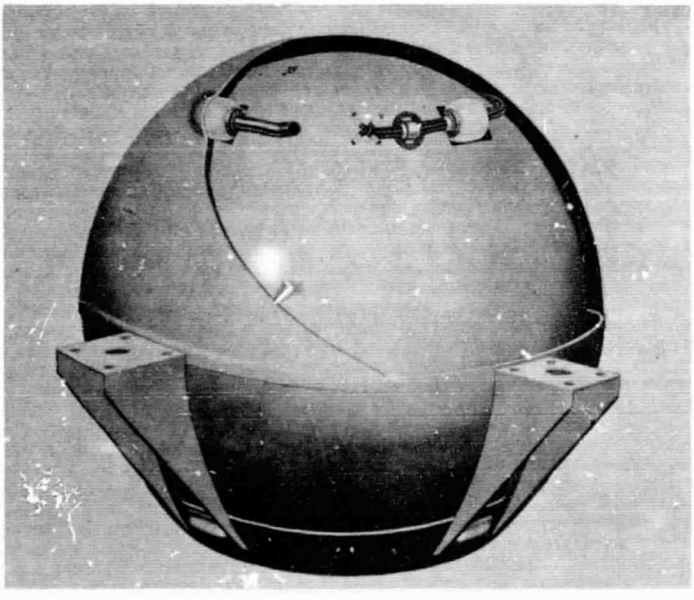


Fig. 2-3

Discrete Shield-Radial Bumper Design

2.2 Dewar Insulations

Several insulation concepts are reviewed in the following discussion. In general, only those concepts are considered that have been examined and tested with the objective of obtaining very low heat leak with stable shelf life static vacuum conditions.

2.2.1 Pure Vacuum Insulation

Assuming a dewar made of an inner pressure vessel and a rigid outer vacuum jacket for all practical tankage insulation techniques, then comparatively the pure vacuum insulation weighs nothing and consumes the least volume, thus allowing the smallest and lightest rigid outer vacuum jacket. For critical low heat leak tank applications, the insulation properties of pure vacuum are limited, but it is important to establish and know the extent of this limitation, because it is only for thermal property requirements beyond this limitation that it can possibly be weight economical to add supplemental insulation. Carrying the rigid vacuum wall assumption one step further, it is seen that - irrespective of the type of supplemental insulation added - if it were momentarily removed, a basic pure vacuum vessel would remain; the basic vacuum vessel design establishes the basic thermal (and physical) properties of the tank. The supplemental insulation is intended to improve these properties; again, it is important in development and analysis to know the extent of the improvement, i.e., what thermal values can be credited to what design features.

The records of some 20,000 pure vacuum flight design dewars manufactured at I & L S Division were analyzed for the purpose of estimating the best surface radiation and component conduction properties attained in the different tank designs. This exercise resulted in a "basic vacuum vessel heat leak curve" which is shown as "Curve B" of Figure 2-4. Curve B is plotted from hypothetical dewars comprised of the best components from the best recorded radiation and conduction data obtained on Instruments & Life Support production units. This curve is considered to be at the lower edge of the existing state-of-the-art for pure vacuum insulation vessels, i.e., the best possible with current knowledge. The present state-of-the-art is a reasonable band area above the curve.

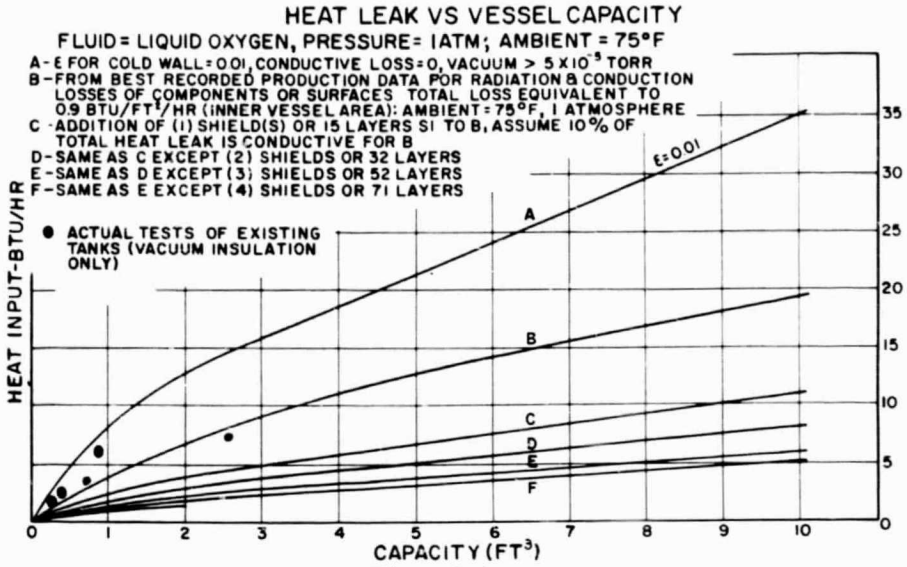


Fig. 2-4

Heat Leak vs. Vessel Capacity

The effect of surface emissivity upon the theoretical radiation heat leak per square foot of inner vessel surface is shown in the following Table 2-1. The heat leak is given in Btu/hr-ft$_i^2$ (i = inner vessel surface), and is for liquid oxygen vented to an NTP environment. The spherical surfaces have a spacing of approximately 1/2" and an inner/outer surface area ratio = .7055. The emissivity data in Table 2-1 is from NBS-AEC report 54-9, by M. Fulk and M. M. Reynolds.

TABLE 2-1

OXYGEN HEAT LEAK - BTU/FT$_i^2$-HR.

INNER VESSEL Outer Surface -297°F	OUTER VESSEL Inner Surface +78°F			
	Silver e=.022	Copper e=.018	Stainless e=.074	Blackbody e=1.0
Silver e=.006	0.74	0.71	0.83	0.87
Copper e=.015	1.49	1.38	1.93	2.18
Stainless e=.048	2.79	2.45	4.91	6.99
Blackbody e=1.0	4.50	3.69	14.82	145.71

The analysis of production dewar tanks at I & L S Division shows that the radiation heat transfer for $\Delta T = 375°F$ must be between 0.7 and 0.9 Btu/ft^2_i hr. for the best recorded units which correlates favorably with the silver$_i$ values above.

The technique of obtaining very low emissivity surfaces has been well established on prior vacuum vessel programs; however, it has been accomplished only on rigid, well-prepared surfaces such as tank hemisphere walls or stable configuration radiation shields. Aluminum foils and aluminum vapor coatings appear on the order of e = 0.03 to 0.05 and above.

2.2.2 Supplementing Vacuum Insulation

Curves C, D, E, and F of Figure 2-4 show the effect of adding discrete shields, or equivalent units of laminar insulation at K = 0.00004 Btu/ft^2-hr-°F/ft, to the basic Curve B tanks and, therefore, also represents the best possible values for those respective vessels.

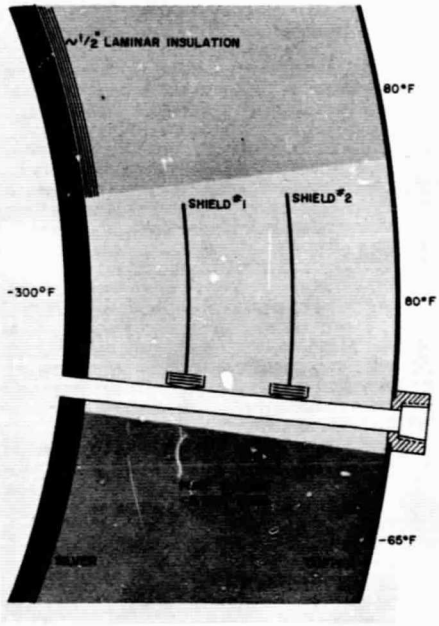


Fig. 2-5
Equivalent Heat Transfer Configurations

Figure 2-5 at left is a cross section view of a dewar vacuum space and depicts apparent equivalent heat transfer configurations. If we take a pure vacuum insulated dewar with a low fraction of conductive heat input, we can reduce the heat input about 65% by:

(a) Reducing the evnironment temperature to -65°F

(b) Adding two discrete radiation shields

or

(c) Adding 1/2" laminar insulation (K = .00004 Btu/ft^2-hr-°F/ft)

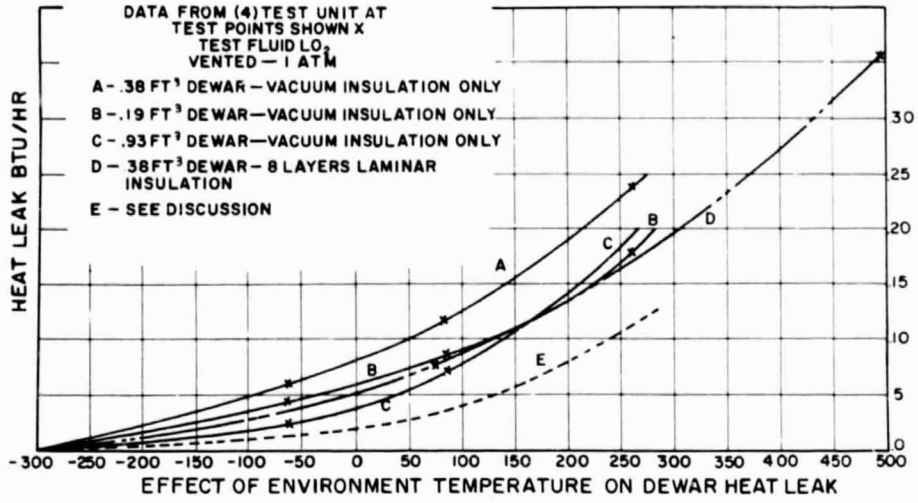


Fig. 2-6
EFFECT OF ENVIRONMENT TEMPERATURE ON DEWAR HEAT LEAK

In actual practice (a) is quite effective as seen by Curve C of Figure 2-6; (b) is nearly attainable as evidenced by the Phase A and Phase B oxygen two discrete shield units fabricated at I & L S Division and discussed in this report; however, (c) is generally off by a factor of 2 or more in actual application as subsequently discussed. From (a) and (b) it follows in actual application that the innermost shield must be about -65°F if the actual heat transfer is to compare to (a).

It is generally convenient from a design, test, analysis and discussion point of view to separate the conductive and radiation modes of heat transfer. Further, it is convenient and practical to consider the radiation heat transfer in terms of "per square foot of inner vessel surface," since the inner vessel is the "receiver" of all heat input.

Thermal conductivity tests on the existing radial bumper suspension design have shown that the total conductive heat leak into a cryogenic tank with this design will be less than (1) Btu/hr. in a (1) g NTP environment. This will reduce to about 0.2 - 0.3 Btu/hr in a zero-G environment where there is no load on the bumpers and the major conductivity paths are disrupted.

In the subsequent discussion the conduction heat transfer component will be ignored with regard to the pure vacuum and discrete radiation shield comparisons because it is sufficiently low as to not alter the conclusions.

$$Q = \sigma A \frac{E}{(n+1)} (T_2^4 - T_1^4)$$

Where
σ=Stefan-Boltzmann constant
A=Enclosed surface area
E=Emissivity factor
n=no. of shields
T_2=Abs. Temperature of enclosing surface
T_1=Abs. Temperature of enclosed surface
Q=Heat transfer rate into system

2.2.3 Discrete Shield Insulation

A discrete radiation shield is a low emissivity radiation barrier placed in the vacuum space and isothermally mounted to some support structure. At equilibrium, it assumes some intermediate temperature between the inner and outer vessel surface temperatures.

The use of discrete shields with good thermal isolation in the vacuum space will substantially reduce the radiant heat transfer. For example, when the emissivity factors are the same between all pairs of surfaces in a dewar, and shields are thermally isolated, the thermal transfer rate to the inner tank varies according to the factor 1/(n+1), where n = the number of shields placed between the inner and outer tank surfaces. This is expressed in the equation at left.

Applying shields to the reasonable silver-stainless values of 0.83 Btu/ft_i^2-hr from Table 2-1 and assuming $_o$ equivalent emissivities, we obtain Table 2-2.

TABLE 2-2

N. Shields	Factor of $\frac{1}{n+1}$	Radiation Heat Transfer Btu/hr-ft_i^2
0	1	0.80
1	1/2	0.415
2	1/3	0.277
3	1/4	0.207
4	1/5	0.166

2.2.4 Laminar (Super) Insulation

Heat transfer through other type radiation barrier insulations can also be compared to pure vacuum or discrete shield type insulation on a per ft_i^2-hr basis.

Table 2-3 shows the heat transfer in Btu/ft_i^2-hr for various thicknesses of laminar (super) insulation over a range of K values. The column for "ΔT = 380°F" represents liquid oxygen testing and assumes an outer laminar surface temperature close to ambient which generally occurs if over 8 to 10 layers are used.

TABLE 2-3

HEAT TRANSFER THROUGH SUPERINSULATION* AT VARIOUS K VALUES

K** BTU/HR FT^2 °F/FT	BTU/FT_i^2 HR For 1/2" Insul. ΔT = 380°F	For 1/8" Insul. ΔT = 380°F	For 1/8" Insul. ΔT = 300°F	For 1/8" Insul. ΔT = 190°F
0.00001	0.0912	0.3648	0.2882	0.1824
0.00002	0.1824	0.7296	0.5764	0.3648
0.00003	0.2736	0.9944	0.7856	0.4972
0.00004	0.3648	1.4592	1.1527	0.7296
0.00005	0.4560	1.8240	1.441	0.9120
0.00006	0.5472	2.1888	1.729	1.0944
0.00007	0.6384	2.5536	2.017	1.2768
0.00008	0.7296	2.9184	2.305	1.4592
0.00009	0.8208	3.2832	2.594	1.6416
0.00010	0.9120	3.6480	2.882	1.8240

* Alternate layers of 'dexiglas' fiber glass paper and aluminum foil.

** Effective Flat Surface Thermal Conductivity: The use of flat plate data provides a conservative comparison with shields and pure vacuum. For example, the insulation thickness for a 5 ft^3 vessel spherical surface with an effective flat plate K = 0.00004 Btu/Hr °F-Ft and 0.3648 Btu/Hr-Ft^2 heat transfer would be 0.52" rather than the 0.50" noted above; i.e., the effective spherical surface thermal conductivity is higher.

Bendix Instruments & Life Support Division

The basic heat transfer mode for laminar or powder type insulations is thermal conductivity with radiation reinforcement or suppression in the interstices depending mainly upon the particle conduction and/or surface characteristics.

The transition from pure vacuum insulation to the addition of nonisothermally installed insulation is best considered with an example: Consider from Table 2-1 a practical heat transfer value between $silver_i$-$stainless_o$ surfaces (LO_2 to NTP) of 0.83 Btu/ft_i^2-hr: In this example, the radiation transfer is 0.83 Btu/ft_i^2-hr, the conductive heat transfer is zero. A spacing of 1/8" in practice is not uncommon. The addition of radiation opaque insulation to the system (non-isothermally installed powders, super insulation, laminae, etc.) is, in effect, attempting to reduce the unit radiation heat transfer at a greater rate than conductive* heat transfer is added to the system; assuming pure opacity for the example, the unit conductive heat transfer for the added insulation must be below 0.83 Btu/ft_i^2-hr to be of any value to the system. Referring to Table 2-3, 1/2" of laminar insulation at a reasonable K = 0.00009 Btu/ft^2-°F-hr/ft will suffice, but note that the weight of 1/2" of insulation has been added plus the necessary 1/2" spacing merely to arrive at an equivalent situation for operation at 75 to 80°F. Comparatively, one discrete shield could have been added for a weight less than 1/4" laminar insulation (in a 5 ft^3 vessel size) and reduced the heat transfer about one-half by blocking the radiant transfer without addition of conductive heat transfer to the system.

This is why, in designs requiring light weight, where construction costs permit processing high quality vacuum space surfaces, there is no useful - normal temperature - application for laminar insulations below 1/2" or powders below about 1" since these thicknesses are required in actual practice merely to compete favorably with low emissivity-pure vacuum insulation at the current state-of-the-art.

* The Complex conductive-radiative process that occurs in superinsulation is herein called conduction.

Referring to further examples from Table 2-3, we can compare the 1/2" of super insulation at $\Delta T = 380°F$ with two discrete radiation shields from Table 2-2. The heat transfer for the two shields is 0.277 Btu/ft$_i^2$-hr, therefore, the 1/2" super insulation must have a K = 0.00003 Btu/ft^2-°F-hr/ft to compare. This has not apparently been practicably attained on complete cylindrical tankage configurations and, therefore, is not considered possible with present material on spherical tankage surfaces.

A further example is that of a four shield unit from Table 2-2; the heat transfer is 0.166 Btu/ft$_i^2$-hr. From Table 2-3 it is seen that one inch of superinsulation at K = 0.00004 Btu/ft^2-hr-°F/ft or about two inches of superinsulation at K = 0.00008 Btu/ft^2-hr-°F/ft is required. The latter is the more practical K value, however, discrete shields would be lighter even at the lower K value.

Table 2-4 is a summary of one laminar insulation test program performed at I & L S Division in 1959 on Contract AF33(600) 39882 and reported in ASD-TDR-62-84. It amply shows how improvement can be miscounstrued.

The test calorimeter used in the Table 2-4 test work was cylindrical. Several different materials were tested; the type insulation #4 was composed of alternate layers of Dexiglas paper and aluminum foil which became a popular superinsulation material.

The following insulating materials were tested:

Insulation 1. Style 116 glass cloth, heat cleaned, .005 in. thick. Exeter Manufacturing Co.

Insulation 2. C-100-28 Refrasil cloth, .013 in. thick. H. I. Thompson Fiber Glass Company.

Insulation 3. Glass fiber surfacing mat, silane treatment polyester binder, .005 in. thick, Modiglas Fibers, Inc.

Insulation 4. P. R. #500 - .008B Dexiglas glass fiber paper, .008 in. thick. H. I. Thompson Fiber Glass Company.

All insulations were constructed with equal numbers of alternating layers of the insulating material and 0.001 in. thick aluminum foil.

TABLE 2-4

INSULATION TEST - HIGH TEMPERATURE VESSEL PROGRAM

TEST	TYPE INSULATION	CONFIGURATION	TOTAL HEAT LEAK BTU/HR	CONDUCTIVE HEAT LEAK (EST.) BTU/HR	TOTAL RADIATION HEAT LEAK BTU/HR	EST. RAD. HEAT LEAK INSULATED SURFACE $BTU/FT^2/HR$	EFFECTIVE FLAT PLATE K $BTU/FT^2-°F-HR/FT$
1	Vacuum Only		19.0	4	15	No Insulation	
2	1	18 continuous layers	12.67	4	8.67	5.06	0.00028
3	2	18 continuous layers	16.63	4	12.63	8.51	0.00048
4	3	18 continuous layers	13.78	4	9.78	6.03	0.00033
5	4	18 continuous layers	12.67	4	8.67	5.06	0.00028
6	4	18 separate layers	11.08	4	7.08	3.67	0.0002
7	4	9 separate layers	11.08	4	7.08	3.67	0.0001
8	4	7 separate layers	12.17	4	8.17	4.62	0.0001
9	4	4 separate layers	12.67	4	8.67	5.06	0.00007
10	4	9 separate layers on cylinder. 9 layers on ends	7.6	4	3.6	2.53	0.00007

Test Calorimeter inner vessel cylinder 5" diameter x 10.5" long.

Test 2 through 9 had insulation layers on cylindrical surface only.

Test 10 had insulation layers on both cylindrical and end surfaces.

Cylindrical surface area = 1.145 ft^2; cylinder ends area = 0.2726 ft2.

Bendix Instruments & Life Support Division

It is seen in Table 2-4 for the type (4) insulation that slight improvement occurred with separated layers over continuous wrap layers; that no improvement occurred between 9 and 18 layers on the cylindrical surfaces only; that a large improvement occurred in test 10 by adding layers to the cylinder ends. Most significant is to note that the dewar was improved from 19 Btu/hr with pure vacuum insulation to 7.6 Btu/hr with 1/8" insulation added to all surfaces; an improvement of 60%. Actually, the resulting heat transfer was approximately 2.53 Btu/ft^2_i-hr which corresponds to an effective flat surface K = 0.00007 Btu/ft^2-hr °F/ft. This is three times higher than pure vacuum insulation with low emissivity surfaces such as $silver_i$-$stainless_o$ = 0.83 Btu/ft^2_i-hr from Table 2-1.

Thus, in this test example, the insulation improved the heat transfer of a dewar because of the very high (poor) surface emissivity characteristics. Alternately, it would have degraded a dewar with low emissivity surfaces.

The fact that small thicknesses of laminar insulation will actually degrade a pure vacuum vessel with low emissivity surfaces is not generally recognized. An excellent example that demonstrates this comparison occurred on an instrument dewar program, contract Schlumberger 0-12777, during the 1959-1960 period at I & L S Division.

The cylindrical dewars for the program were one liter capacity and the inner vessels were approximately 2" diameter x 23" long. The annular spacing was 0.140". The initial dewars had pure vacuum insulation with silver-copper annular surfaces. Later dewars had 7-9 layers each of aluminum foil and glass fiber paper in order to meet the contract specifications.

The contract test procedure for the instrument dewars was to fill the dewar with 190°F water, apply a specific stopper to the opening and measure the time versus temperature drop of the contents to 130°F. The test was performed in an NTP environment.

Test data exists on four dewars that were tested for heat leak both with hot water and LO_2 as the test mediums. Only the pertinent data from the laboratory records is shown in the following Table 2-5.

TABLE 2-5

UNIT	INSULATION	NECK TUBE CONDITION	HOT WATER HEAT LEAK	LO_2 HEAT LEAK
E-1	Vacuum	Regular	Too High	4.53 Btu/hr
E-2	Vacuum	Regular	Too High	4.53 Btu/hr
E-3	Vacuum	Cut Down	Too High	4.05 Btu/hr
E-Test	Laminar Insul.	Cut Down	Within Spec.	5.00 Btu/hr

The initial units E-1 thru E-3 had pure vacuum insulation with low emissivity silver plated surfaces. They failed the hot water test but had lower LO_2 heat leaks than the laminar insulated E-Test unit. Units E-3 and E-Test are identical except for the insulation in that both had under cut (thinner) neck tube sections and both had silver-copper annular surfaces.

The cylindrical surface area of the inner cylinder is 0.924 ft^2. If we assume normal prototype emissivity characteristics, the pure vacuum radiation heat transfer to the cylindrical surface is approximately 0.8 to 1.0 Btu/hr (ref. Table 2-1). Thus, the addition of 0.140" insulation approximately doubled the cylindrical surface heat transfer in the LO_2 test. Referring to Table 2-3, the equivalent flat plate thermal conductivity must have been about 0.00005 to 0.00006 Btu/hr. ft. °F/ft. for this cylindrical surface application.

Therefore, both the relative effect and proper application of laminar insulation in cryogenic tankage are demonstrated. First, the relative effect is that thin applications of laminar insulation will increase the heat transfer between low emissivity surfaces for normal temperature cryogenic applications. Second, low conductivity (laminar type) insulation should be used at the outer tank surface to retard heat transfer particularly for high temperature applications where the fourth power difference would have a large effect on pure radiation heat transfer.

I & L S Division had three contract programs that required laminar insulation which contributed to about three years investigative work on laminar insulation techniques. The insulation programs were successful in that they were adequate for the special

development problems at that time, but the results would not be considered successful for general application to current space mission requirements. It is apparent, however, that the laminar or opaque fiberglass type insulations will be required for specific space system applications. These should be integrated with discrete radiation shields for maximum efficiency.

As an example, laminar insulation was effectively used on two high temperature liquid oxygen systems for operation at 500°F and 700°F on contract AF33(600)39882. The heat leak curve for one of these units is shown as Curve D of Figure 2-6. The laminar insulation reduced the slope of the heat leak versus environment temperature curve thus indicating the dominant conductive rather than radiant mode of heat transfer. The heat transfer in the normal temperature region was actually worse for the addition of insulation, but was significantly improved at the higher temperature region. These units also had vapor cooling coils wound through the insulation for precooling during flow periods.

2.2.5 Conductive Versus Radiation Heat Transfer

The insulation temperature environment is a significant factor in the design and selection of the insulation barrier.

Conductive heat transfer varies directly as the difference in absolute temperature whereas the radiation heat transfer varies as the difference of the fourth power of the temperatures. The low temperature operating regimes of the cryogenic fluids are relatively fixed, although the external environmental temperature during a space mission can vary significantly. Also, a marked temperature profile exists through an insulation package. It is noted on radiation heat leak versus environment temperature curves for cryogens that the slopes of the curves increase significantly at the higher temperature regions where the fourth power difference has a large effect; the curves are fairly shallow for low temperature region ΔT's. Conduction, on the other hand, is more uniform over the entire temperature region, varying only as the material thermal conductivity varies. As a general design observation, pure radiation heat transfer should dominate the low temperature heat transfer region and conduction should be used to limit the heat transfer process at the higher temperature region. The only way to preserve pure radiation heat transfer at the low temperature region for the heat transfer surfaces that view or are adjacent to the inner cryogen vessel, is to thermally isolate the radiation viewing surfaces in the proximity of the inner

vessel; this is the function of the discrete radiation shield. The radiation surfaces should, in turn, be comprised of well prepared silver or copper plating to represent the actual state-of-the-art.

The warmer region, particularly the outer surface region in a high temperature tank application, can very effectively utilize a low thermal conductivity insulation such as certain glass fiber or mineral fiber felts or papers to minimize the high temperature heat transfer and reduce the surface temperature that views the inner radiation heat transfer control surfaces and assembly.

Figures 2-7 and 2-8 compare the heat input in Btu/ft_i^2-hr versus tank outer surface temperature for discrete shield and laminar insulation. Figure 2-7 compares a discrete shield effective emissivity of 0.005 with a laminar insulation FTC = 3 (Avg. normal temp. K - 7.5×10^{-5} for O_2). These are considered the best possible overall values that can be obtained for spherical tanks with the existing materials and design technology. Figure 2-8 compares a discrete shield effective emissivity of 0.006 with a laminar insulation FTC = 4 (Avg. normal temp. K = 1×10^{-4} for O_2).

The importance of isolating the radiation heat transfer mode from the conduction mode is now apparent. It is compatible with the problems attending analysis, design and test, but more important the function of each mode is now apparent. It is compatible with the problems attending analysis, design and test, but more important the function of each mode is suited to a different temperature region in actual application, and isolation or separation is necessary to attempt effective control at each temperature region depending upon the application and environment.

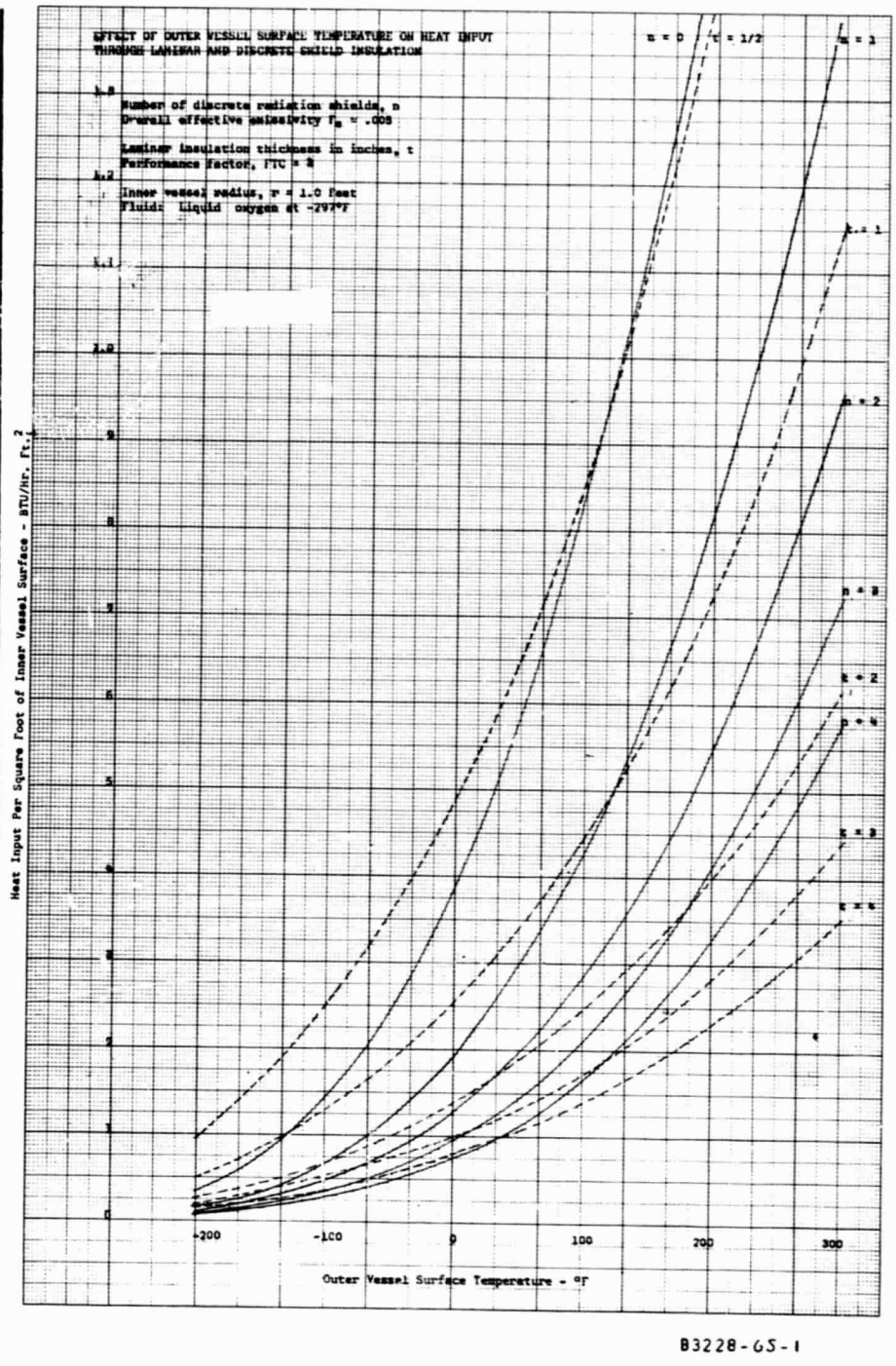


Fig. 2-7

Effect of Outer Vessel Surface Temperature
On Heat Input
Through Laminar and Discrete Shield Insulation

F_e=.005 FTC=3

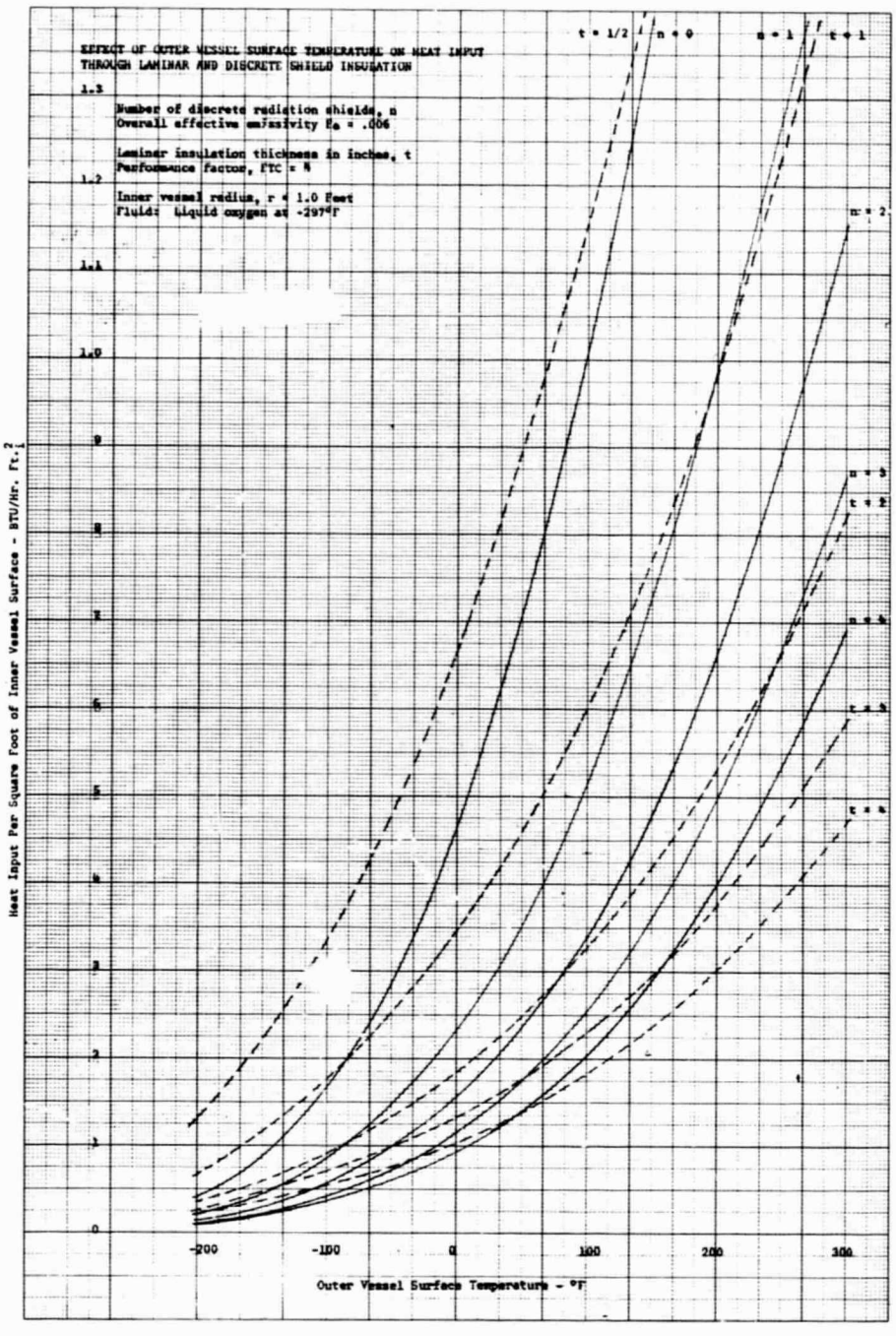


Fig. 2-8
Effect of Outer Vessel Surface Temperature
On Heat Input
Through Laminar and Discrete Shield Insulation
F_e=.006 FTC=4

2.2.6 Growth Potential of Insulation Concepts

It is reasonable to conclude or assume at this time that the two insulation techniques, "discrete shielding" and "laminar wrap" are the only basic insulation forms that merit comparison. There are, of course, numerous variations of each basic form.

Each insulation concept is composed of a multiplicity of reflective shields to limit radiation heat transfer, and each is separated by a low conductivity spacer to retard thermal conductivity heat transfer between the shields. It is thus seen that the reflective and insulation qualities of the alternate layers, and the effective weight-volume characteristics of each, are the important aspects for comparison.

The discrete shield is a thin but self-supporting member, sufficiently rigid to be processed to the lowest possible surface emissivity characteristics for the specific temperature region. It is supported by a (near) isothermal mounting and each shield is separated by a high vacuum. Therefore, the radiation reflective characteristics are the highest possible with current technology, the high vacuum separation and isothermal mounting approaches zero thermal conductivity heat transfer and is, therefore, the lowest at the current technology. Heat transfer with the discrete shield concept is essentially radiation. Improvement lies in developing thinner, closely spaced, multiple shield assemblies without increasing conductive heat transfer between the shields.

Laminar wrap insulation utilizes very thin alternate layers of reflective foil or reflective coating and low thermal conductivity spacer material.

The reflector surfaces are generally aluminum, the spacer materials are generally forms of fiberglas or mylar. In comparison with the discrete shield, the emissivity of aluminum is several times higher than the rigid surface silver or copper used on the discrete shield. Also, the spacer materials of fiberglas or mylar provide an effective (though low) conductivity path compared to the isothermal mounting and pure vacuum used with the discrete shield. To compensate for the poorer reflector and conductivity properties of the laminar layers, many very thin layers are used.

Because of the relatively poor emissivity properties of the aluminum and the contact proximity of each layer, the primary mode of heat transfer is thermal conductivity.

The difference in emissivity characteristics that can be processed on various surfaces has a large effect on the heat transfer of the various insulation concepts. Because of the relatively poor radiation surface characteristics of the available aluminum foils and vapor coatings used in laminar insulations, it takes 20 to 35 of the combination laminae on an inner vessel surface merely to reduce the insulation thermal conductivity to a value comparable to the pure vacuum radiation transfer between two (2) low emissivity surfaces. Beyond this, approximately 10 to 20 layers of laminar insulation compares to one (1) discrete shield for normal temperature environment application.

Heat transfer for the discrete shield is predominantly by radiation, therefore, discrete shields will be most effective at the low temperature region. Heat transfer for laminar insulation is predominantly thermal conductivity, therefore, laminar insulation will be most effective at the high temperature region.

In terms of comparative growth potential for normal to low temperature region applications, the low conductivity layer of the laminar insulation must approach the conductivity of high vacuum used for the discrete shield concept; the aluminum foils or coatings must be replaced by reflector surfaces which approach the effective emissivity of the silver-copper surfaces used for the discrete shields. It appears that the present emphasis and expenditure upon laminar insulation "lay-up" techniques with existing materials is somewhat optimistic since the problem lies in the reflective and conductivity properties of the basic materials.

2.2.7 Improvement Concepts For The Radial Bumper-Discrete Shield Design

2.2.7.1 Characteristics of The Basic Design

The design improvement tasks for flight tankage in the 1955 to 1960 period were mainly concerned with reducing the thermal conductivity and improving the structural integrity of the annular mounting suspension design. It was during this period that the "radial bumper suspension" design evolved which has proved extremely successful in subsequent applications.

The period 1958 - 1961 was marked by considerable effort and money expended to improving the radiation heat transfer by various wrapped, laminar and powder insulation techniques. This work was performed mainly with spherical tanks of (1) ft^3 capacity or less, and could not be

construed as successful for present requirement low heat leak applications.

In 1962 I & L S Division reoriented the main cryogenic tankage insulation effort to the discrete shield concept and this work has been successful from the beginning. The most encouraging aspect of the radial bumper-discrete shield design is the consistency of results. The artisan techniques of assembly have been essentially eliminated. The design is straight forward and the thermal-physical properties of a specific design can be defined and described within reasonable limits.

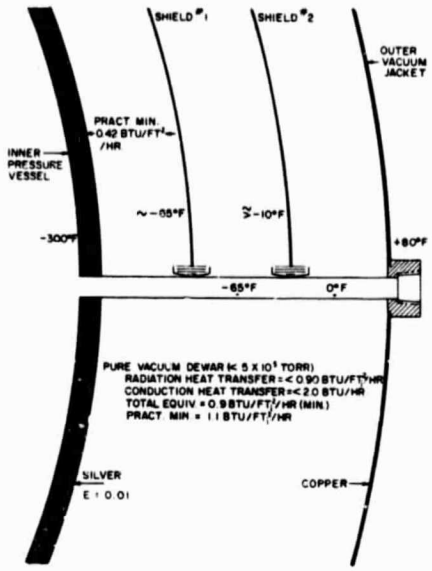


Fig. 2-9

Phase A Schematic

Figure 2-9 at left schematically represents the Phase A Supercritical Oxygen Tank discussed in Section III of this report. The values shown were considered a reasonabl expectation for the first prototype. The conductive loss was approximately 1.5 Btu/hr, but the radiation heat transfer was approximately 0.45 Btu/ft^2-hr due to surface plating and assembly problems that caused surface degradation, as discussed in Section III. The conductive loss has since been reduced to approximately 0.5 Btu/hr for an equivalent suspension design and the radiation surface procedures have been improved.

2.2.7.2 Laminar Insulated Shields

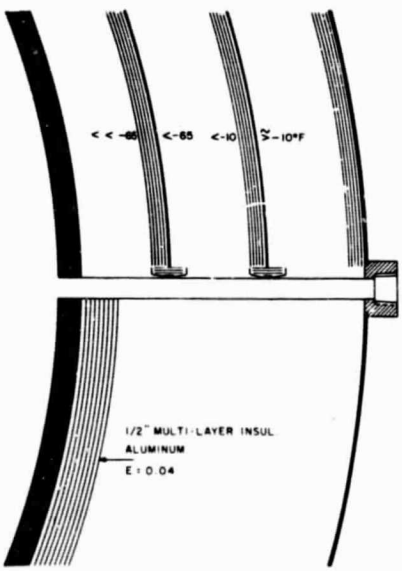


Fig. 2-10

Laminar Insulated Shields

Referring to Figure 2-10 at left, it has been considered that adding a laminar type low conductivity insulation to the emitting (least critical) side of the discrete shield may effectively reduce the heat transfer across the shield. The question, of course, is whether the additional laminar insulation would weigh less than an additional discrete shield to effect the same reduction in heat transfer. At the current state-of-the-art for laminar materials, an additional discrete shield would weigh less; yet very little is known about applying laminar insulations while preserving low emissivity surfaces at key intervals as depicted by Sketch B. It is improbable that laminar insulated shields would be effective at the inner cold temperature regions. Applying outer surface laminae may be effective for high temperature applications.

2.2.7.3 Integral Structure, Multiple Discrete Shield Assemblies

The successful performance indicated for discrete shields suggests a concentrated effort to further weight improvement of the discrete shield concept. The approach is to produce the essential low emissivity surfaces and isothermal mountings using the thinnest and lightest shield hemispheres as the structure bases for the electroplated surfaces. For compact, multi-shield assemblies, each thin shield must structurally reinforce and rigidize the whole shield assembly through miniaturized isothermal mounting connections; i.e., comparable to thin wall sandwich construction sheet.

The first application of multi-shield subassemblies was in the Phase B oxygen and hydrogen tanks, discussed in Section IV, in which miniaturized low conductivity mounting connections were used to connect dual shield subassemblies together. The next steps would be to reduce shield wall thickness, reduce shield spacing and increase the number of shields in a subassembly.

2.2.7.4 Vapor Cooling

Whenever a flow situation prevails with a cryogenic dewar - such as with a venting type standby or a normal usage flow, the heat input to the dewar can be minimized by feeding the cold venting fluid through the insulation for precooling This is called vapor cooling or vapor expansion cooling, depending upon whether fluid expansion subcooling is employed.

Computer analyses have shown that the most efficient use of the cooling vapor occurs when the vapor cooling heat exchanger is applied in the cold temperature region in the shield adjacent to the inner vessel. It has been shown that the radiation mode of heat transfer control is most effective in this region; it therefore follows that efficient use of the available specific heat in the cooling vapor will occur through application with the isothermally mounted discrete radiation shield.

Vapor cooling can reduce the static shielded insulation heat input by 50-80%, therefore, it is very important to weight optimization of long standby and/or very low mission flow rate systems, and it is most effective for the low density cryogenic fluids such as hydrogen and helium.

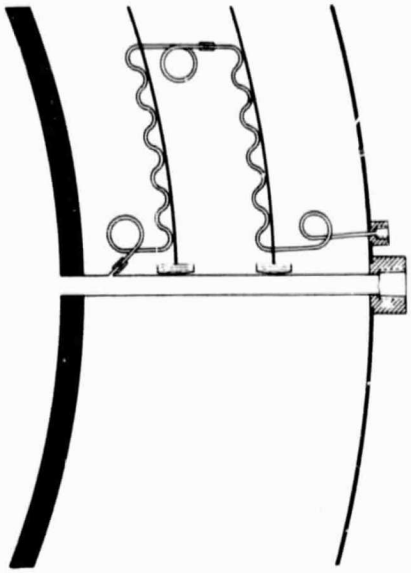


Fig. 2-11
Vapor-Cooled Shield

Figure 2-11 pictorially shows the supply cooling coil attached to the discrete radiation shields. The objective is to cool the shield emitting surface temperature below the static heat transfer equilibrium temperature by absorbing shield heat into the cold flowing fluid. As the shield temperature is reduced, there is an increase in heat radiation to the shield due to the larger ΔT can be maintained across the shield and sustain a low temperature at the emitting surface.

It presently appears that development work on the vapor cooled laminar shield should follow a reasonable vapor cooled shield development program which will obtain basic vapor cooling data for subsequent comparative evaluation purposes.

Computer programs have been prepared for evaluating and comparing multi-shield designs with vapor cooling of one and two shields. There tentatively appears to be little value in vapor cooling more than two shields.

2.3 Insulation Summary

There is an extensive history to the development of cryogenic tankage insulation as related herein and summarized as following:

Thermal Conductivity Heat Input - Numerous annular suspension designs have been constructed and sold in competition for thousands of aircraft systems. The radial bumper design has the lowest basic thermal conductivity of any known design. It is the most uniform and repeatable of the known support mechanism concepts.

Pure Vacuum Insualtion - Pure vacuum insulation with low emissivity surfaces is the only form of radiation deterrent insulation effectively developed to a high state-of-the-art. Its limitation without further shielding has apparently been reached.

Reflective Powder Insulations - This insulation is heavy and bulky. Thin applications degrade pure vacuum insulations; thicker applications effect proportionate heat transfer reduction; economical when used for low heat leak ground applications. Based upon extent of prior development and application, the present properties are probably approaching a limitation to the art for existing materials.

Laminar (Super) Insulation - Thin applications degrade pure vacuum insulation; thicker applications effect proportionate heat transfer reduction; lighter than

powders; markedly degraded by compression or application to spherical surfaces. Assembly of insulation is difficult; resulting heat transfer is not uniform. Stable static vacuum characteristics are poor. Based upon the extent of prior development time and expense, the present properties are probably approaching a limitation to the art with present materials.

Discrete Radiation Shields - Application with low emissivity surfaces agree favorably with theory and improves pure vacuum insulation for single or multiple shield application. These shields are applicable to spherical surfaces; reasonable to design and assemble with consistent, repetitive results; considerably lighter than other insulation from small tanks; weight competitive for large tanks because of poor thermal properties of applied laminar insulation; and stable vacuum characteristics are good.

Vapor Cooling - A small amount of vapor cooling exists in all cryogenic tanks. Only recently has much effort been applied to design efficient vapor cooling into a tank. It appears from present computer studies that most efficient use of available fluid occurs in the cold temperature region adjacent to the inner tank and by limiting the mode of heat transfer to radiation. The isothermally mounted discrete shield appears the only way to accomplish this.

Weight Comparison - It is difficult to define a weight comparison between discrete shields and laminar insulation that will serve for all tankage sizes and applications. It varies significantly with tank size and allowable heat input to the inner vessel per unit area. For example, it is impractical to consider laminar wrapped insulation for small tanks (10-20" diameter) because of the small radius effect upon wrapped insulation efficiency. Discrete shields are not affected by tank radius or size.

Recent analyses which have examined the insulation thickness and weight plus outer shell weight to meet a spectrum of heat input requirements show the following weight comparison for a normal temperature environment.

If the heat input requirement is above 0.5 Btu/ft_i^2-hr the discrete shield weight will trade off with laminar wrap insulation at approximately K = 3 x 10^{-5} Btu/ft^2-hr°F/ft.

If the heat input requirement is below 0.5 Btu/ft_i^2-hr the discrete shield weight will trade off with laminar

wrap insulation at approximately K = 5 x 10^{-5} Btu/ft^2-hr°F/ft.

A laminar wrap insulation having an effective flat plate K = 8 x 10^{-5} Btu/ft^2-hr°F/ft will have approximately twice the insulation weight as discrete shields in the 2-10 ft^3 capacity tank range.

SECTION III

PHASE A PROGRAM

3.1 System Description and Operation

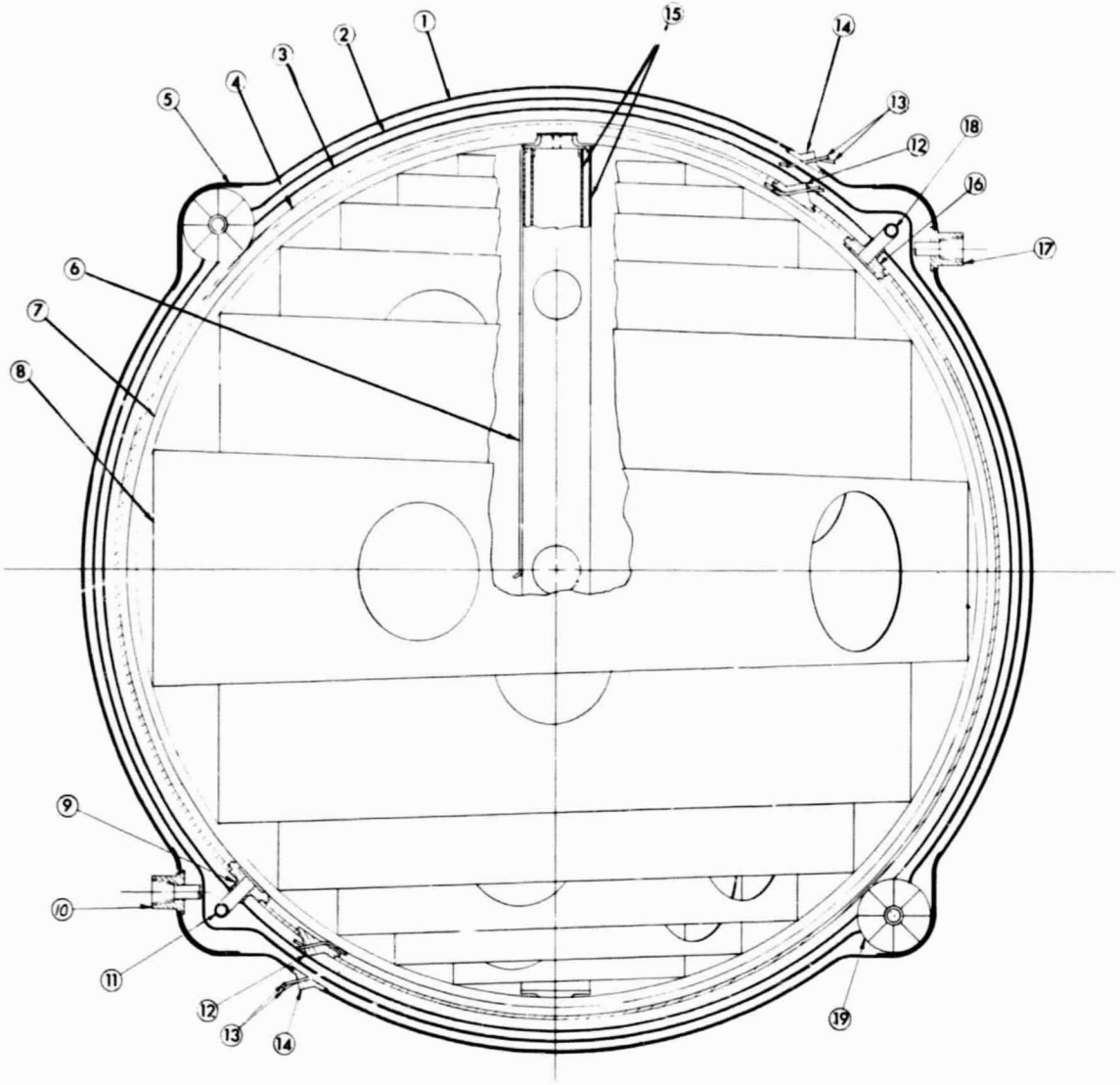
The following paragraphs describe the dewar itself, the complete system, and the operation of the complete system.

3.1.1 Dewar Description

The Phase A Dewar Assembly is shown in Figure 3.1-1. Physical characteristics of the dewar are presented in Table 3.1-1.

The pressure vessel consists of a spherical inner shell fabricated from two hydroformed Inconel 718 hemispheres. Located within the pressure vessel are a static thermal conductor, a capacitance-type quantity sensor (non-functional), and a copper-constantan thermocouple. The thermal conductor and quantity sensor are mounted in a support ring which is mounted within the pressure vessel at the fluid fill and vent fittings.

The static thermal conductor consists of a spiral wound sheet of aluminum assembled to a support ring mounted in the inner vessel. The conductor was included to limit temperature stratification in the fluid contents by diffusing heat throughout the vessel by means of conductive heat transfer. The spiral is made of 0.025" thick 5052 aluminum sheet, 214" long, with steps from 4-1/16" wide at the narrow external end to 19-13/32" wide at the inner end to obtain the spherical configuration. Eighteen 3-inch diameter holes throughout the length provide good liquid communication and minimize the unit weight. The spiral spacing is 1.3" and total surface area is 41.4 ft^2. The conductor is mounted within an aluminum 6061 channeled ring which is secured to the inner vessel at the inner portion of the inlet and outlet tube fittings. In addition, spring clips located on the ring contact the inner vessel walls and are compressed when the inner vessel hemispheres are assembled; this allows for thermal expansion and contraction differences between the pressure vessel material (Inconel 718) and the aluminum thermal conductor assembly, while maintaining rigidity.



1. OUTER SHELL
2. OUTER RADIATION SHIELD
3. INNER RADIATION SHIELD
4. PRESSURE VESSEL
5. OUTER SHELL DOUBLE STRIP
6. THERMOCOUPLE
7. SUPPORT RING
8. THERMAL CONDUCTOR
9. INNER FILL FITTING
10. OUTER FILL FITTING
11. FILL TUBE
12. INNER ELECTRICAL LEAD FITTING
13. ELECTRICAL LEAD
14. OUTER ELECTRICAL LEAD FITTING
15. QUANTITY SENSOR
16. INNER VENT FITTING
17. OUTER VENT FITTING
18. VENT TUBE
19. SEGMENTED BUMPER

ASSEMBLY - PHASE A DEWAR

FIGURE 3.1-1

E-3873-67-235

TABLE 3.1-1

PHASE A DEWAR PHYSICAL CHARACTERISTICS

		WEIGHT, LB.
INNER VESSEL		36.200
Material	Inconel 718 (Aged)	
Inner Diameter	20.344 in.	
Wall Thickness	0.084 in.	
Usable Volume	2.50 ft^3	
Operating Pressure	900 psig	
INNER SHIELD		2.700
Material	Aluminum 5052	
Inner Diameter	21.000 in.	
Wall Thickness	0.017 in.	
OUTER SHIELD		2.900
Material	Aluminum 5052	
Inner Diameter	21.500 in. (nom.)	
Wall Thickness	0.017 in.	
OUTER SHELL		21.000 (with doublers)
Material	Stainless Steel 304L	
Inner Diameter	22.000 in. (nom.)	
Wall Thickness	0.035 in.	
FITTINGS (4)		
Material		
Inner	Inconel 718	
Outer	Stainless Steel	
Tubes Inner (2)		0.300
Tubes Outer (2)		0.200
Leads Inner (2)		0.150
Leads Outer (2)		0.100
FILL & VENT TUBING		
Material	Stainless Steel 304L	
Outer Diameter	0.3125 in.	
Wall Thickness	0.016 in.	

TABLE 3.1-1

P''ASE A DEWAR PHYSICAL CHARACTERISTICS
(Continued)

		WEIGHT,LB.
BUMPERS (6)		1.398
Type	Segmented	
Material	25% Glass-Filled Teflon	
Assembly Outer Diameter	1.772 in.	
SPIRAL THERMAL CONDUCTOR		7.550
Material	Aluminum 5052	
QUANTITY SENSOR (non-functional)		0.700
Material		
Inner Tube	Aluminum 6061	
Outer Tube	Stainless Steel 321	
INNER SUPPORT RING		0.500
Material	Aluminum 6061	
THERMOCOUPLE AND LEAD		
Type	Copper-Constantan	
QUANTITY SENSOR LEAD (non-functional)		0.100
HEATER LEAD (non-functional)		0.130
GETTER		0.090
Type	Barium	
BURST DISC		0.100
	TOTAL DEWAR WEIGHT	74.618

A capacitance type quantity sensor, consisting of two concentric tubes (one aluminum 6061 and one stainless steel 321), is mounted in the support ring in the center of the spiral thermal conductor. No electrical leads are connected to the sensor, thus the unit is not functional. However, it was included in the system to represent the weight of such a unit in a completely functional system and also to represent the thermal conductivity effects of a full length probe, acting as a static thermal conductor. The thermocouple is mounted between successive layers or segments of the thermal conductor near the center of the vessel. No heater element was included in the system, since the Phase A unit was not intended to be functional but to serve as a test vessel to verify the low heat leak properties and structural integrity of the discrete shield-radial bumper design.

Two pick-up tubes, silver-brazed to the inner fill and vent fittings, extend from the fittings along the inside surface of the vessel to the top and bottom points of the vessel. Locating tubes in this manner permits essentially 100% fill and 100% depletion, even though the fill (or supply) and vent fittings are not located at the vessel poles.

The thermocouple, quantity sensor and electrical heater leads exit from the pressure vessel through silver-brazed joints in two electrical lead fittings located in the same 45° horizontal planes as the fluid fittings. The two quantity sensor leads and the electrical heater leads are non-functional, but are included in the dewar to provide the conductive heat transfer obtained from such leads in a completely operable system. All leads consist of conductors enclosed within, and electrically insulated from, a stainless steel sheath. The conductor insulation material is magnesium oxide.

Stainless steel 304L fill and vent tubes exit from the pressure vessel at silver brazed joints in the two fluid fittings located 45° above and 45° below the girth line. The tubes extend circumferentially approximately 360° through the vacuum void before exiting from the dewar. In like manner, the four electrical leads follow the tubes through the vacuum void and exit thru fittings in the outer shell. Both tubes and leads pass through and are supported by the six radial bumpers utilized for supporting the pressure vessel within the outer shell.

The low thermal conductivity of this type of vessel support and the small contact area at support locations result in very low conductive heat transfer from the environment to the fluid contents. The pressure vessel is silver plated to provide a low emissivity surface for minimization of radiation heat transfer to the stored cryogen.

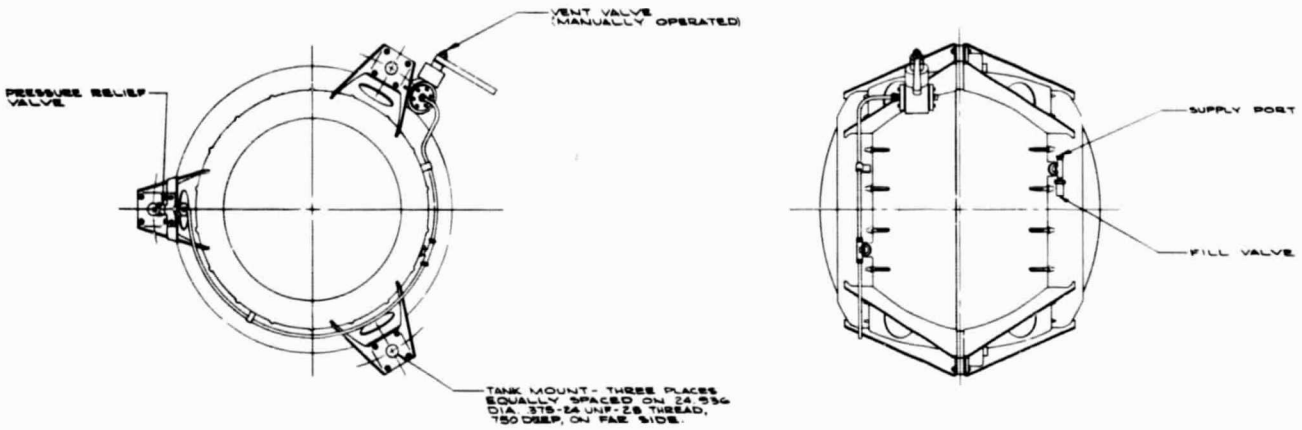
Two radiation shields are located around the pressure vessel in the vacuum annulus to further reduce radiation heat transfer to the fluid contents. The shields consist of hemispheres (inner shield) and hemispheroids (outer shield), hydroformed from aluminum 5052 and mechanically fastened at the girth. A doubler is riveted to one half-shell of each of the shield assemblies for further rigidity of the individual shield assemblies. The inner shield is spherical; the outer shield is essentially spherical and concentric to the inner vessel but deviates from this in that there are two tunnels formed horizontally around each shield hemispheroid through which the fill and vent tubing and leads pass. Cut-outs in the shields are provided to fit around the bumper assemblies and to permit the passage of the fill and vent tubes and leads to the outer shell. The cut-outs were oversized for ease of assembly and installation. To minimize the radiant heat shorts through the shields resulting from the oversized cut-outs, small contoured covers are mechanically fastened to the shields over the portions of the holes not required for feed-through. Adequate clearance is left in order that no physical contact occurs between the shields and the tubes and leads, which would result in a conductive heat short. The radiation shields provide essentially 100% coverage of the pressure vessel. The two shields are supported in the void by low thermal-conductivity Teflon hangers located in the fill and vent tubes, thus thermally isolating the shields from the tubes. To provide low emissivity surfaces for minimization of radiant heat transfer, both shields are silver plated on all surfaces.

The fill and vent lines, as well as the electrical leads, exit from the dewar through silver-brazed joints in the stainless steel outer shell fittings, which are in turn heliarc welded in the outer shell, or vacuum jacket. The outer shell consists of two hydroformed stainless steel 304L hemispheres heliarc welded at the girth. The vacuum annulus is evacuated to a high vacuum of 10^{-7} mm Hg or more to eliminate convective heat transfer to the fluid contents. A barium getter on the outer shell wall assists in maintaining a high, stable vacuum. The inner surface of the outer shell,

being essentially at environmental temperature, is copper-plated to provide a low-emissivity surface at this relatively higher temperature. The conductive heat transfer to the stored cryogen through the tubing and leads is minimized by the long lengths of these heat paths.

3.1.2 System Description

The Phase A Tankage Assembly is shown in Figure 3.1-2. Physical characteristics of the system are presented in Table 3.1-2.



TANKAGE ASSEMBLY
SUPERCRITICAL CRYOGENIC OXYGEN

NAS 9-2978 PHASE A

FIGURE 3.1.2

D-3873-67-234

The dewar assembly is supported within a mount carriage at the points of contact between the radial bumpers and outer shell so that all vessel loads are carried directly from the bumpers through the outer shell and into the mount carriage. The mount structure configuration conforms to that of the outer shell in the horizontal plane tunneled regions; three gusseted support members in each half of the carriage assembly connect the horizontal contoured rings to the system mounting points. Three anti-shock and vibration dampers are provided between the gusseted supports and the mounting locations. This

TABLE 3.1-2

		WEIGHT, LBS.
MOUNT CARRIAGE		9.500
Material	Aluminum 6061	
VIBRATION MOUNTS		1.060
Manufacturer	Lord	
VENT VALVE		3.100
Manufacturer	Hydromatics	
Type	Manual Ball Valve	
Orifice	0.375 in.	
Seats	Teflon	
FILL VALVE		0.100
Manufacturer	Essex	
Type	Quick-Disconnect	
PRESSURE RELIEF VALVE		0.350
Manufacturer	Circle Seal	
Cracking Pressure	950 psi	
ION PUMP		0.180
Manufacturer	Ultek	
Capacity	0.2 ltr/sec 10^{-5} to 10^{-8} torr.	
MISC. PLUMBING		0.700
TOTAL EXTERNAL COMPONENT WEIGHT		14.980
TOTAL DEWAR WEIGHT (FROM TABLE 3.1-1)		74.618
TOTAL DRY SYSTEM WEIGHT		90.598
TOTAL WET SYSTEM WEIGHT (178.1 lb LO_2)		268.698

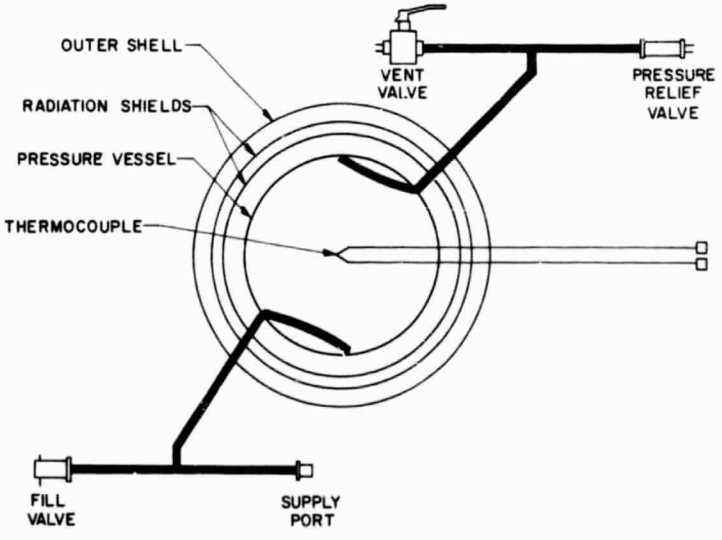
type of support structure is suitable for vehicle attachment in the horizontal plane.

External components include a manually operated vent ball valve, a pressure relief valve, and a quick-disconnect fill valve. The vent valve and pressure relief valve are attached to the gusseted support members of the mount carriage.

An ion pump attached to the evacuation tube of the tank (not shown in Figure 3.1-2) is included for two reasons. It is used to remove outgassed materials from the vacuum annulus, and to provide a means of determining the pressure within the vacuum annulus. The ion pump operates from a separate power supply provided with the system.

3.1.3 System Operation

Because of the objective of the Phase A program, i.e., to develop and build a large flight-type cryogenic storage test vessel for purposes of verifying the discrete shield-radial bumper thermal-physical design, some functions required for pressure-flow control were not included. These included destratification fans for mixing the fluid, heaters for system pressurization, and pressure switches for controlling these functions. Therefore, the system operation is simplified and straight forward. (Refer to Figure 3.1-3).



SCHEMATIC—SUPERCRITICAL CRYOGENIC OXYGEN NAS 9-2978 PHASE A

FIG. 3.1-3 A-3873-67-229

The fill process consists of connecting the liquid oxygen supply source to the system fill port and closing the supply port by means of a downstream valve. With the vent valve open, the liquid oxygen supply source should be pressurized to 15-30 psig to insure a continuous flow of liquid into the vessel. Initial liquid flow into the storage vessel will result in vaporization of oxygen until the vessel wall is cooled to liquid oxygen temperature, at which time the vessel will begin to fill. Continued transfer to the system will eventually result in liquid oxygen issuing from the vent valve when the container is 100% full. Some liquid will be vaporized after the supply source is disconnected, due to the liquid turbulance created by filling. Therefore, the vessel cannot be filled 100% full with liquid cryogen; the maximum fill obtained with the system has been 98.8%.

When the predetermined or required quantity of oxygen is "onboard", the filling is stopped, the liquid oxygen supply source is disconnected, and the vent valve is closed. The system is now in the standby period, during which time the oxygen pressure and temperature gradually increase due to heat input from the environment surrounding the system. The time required for the Phase A system to pressurize to 800 psig, when 96% filled with liquid oxygen and in a 70°F environment, is approximately 100 hours. To protect the system against malfunction, excessive heat leak, increased standby, etc., the pressure relief valve is provided to prevent a pressure rise above a safe limit (950 psig).

Flow from the system is initiated by opening a supply control valve downstream of the system supply port. If in a 1-g environment and the system is in its normal orientation, liquid oxygen will be obtained from the supply port and gaseous oxygen will exit through the vent valve (if opened) when the fluid contents are in the two-phase subcritical condition. If the oxygen is at or above oxygen supercritical pressure, i.e., the fluid contents are single phase, the fluid may be withdrawn from either the vent valve or from the supply port.

3.2 Program Description

The objective of the Phase A program of Contract No. NAS 9-2978 was to fabricate a prototype supercritical oxygen storage system in a short time period for demonstrating and evaluating the radial bumper-discrete radiation shield thermal-physical dewar design. The

design, development and fabrication assembly features and techniques gained from the Phase A program were then to be utilized to the fullest extent in the Phase B program, which was fully hardware oriented. Specific major tasks of the Phase A program included the following:

1. Development testing of dewar components for design optimization.

2. Development testing of fabricating and processing techniques.

3. Survey of current dewar shell fabrication methods and vendors.

4. Design of a supercritical oxygen storage system.

5. Fabrication of a supercritical oxygen storage system.

6. Thermal and structural testing of the system.

3.2.1 Vendor Survey

Stable static vacuum cryogenic vessels require absolute zero leakage or diffusion through the vessel walls and joints by optimum mass spectrometer standards, and extremely low material out-gassing characteristics. This has been routinely accomplished with the materials, design, fabrication and process procedure used in aircraft systems. Because of the importance of maintaining these characteristics in the selection of materials, fabrication processes and procedures used in space system tankage, a vendor survey was conducted during the period December 1963 to October 1964. The purpose of the survey was to review and observe the methods, techniques, processes, equipment and general experience, capability and capacity in the country for fabrication of hemispheres and pressure vessels suitable for cryogenic vacuum vessel manufacture.

The objectives of the survey were twofold:

1. Establish the availabiltiy and suitability of equipment, processes and procedures for the fabrication of light weight cryogenic vacuum tankage in the size range 23" to 72" diameter.

2. Provide direct familiarity and exposure for vendor selection and project personnel so that sound design, fabrication and process control procedures can be effected.

The following personnel performed the vendor survey and solicitation program. Each individual visited one or more companies in each of the process categories subsequently described. At the time of the survey, each individual had over eight years experience in his respective field at Bendix, Instruments & Life Support Division, associated with cryogenic tankage.

Mr. P. Gardner - B.S. Chem. - Mgr. Cryogenic Systems

Mr. D. Hankins - B.S.M.E. - Sr. Eng. Cryogenic Sys.

Mr. D. Wiele - B.S. Metallurgy E g. - Sr. Metallurgist

Mr. D. McKeon - Mgr. - Engineering Machine Shop

The specific items reviewed consisted of the following:

1. Specific Prior Experience

   (a) Hemispheres, spheres and/or cylinders actually fabricated

   (b) Materials used

   (c) Sizes

   (d) Wall thickness

   (e) Processes and procedures required

2. Inspection Procedures

3. Heat Treating Equipment or Source

4. Plating Equipment

5. Machining Equipment or Source

6. Welding Equipment or Source

7. Polishing Equipment

8. Leak Detection Equipment

9. Metallurgy and Process Control Laboratory or Source

10. Tooling Lead Time and Source

11. Piece Part Lead Time

12. Hemisphere and Sphere Tolerance Control

    (a) Wall thickness

    (b) Diameter

    (c) Sphericity

    (d) Reproducibility

In the selection of companies for review, it was intended to discover the major capability in the country for the fabrication of cryogenic vessel shells. Companies were visited that represent each of the major and applicable processes, and both large and small business establishments were included.

The companies are listed according to process capability, therefore some company duplication exists. The first number following the company listing indicates the number of personnel visits; the second number is a relative composite of personnel and facility resources and experience varying from (1) "major" to (2) "satisfactory" to (3) "limited" based upon the requirements for a major cryogenic tankage program.

A. Forging

    1. Ladish Company, Cudahy, Wisconsin 2-1

    2. Taylor Forge, Chicago Illinois 2-2

    3. Cameron Iron Works, Houston, Texas 1-1

    4. Interstate Forge, Milwaukee, Wisconsisn 2-3

B. Machining

    1. Airite, Los Angeles, California 6-2

    2. Airtek Dynamics, Compton, California 4-2

    3. Menasco, Burbank, California 6-1

    4. A. R. Gieringer Tool Corporation
       Milwaukee, Wisconsin 2-3

    5. Stanek Tool, Milwaukee, Wisconsin 2-3

6. Petersen Tool, Chicago, Illinois 2-3

7. Goodwin Engineering, Chicago, Illinois 1-3

8. E. W. Bliss, Canton, Ohio 1-2

9. Merz Engineering, Indianapolis, Indiana 2-1

10. Martin Company, Baltimore, Maryland 1-1

11. Diversey Engineering, Chicago, Illinois 1-3

12. California-General, Chula Vista, California 3-2

C. Spinning

1. Phoenix Products, Milwaukee, Wisconsin 3-2

2. Spincraft, Milwaukee, Wisconsin 3-2

3. C. A. Dahlin, Elk Grove Village, Illinois 5-3

4. C. B. Kaupp, Maplewood, New Jersey 1-2

D. Mechanical Drawing

1. California Hydroforming, El Monte, Califor[illegible]-3

2. General Metals, St. Louis, Missouri 1-2

3. Barth Corporation, Cleveland, Ohio 1-1

4. C. B. Kaupp, Maplewood, New Jersey 1-3

5. Martin Company, Baltimore, Maryland 1-2

6. Tyce Engineering, Chula Vista, California 1-2

7. Bendix, Kansas City, Kansas 0-2

E. Hydroforming (up to 22" diameter)

1. Cincinnati Milling Machine, Cincinnati, Ohio
2 - equip, only

2. Jones Metal Products, West Lafayette, Ohio 6-1

3. California Hydroforming, El Monte, California 3-3

4. C. B. Kaupp, Maplewood, New Jersey 1-1
(Max. 14" diameter)

5. Diversey Engineering, Chicago, Illinois 1-1

F. Hydraulic Bulge Inturgescent Forming

1. Jaycraft Engineering, El Cajon, California 10-2 (limited resources)

2. Multiplex, El Cajon, California 1-(no capability)

G. Chemical Milling

1. Chemtronics, Santee, California 3-1

2. Brooks & Perkins, Detroit, Michigan (communication only)

3. Straza Company, El Cajon, California (communication only)

H. Welding

1. Menasco, Burbank, California 6-1

2. Airite, Los Angeles, California 6-1

3. Airtek Dynamics, Compton, California 4-2

4. Arde, Inc., Paramus, New Jersey 12-1

5. Arde, Inc., Portland, Maine 6-2

6. California-General, Chula Vista, California 3-3

I. Cryoforming

1. Arde, Inc. Paramus, New Jersey 12-2

2. Arde, Inc., Portland, Maine 6-2 (limited resources)

J. Plating

1. Precision Plating, Chicago, Illinois 6-1

2. Superior Plating, Minneapolis, Minnesota 0-3

3. Electro Coating, Inc., Moline, Illinos 2-3

4. Mason Company, Inc., Davenport, Iowa 2-3

5. Adolph Plating Company, Chicago, Illinois 1-2

K. Materials

1. TMCA, Toronto, Ohio 2
2. Crucible Steel, Pittsburgh, Pennsylvania 2
3. Battelle Memorial Institute, Columbus, Ohio 1
4. Martin Company, Denver, Colorado 1
5. Denver Research Laboratory, Denver, Colorado 1
6. North American, Downey, California 1

L. Brazing

1. Research Inc., Minneapolis, Minnesota 1
2. TMCA, Toronto, Ohio 2
3. Crucible Steel Company, Pittsburgh, Pennsylvania 2

M. Miscellaneous

1. Lockheed-Burbank-Explosive Forming & Spin Forging
2. NAA-Downey - General Experience
3. McDonnel - St. Louis - General Experience
4. Boeing - Seattle - X-20 Tankage Experience
5. Lear Sigler - Los Angeles - Spin Forging
6. Bendix - Kansas City - High Energy Forming

Summary of Survey

The following conclusions were summarized and reported in the August 1965 Interim Report #16A.

The principle processes applicable to cryogenic vacuum vessel hemisphere fabrication are:

1. Mechanical drawing
2. Spinning (and machine)
3. Hydroforming
4. Forge and machine
5. Hydraulic bulge (Inturgescent) forming

The principle procedures applicable to cryogenic pressure vessel fabrication are:

1. Welding of shapes produced by above processes with or without interstage or subsequent heat treatment. All cryogenic materials are applicable.
2. Cryogenically stretch forming of vessels fabricated of shapes produced by the above processes. (only low Si 301 SS)

An objective of this process study was to determine the existing equipment and process capability in the country for producing large and light weight cryogenic vessels. Equipment and process limitations, tool and piece part cost and delivery, reproducibility, applicable materials and compatibility with good vacuum vessel design practice are the important factors. The prior and extensive cryogenic pressure vessel and vacuum vessel design and processing procedures were used as a guide in the evaluation of procedures for fabrication of large vessels to maintain a high design and fabrication assurance level. Therefore, four basic assumptions were made for evaluation purposes that were justified by prior experience and/or lack of alternate procedure experience and evidence.

a. Integral vs welded bosses: There is no substantial evidence that either technique is superior from a pressure, structural, weight or leak tight aspect if comparable design and process control procedures are employed. Welded bosses provide greater process flexibility and reduced cost, and have been most extensively used in flight type cryogenic tankage. Therefore either procedure is acceptable and the latter is preferred.

b. Forged vs formed shapes: All prior cryogenic tankage with proven stable static vacuum characteristics have been fabricated from polished surface, deep drawn or hydroformed shells; i.e., from basic, smooth, mill rolled materials in which the inclusions are routinely well controlled and which run perpendicular to the direction of potential leakage or diffusion.

Large forged shapes require stringent materials control on each piece and machine removal of approximately 90-95% of the basic forge stock. The surface finish is > 63 RMS except with special polishing. Leakage and diffusion characteristics are questionable since there is no proven prior experience with forged thin wall shells on stable static vacuum tanks.

For the above reasons, formed shells are preferred.

c. Surface Finish: The surface finish of the annular space walls or shields is important to provide good vacuum space cleanliness, minimize gas occlusion, and provide for extremely low emissivity surfaces. This is consistent with prior and proven vacuum vessel practice, therefore, forming processes and procedures that yield smooth surface characteristics are preferred.

d. Materials: Materials used in the vacuum space must have a vapor pressure below 10^{-6} mm Hg and be readily outgassed to a stable vapor pressure condition. Aluminum, copper, nickel, silver, stainless steel, teflon, Kel-F and mica are the materials with which most satisfactory experience exists. Stainless steels and some nickel-iron alloys have, in the past, been preferred for the pressure and vacuum vessel shells because of the vacuum, weld, cryogenic and tube joint compatibility. If weight and other factors are comparable, preference will be given to materials with which prior and satisfactory vacuum vessel experience exists. A brief summary of the results of the hemispheres study is as follows:

Hemisphere Size	Wall Thickness	Preferred Process
<22" dia.	<0.2"	Hydroform
>22" dia.	<0.150"	Hydraulic bulge forming
<35" dia.	>0.150"	Forge & machine
>30-35" dia.	>0.20"	Shear spin or spin forge & machine

All processes or process combinations reviewed are capable of producing hemisphere shapes with wall thicknesses within ± 0.002", and diameters within ± 0.005" with proper fixturing and tooling and for nominal 30" diameter pieces. This order of dimensional control is considered adequate for the application and pertains to the commonly considered materials such as aluminum, stainless steel, inconel and titanium.

Minimum practicable wall thicknesses are on the order of 0.008" to 0.010" by the hydroform, mechanical draw and inturgescent processes although wall thicknesses down to 0.003" have been produced on 18-20" diameter hemispheres.

A minimum practicable wall thickness for pressure vessels is approximately 0.020" particularly in the 20" - 30" diameter range due to welding, handling, processing and for uniform test properties.

The low carbon and stabilized stainless steels, inconel, low silicon 301 cryoformed stainless, aluminum and copper materials have, with proper control, exhibited suitable ductility and compatibility for use with all cryogenic fluids. Titanium alloys, with proper control, are suitable for all cryogenic fluids except oxygen.

From prior application experience and evidence, strength to weight analyses and cost analyses, cryoformed stainless offers the best growth potential for cryogenic fluid application.

The hydroform process is suitable for producing uniform wall thickness shapes up to 22" diameter with wall thickness between 0.010" and 0.200". It is the most economical tooling and piece part process for a small quantity of parts.

The hydraulic bulge forming process (inturgescent forming) is a comparable forming technique to the hydroform process, but due to the higher tooling and piece part cost, it is not competitive below 22" diameter. It is an excellent process for the fabrication of uniform thin wall shapes in the range of 22" diameter to 110" diameter, and also provides the lowest tooling piece part cost for small quantities in this size range.

Mechanical deep drawing is applicable up to 30-35" diameter pieces, however the tooling cost is extremely high and drawing presses are limited.

The forge and machine process is primarily applicable to shapes in the size range from 22" diameter to about 35" diameter. Above 30-35" diameter the tooling and piece part costs become prohibitive. With the advent of the inturgescent process, the need for forge and machine has diminished for thin wall shapes.

Shear spinning and spin forging are applicable to all sizes, but because of material control problems and the polishing or machining requirement, it is not as economical or well suited to the large thin wall shapes as the inturgescent process.

Explosive and spark type high energy forming techniques have not proven suitable or reproducible for thin wall shapes.

Electroforming (electrolytic deposition) is not applicable to light weight shells because of the limitation of applicable materials to the process.

The cryoform process can utilize any of the processes that produce uniform hemispherical shapes for the vessel preforms, which are subsequently cryogenically stretch formed to the desired size and shape. The hydroform and inturgescent processes provide the most economical hemisphere preform.

Alternately, "Composite Structure Cryoforming" utilizes sheet material which is properly cut, rolled and welded to form truncated cones, cylinders and circles which are assembled, welded and stretch formed to cylindrical or spherical shapes.

The cryoforming process is therefore quite versatile for utilization of existing materials forming equipment in the country, and for the fabrication of large pressure vessels.

Several graphs were prepared to show cost, weight and materials comparison data pertaining to hemisphere and pressure vessel fabrication.

Figure 3.2-1 shows the subcontractor tooling cost vs hemisphere diameter for the five common forming procedures. This cost will vary somewhat, depending upon the material and wall thickness.

Figure 3.2-2 shows the nominal subcontractor hemisphere piece part cost vs diameter for the five common forming procedures. The piece part cost can vary significantly depending upon the material, wall thickness, tolerance and surface finish requirements.

Figure 3.2-3 shows the material in the final part vs starting material requirements. This is significant for the high process expense materials because it is an indication of the potential cost reduction through development improvement. For example, very little cost improvement can be expected for the forge and machine process since the excess material and fabrication labor are inherent in the process.

Figure 3.2-4 is an estimate of the cost of obtaining an 8 RMS surface finish on the vacuum exposed surfaces. These costs must be added to the piece part costs of Figure 3.2-2.

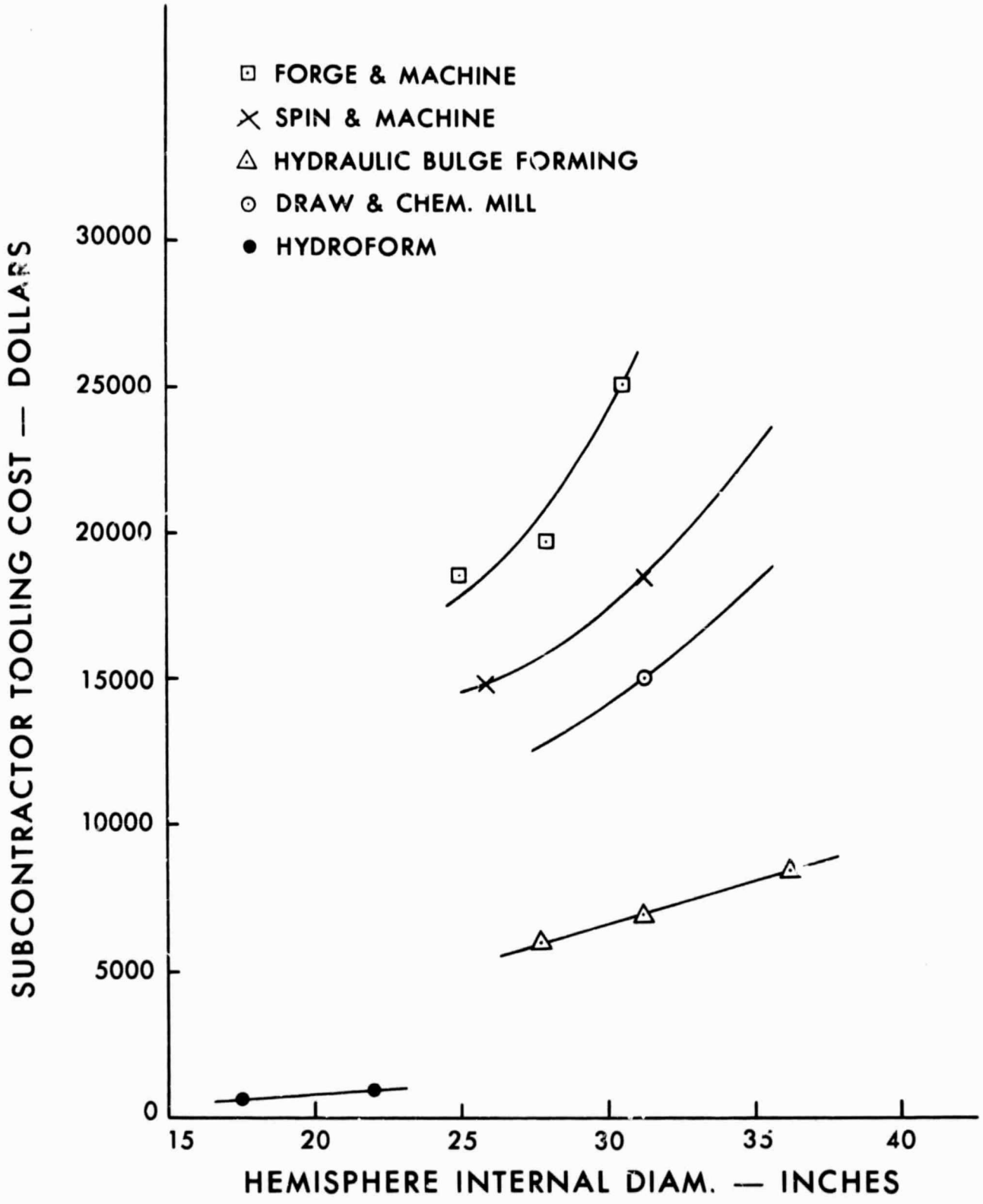
Figures 3.2-5, 3.2-6 and 3.2-7 show a comparison of the relative strength properties of cryoformed stainless steel with other cryogenic pressure vessel materials. These strengths have been related to stainless steel for this comparison.

Figure 3.2-8 includes several plots of outer vacuum shell weight vs diameter for several materials and buckling conditions. Only the "2" and "4" curves are significant on the basis of recent buckling test data.

Figures 3.2-9 and 3.2-10 are plots of spherical pressure vessel weight vs diameter for burst pressures of 500 and 1500 psi. Cryoform stainless and titanium 5 Al 2.5 Sn are compared.

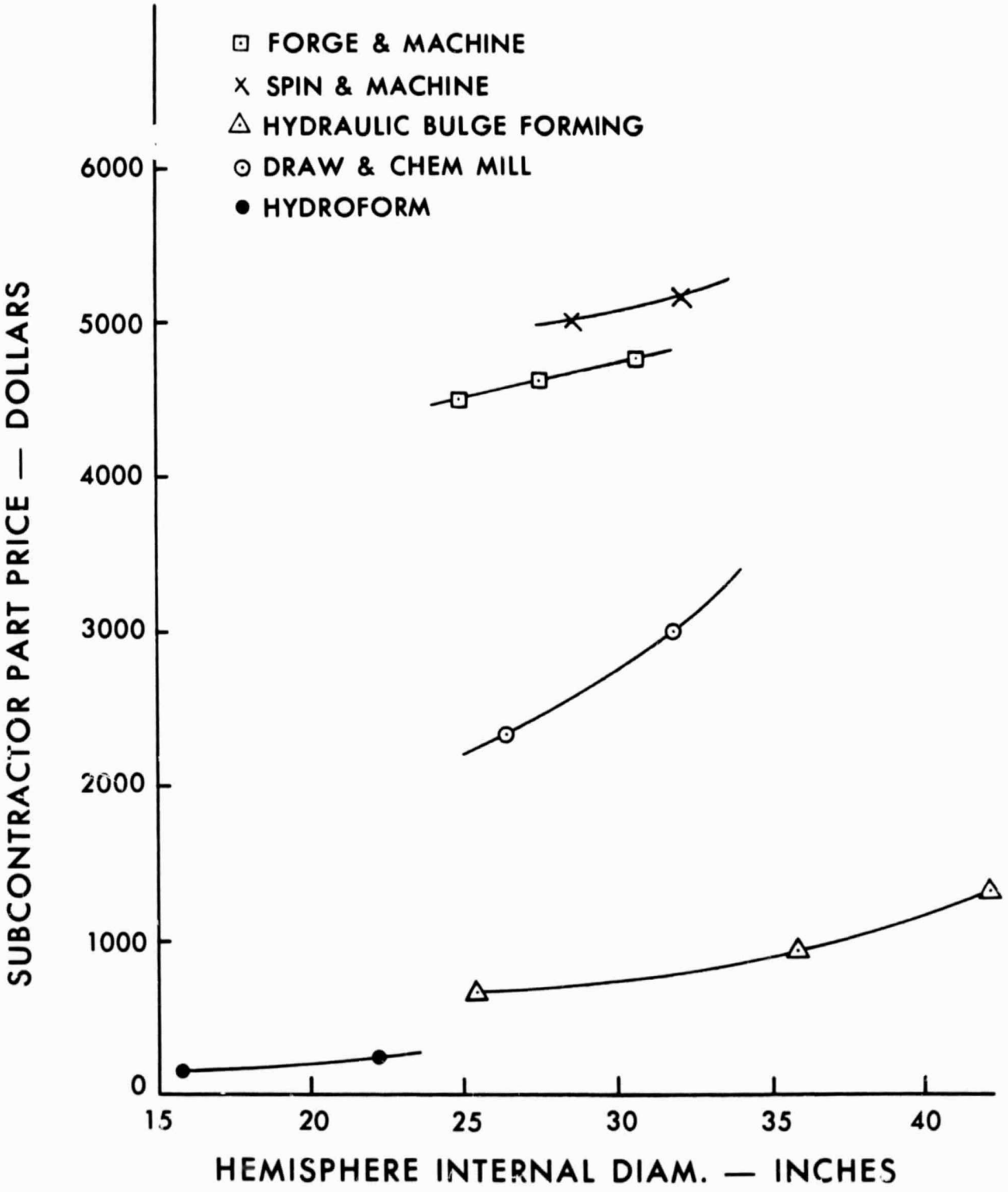
Figures 3.2-11 and 3.2-12 present comparative estimates of basic pressure vessel tooling and fabrication costs for several fabrication procedures.

Table 3.2-1 is a generalized summary rating of the hemisphere survey program.



SUBCONTRACTOR TOOLING COST
FIG. 3.2-1

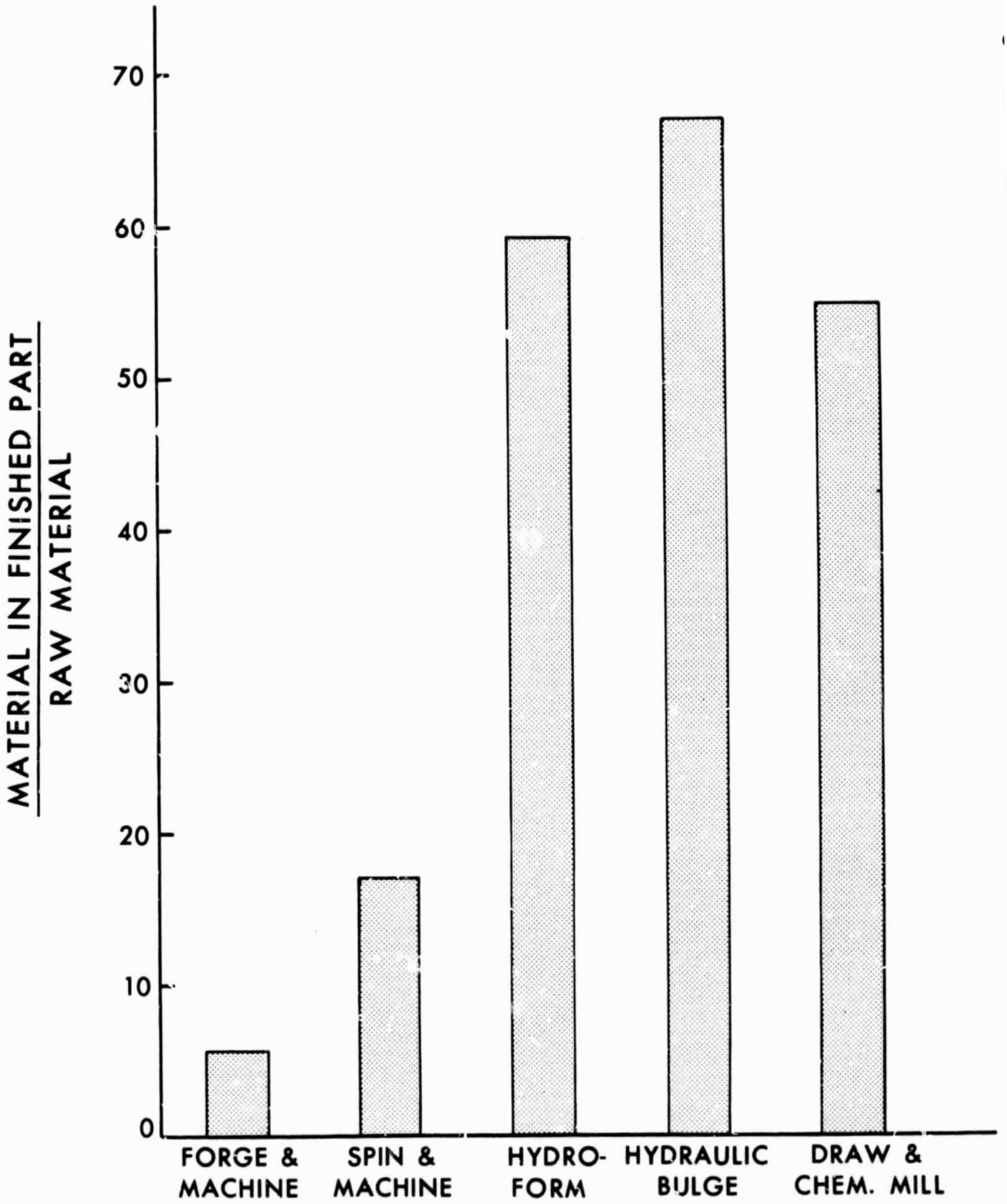
A-3873-67-209



SUBCONTRACTOR PART COST

A-3873-67-210

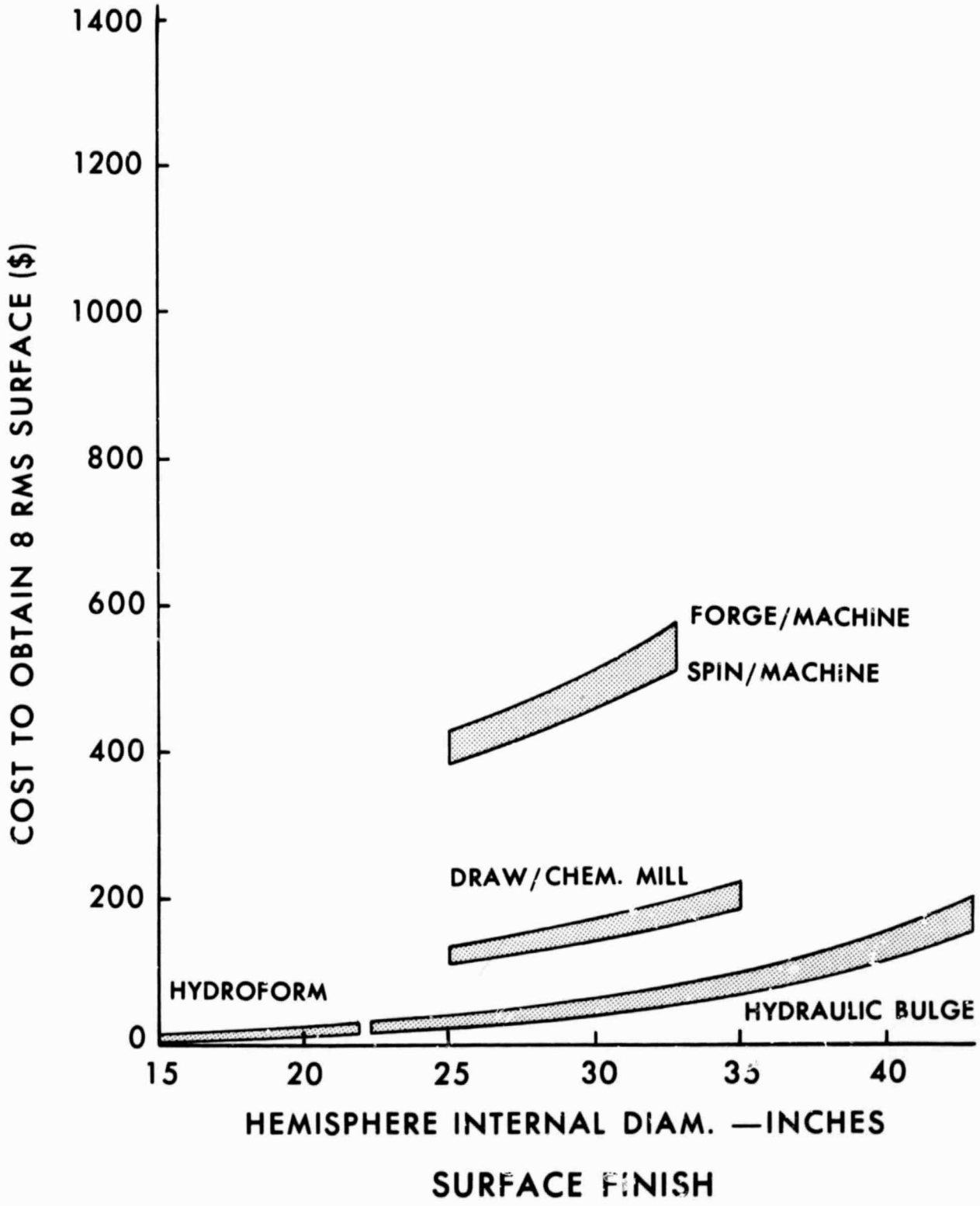
FIG. 3.2-2



MATERIAL CONSERVATION

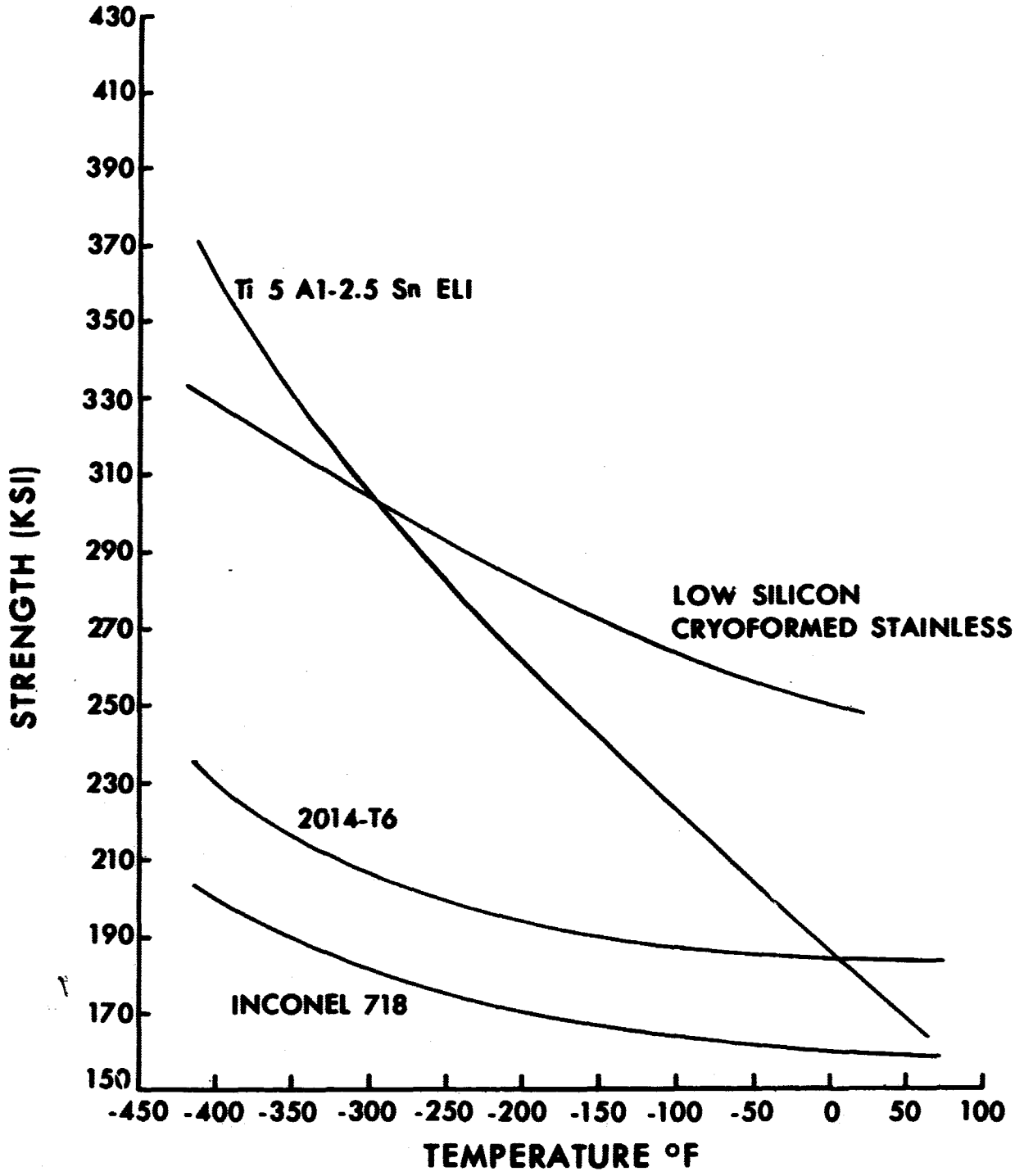
A-3873-67-211

FIG. 3.2-3



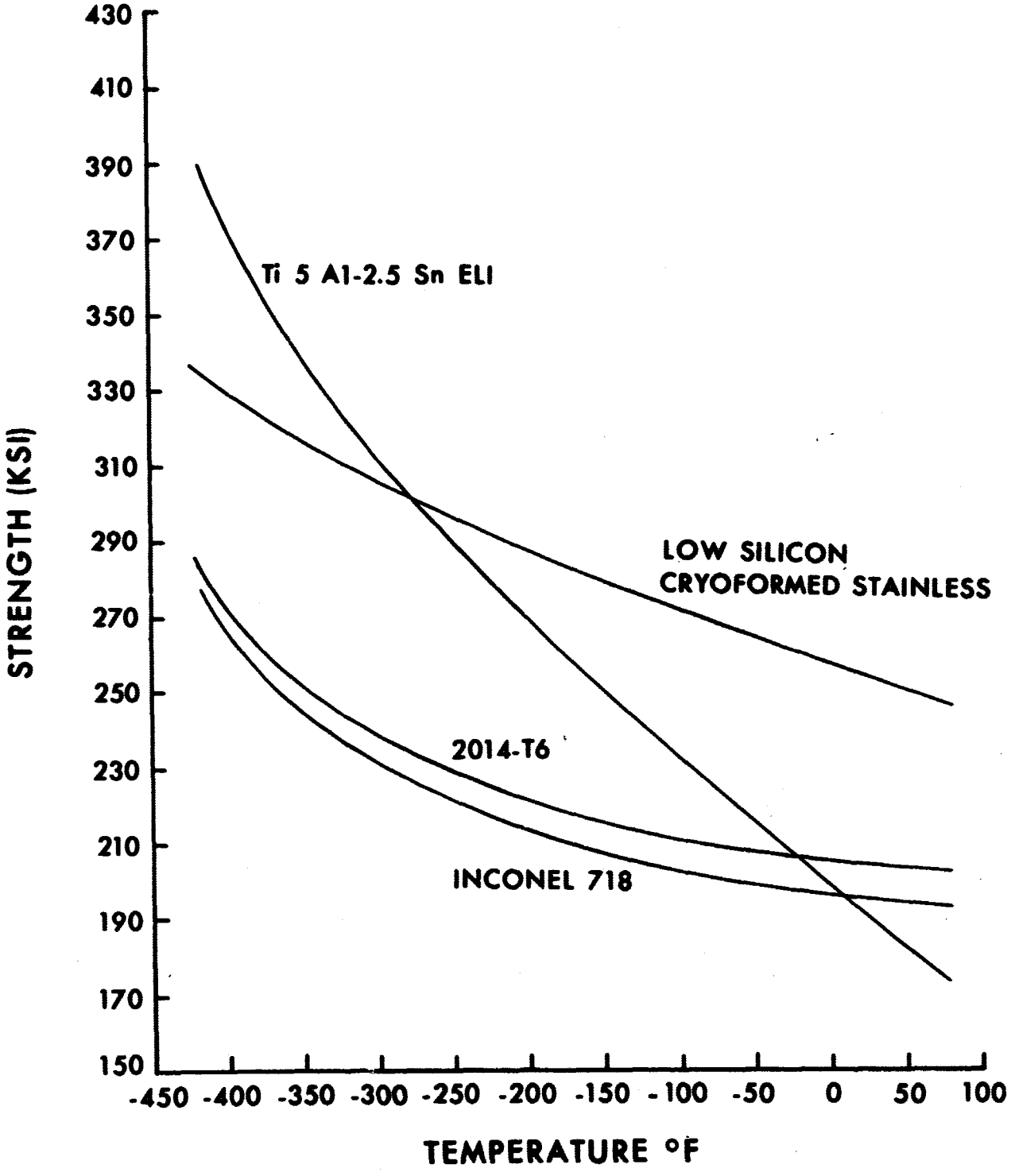
A-3873-67-212

FIG. 3.2-4



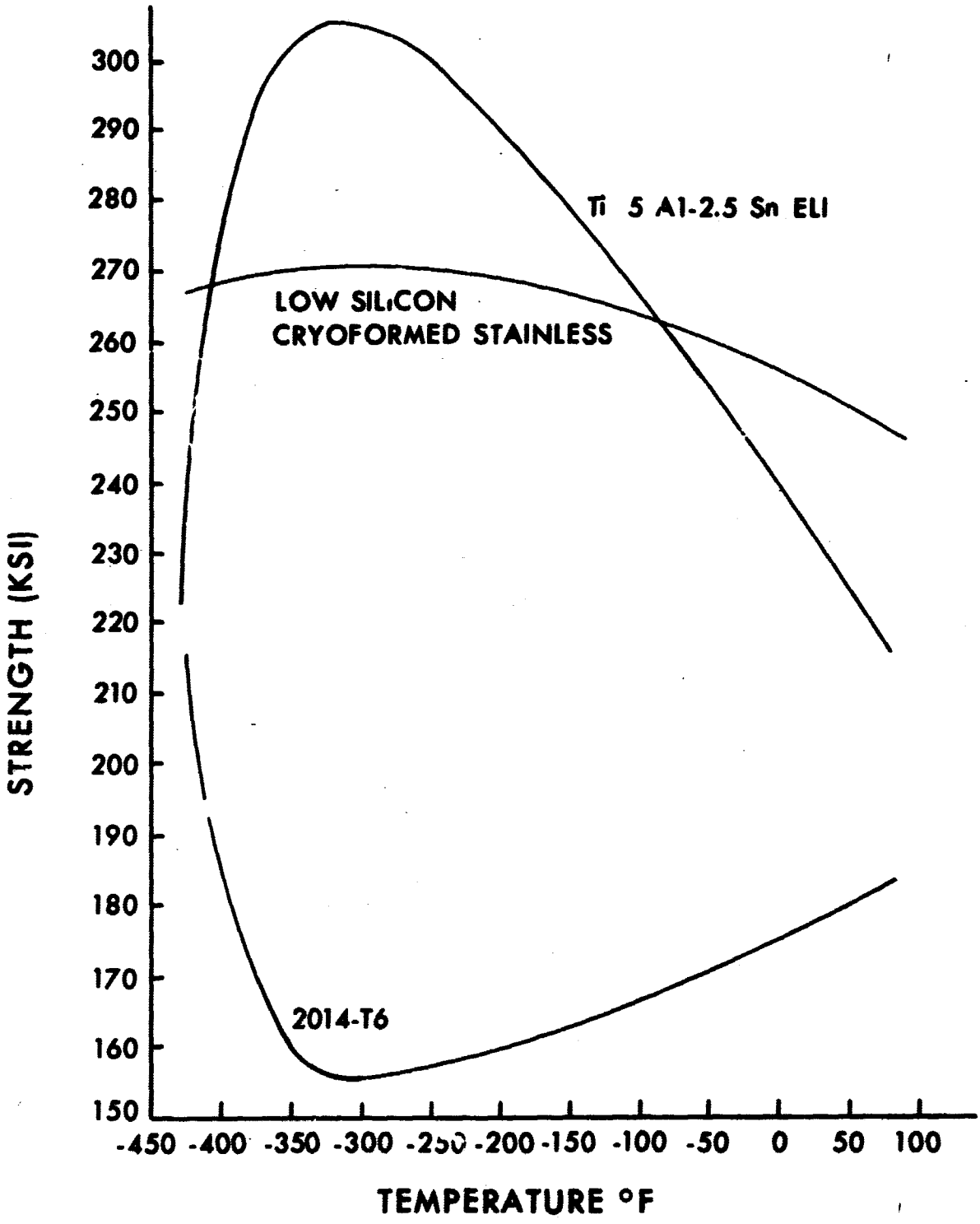
.2% YIELD STRENGTH EQUIVALENT TO STEEL

FIG. 3.2-5 A-3873-67-213



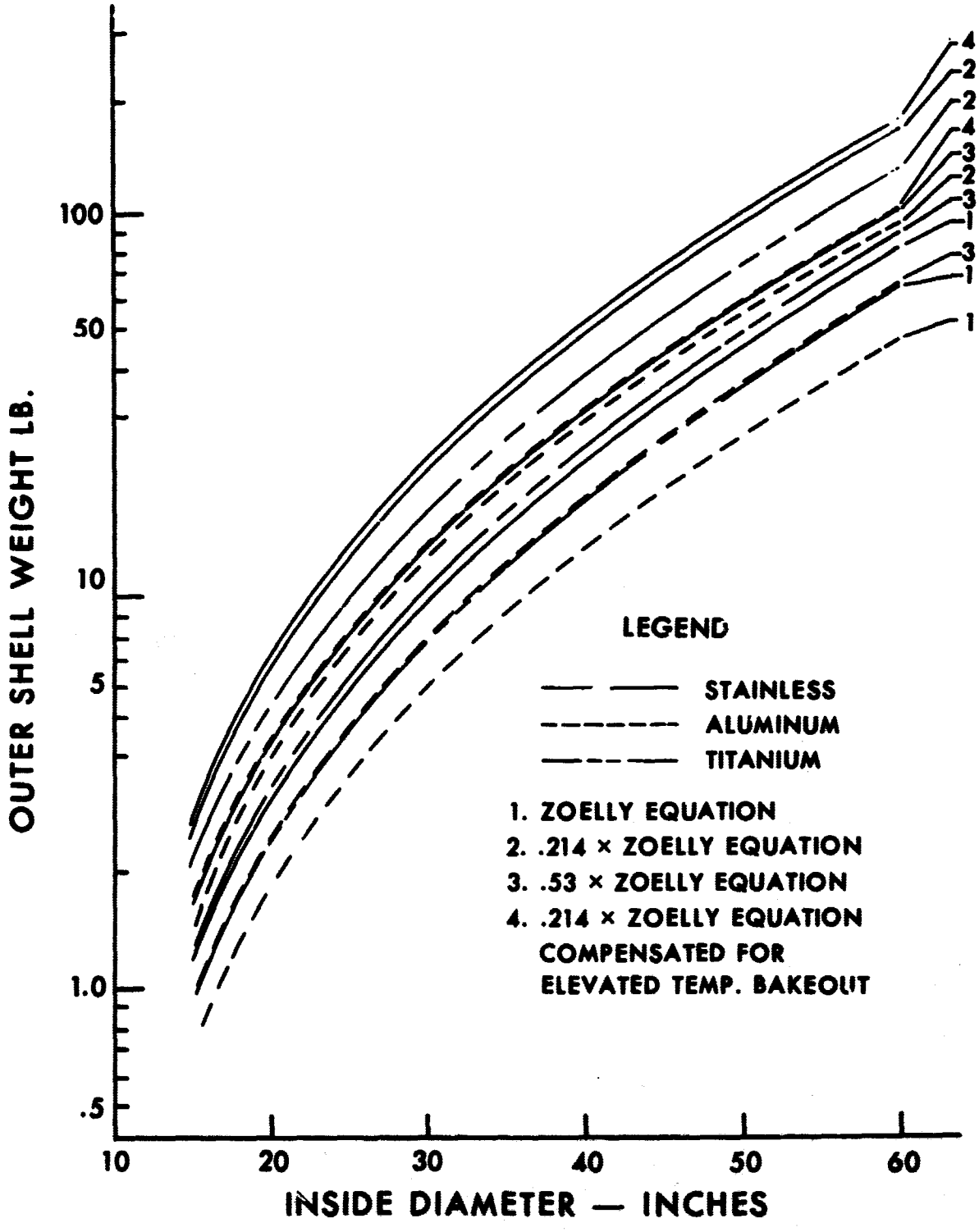
ULTIMATE TENSILE STRENGTH EQUIVALENT TO STEEL

FIG. 3.2-6 A-3873-67-214



NOTCH TENSILE STRENGTH EQUIVALENT TO STEEL

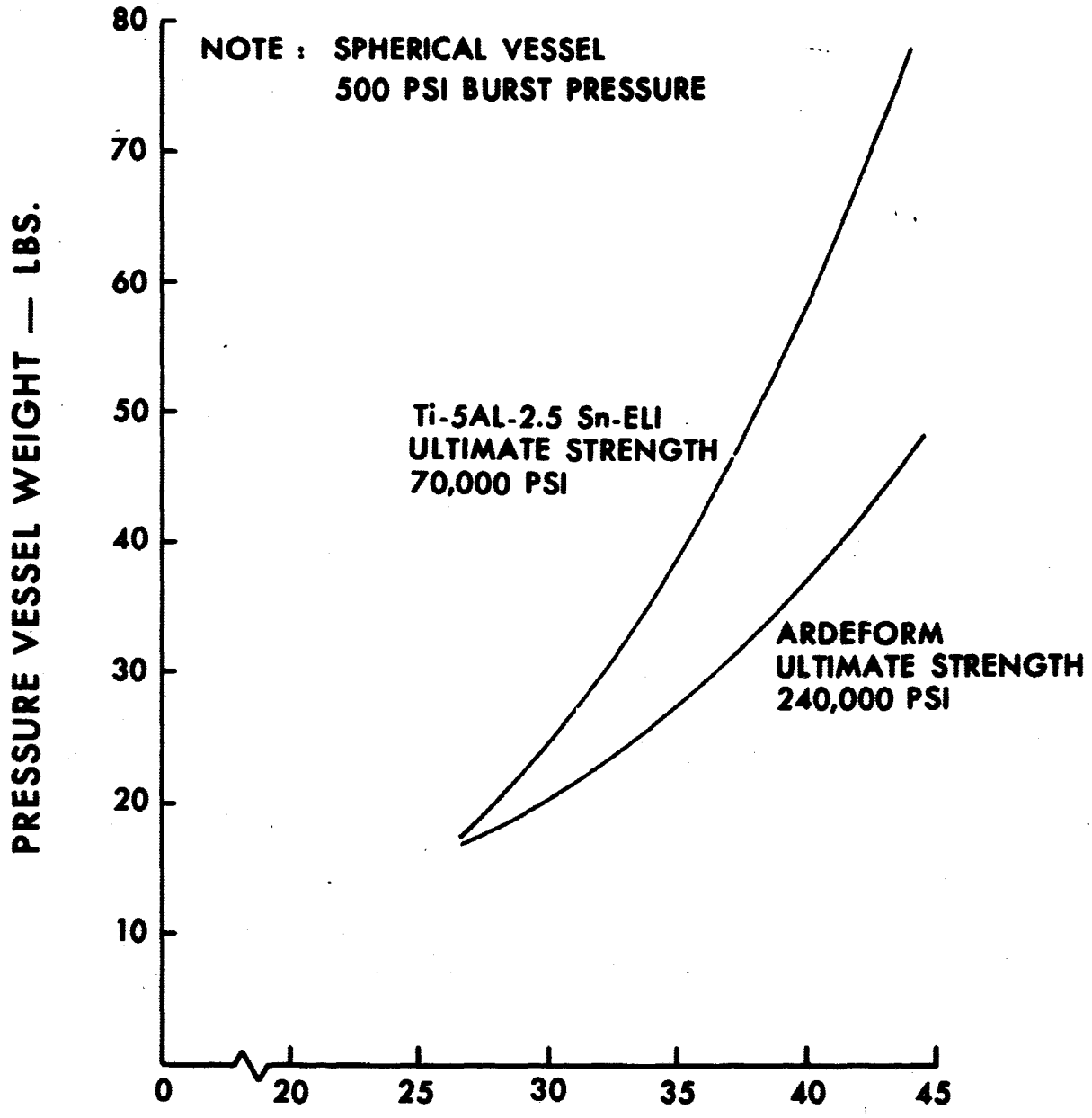
FIG. 3.2-7 A-3873-67-215



OUTER VESSEL WEIGHT
WEIGHT VS. DIAMETER
ΔP = 20.0 PSI

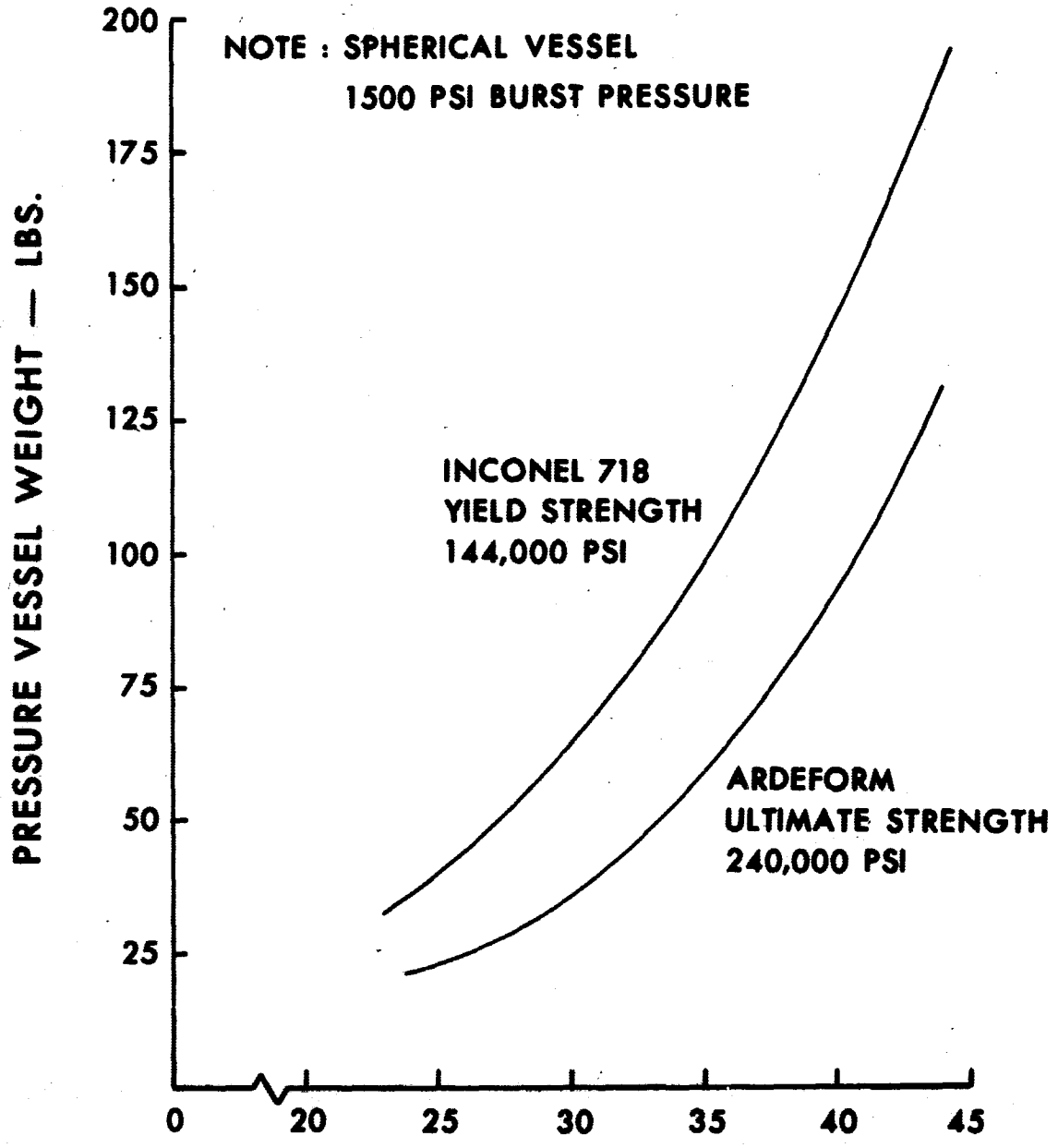
A-3873-67-216

FIG. 3.2-8



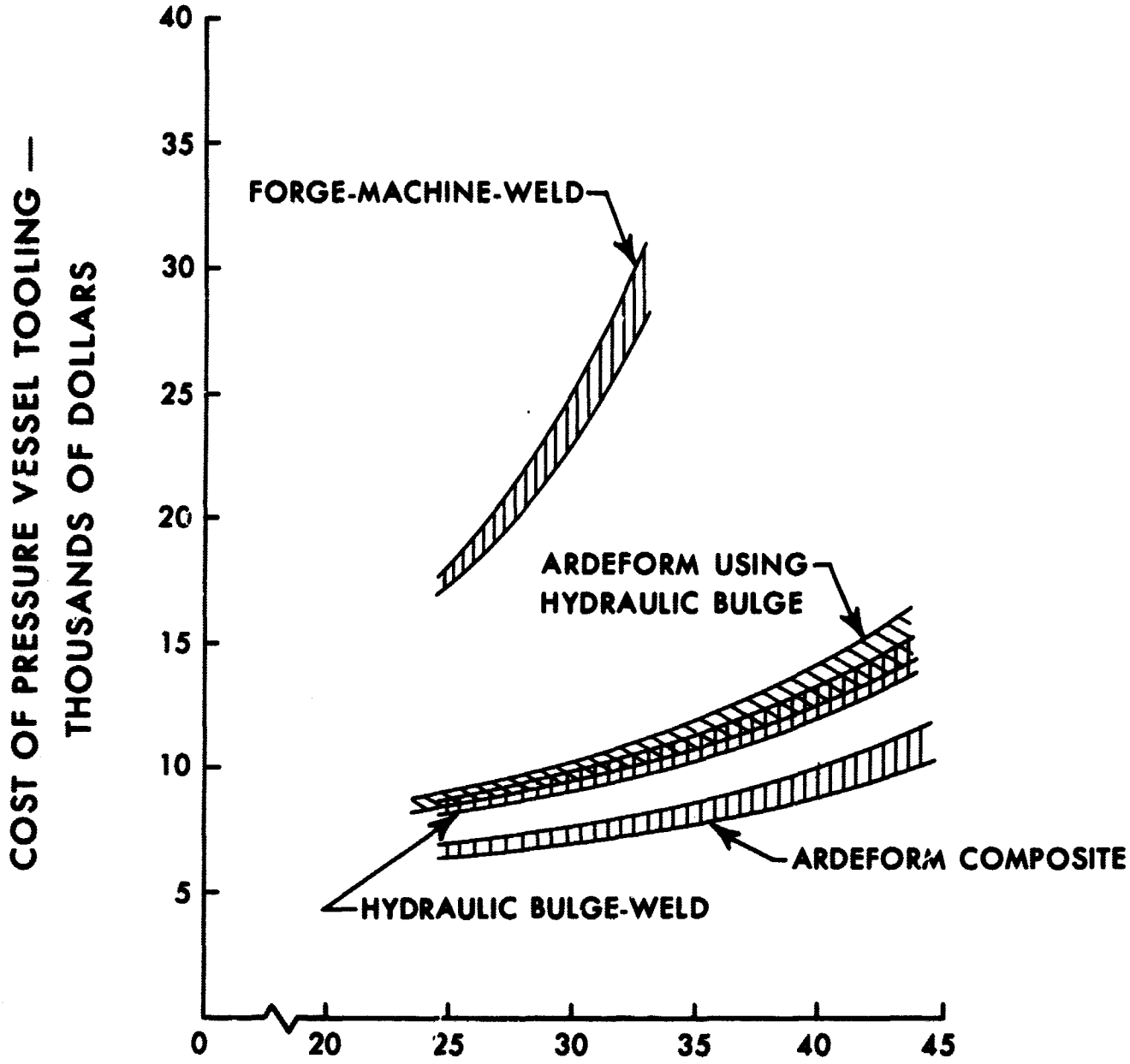
PRESSURE VESSEL WEIGHT AS A FUNCTION OF INSIDE DIAMETER

FIG. 3.2-9 A-3873-67-217



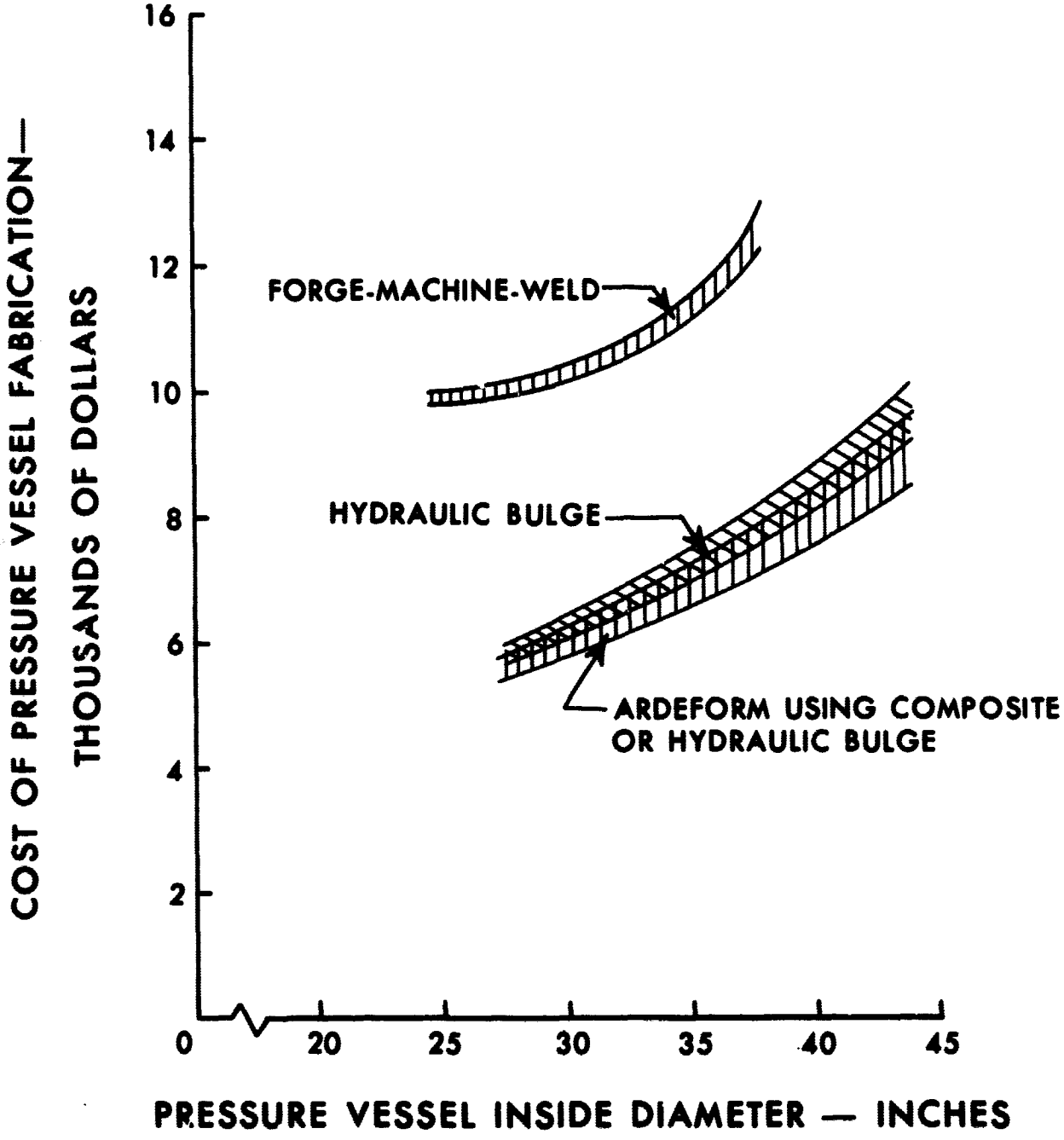
PRESSURE VESSEL WEIGHT AS A FUNCTION OF INSIDE DIAMETER

FIG. 3.2-10 **A-3873-67-218**



PRESSURE VESSEL TOOLING COST AS A FUNCTION OF INSIDE DIAMETER

FIG. 3.2-11 **A-3873-67-219**



PRESSURE VESSEL FABRICATION COST AS A FUNCTION OF INSIDE DIAMETER

FIG. 3.2-12 **A-3873-67-220**

TABLE 3.2-1

SURVEY SUMMARY

	SIZE	TOOL COST	PART COST	MATERIAL CONSERVATION	MATERIAL SELECTION	SURFACE FINISH	WALL THICK UNIFORMITY	SPHERICITY UNIFORMITY	VACUUM INTEGRITY	EQUIP. AVAIL.	REDESIGN TIME
FORGE/ MACHINE	2	3	3	3	1	3	2	1	3	1	2
SPIN MACHINE	1	3	3	3	2*	3	2	1	3	2	2
HYDRAULIC BULGE FORM	1	2	2	1	2*	1	2	2	1	3	1
DRAW & CHEM MILL	2	3	3	2	2*	2	1	2	2	2	3
HYDROFORM	3	1	1	1.5	2*	1	2	2	1	3	2

1. EXCELLENT
2. GOOD
3. POOR

* Need Development to fabricate Titanium Alloys.

Bendix Instruments & Life Support Division



Fig. 3.2-13
OUTER SHELL HEMISPHERE

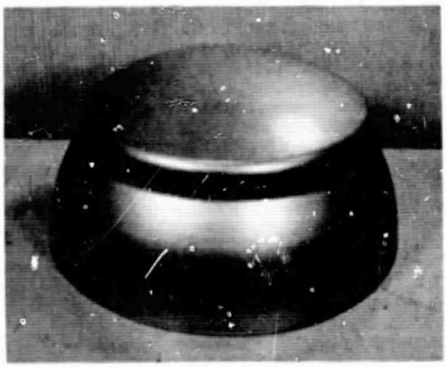


Fig. 3.2-14
OUTER SHELL HEMISPHERE

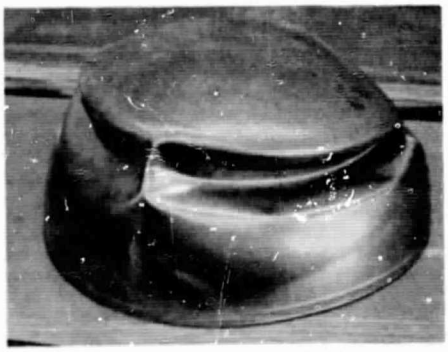


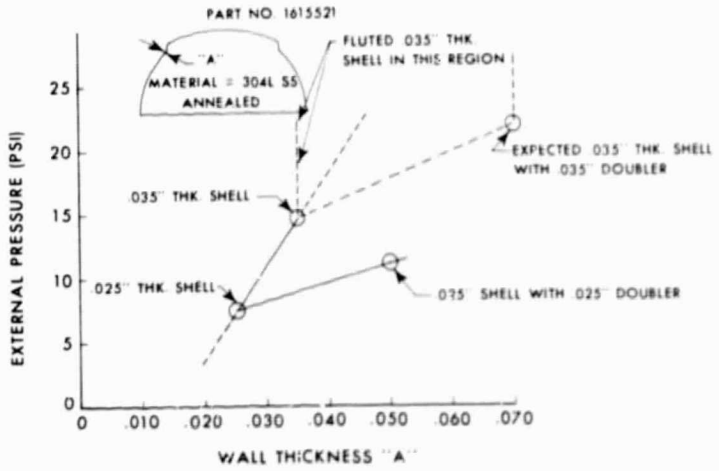
Fig. 3.2-15
BUCKLED HEMISPHERE

3.2.2 Outer Shell Tests

The outer shell configuration is extremely difficult to analyze in terms of external pressure loading and buckling characteristics. This problem was realized as a result of design and test work performed on production tank shells for aircraft equipment and on larger hemispheres (see Appendix A). Four different 304L stainless steel outer vessel shells were procured for the Phase A program. Figures 3.2-13 and 3.2.-14 show the two outer vessel shapes obtained. The buckling problem occurs at the tunnel sections, i.e., at the sections deviating from the true spherical shape. Brief analyses of the spherical and cylindrical sections of the outer shell shown in Figure 3.2-14 are presented in Appendix B. The top relatively flat section was analyzed as a Belleville washer and as a flat plate. No suitable analysis for buckling at the intersection of the cylindrical and spherical sections was available.

Shells with wall thicknesses of 0.020" and 0.0303" minimum were specified for each shape; due to material availability the wall thicknesses become a nominal 0.025" and 0.037" for each of the two shapes.

Figure 3.2-15 shows a 0.035" wall outer shell of the configuration in Figure 3.2-14. Buckling occurred at 14.7 psi differential, (shell evacuated) after standing at this condition for a short period of time. The buckling pressure was approximately 10 psi lower than expected. Subsequently an 0.025" wall outer shell of the same configuration was evacuated and buckled at 7.5 psi differential. A plot through these two points (see Figure 3.2-16) indicated that the wall thickness



BUCKLING TESTS—PHASE A 22" DIA. OUTER SHELL

A-3873-67-202 FIG. 3.2-16

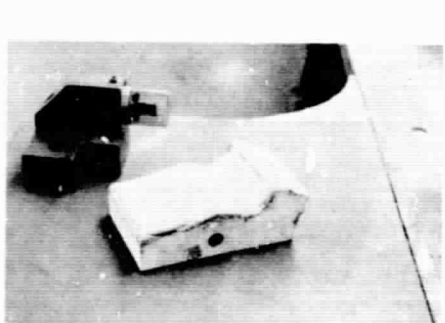


Fig. 3.2-17
TOOLING FOR FLUTES



Fig. 3.2-18
FLUTED OUTER SHELL

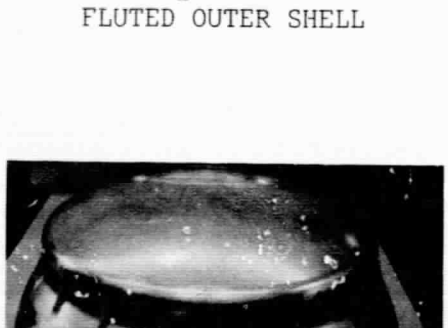


Fig. 3.2-19
FLUTED OUTER SHELL
WITH DOUBLER

at the cylindrical-spherical radius intersection would have to be approximately 0.045" thick for a safety factor of 1.5, i.e., for a buckling pressure of 22.1 psid. As a result of this, a 0.025" thick doubler section was welded into a 0.025" shell giving a total thickne in the immediate area of 0.050". Upon evacuation, the shell buckled at 11 psi, an increase of about 50% of the original buckling load. Results of this test indicated that the addition of a 0.035" thick doubler band to the inner surface of a 0.035" shell would give the required 1.5 safety factor to the outer shell (see Figure 3.2-16). This solution, however, is not entirely satisfactory in that it results in a fairly large and tight trapping area for chemical contamination in the vacuum void.

To strengthen the outer shell, but to eliminate contaminant trapping, it was decided to form fluted gussets in the shells at the tunnel area. A number of tooling modifications were required to obtain flutes which blended well in the compound curves. The final tooling utilized is shown in Figure 3.2-17.

A 0.035" outer shell of the type shown in Figure 3.2-14 was modified to result in a configuration similar to that of Figure 3.2-18. No buckling occurred after a sustained evacuation of 14.7 psi differential; no evidence of deformation or movement was noted. The same outer shell was then heated to 330°F during evacuation, and buckled at 14.7 psi differential.

The final outer shell modification consisted of welding a 0.035" thicker doubler section into the fluted 0.035" shell. This configuration is shown in Figure 3.2-19 and 3.2-20. No buckling occurred with this configuration when tested at 330°F and a 14.7 psi differential.

To determine the wall thickness uniformity of the hydroformed outer shells, a 0.035" thick outer shell was sectioned and measured. The original sheet thickness was approximately 0.037"; total wall thickness variation was found to be 0.003" with the minimum thickness of 0.035" occurring at the intersection of the tube tunnel cylindrical section with the middle spherical section. The wall thickness variation was within 10% of the original material thickness as originally discussed with the fabricator. Figure 3.2-21 shows the dimensional layout of the sectioned outer shell.

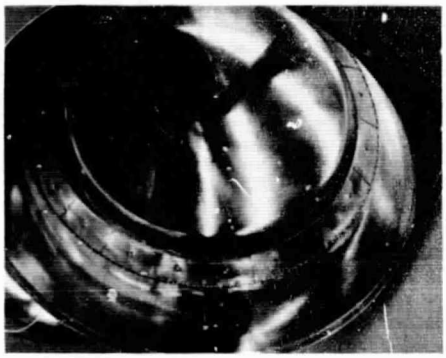


Fig. 3.2-20
INTERNAL VIEW OF DOUBLER

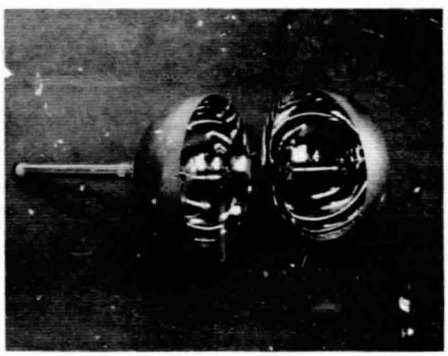


Fig. 3.2-22
TEST CALORIMETER OUTER SHELL

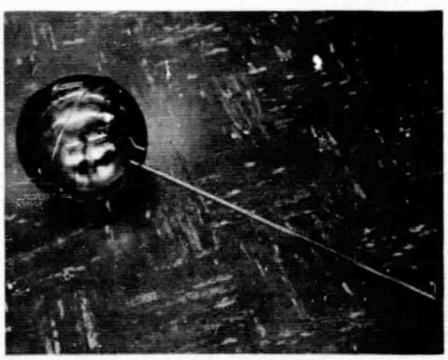
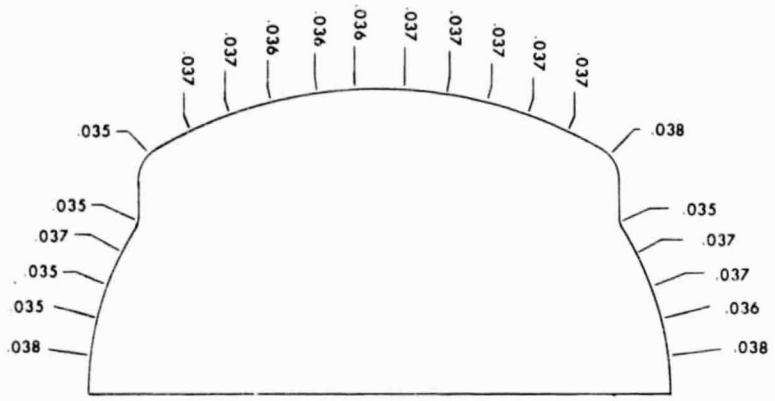


Fig. 3.2-23
TEST CALORIMETER
INNER VESSEL



WALL THICKNESS—PHASE A 22" DIA. OUTER SHELL

FIG. 3.2-21 A-3873-67-201

3.2.3 Bumper Tests

Thermal evaluation of the segmented radial bumper design was performed utilizing a test dewar calorimeter. The purpose of this testing program was to determine quantitatively the effective conductive heat transfer of Phase A bumper assemblies.

Figures 3.2-22, 3.2-23, and 3.2-24 show the test dewar and test set-up used in the test program. The test dewar consists of a 10.8" diameter inner vessel suspended by a 20" long x 1/2" diameter neck tube in a 15.4" diameter outer vessel which also has an 18" long x 1.6" diameter neck tube vacuum jacket. The unit has an ionization gauge attached to the top outer shell for relatively accurate vacuum measurement. The vessel design is readily amenable to repeated assembly and disassembly for testing of various bumpers by separation of a girth seam soldered tear strip and one top neck tube solder joint. Evacuation of the annular space to less than 10^{-6} mm Hg is accomplished by a mechanical roughing pump and an ion pump.

A bellows assembly attached to the inner vessel neck tube permits the inner vessel to be raised and lowered with respect to the outer vessel. When raised, the inner vessel is not in contact with the bumpers. The inner vessel can be lowered onto the bumpers and spring loads can be added to the inner vessel, loading the bumpers to determine the effects of loads on bumper thermal conductivity. When the inner vessel is lifted free of the bumpers, the heat input, as measured by the quantity of the cryogen boiling off, can be attributed primarily



Fig. 3.2-24
TEST CALORIMETER

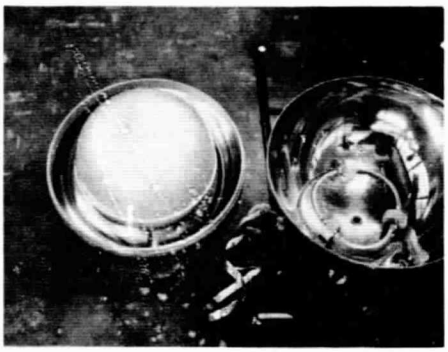


Fig. 3.2-25
TEST CALORIMETER
BUMPER ARRANGEMENT

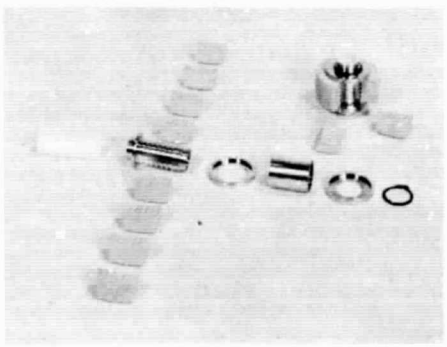


Fig. 3.2-26
PHASE A SEGMENTED BUMPERS

to radiation and conduction through the neck tube. When lowered so that the inner vessel rests on the bumpers, the heat input is due to radiation, neck tube conduction, and bumper conduction. Bumper conduction can, therefore, be isolated by determining the difference of the two heat inputs. Figure 3.2-25 shows the test arrangement for the bumper tests in the bottom of the calorimeter. Figure 3.2-26 shows the Phase A segmented bumper assembly; one disassembled bumper is displayed in exploded view and one is shown with two segments removed. Each bumper has 8 glass-filled teflon segments. The outer diameters of the bumpers (after bakeout) ranged from 1.770-1.774 inches.

Tests #1 and #2 were performed to determine the effect of the vacuum-bakeout process on the conductivity of the bumpers. In test #1 the three bumpers were "as machined" and not baked out. As such, the bumper segments and components were all tight fitting which contributed to a high thermal conductivity value. The bumper conductivity in this test was 0.54 Btu/hr for each bumper.

Test #2 was performed on bumper assemblies which had been heat treated to simulate the condition of the bumpers after bakeout. During the bakeout process, the teflon components expand more than the metal components, and as a result, the bumper segments loosen. The segment spacing therefore contributes more as a barrier to heat flow, reducing heat transfer between the outer shell and the inner vessel. Dimensional variations of the bumper assemblies used in this test are given in the following table. The assemblies were heated in air for 5 hours at 520°F, followed by oven cooling. Prior to heating, the components were all tight fitting. After heating the Teflon sleeve would slide freely; the segments and segment retainer rings could be moved, but not freely.

TABLE 3.2-2
EFFECT OF BAKEOUT ON BUMPER DIMENSIONS

BUMPER ASS'Y	O.D. BEFORE HEATING IN.	O.D. AFTER HEATING IN.
1	1.755 - 1.757	1.772 - 1.774
2	1.753 - 1.755	1.771 - 1.773
3	1.752 - 1.753	1.770 - 1.773

The results of Test #2 indicated a conductivity of 0.49 Btu/hr for each bumper. A net reduction in conductivity of 0.05 Btu/hr was thus observed due to the vacuum bakeout process.

A laminated wrapped metal core is shown in Figure 3.2-26. The boundary between successive laminations acts as a barrier to conduction heat transfer. The purpose of Test #3 was to determine the effectiveness of this configuration. To do this, the wrapped laminar core was replaced with a three-segment teflon core. The results of Test #3 showed a conductivity of 0.55 Btu/hr for each bumper, a net increase of 0.06 Btu/hr over the results of Test #2. It thus appeared that the heat transfer was effectively minimized in the wrapped laminar core.

Test #4 was performed to determine the heat transferred from the axial tube to the periphery of the bumper assembly or vice versa. To accomplish this, brackets were attached to the tube at each segmented bumper assembly. These brackets were longer than the radius of the bumpers, hence the bumpers did not contact the outer shell. Heat transfer, therefore, followed a path from the outer shell, through the bracket to the tube, through the tube to the center of the inner sleeve of the bumper (the center of the tapered sleeve being the only part of the bumper assembly in contact with the tube) and through the bumper assembly to the inner vessel. Thermal conductivity was found to be 0.74 Btu/hr for each modified bumper assembly.

The first four bumper thermal conductivity tests were performed on 8-segment glass-filled teflon bumpers, O.D. = 1.770 - 1.774 inches (after bakeout). Test #5 was performed on non-segmented Kel-F bumpers, O.D. = 1.124 - 1.126 inches. These bumpers had no core; rather, the tube passing through contacted the bumper hole.

Kel-F has a lower coefficient of thermal conductivity than does glass-filled teflon. However, because of its lower melting point, Kel-F cannot withstand the high bakeout temperatures used with glass-filled teflon; bakeout temperatures are limited to 300°F. The purpose of this test was, therefore, to determine the effectiveness of Kel-F as bumper material for future vessels.

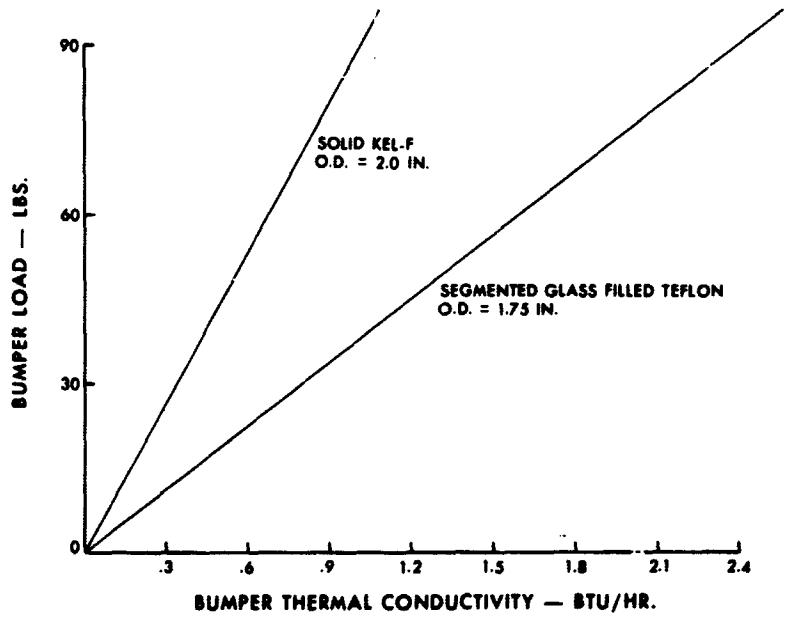
Results of Test #5 showed a thermal conductivity of 0.23 Btu/hr for each solid Kel-F bumper.

Test #6 also employed Kel-F as bumper material. The test bumpers were segmented, however, and had outer diameters of 2.005 - 2.010 inches. The average thermal conductivity for each bumper was found to be 0.20 Btu/hr.

Test #7 was performed on three eight-segment, glass-filled teflon bumpers with outer diameters of 1.138 - 1.143 inches. These bumpers employed eight segments, well insulated from the axial tube through low conductivity interfaces and laminar wrapped titanium core. Average thermal conductivity was 0.55 Btu/hr for each bumper.

Results of Phase A bumper thermal conductivity tests are presented in Table 3.2-3.

Figure 3.2-27 compares bumper conductivity vs bumper load for solid Kel-F bumpers as used in Test #6 and the segmented glass-filled teflon bumpers used in Tests #1 through #4. These curves were derived from data obtained in the bumper thermal evaluation test program.



BUMPER CONDUCTIVITY VS. LOAD ΔT = -297°F TO +75°F

FIG. 3.2-27 A-3873-67-222

TABLE 3.2-3

PHASE A BUMPER THERMAL CONDUCTIVITY
TESTING SUMMARY

TEST	BUMPER MATERIAL	BUMPER TYPE	BUMPER OD, IN.	PURPOSE	LOAD PER BUMPER, LB.	THERMAL CONDUCTIVITY PER BUMPER BTU/HR
1	Glass-Filled Teflon	8 Segment	1.752 / 1.757	Thermal Conductivity of "As Machined" Bumper Assembly	18.83	0.54
2	Glass-Filled Teflon	8 Segment	1.770 / 1.774	Thermal Conductivity of Heat-Treated Bumper Assembly	18.50	0.49
3	Glass-Filled Teflon	8 Segment	1.771 / 1.773	Effectiveness of 3-Segment Teflon Core	18.50	0.55
4	Glass-Filled Teflon	8 Segment	1.771 / 1.773	Thermal Conductivity Between Tube & Bumper Periphery	19.00	0.74
5	Kel-F	Solid	1.124 / 1.126	Thermal Conductivity of Non-Segmented Kel-F Bumper	19.90	0.23
6	Kel-F	8 Segment	2.005 / 2.010	Thermal Conductivity of Segmented Kel-F Bumper Assembly	18.61	0.20
7	Glass-Filled Teflon	8 Segment	1.138 / 1.143	Thermal Conductivity of Segmented Bumper Assembly	18.89	0.54

Bendix Instruments & Life Support Division

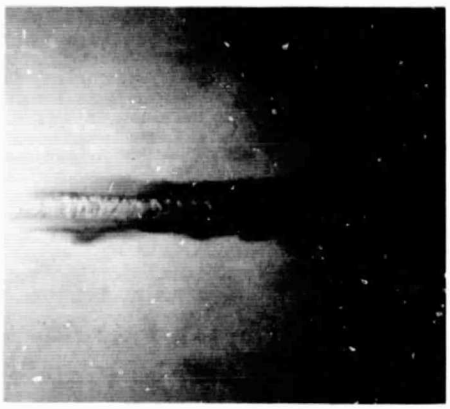


Fig. 3.2-28
PROOF PRESSURE VESSEL
GIRTH WELD

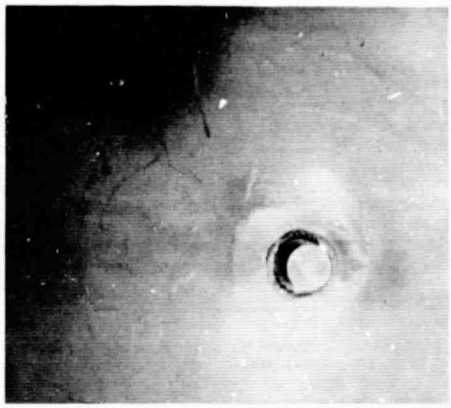


Fig. 3.2-29
PROOF PRESSURE VESSEL
FITTING WELD

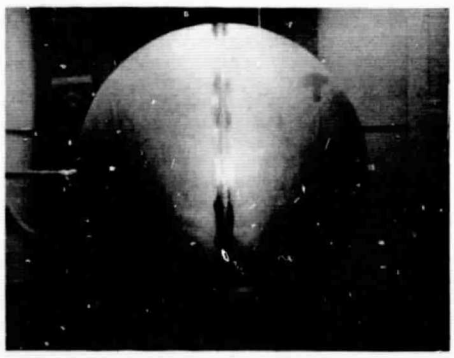


Fig. 3.2-30
PROOF PRESSURE VESSEL

3.2.4 Pressure Vessel Weld and Heat Treat Testing

The pressure vessel was fabricated from Inconel 718 for several reasons. Not only is this material more economical than a material such as titanium, but more knowledge and data are available concerning fabrication techniques. Inconel 718 is oxygen-compatible, it has adequate ductility over cryogenic temperatures, and it can be age-hardened for weight optimization. Finally, the material is readily formable by the hydroform process, which was used for fabrication of all Phase A shells.

Four hemispheres were procured for the program, two of which were used to fabricate an experimental pressure vessel for investigation of the girth and fitting welds and for proof pressure testing in the annealed condition. The experimental vessel was TIG welded, using a two-pass 45° bevel butt weld at the girth. The first pass was a parent metal weld, and the second pass was with Inconel 718 filler rod. The tank was fixtured in a horizontally rotating welding lathe; however, semi-automatic operation of the girth welding could not be controlled because minimum speed of the rotary head was too high. The welding was therefore done by hand with manual rotation. Radiographic inspection showed two spots of incomplete penetration, which were later repaired. Figure 3.2-28 shows the experimental vessel girth weld.

For the proof pressure testing on the experimental vessel, two fittings were TIG welded, one at each pole. A pressure type fitting design was used at one pole with a parent metal weld at the inner pressure flange (prior to girth welding) and a scarfed butt weld with filler rod at the external surface. The second fitting design and weld were similar to the first, with provisions in the second fitting for pressurization of the tank. Figure 3.2-29 shows one such fitting weld.

The completed experimental pressure vessel, shown in Figure 3.2-30, was proof tested in the annealed condition. Figure 3.2-31 shows the booster pump used for performing the hydrostatic PVE (Permanent Volumetric Expansion) tests. Flexible "Pi" measuring tape was used for determination of dimensional variations. PVE exceeded 10% for a test pressure of 1200 psig. At approximately 1300 psig, a minute crack developed in one of the fitting weld joints. A second fitting of the same design but using a 2-pass 30° bevel-butt weld joint at the outer joint region pressurized satisfactorily. This modified fitting design was subsequently used on the final vessel.

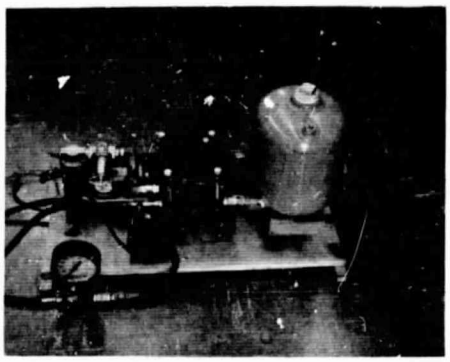


Fig. 3.2-31
PRESSURIZATION SYSTEM

It was apparent from the pressure testing performed on the annealed vessel that age hardening would be required to meet the proof pressure requirements of the final vessel with the vessel wall thickness used. The yield stress required after age hardening was determined from the following calculation:

$$\sigma = \frac{P \times S.F. \times D}{4t} = \frac{975 \times 1.5 \times 20.344}{4 \times 0.084} = 88,551$$

where P = relief valve pressure = 975 psig

S.F. = proof safety factor = 1.5

D = vessel inner diameter = 20.344 in.

t = vessel wall thickness = 0.084 in.

σ = required yield strength = 88,551 psi

Yield and tensile strength tests were performed on welded, heat treated .062" thick strips of Inconel 718, to determine the time-temperature requirements for developing a 90,000 psi yield strength in the vessel material. Table 3.2-4 summarizes the results of these tests.

TABLE 3.2-4

HEAT TREATED INCONEL 718

YIELD AND TENSILE STRENGTH TESTS

TEST NO.	TEMP. °F	TIME AT TEMP. HRS.	YIELD STRENGTH PSI	TENSILE STRENGTH PSI
1	AS-ANNEALED		54,500	117,400
2	1,000	24	70,100	108,800
3	1,100	24	101,800	126,900
4	1,200	24	130,000	152,800
5	1,000	36	76,500	115,000
6	1,050	36	88,100	114,000
7	1,100	36	102,400	131,800
8	1,200	36	134,900	164,000

Because the final Phase A pressure vessel contained an aluminum thermal conductor and quantity sensor, it was planned to age the vessel at a temperature below 1100°F. Aluminum specimens, simulating the thermal conductor and quantity sensor, were heated to 1050°F. and 1100°F; no marked deterioration of bend properties or surface was noted.

Based upon the Inconel and aluminum tests, it was concluded that an approximate 1075°F age for 36 hours in an argon atmosphere would develop an approximate 90,000 psi yield strength in the pressure vessel, with no effect on the aluminum thermal conductor.

3.2.5 Pressure Vessel Plating Tests

The experimental pressure vessel utilized for heat treating, weld, and pressure tests (see Section 3.2.4) was also used as a test plating vessel to determine what problems would exist in the plating process.

The electroplating step process was as follows, with water rinses between each step:

1. Alkaline electro-clean
2. 50% muriatic acid
3. Nickel strike - positive
4. Nickel strike - negative (plate)
5. Copper plate
6. Silver plate

Several problems in fixturing and obtaining proper current density were encountered. The principal problem was obtaining a high current density for the relatively inefficient nickel strike process and resulting poor adhesion.

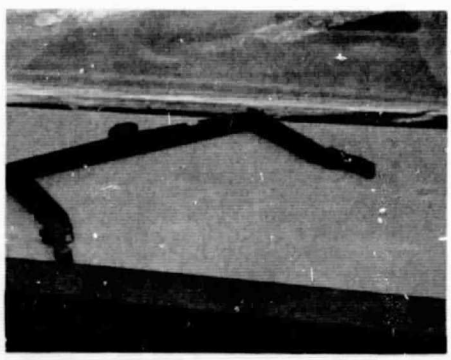


Fig. 3.2-32
INITIAL PLATING FIXTURE

Figure 3.2-32 shows the plating fixture used for the experimental plating tests. The vessel was supported at the fittings and current was delivered through the fittings. This resulted in inadequate electrical contact area to the vessel. In addition, the reversing switch at the nickel strike tank control panel had inadequate current capacity. As a result of the first plating exercise, the following changes were made:



Fig. 3.2-33
HANDLING CRADLE

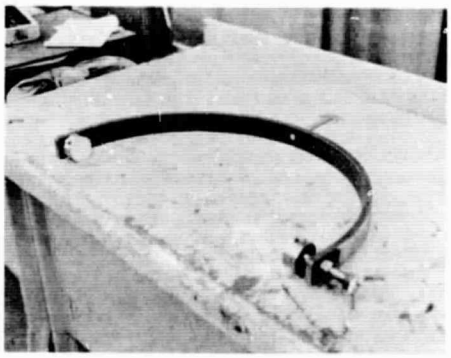


Fig. 3.2-34
FINAL PLATING FIXTURE



Fig. 3.2-35
PRESSURE VESSEL FITTING WELDS

1. A larger capacity reversing switch was obtained for the nickel strike tank and multiple cables installed.

2. A quick detachable handling cradle (cable construction) was fabricated for transporting the vessel between plating tanks (see Figure 3.2-33).

3. A spring type electrical contact fixture (Figure 3.2-34) with 1-1/2 in. diameter contoured copper contacts was fabricated. This fixture design was intended to permit the electrical contacts on the vessel surface to be rotated during plating for 100% plating coverage.

Concurrently, Inconel 718 samples were silver plated using various current densities and surface preparations to determine the optimum plating procedures.

3.2.6 Fabrication and Assembly

All hemispheres used in fabrication of the Phase A dewar were hydroformed by Jones Metal Products. These included the pressure vessel, radiation shield, and outer shell hemispheres. The hydroform process was selected because shells in the diameters (up to 22 in.), materials (Inconel 718, aluminum 6061, and stainless steel 304L), and wall thicknesses (.084 in. for Inconel 718 pressure vessel) required for the system could be rapidly, economically, and accurately produced by this process.

3.2.6.1 Pressure Vessel

Inconel 718 was selected as the pressure vessel material because (1) the material is readily and economically formable by the hydroform process, (2) it is oxygen compatible, (3) it has adequate ductility at cryogenic temperatures, and (4) it can be age-hardened for weight optimization. Tests performed on Inconel 718 samples and on an experimental pressure vessel identical to that employed in the Phase A dewar are described in Section 3.2.4. As a result of these tests, the time-temperature relationship for age-hardening the vessel to obtain an approximate 90,000 psi yield strength was determined to be 36 hours at approximately 1075°F.

Pre-assembly operations performed on the pressure vessel hemispheres consisted of piercing holes for the fluid and electrical lead fittings, fitting weld and leak check, and chamfering the girth for welding. The fluid vent and electrical lead fittings welded in the upper pressure vessel hemisphere are shown in Figure 3.2-35. A small locator was heli-arc welded to the inner surface

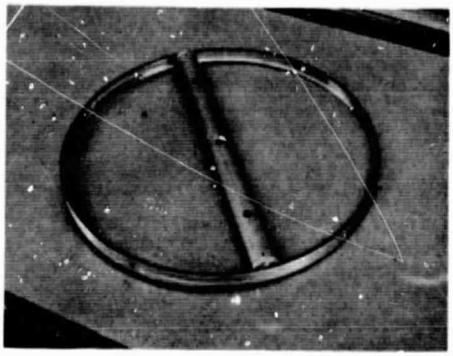


Fig. 3.2-36
INNER SUPPORT RING
AND QUANTITY PROBE

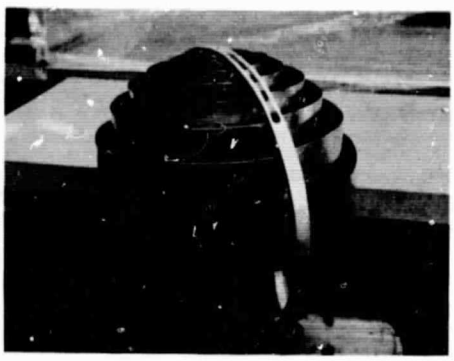


Fig. 3.2-37
SPIRAL THERMAL CONDUCTOR

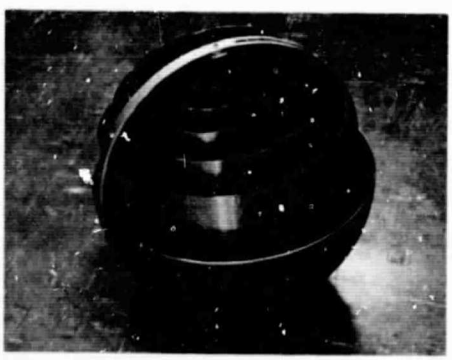


Fig. 3.2-38
INTERNAL ASSEMBLY

of the lower pressure vessel hemisphere to be used for positioning and securing the inner assembly support ring.

The static thermal conductor was originally intended to be fabricated from 0.012" - 0.015" thick aluminum; however, 0.025" thick aluminum was the thinnest (except for foil) that could be obtained in time for the program. Following the cutting and winding of the thermal conductor and mounting within the support ring, the inner assembly was mounted within the lower pressure vessel hemisphere. Figure 3.2-36 shows the internal mounting support ring with the capacitance probe assembly mounted in place. Figure 3.2-37 shows the complete internal assembly with the spiral thermal conductor. The internal assembly mounted in the lower inner vessel hemisphere is shown in Figure 3.2-38.

Following assembly of the pressure vessel hemispheres, with the inner assembly mounted, the pressure vessel girth weld was performed. Figure 3.2-39 shows the vessel in the welding lathe prior to the initial tack-weld. Figure 3.2-40 shows the final weld pass being performed. Helium mass spectrometer leak testing showed zero leakage at 10^{-8} atm - cc/sec. All inner vessel weld joints were 45° bevel-butt seams with one pass parent metal weld followed by one pass fill metal weld. X-ray examination of the welded pressure vessel showed a sound girth weld.

A hydrostatic pressure test was performed on the pressure vessel, prior to heat treating. Zero permanent volumetric expansion (PVE) resulted from pressurization to 850 psig. The pressure vessel was then age hardened by heating in an argon-atmosphere retort at 1050°F for 36 hours. The retort used is shown in Figure 3.2-41. The retort, with the pressure vessel inside and the lid secured by welding, was placed in a heat treating furnace. Argon was circulated in the retort during the aging process through fittings in the lid.

A hydrostatic PVE test was performed on the pressure vessel after aging. The material yield stress for the proof pressure of 1350 psi was calculated from the following:

$$\sigma = \frac{P \times D}{4 \times t} = \frac{1350 \times 20.344}{4 \times 0.085} = 80{,}800$$

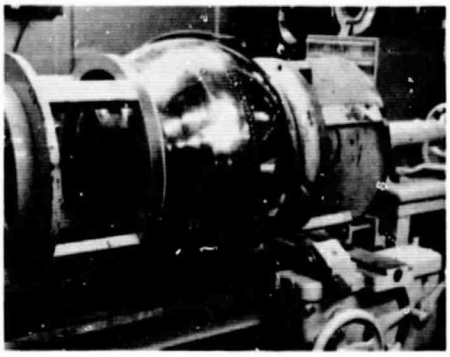


Fig. 3.2-39
PRESSURE VESSEL WELD SET-UP

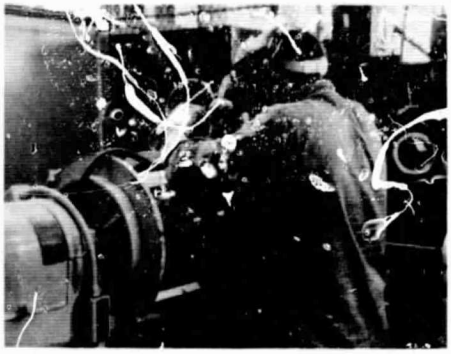


Fig. 3.2-40
PRESSURE VESSEL WELDING



Fig. 3.2-41
AGE HARDENING RETORT

where

P = proof pressure = 1350 psi

D = vessel inner diameter = 20.344 in.

t = vessel wall thickness = 0.085 in. (minimum)

σ = yield strength if yield occurred at given proof pressure = 80,800 psi

Flexible "pi" tape was utilized for determining diameter changes with pressure. The test results are presented in Table 3.2-5.

Total diameter increase was 0.027 in. at the proof pressure of 1350 psig. Total permanent stretch indicated was a negative 0.002 in., after increasing to proof pressure and decreasing to zero psig. The discrepancies in measurement were attributed to error in reading the "pi" tape as well as to temperature change in the vessel shell after filling with water (pressure medium). It was apparent from this test that since zero PVE resulted, the aging process of 1050°F for 36 hours raised the yield strength to a point above 80,800 psi. The results of testing Inconel 718 samples at various time-temperature relationships showed a yield strength of 88,100 psi for a similar 1050°F - 36 hour aging process (see Section 3.2.4, Table 3.2-4). It was felt that the Phase A pressure vessel aged yield strength was of similar magnitude.

TABLE 3.2-5

PVE TEST OF NAS 9-2978 PHASE A INCONEL 718 PRESSURE VESSEL AFTER AGE HARDENING

PRESSURE PSIG	VESSEL OUTER DIAMETER IN.
0	20.478
900	20.495
1000	20.498
1100	20.500
1140	20.501
1200	20.502
1260	20.503
1280	20.504
1300	20.504
1350	20.505
950	20.505
750	20.495
525	20.490
375	20.487
250	20.486
200	20.485
0	20.476

3.2.6.2 Radiation Shields

Aluminum 5052 was selected as the radiation shield material because of its light weight and ease of forming by the hydroform process.

Figure 3.2-42 shows one 21 in. I.D. inner radiation shield hemisphere. Wall thickness is 0.017 in. minimum. Figure 3.2-43 shows one 21.5 in. I.D. outer radiation shield hemisphere, with wall thickness of 0.017 in. minimum.

The inner shield assembly is shown in Figure 3.2-44. The contoured section in the bumper plane was originally intended to provide clearance for a chabazite absorbent container, shown in Figure 3.2-45. The container was basically a flat tube contour-formed to the inner vessel spherical configuration with silver soldered fine screen windows to allow for residual gas adsorption. The container was to be attached to the outer wall of the inner vessel at a position between two bumpers. Due to clearance problems encountered in pre-assembly fit-up, the container was removed and a barium getter attached to the outer shell wall was used instead. The final inner shield assembly did not contain the contoured section.

Figure 3.2-46 is a closeup view of the type fasteners used to secure the shield girth joints.

Figures 3.2-47 and 3.2-48 show the inner shield hemisphere bumpers and tube cut-outs and the shield patches used around the bumpers. Figure 3.2-49 shows the shield patches around the tube and electrical lead feed-through ports on the inner shield.

Figure 3.2-50 is an exterior view of an outer shield shell and shows the shield patches used around the bumpers. Figure 3.2-51 is an internal view of the same shell. Figure 3.2-52 shows the tube port shield brackets that are attached to the outer shield after shield assembly to the inner vessel.

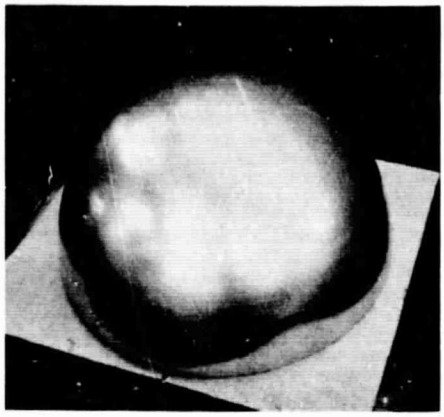


Fig. 3.2-42
INNER SHIELD HEMISPHERE

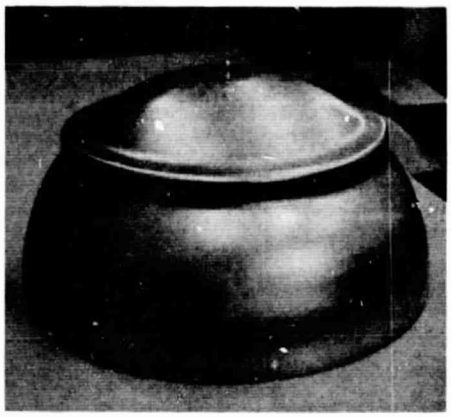


Fig. 3.2-43
OUTER SHIELD HEMISPHEROID

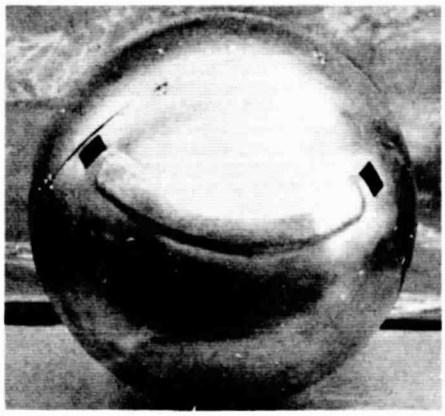


Fig. 3.2-44
INNER SHIELD ASSEMBLY

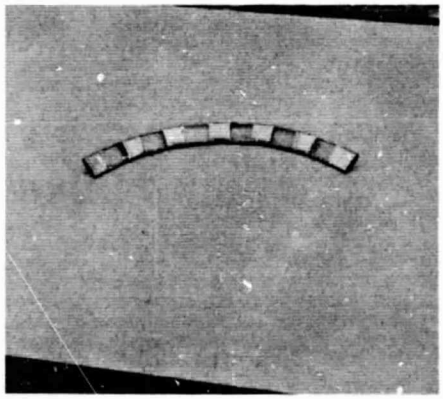


Fig. 3.2-45
ADSORBENT CONTAINER

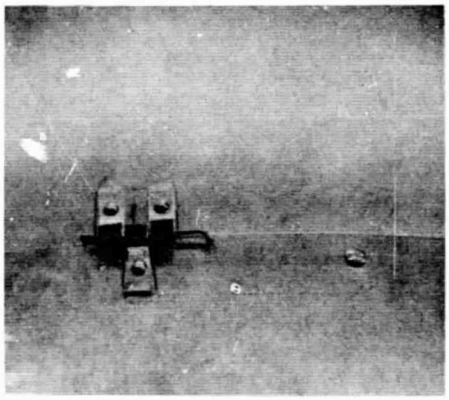


Fig. 3.2-46
SHIELD ASSEMBLY LATCH

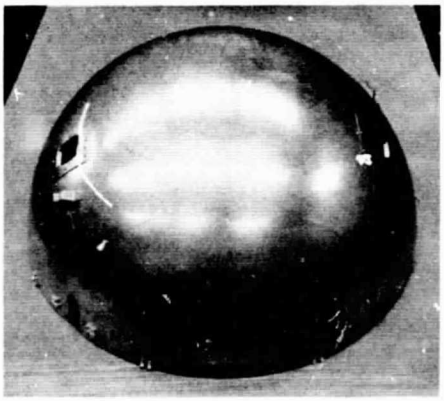


Fig. 3.2-47
INNER SHIELD HEMISPHERE

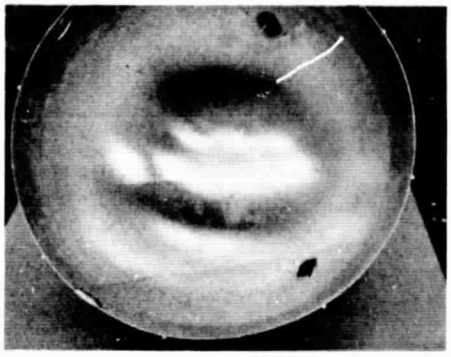


Fig. 3.2-48
INSIDE OF INNER
SHIELD HEMISPHERE



Fig. 3.2-49
FEED-THROUGH
SHIELD SEGMENTS

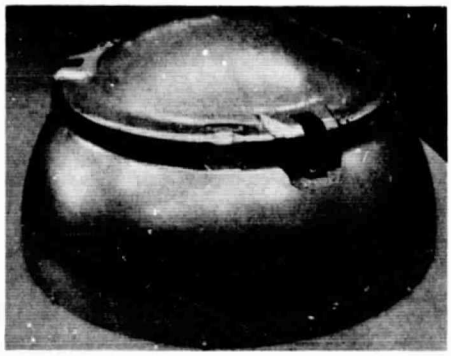


Fig. 3.2-50
OUTER SHIELD HEMISPHEROID

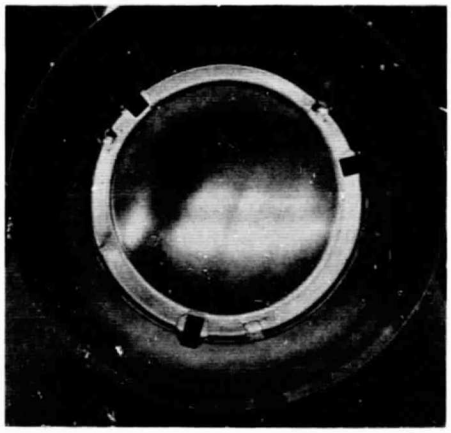


Fig. 3.2-51
INSIDE OF OUTER
SHIELD HEMISPHEROID

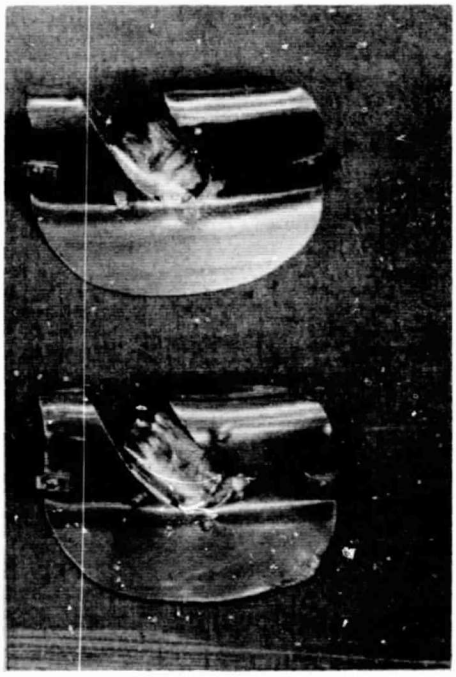


Fig. 3.2-52
FEED-THROUGH
SHIELD SEGMENTS

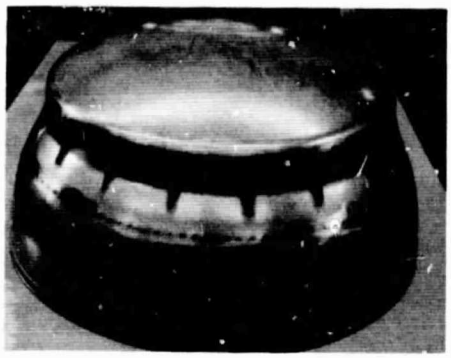


Fig. 3.2-53
FLUTED OUTER SHELL
WITH DOUBLER

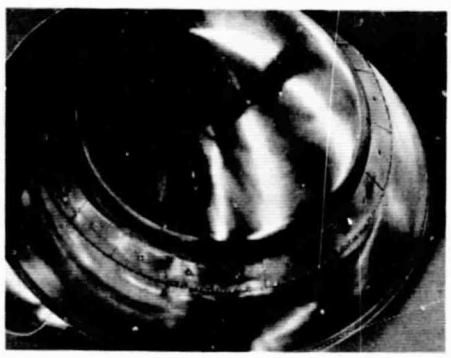


Fig. 3.2-54
INTERNAL VIEW OF DOUBLER

3.2.6.3 Outer Shell

The outer shell design was determined from the results of developmental buckling tests described in Section 3.2.2. Figure 3.2-53 is an external view of one outer shell which shows the flutes required to improve the tunnel region structure and also the weld marks from the doubler welded to the inner surface. Figure 3.2-54 is an internal view of the shell showing the welded doubler, required for further strengthening the shell in the tunnel region.

Stainless Steel 304L was selected as the outer shell material over aluminum because of the necessity for fabricating the dewar in a short period of time. Much experience was available in fabricating dewars with stainless steel vacuum jackets, whereas only limited experience had been obtained for aluminum outer shells. Use of stainless steel eliminated the need for stainless steel-aluminum transition joints for the fluid and electrical lead external fittings. Finally, the use of stainless steel did not offer a serious weight penalty.

3.2.6.4 Dewar Assembly

Upon completion of the pressure vessel, radiation shields, and outer shell subassemblies, pre-assembly fit-up was performed. Figures 3.2-55 through 3.2-66 show the fit-up sequence. Figure 3.2-55 is of the pressure vessel and shows the fluid ports and thermocouple lead. The fill and vent tubes are not yet located in their respective fluid fittings in this figure.

Figure 3.2-56 shows the two inner shield hemispheres partially assembled to the inner vessel.

Figure 3.2-57 shows the inner shield assembled to the inner vessel. Tube feed-through shield brackets, leads and bumpers are all in place.

Figure 3.2-58 is a top view of the inner shield assembly, showing the vent tubing and leads. The three inner shield support hangers are shown on the tubing, along with the three spools to be subsequently used for supporting the outer shield on the tube.

Figure 3.2-59 shows one outer shield shell in position on the inner shield-inner vessel subassembly.

Figure 3.2-60 is the opposite view of Figure 3.2-59.

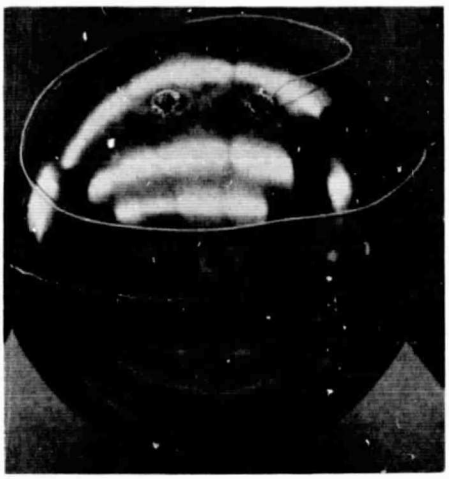


Fig. 3.2-55
PRESSURE VESSEL

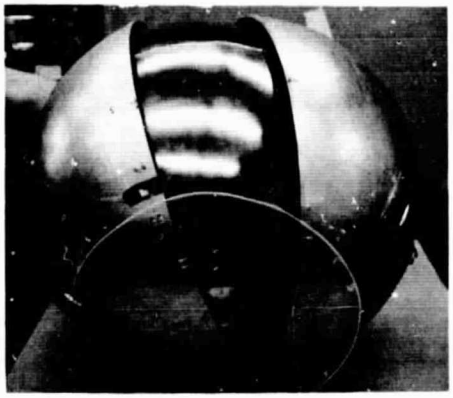


Fig. 3.2-56
INNER SHIELD ASSEMBLY

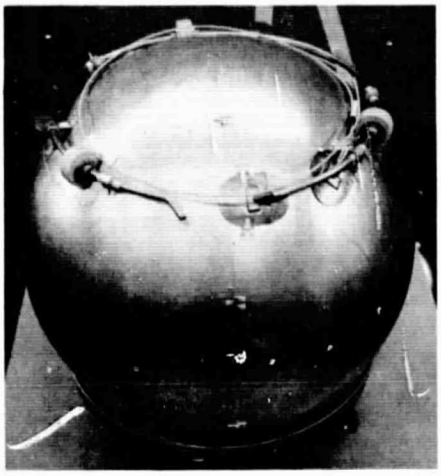


Fig. 3.2-57
INNER SHIELD ASSEMBLED

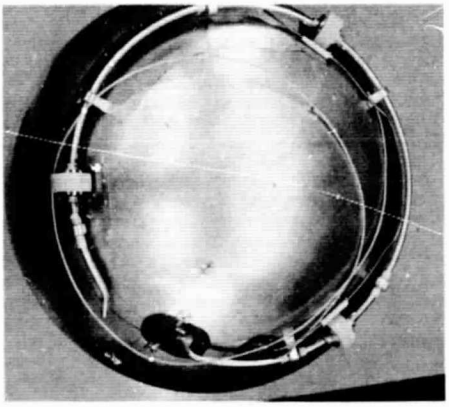


Fig. 3.2-58
FLUID PIGTAIL TUBING
AND BUMPERS

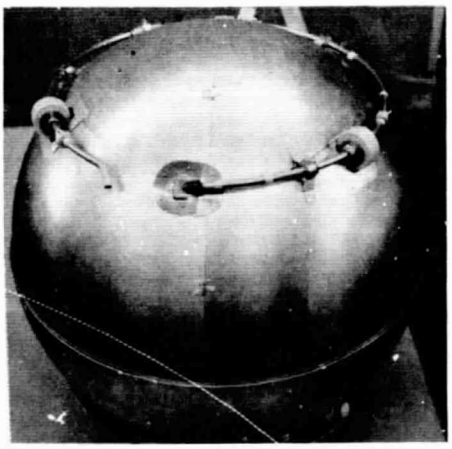


Fig. 3.2-59
OUTER SHIELD
PARTIALLY ASSEMBLED

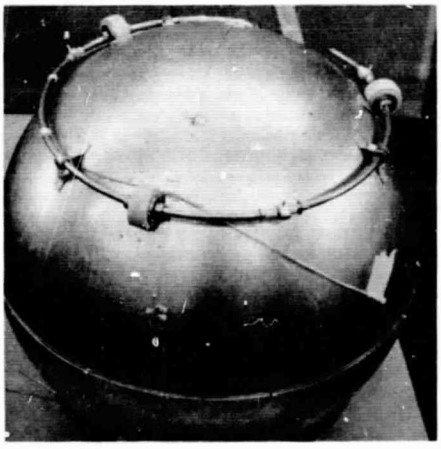


Fig. 3.2-60
OUTER SHIELD
PARTIALLY ASSEMBLED

Figure 3.2-61 shows the complete shield-inner vessel subassembly with both shields assembled and supported on the fluid fill and vent tubing. The outer fill and vent fittings can be seen at the ends of the tubes protruding through the outer shield.

Figure 3.2-62 shows the electrical leads protruding through the outer shield.

Figure 3.2-63 is a close-up view of the tube feed-through in the outer shield and the shield bracket that is assembled to cover the large tube feed-through hole following outer shield assembly.

Figure 3.2-64 is a top view of the outer shield assembly, with one outer shell assembled.

Figure 3.2-65 is a side view of Figure 3.2-64, again showing one outer shell assembled.

Figure 3.2-66 shows the tank unit with both outer shells assembled in place.

The shield hemisphere components and complete shield assemblies went very well in terms of design simplicity, assembly, and thermal-physical mounting characteristics up to the final fitup stage. The final stages of assembly involved fitup adjustment and electrical continuity testing to establish proper spacing to assure that distortion from vibration, thermal contraction, etc. did not cause heat shorting. This final fitup, adjustment and test phase was far more time consuming than planned. One of the major problem areas was contouring the inner shield to be properly spaced from the adsorbent container located on the inner vessel. As discussed previously, the adsorbent container was removed to prevent further program delay, and a barium getter was used on the outer tank wall instead.

Following final fitup, the unit was disassembled and all components were prepared for electroplating of all vacuum exposed surfaces.

The radiation shields were silver plated on all surfaces and plating quality was considered fairly good. The shield surfaces were "as formed", i.e., neither mechanically nor chemically polished. Only one set of shields was plated; no trial plating runs were performed. It was concluded that future shield plating should be accomplished on chemically polished surfaces. This

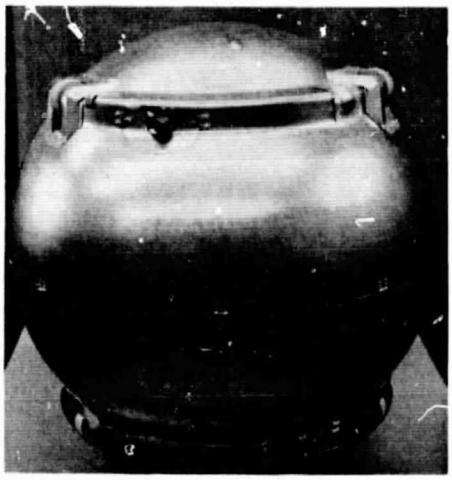


Fig. 3.2-61
OUTER SHIELD ASSEMBLED

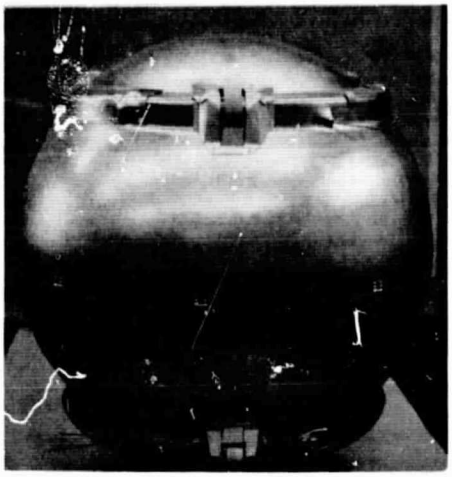


Fig. 3.2-62
OUTER SHIELD ASSEMBLED

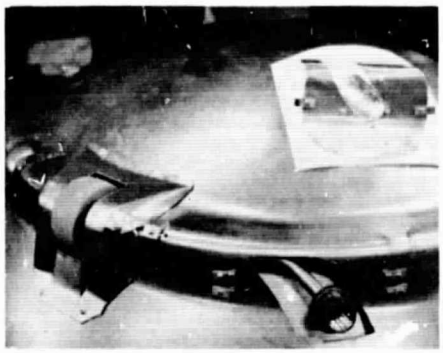


Fig. 3.2-63
FLUID TUBE FEED-THROUGH
AND SHIELD SEGMENT

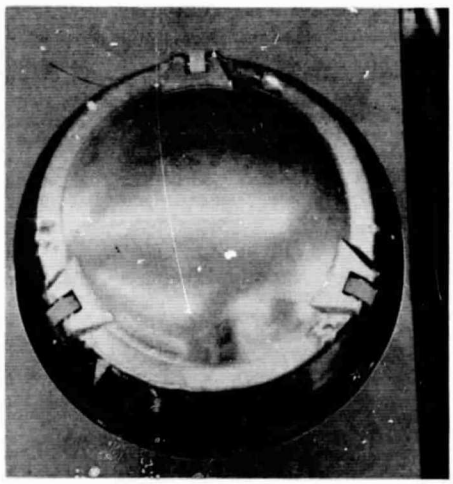


Fig. 3.2-64
TOP VIEW-ONE
OUTER SHELL ASSEMBLED



Fig. 3.2-65
ONE OUTER
SHELL ASSEMBLED

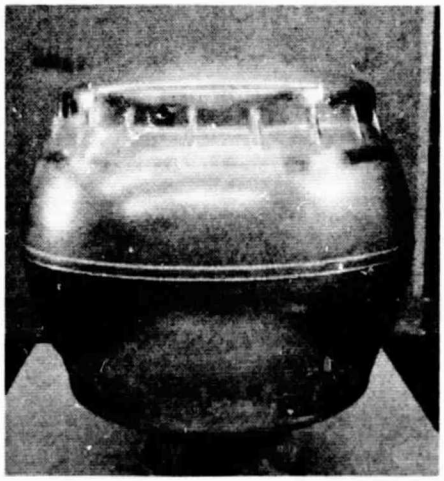


Fig. 3.2-66
DEWAR
ASSEMBLED

procedure was planned for the Phase B portion of the NAS 9-2978 program.

The silver plating quality of the inner vessel was considered fairly poor. The sliding contact fixture did not work as planned; two contact areas of about 2-1/2 in^2 each were not plated on the outer surface of the pressure vessel.

The outer shells were copper-plated on the inner surface. The plating quality was considered fairly good; however, the long assembly standby time prior to evacuation, described later, could have been detrimental to the plated surfaces.

A general summary of the plating quality, particularly in view of the excessive assembly handling and long assembly standby time, was that it was only a fair quality.

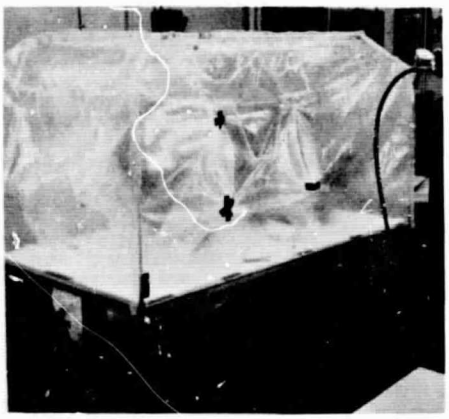


Fig. 3.2-67
ARGON ASSEMBLY BOOTH

Following the plating process all tank components were given the standard vacuum surface cleaning treatment which consisted primarily of the following steps: water-detergent wash; distilled water rinse; alcohol rinse; acetone rinse. The parts were then put in the constant flow-pressurized argon atmosphere assembly booth for the final assembly operation. Figure 3.2-67 shows the assembly booth used for Phase A assembly. Figure 3.2-68 shows the procedure by which the dewar was assembled when in the booth.

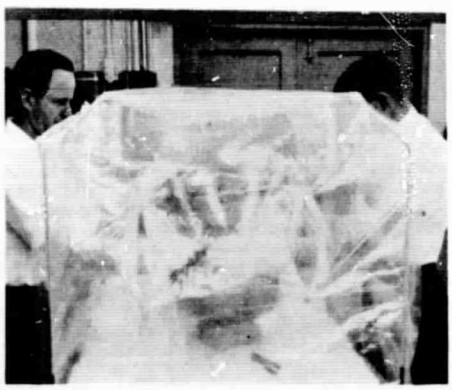


Fig. 3.2-68
ARGON ASSEMBLY BOOTH

Considerable difficulty was again experienced in the final assembly buildup for eliminating contact heat shorts to the extent that the final assembly was not completed until nine days after the outer shells were plated (ten days after pressure vessel and inner shield plating and eleven days after outer shield plating). This meant that the radiation surface components were at ambient pressure and temperature for 10 or 11 days prior to final weld and evacuation. Although the components were in an argon atmosphere over 80% of the time, the extensive handling due to the final assembly buildup and checkout problems and the excessive time prior to evacuation caused marked deterioration of the radiation surfaces. A 1957 program at Instruments & Life Support Division on approximately 2000 dewars clearly showed a deterioration of 1 to 1-1/2 Btu/hr on dewars with inner vessel areas of 1-1/2 to 2 square feet when final assembly occurred over 24 hours after plating, final cleaning and argon protection.

Following final assembly, the tank unit was sealed in an argon atmosphere bag and transported to the final heliarc welding area. This involved fixturing the unit and performing the outer girth weld, two external tube fitting welds, two external electrical feed-through fitting welds and four electrical lead feed-through silver braze joints. The external welding operation was performed in two hours and was completely satisfactory. The complete time from final assembly and removal from the argon assembly booth until the welded unit was placed on the helium mass spectrometer evacuation stand was four hours.

The initial evacuation of the vacuum void following welding resulted in less than 0.1 micron pressure in thirty minutes, which indicated no excessive leakage. Following further evacuation, the weld and silver braze joints were leak tested to prove zero leakage at 10^{-8} atm-cc/sec.

Prior to the evacuation-bakeout processing, two liquid oxygen dynamic heat leak tests were performed on the unit. These tests are described in Section 3.2.7.

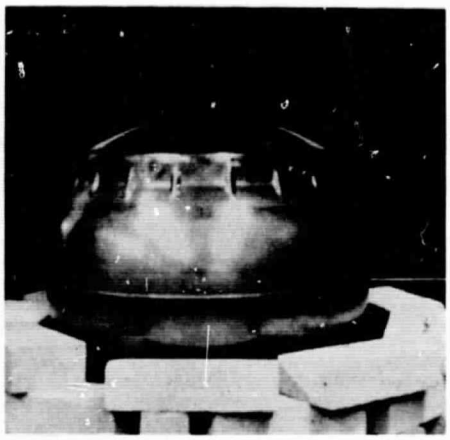


Fig. 3.2-69
DEWAR IN BAKEOUT OVEN

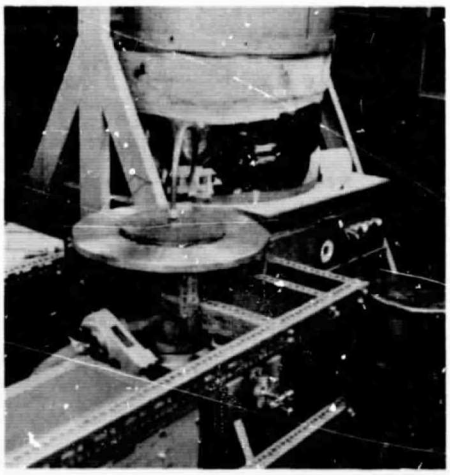


Fig. 3.2-70
EVACUATION-BAKEOUT SET-UP

Figure 3.2-69 shows the completed unit on the evacuation-bakeout stand, with the bakeout oven hood raised. Figure 3.2-70 shows the evacuation-bakeout process set-up, with the ion pump used for evacuation in the foreground. The heating system consisted of a calrod heater-blower system located separately from the bakeout oven, with hot air circulated through the oven. Thermocouples were attached at various locations on the tank unit surface. The vessel was evacuated to 1×10^{-6} torr at which time heat was gradually applied to the system at a controlled rate such that the outgassing rate did not raise the pressure in the vacuum void above 4×10^{-6} torr. Maximum temperature during this bakeout was controlled at 300°F. The unit was held at the maximum temperature for five days, at which time the vacuum pressure reached 1.05×10^{-6} torr. Following a slow cool-down to room temperature over a 32-hour period, the unit was "tipped off".

The evacuation tube on the unit was a 3/8" diameter oxygen-free copper tube silver brazed to the outer tank wall. Tip off sealing of the tube was performed with a hydraulic device that closes precision 5/16" diameter rollers, thus cold compression welding and sealing the evacuation tube. The tip off process is performed quite rapidly due to the operational characteristics of the tip off tool.

Following tip off, the tank was charged with liquid oxygen to determine vacuum integrity. Due to the excessive boil off observed, it was apparent that the void pressure was relatively high. It was suspected that a vacuum leak developed at the pinch-off joint. Therefore, the unit was prepared for re-evacuation and bakeout.

The pinch off operation of a vacuum tank is a critical operation and is treated as such. Pinch off failure occurs on a fraction of a percent of production units. This was the first apparent pinch-off failure of an Engineering development unit at Instruments & Life Support Division in over two years. The pinch-off performed is termed a cold weld pinch-off since heat is not applied. In the 1957-58 period, Bendix developed a hot pinch off technique. It is more time consuming and costly than the cold weld procedure because several high temperature outgassing steps are required at the pinch-off region. However, a more sound and reliable weld joint results. It was planned to perform a hot pinch-off on the unit after re-evacuation and bakeout.

The second re-evacuation and bakeout was performed at the same temperature and over an eight-day period, following which a hot pinch-off weld joint was made to seal off the vacuum space. The procedure consisted of heating the tube in the tip-off area several times a day prior to tip off to outgas the tube. At the time of tip off, the tube was again heated (to the 1350°F range) prior to the hydraulic compression.

Vacuum decay again occurred following the second pinch-off as evidenced by a gradual increase in liquid oxygen heat leak. No evidence of leakage was found when leak tested on the helium mass spectrometer.

It was then speculated that some rather large quantity of outgassing was occurring from some trapping area such as the laminated titanium foil wrapping in the segmented bumpers or in the interstices created by riveted brackets on the shields or the weld doubler on the outer vessel. It was suspected that the large area space between the weld doubler and the outer shell may not have been thoroughly rinsed of high vapor pressure trace contamination at final cleaning.

Although the unit had to be re-evacuated and baked out, the tank was put on a vacuum system to demonstrate dynamic heat leak to NASA-Houston personnel. Following the dynamic heat leak test, the unit was pinched off

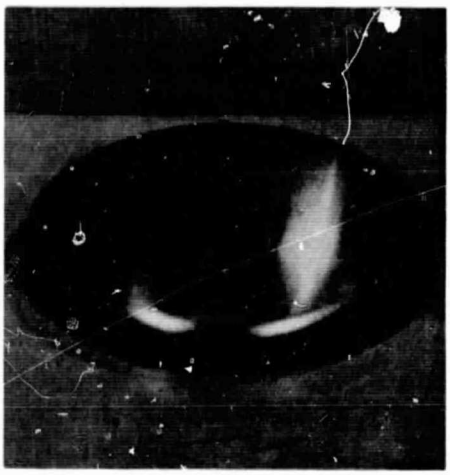


Fig. 3.2-71
MOUNTING RING FORM



Fig. 3.2-72
MOUNTING RINGS



Fig. 3.2-73
MOUNT FRAME

and a vibration search was performed in the presence of the NASA representative. These tests are described in Section 3.2.7.

Following the test demonstration, the unit was rigorously leak tested to re-establish the leak tight integrity of the vessel. Upon proving zero leakage at 10^{-8} atm-cc/sec, the unit was assembled on the evacuation stand with very short evacuation plumbing between the tank and the pump system. A long term re-evacuation-bakeout was performed to clean up residual outgassing in the annular space. Heat leak tests performed after pinch-off indicated a stable static vacuum.

The unit was placed on vented liquid oxygen heat leak testing for over two months following the third evacuation-bakeout and pinch off. Because the vented heat leak showed a gradual increase over the period, it was decided to re-evacuate the unit at a slightly higher temperature for complete removal of trapped gas from the outer shell doubler ring attachment. Prior to the evacuation-bakeout, a small ion pump was silver brazed to the evacuation tube for occasional pumping if the outgassing persisted. The unit was pinched off after a lengthy evacuation bakeout period of two weeks. Tests conducted on the unit throughout the remainder of the program indicated that the vacuum was indeed stable after this final thermal-vacuum processing.

3.2.6.5 Mounting Frame

The mounting frame, fabricated from aluminum 6061, consisted of two mounting rings and six support legs. Figure 3.2-71 shows one of the hydroformed mounting ring forms as received from Jones Metal Products. Figure 3.2-72 shows the upper and lower mounting rings after material removal and fluting to conform to the dewar outer shell configuration. The complete mounting frame assembly is shown in Figure 2.2-73, positioned through vibration isolators on the vibration fixture utilized in tests described in Section 3.2-7. The frame was assembled on the Phase A dewar such that the three support legs welded to the mounting ring in each half were centered at the bumper locations.

3.2.6.6 Weight Summary

The component and system weights resulting from the Phase A tankage program are summarized in Tables 3.2-6 and 3.2-7. Major weight variant components are discussed following the tables.

TABLE 3.2-6
PHASE A DEWAR WEIGHT REVIEW

COMPONENT	PROPOSED WEIGHT, LB.	ACTUAL WEIGHT, LB.	SUMMARY	ADJUSTED OBTAINABLE WEIGHT, LB.
Inner Shells	30.650	36.200	Closest available sheet stock .015" oversize	Min. 30.650
Outer Shells	8.750	17.200	Buckling problem increased all thickness.	Min. 13.040
Doublers	---	3.800	Added to overcome buckling problem	.----
Bumpers	1.376	1.398	20-25% wt. reduction possible by excess material removal	1.120
Tubes	.360	.450	Proposed estimate too low	0.450
Fittings	.250	.750	Proposed estimate too low	
Tubes Inner		(.300)		.300
Tubes Outer		(.200)		.200
Leads Inner		(.150)		.150
Leads Outer		(.100)		.100
Thermal Conductor	1.750	7.550	Not in contract; added for H. T. data	1.750
Quantity Sensor	.360	.700	Heavier sensor readily available; .360-lb can be obtained	.360
Getter		.090		.090
Blowout Disc	.150	.100	Disc Fitting ring wt. estimate low	.100
Mount Ring (internal)	.200	.500	Used heavier thermal conductor	.200
Shields	5.570	5.600	20-25% wt. reduction practical	
Inner		(2.700)		2.160
Outer		(2.900)		2.320
Thermocouple	.200	.050	Changed from PRT to thermocouple	.050
Probe Lead	---	.100		.100
Heater Lead	---	.130		.130
	49.616			53.270
+ 8% Mfg. Tol.	3.969		+ Max. .003" outer shell dia. variation	1.510
TOTAL	53.585	74.618	+ Max. .004" inner shell dia variation	1.570
			TOTAL	56.350
			Minimum with 8% mfg. tol. removed	52.088

TABLE 3.2-7

PHASE A EXTERNAL COMPONENTS WEIGHT REVIEW

COMPONENT	PROPOSED WEIGHT, LB.	ACTUAL WEIGHT, LB.	SUMMARY	ADJUSTED OBTAINABL WEIGHT, L
Mounting Frame	4.250	10.550	Frame considered	4.250
Rings		(3.600)	Over-designed; used	
Brackets		(3.300)	Al rather than Mg	
Vib. Mounts		(1.050)	Not estimated originally	1.050
Nuts, Bolts		(.300)		
Spacers		(1.200)	Not originally planned	
Gasket		(1.000)	Not originally planned	
Pads		(.100)	Not originally planned	
Fill Valve	.310	.100	Changed to Essex valve	.100
Vent Valve	.300	3.100	Changed to GSE Manual Valve (other available)	.300
Pressure Relief Valve	.380	.350		.350
Pressure Gage	---	.050	Added for test	---
Misc. Plumbing	.700	.700 est.		.700
Net Weight	5.940			
+ 8% mfg. tol.	.475			
TOTAL	6.41	14.850		6.850

The principle components representing the design concept investigated on the Phase A program are the segmented bumpers and discrete radiation shields. These components came within 1.6% and 0.54% respectively of the proposed weight estimates.

In the tables, "proposed weight", "actual weight" and "adjusted obtainable weight" columns are presented. The first two columns are self-explanatory; the latter is the result of examining the actual Phase A components and the weight variant problems and determining an attainable weight for the proposed design concept. Thus a realistic attainable weight for the Phase A tank with manufacturing tolerance is 56.350 lbs; the comparable proposed weight was 53.576 lbs. The main difference lies in the variation of actual outer shell buckling characteristics from conventional theory.

Several of the component weight variations were due to selection compromise to obtain short delivery (particularly the inner shells) or to overdesign to minimize the possibility of marginal design failure problems (the mounting frame, for example).

The inner pressure vessel shells were 5.55 lbs. overweight. The reason was largely due to selection of the closest available sheet stock one standard gauge over the minimum thickness required prior to forming. The material was ordered concurrent with tooling fabrication and without the precise knowledge of wall thickness reduction due to hydroforming.

The inner vessel shells (Inconel 718) were heat treated to only 90,000 psi yield, therefore this item was not planned as weight optimum.

Buckling problems were experienced due to a non-spherical configuration of the outer tank shells. This was partly anticipated since two different wall thicknesses of two shell designs were originally ordered. The problem was more severe than anticipated from conventional buckling analysis.

The outer shell is noted as the largest weight variant item. It was found necessary to flute the tunnel areas and add doubler reinforcement bands to the tunnel region of the outer shells. This added 12.26 lbs. to the proposed weight estimate.

As a result of the outer shell buckling problem, a number of hemispheres were obtained and buckling failure tests were run to obtain a reasonably accurate empirical formula for determining the outer shell wall

thickness required. This work is reported in Section 3.2.2; the effect is reflected in the outer tank weight in the "Adjusted Obtainable Weight" column.

The weight of the bumpers can be significantly reduced by removal of excess, non-structure supporting material. This was accomplished on a subsequent design.

The proposal estimate for fittings took into account the tank material removed to accommodate the fitting. The estimates were considered too low. The actual fitting weights are shown.

The thermal conductor was removed from the contract program. However, a heavier conductor was added at Instruments & Life Support Division expense to obtain stratification data for comparison with a smaller unit containing a thermal conductor with proportionate physical characteristics.

The structural rigidity and stability of the shield hemispheres for fabrication, handling and assembly was very good. The wall thickness of the shields was nominally 0.017". The preliminary vibration test did not impair the shield characteristics and a 20-25% weight reduction appeared practical for a nominal effort program.

The mounting frame was overdesigned due to direct design extrapolation from a smaller design frame that had been successfully vibrated to the complete Apollo tankage vibration specification.

It was necessary to limit the mounting frame effort to compensate for the excessive effort required to solve the outer shell buckling problem.

The mounting frame spacers and gaskets were added to compensate for dimensional variation since the frame had to be constructed prior to final tank assembly fitup dimension examination. Also with this design it is possible to alter the dynamic characteristics of the mounting frame - tank assembly for vibration testing.

The vent valve was changed to a good quality, cryogenic, industrial, manual valve for ground support use since lightweight standard off-the-shelf valves generally wear out rather quickly and have little G.S.E. value.

The proposed manufacturing tolerance of 8% over normally minimum weight estimates was somewhat low for a nominally funded program that cannot support substantial tooling, process refinement and contour machining.

The weight variation of the Phase A tank was due largely to the buckling problem encountered on the outer shells. The results of the buckling test program showed that the proposed outer shell weight was not practicably attainable for a single wall spherical structure. The effect was a weight increase to the system and thus pointed up the importance of developing alternate design outer shell structures such as sandwich or honeycomb construction hemispheres.

3.2.7 Testing

Successful performance of the system demonstrating the radial bumper-discrete shield dewar design are evidenced by the results of the thermal and structural tests performed on the unit.

3.2.7.1 Thermal

The following thermal tests performed on the dewar demonstrated the insulating qualitites of the concept.

3.2.7.1.1 Vented Heat Leak

Vented heat leak results for the Phase A dewar are presented in Table 3.2-8. All tests were performed with the test fluid at local atmospheric pressure and in a laboratory environmental temperature of 75 - 80°F. The cryogen loss rate from the dewar for Tests 1 through 3 was determined by measuring the vented flow with a wet test meter. The loss rate for the remainder of the tests was determined by measuring the weight change with a recording scale.

TABLE 3.2-8

VENTED HEAT LEAK TESTING - PHASE A DEWAR

TEST NO.	TEST FLUID	HEAT LEAK BUT/HR	COMMENTS
1	LO_2	10.50	Dynamic test immediately after tank welding; 42-hour cold pump down; stabilization 17 hours after LO_2 fill.
2	LO_2	7.61	Dynamic test on higher capcity pumping station; 40-hour cold pumpdown; stabilization 21 hours after LO_2 fill.
3	LO_2	8.84	Dynamic Test after second evacuation bakeout; 22 hours cold pumpdown.
4	LO_2	8.08	After tip-off of cold (un-baked) tank, before third evacuation-bakeout. Witnessed by NASA personnel.
5	LO_2	6.80	After third evacuation-bakeout and tip-off; 96 hours after LO_2 fill.
6	LO_2	7.30	1 month after third evacuation bakeout and tip-off.
7	LO_2	7.31	After fourth evacuation-bakeout and tip-off; 96 hours after LO_2 fill.
8	LO_2	7.29	1 month after fourth evacuation bakeout and tip-off.
9	LN_2	6.80	Dewar cool-down prior to LH_2 fill.
10	LH_2	5.10	Averaged over seven-day period.

3.2.7.1.2 Pressure Build-up

Pressure build-up tests were performed to determine the time required for cryogen pressure to increase from atmospheric to supercritical pressure, due to environmental heat input alone. Both hydrogen and oxygen were used as the test fluid. Oxygen pressure build-up test results are shown in Figure 3.2-74; hydrogen results

are shown in Figure 3.2-75. Differences in build-up time for the two tests shown in each figure are attributed to the differences in initial cryogen fill percentage.

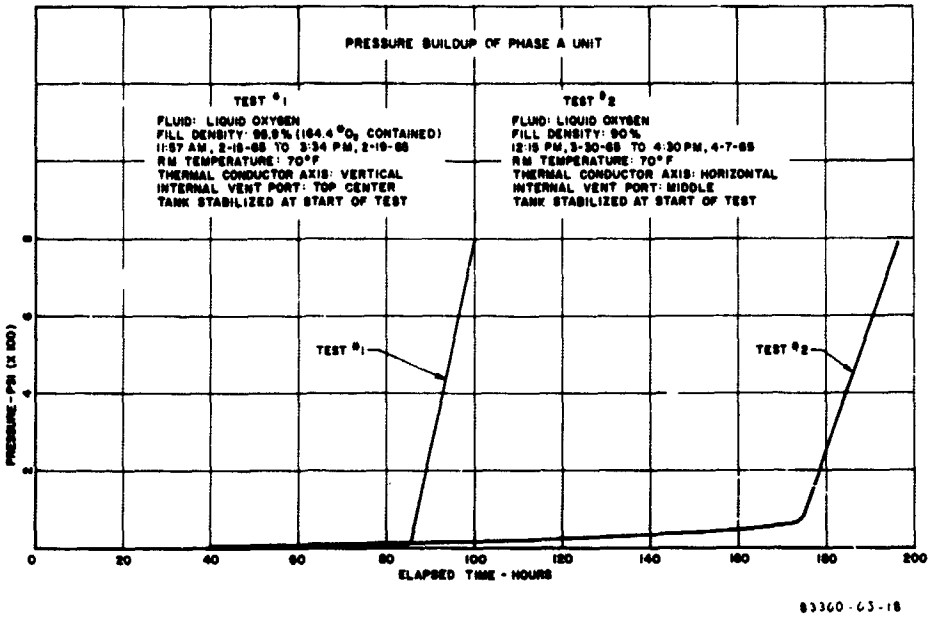
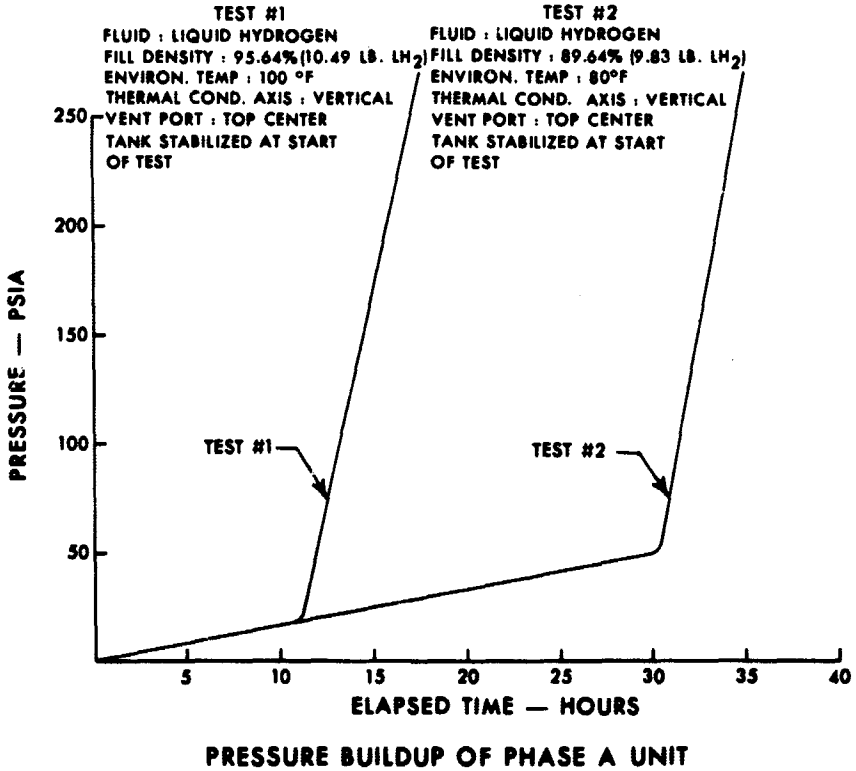


Fig. 3.2-74
PRESSURE BUILDUP OF PHASE A UNIT

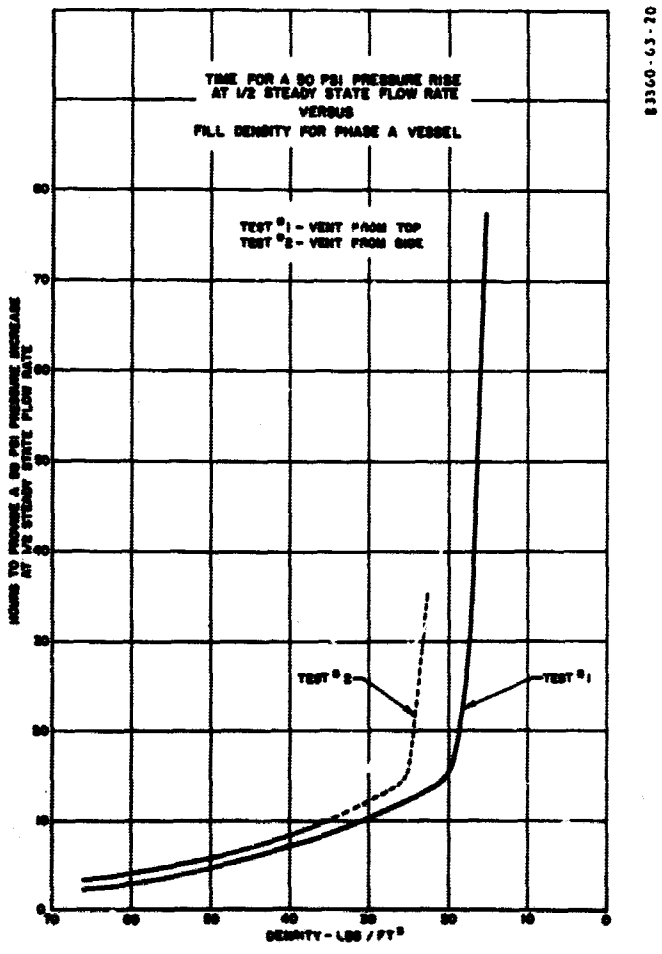


PRESSURE BUILDUP OF PHASE A UNIT

FIG. 3.2-75 A-3873-67-224

3.2.7.1.3 Operational

Tests were performed to determine the time for a 50 psi pressure rise when the oxygen supply flow rate from the dewar was maintained at one-half the steady state flow rate. The vessel was set up to flow through a solenoid valve actuated by a pressure switch that operated between 785 and 800 psig. The vessel attained the operating pressure by pressure build-up from atmospheric, as shown in Figure 3.2-74. The 50 psi pressure build-up test was performed once each day after attaining operating pressure. The procedure consisted of opening the solenoid valve and adjusting a needle valve downstream in the supply line, until the flow rate as measured by a gas flowrator column remained constant for 30 minutes. That flow rate was then reduced by one-half as measured on the flowrator column and the time for an approximate 50 psi pressure rise was observed. Results of the two such tests performed on the unit are presented in Figure 3.2-76.



As noted previously on Figure 3.2-74, the dewar orientation differed in Tests 1 and 2 in that the internal supply port (denoted as vent port on Figure 3.2-74) was located at the top of the vessel in Test No. 1 and at the side of the vessel in Test No. 2. The variations in equilibrium flow rates and therefore in the 1/2-equilibrium flow rates between Tests 1 and 2 are due to the port orientation differences and are attributed to temperature stratification within the cryogen.

3.2.7.1.4 Equilibrium Flow Rate

The equilibrium or steady state flow rates obtained during the oxygen 1/2-steady state flow rate tests of Figure 3.2-76 are shown in Figure 3.2-77. These flow rates represent that flow required to maintain a constant 800 psig oxygen pressure over the fluid density range studied. Fluid port location effects are evident in the figure.

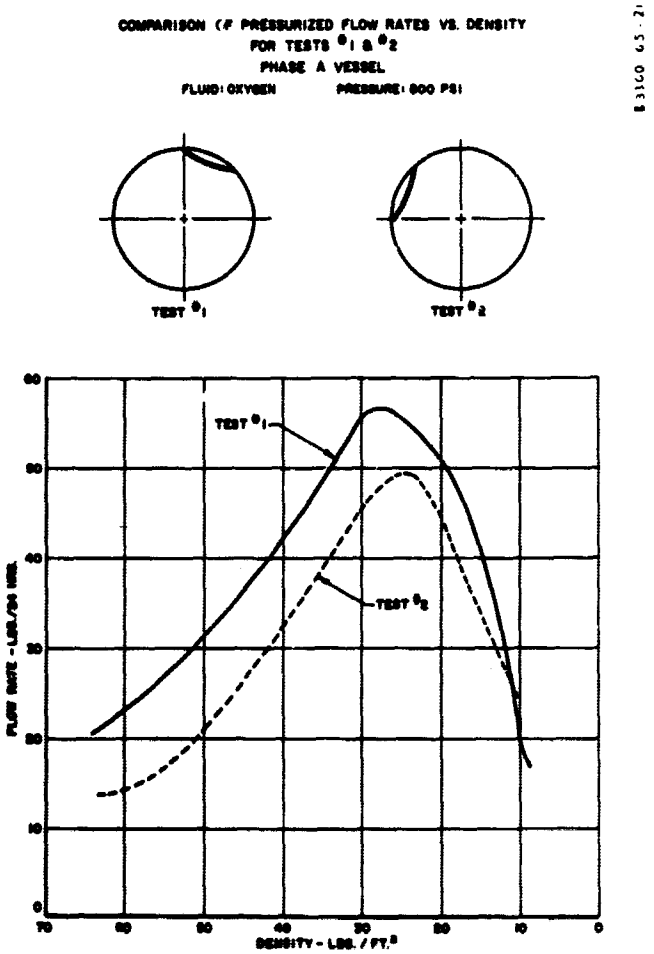


Figure 3.2-78 shows equilibrium flow rest results performed with hydrogen. These results were obtained in conjunction with the two hydrogen pressure build-up tests described in Figure 3.2-75. In both Tests 1 and 2, the supply fluid internal port was located at the top of the vessel.

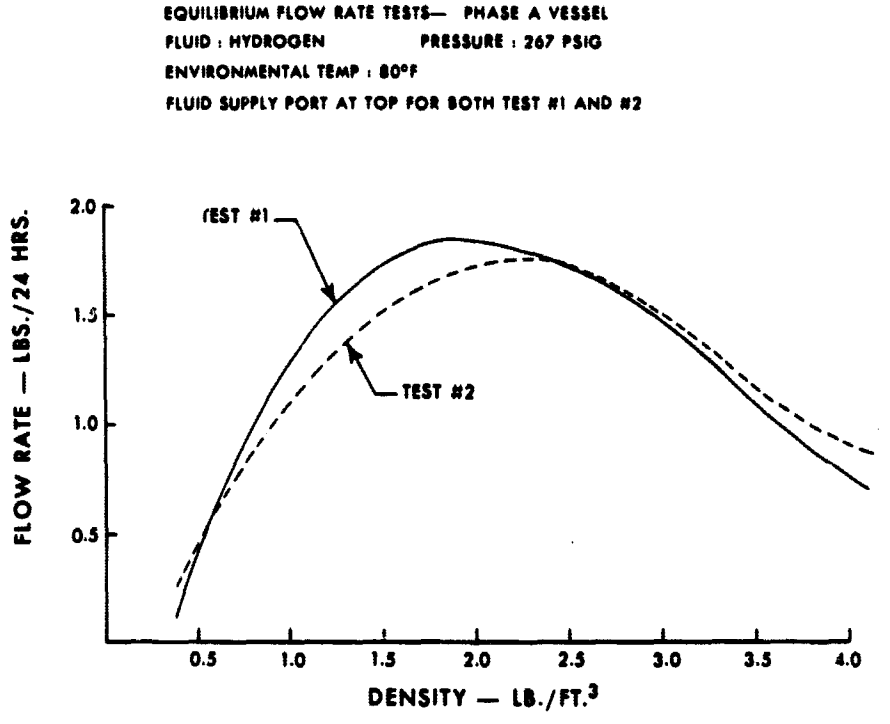


FIG. 3.2-78 A-3873-67-223

3.2.7.1.5 Effect of Load on Conductive Heat Leak

Testing was performed to determine the effect of varying the internal liquid oxygen load on bumper conductivity heat leak. Three oxygen load conditions were examined. All tests were performed with liquid oxygen at local atmospheric pressure and in a laboratory environmental temperature of 74°F. Each test duration was 24 hours. Test results are presented in Table 3.2-9.

TABLE 3.2-9

VENTED HEAT LEAK VS LO_2 LOAD - PHASE A DEWAR

TEST NO.	OXYGEN LOAD, LBS. START	OXYGEN LOAD, LBS. END	TOTAL VERTICAL LOAD, LBS.	AXIAL LOAD PER BUMPER LBS.	TOTAL HEAT LEAK, BTU/HR
1	160.3	158.4	224	159	7.10
2	95.8	94.0	160	95	6.87
3	24.9	21.4	88	23	6.69

3.2.7.2 Structural

Vibration testing was performed on the Phase A dewar following the second evacuation bakeout process, described in Section 3.2.6. As discussed therein, the dewar was pinched off after having been evacuated for 22 hours outside the bakeout oven in order to facilitate the thermal-structural demonstration performed at Bendix for NASA personnel.

Prior to the testing, a magnesium vibration fixture was fabricated and resonance tests on the fixture were performed. The fixture is shown in Section 3.2.6 in Figure 3.2-73. Four acceleration pick-ups were mounted at various locations. Significant (unloaded) fixture resonance at the dewar mounting point locations occurred at the 250-350 cps and 650-750 cps regions, which are normally not too critical for dewar tankage; therefore, the fixture was considered adequate for preliminary tests.

Preliminary vibration searching on the dewar-mounting frame assembly consisted only of sinusoidal examination. The unit was loaded with liquid oxygen (approximately 170 pounds) and pressurized to 100 psig. The plane of vibration was vertical, and the driving pickup was mounted on the vibration fixture, adjacent to a tank mounting bolt. The procedure and observations are listed below:

1. Sine Sweep 38 cps to 2000 cps at constant 3.0 g (approximately 10 minutes) - Noted slight shield activity between 110 and 150 cps.

2. Slow Sine Sweep 200 cps to 40 cps at constant 3.0 g (approximately 7 minutes) - Recheck and confirm

apparent shield, lead or tube resonance in annular space between 150 and 110 cps. Did not appear serious at this input level.

3. Sine Sweep 40 cps to 5 cps at constant 0.020" displacement (approximately 4 minutes) - Apparent inner vessel or vessel-mounting frame resonance occurred between 27 cps and 17 cps. No significant or irrelative motion below 17 cps.

4. Sine Sweep 40 cps to 5 cps at constant 0.040" displacement (approximately 4 minutes) - Again, apparent inner vessel resonance set in at 27 cps, gradually increased to peak at 18 cps and cut out entirely at 17 cps. The magnitude was not serious in terms of vessel failure, but did indicate that low frequency snubbing would improve the existing type vibration mounting system.

The preliminary sinusoidal vibration test performed on the dewar indicated that the vessel and mounting configuration were very stable compared to numerous other mounting systems tested at Bendix on different dewars. There was no evidence of serious or destructive shield resonance characteristics. A low energy level resonance noise was intermittently detected between 110 and 150 cps that sounded like the shield mounting spools. The noise also could have been caused by one of the metal sheathed electrical leads.

Following preliminary testing, the Phase A tank containing approximately 170 pounds of liquid oxygen and pressurized to 100 psig was subjected to limited time exposures of sinusoidal, random, and sine and random vibration in the presence of NASA personnel. The vibration tests were performed in accordance with NAA MC 901-0005C page 53 and Tabel V, oxygen subsystem, except as noted. Search sweeps were performed in the following sequence.

1. Sine Sweep 40 cps to 2000 cps at Constant 3 g (approximately 10 minutes).

2. Sine Sweep 40 cps to 5 cps at Constant 0.040" displacement (approximately 2 minutes).

3. Random only 5 g RMS level 1 (approximately .75 min.).

4. Random only 2.5 g RMS (approximately 2 minutes).

5. Random superimposed on Sine

   Random 2.5 g RMS

   Sine 40 cps to 2000 cps at Constant 3.0 g (approximately 5 minutes).

6. Random Superimposed on Sine

   Random 2.5 g RMS

   Sine 2 g at 40 cps to .2 g at 6 cps

7. Random only 2.5 g RMS (approximately 10 minutes).

The sine (only) vibration was performed in an identical manner to that of the preliminary search test. Stability and general unit characteristics looked very good. The random (only) at 5 g RMS appeared to excite significant shield resonance noise. Again, it could not be ascertained whether shield mount to tube noise or electrical lead to shield noise was occurring.

No degradation of thermal performance was observed following the vibration testing program. Thermal testing performed immediately following the vibration testing excercise resulted in heat leak values comparable to those obtained prior to the exercise. Further evidence of the thermal-physical stability of the dewar is borne out in the results presented in Appendix C. This appendix describes thermal testing performed more than 12 months following the vibration test program; thermal performance of the dewar was unchanged.

3.3 Conclusions and Recommendations

The Phase A program achieved the overall objectives set forth at the outset of the program. A supercritical oxygen storage system employing the radial bumper-discrete radiation shield concept was designed, fabricated and tested. The program successfully demonstrated that the concept is feasible for the fabrication of larger tankage and that the thermal-physical qualities of the concept represent significant state-of-the-art advancements.

Certain design and processing problems were encountered during the performance of the program. Because the program was one of concept development and feasibility demonstration, the problem areas and their solutions were valuable for application to the Phase B program and future large cryogenic tankage programs. The problem areas of major importance, their successful solutions, and recommendations resulting therefrom are discussed in the following sections.

2.3.1 Plating

The overall plating quality of the dewar was considered to be only fair. The reason for this situation was twofold: (1) problems arose during the actual plating process, and (2) the time period between plating and final assembly weld was excessively long, causing some plated surface deterioration.

The poorest plating was experienced on the pressure vessel. Handling of the vessel from tank to tank during the silver electroplating process was not satisfactory due to the fact that an overhead hoist-track was not available. Instead, a portable shop hoist was utilized, which resulted in rolling the hoist (to which the vessel plating fixture was attached) from tank to tank. This required more time than would have been needed if an overhead transport system had been available. Rinse times and immersion times were thus adversely affected.

The fixture used to hold the pressure vessel during plating also was not satisfactory. Because the sliding contact features of the fixture did not work as planned, certain areas were left unplated.

The radiation shields were neither mechanically nor chemically polished prior to plating; they were left in the as-formed condition. The silver plating on the shields was not considered optimum.

Recommendations for improvement of the plating process are as follows:

1. Improve plating fixture for pressure vessel.

2. Improve handling and transport of pressure vessel during plating program.

3. Mechanically and/or chemically polish aluminum shields prior to plating.

Deterioration of the plated surfaces between the plating process and the final dewar assembly was minimized by maintaining the surfaces in an argon environment. However, due to the excessive time period of eleven days and the handling of the surfaces during the assembly, surface oxidation was not completely avoided. Discussion of improvements in assembly are discussed in the following section.

3.3.2 Assembly

Considerable difficulties were encountered in the final fit-up and assembly of the dewar. One of the major problems concerned the mounting of the chabazite absorbent; shield interference was experienced. Eventually the adsorbent container was eliminated, and a barium getter was mounted on the outer shell.

Fit-up of the plated shields involved a certain amount of modification during the final assembly, to prevent shield to shield and shield to pressure vessel contact. This problem existed because there was not enough preassembly fit-up performed, due to difficulties in working with all shells at once. The problem could have been minimized if a mock-up pressure vessel had been available for shield fit-up while the final pressure vessel was being assembled.

The numerous small radiation shield segments used to cover holes and openings made purposely large for ease of assembly required a considerable amount of assembly time in fastening to the main shield body. The same type of fasteners were utilized to join the shield hemispheres at the girth, and could be improved for more rapid assembly. The shield hangers, which supported the shields to the pigtail tubes, were adequate and performed their intended function; assembly time could be shortened, however, by improved design.

Handling of the sub-assembled dewar during fit-up and final assembly involved manually rotating the pressure vessel shield subassembly in the argon booth about a horizontal axis when progressing from one half-shell mounting to the next. This procedure was quite cumbersome and involved considerable time and assembly positioning before the next assembly step could be performed.

Recommendations for improvement of the radial bumper-discrete shield dewar concept assembly procedure include the following:

1. Provide a mock-up pressure vessel for parallel subassembly of shields and pressure vessel.

2. Improve shield locking technique and minimize small radiation shield segments.

3. Improve shield hanger technique.

4. Provide improved methods for handling dewar subassembly during final assembly process in argon booth.

3.3.3 Outer Shell

The major program difficulty and delay resulted from development of the outer shell configuration. A tunnel-type of configuration was initially selected, and outer shells of different thicknesses were procured. Buckling tests performed on the various shells at the initial portion of the program indicated that the thickest shell obtained was not structually adequate at the elevated temperatures experienced during bakeout. Fluting in the tunnel region was not in itself sufficient; a doubler strip in the same region was finally utilized in conjunction with the fluting to result in a satisfactory outer shell design.

Design of the basic tunneled outer shell configuration was extremely difficult to analyze theoretically. For this reason the modifications described above were required to supplement the design received from the shell fabricator.

The doubler strip utilized in conjunction with the flutes in the outer shell was considered to be the major cause for the additional evacuation-bakeout process required before the dewar was considered to have a stable vacuum. Large gas-trapping spaces resulted when the strip was welded into each outer shell hemisphere. The high vacuum annulus pressures present after the first three tip-off processes, indicated by excessive dewar heat loss, were surmised to be caused by outgassing resulting from gas trapped in the pockets between the doubler strips and the inner surface of the outer shell. The final evacuation-bakeout was extended such that the trapping areas were apparently cleaned out to partially eliminate the outgassing problem.

It was concluded from the developmental studies on outer shell design conducted in the Phase A program that the optimum outer shell design would be a spherical configuration. This configuration has much theoretical and emperical background data and appears to be more readily applicable to large tankage outer shell design. It was recommended that the outer shell hemispheres of the Phase B program be of the spherical configuration.

SECTION IV

PHASE B PROGRAM

4.1 System Description & Operation

The oxygen and hydrogen systems that were developed and built under the Phase B part of NAS 9-2978 are shown in Figures 4.1-1 and 4.1-2 respectively. Many of the design and functional aspects of both systems are common, thus this section of the report relates to both systems except in cases where differences do exist. Each system was designed for the storage of a required volume of single phase (supercritical) fluid.

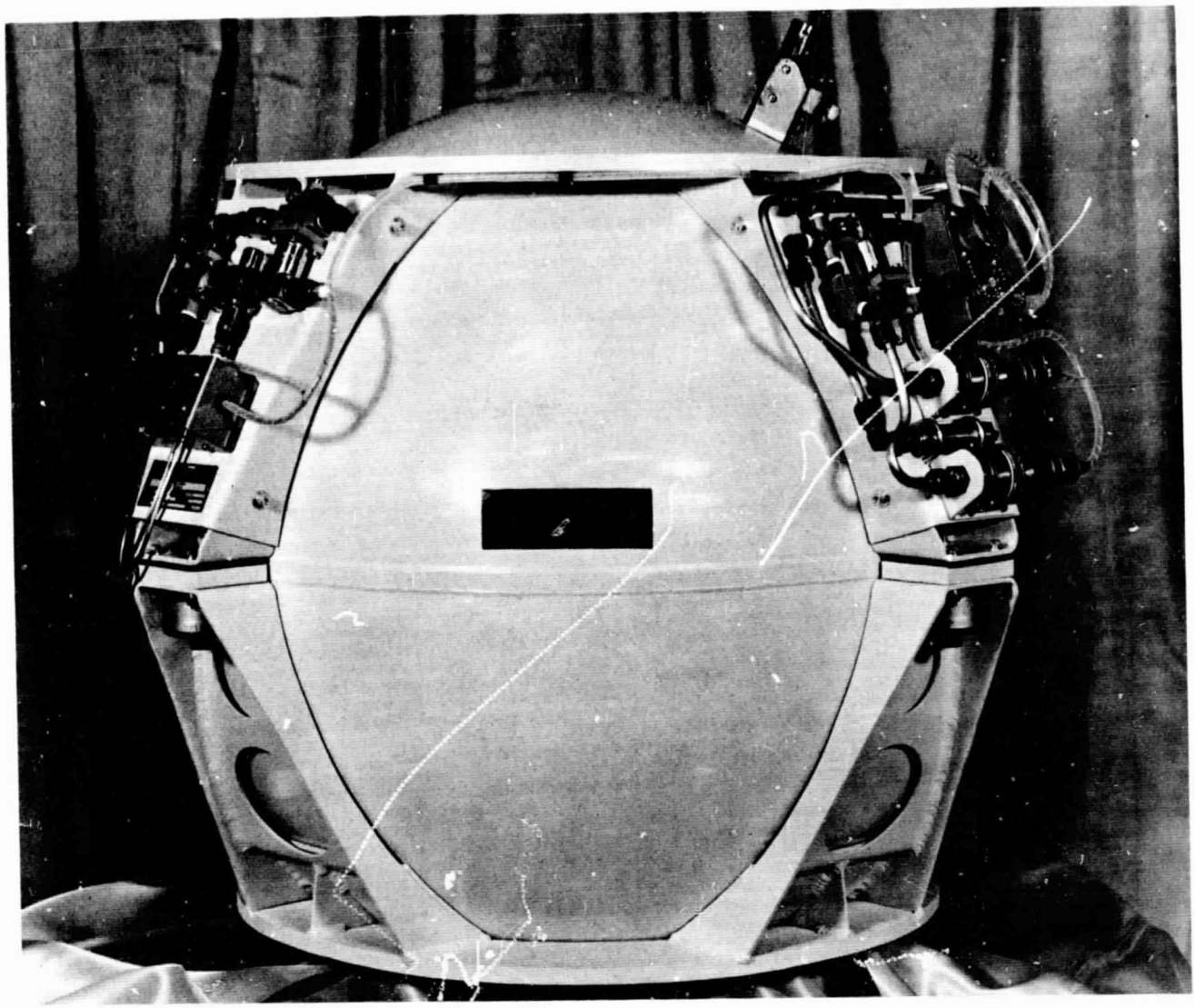
4.1.1 System Operational Concepts

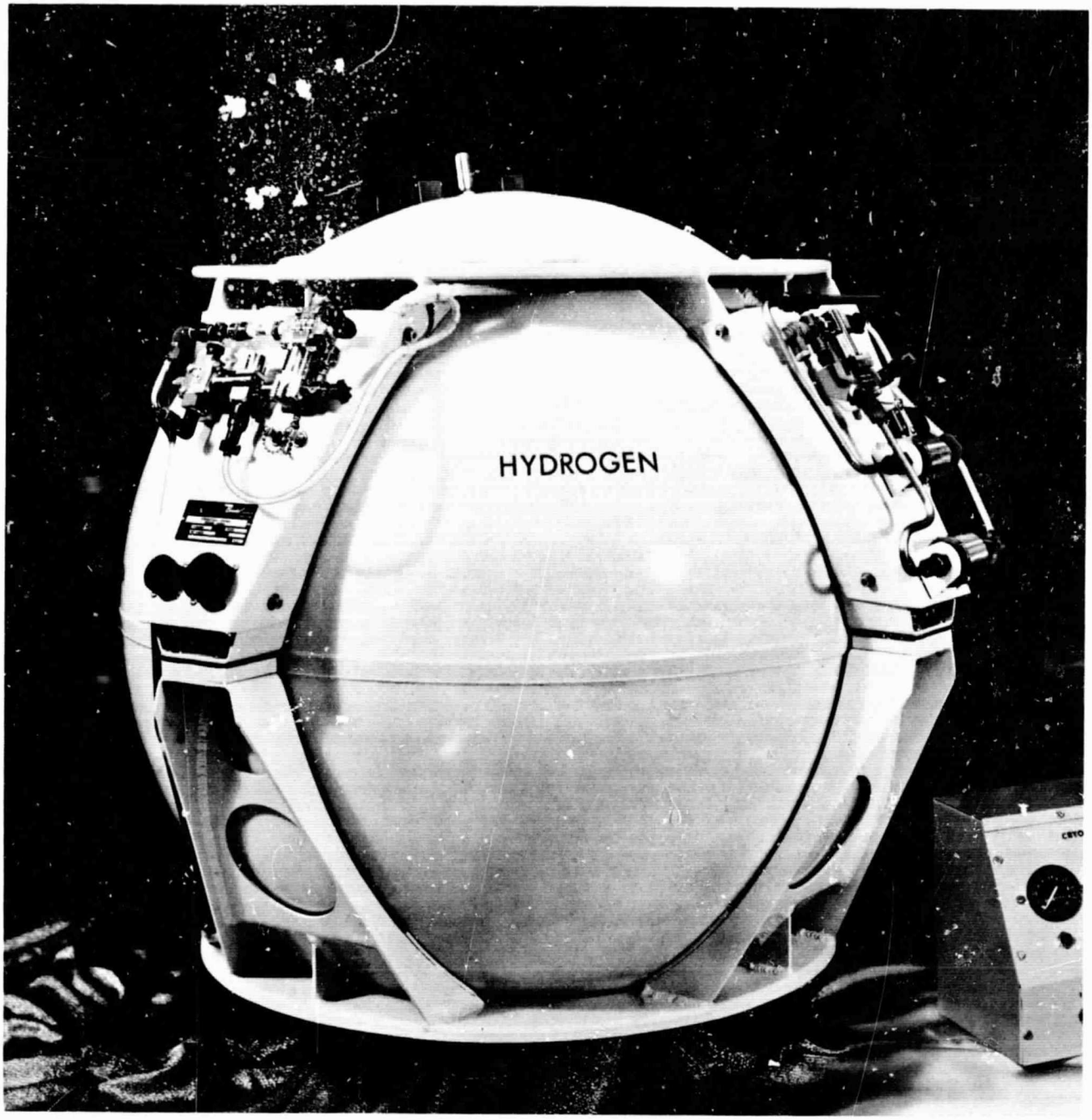
The system operational concepts are essentially the same for both the hydrogen and oxygen systems except that the hydrogen storage tank contains a vapor cooled radiation shield to further reduce ambient heat transfer to the stored cryogen. Schematics of the systems are shown in Figure 4.1.1-1 and 4.1.1-2.

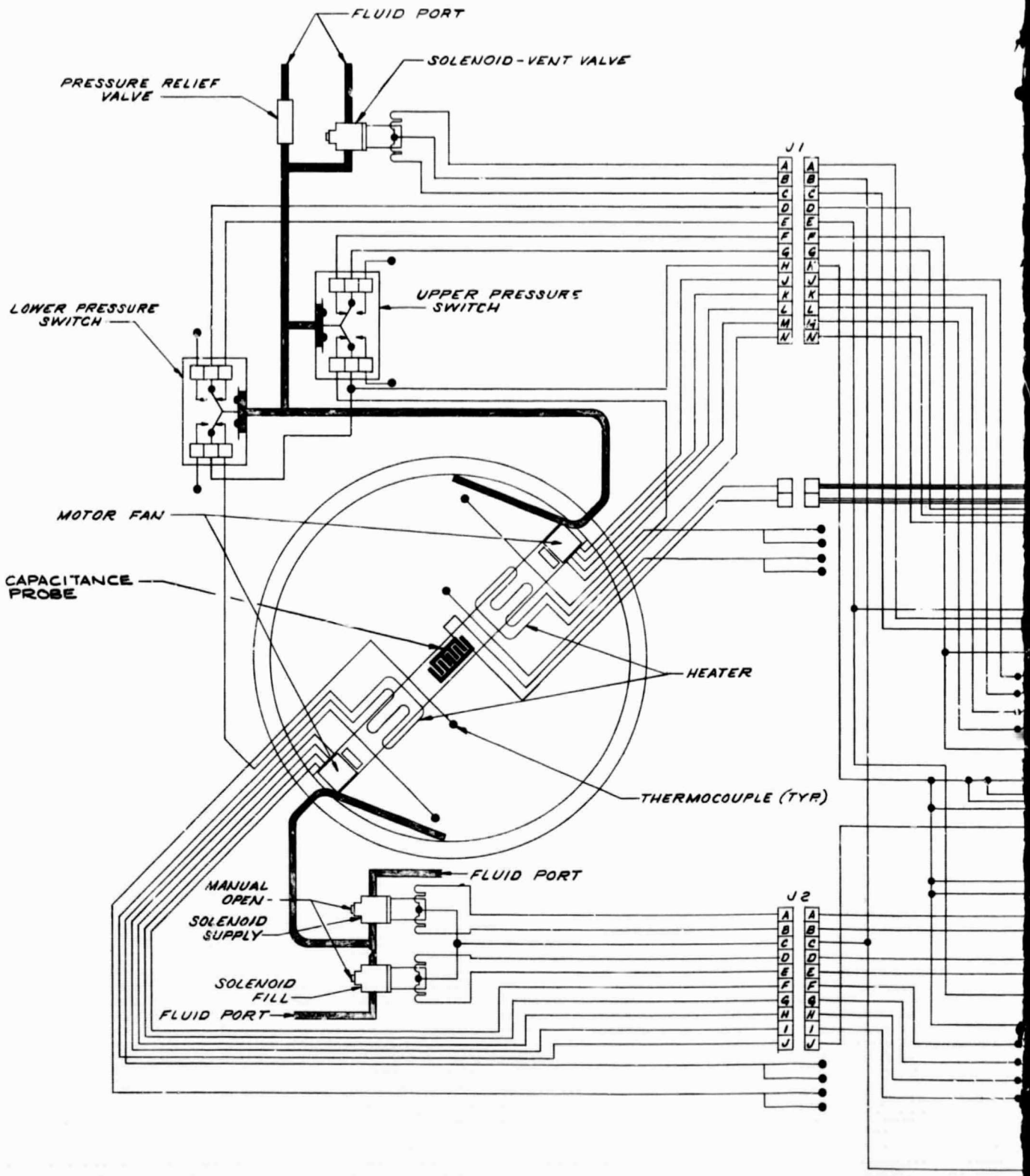
The cryogen is stored in the inner vessel which is insulated from the outer shell by means of a vacuum annulus and low conductivity supports (see Section 4.1.2.1). In addition, the inner vessel is protected from radiant heat by discrete spherical shields which are supported by low conductivity devices within the vacuum annulus. Fill and vent shutoff valves permit filling of the inner container with liquid.

4.1.1.1 Filling

The vessel is filled by connecting the fill shutoff valve to a pressurized source of liquid cryogen. When both the fill valve and the vent valve are opened the system will begin to fill with cryogenic liquid, venting boil-off vapor through the vent valve until the inner vessel has been cooled and the tank is filled with liquid to the desired level. Since the vent line opening is at the very top of the inner vessel, the system may be filled to a level in excess of 97% of the overall tank volume if proper inner vessel cool-down and top-off procedures are observed. When the system has been filled to the desired level, the filling operation is terminated by closing the fill shutoff valve. The stored cryogen at the end of the filling operation is at atmospheric pressure.

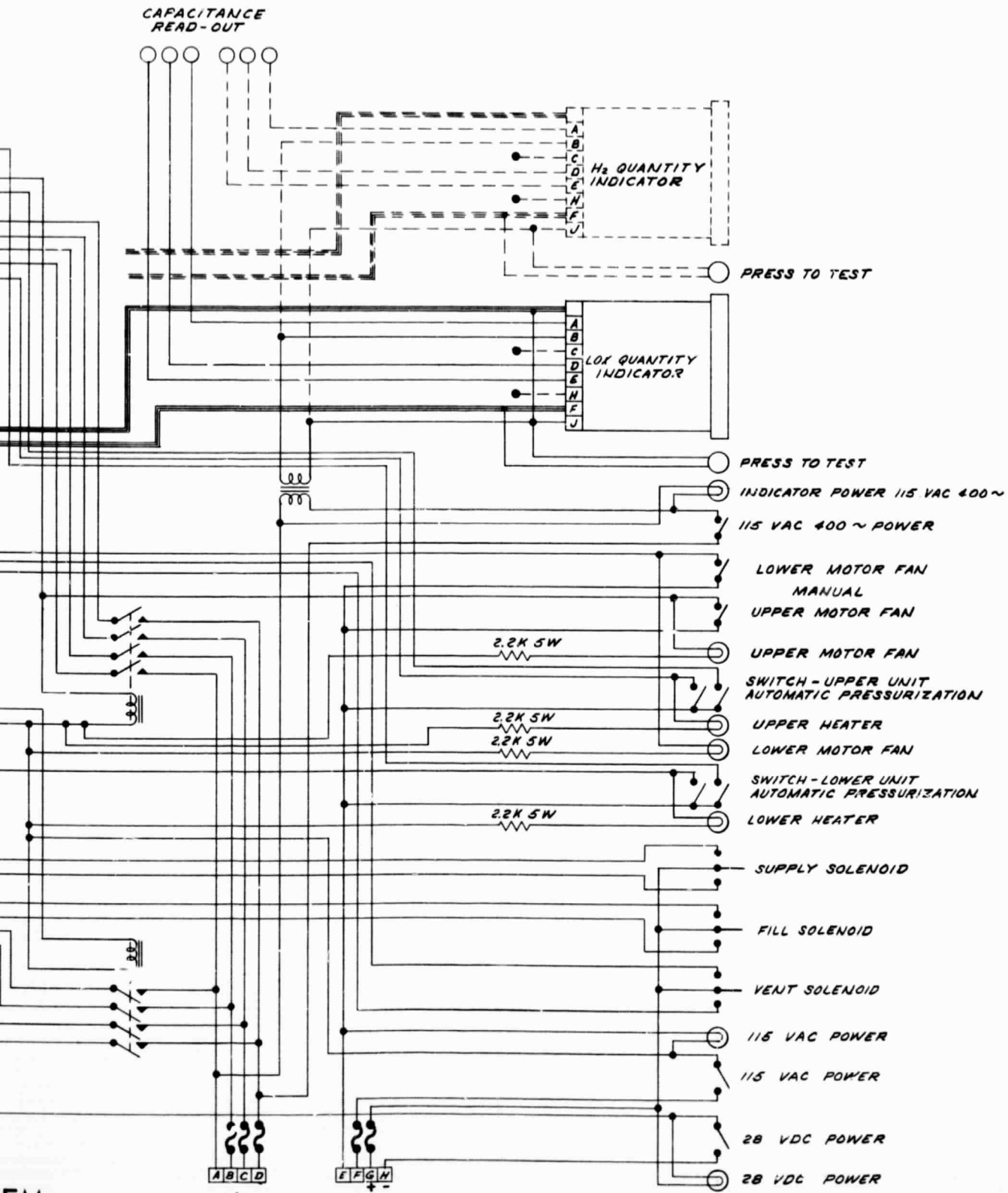



HYDROGEN

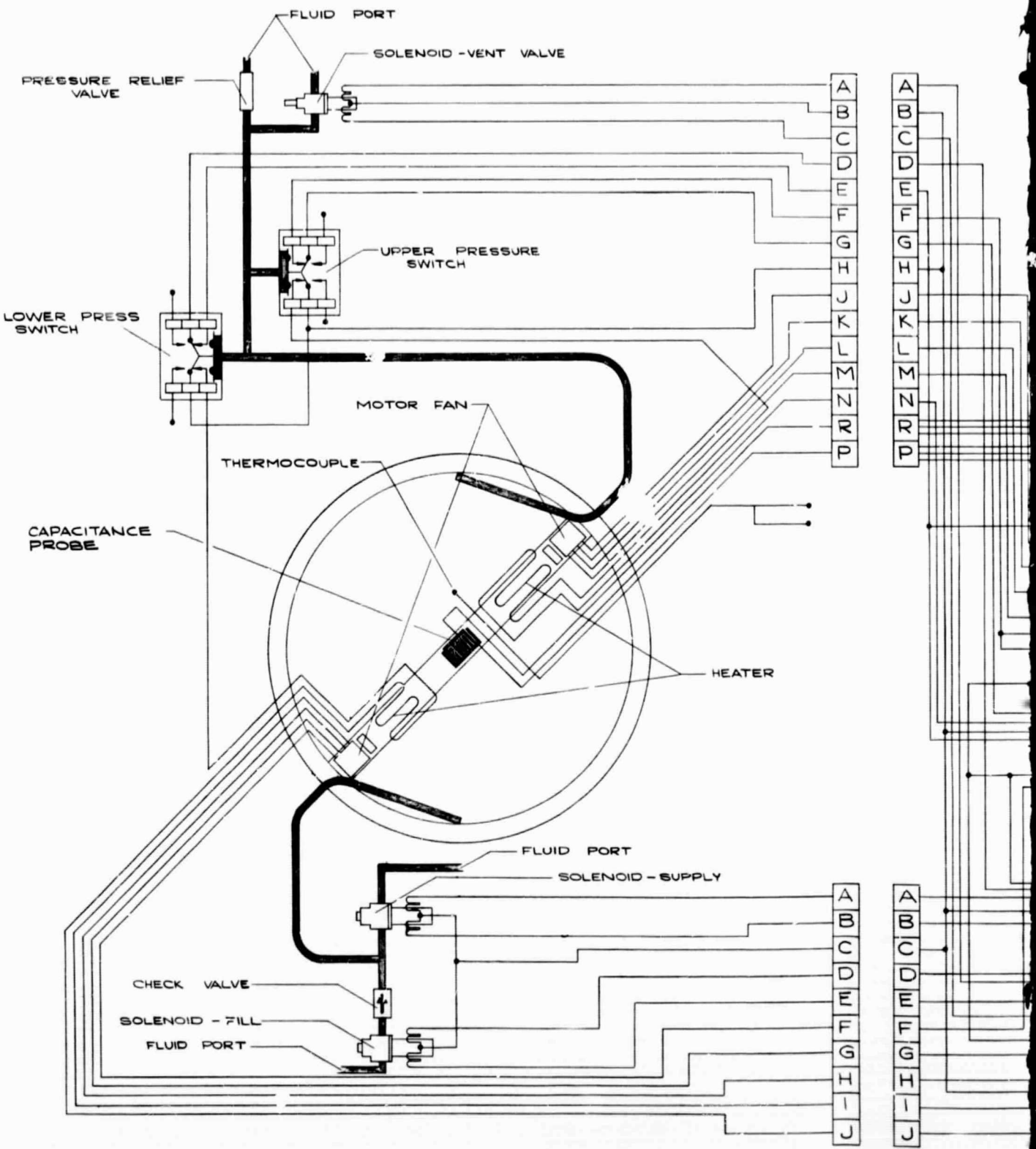


SCHEMATIC-"PHASE B" LOX STORAGE SYSTEM

FIGURE 4.1.1-1

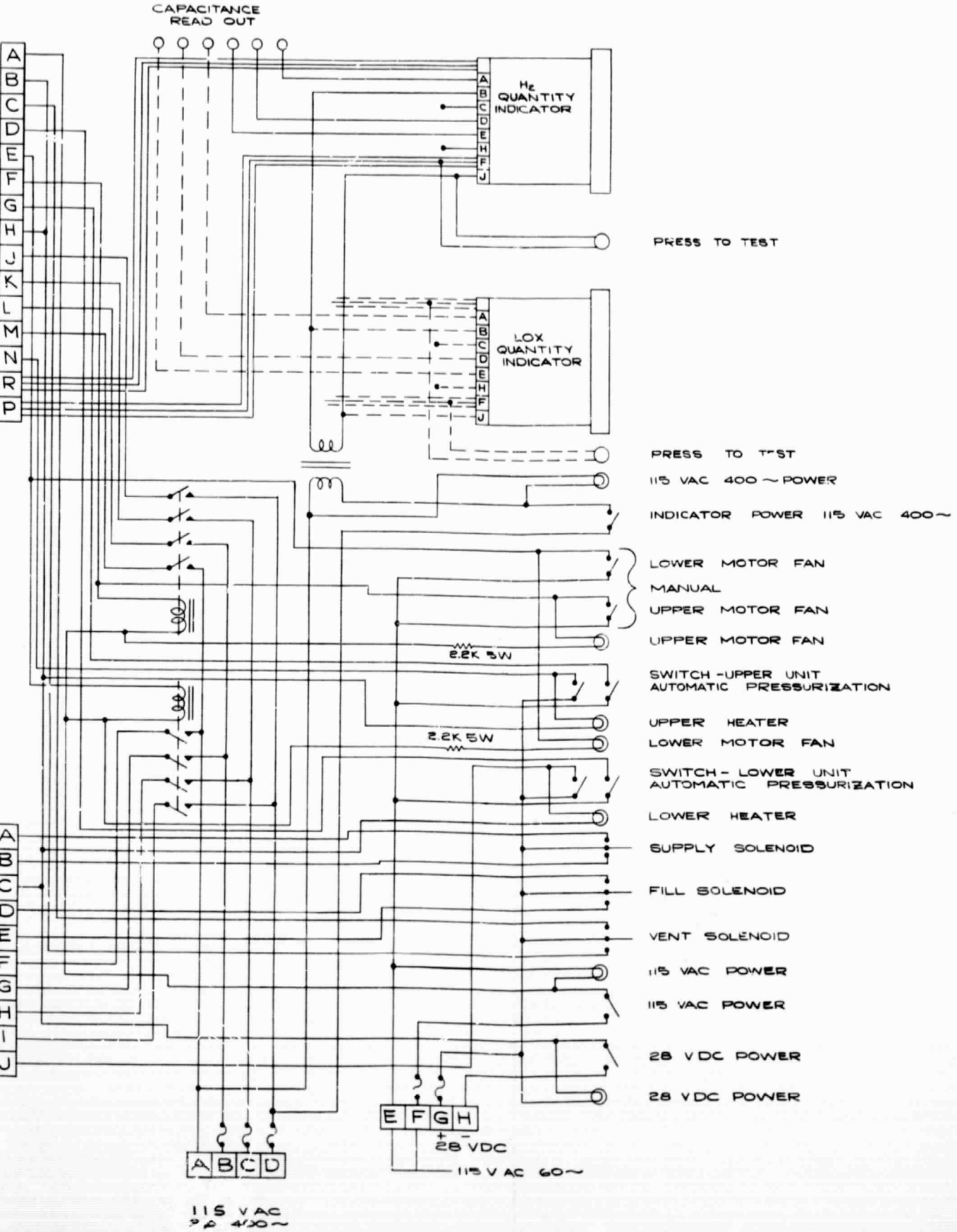

CAPACITANCE READ-OUT
A
B
C
D
E
H
F
J
H2 QUANTITY INDICATOR
PRESS TO TEST
LOX QUANTITY INDICATOR
PRESS TO TEST
INDICATOR POWER 115 VAC 400~
115 VAC 400 ~ POWER
LOWER MOTOR FAN MANUAL
UPPER MOTOR FAN
2.2K 5W
UPPER MOTOR FAN
SWITCH - UPPER UNIT AUTOMATIC PRESSURIZATION
2.2K 5W
UPPER HEATER
2.2K 5W
LOWER MOTOR FAN
SWITCH - LOWER UNIT AUTOMATIC PRESSURIZATION
2.2K 5W
LOWER HEATER
SUPPLY SOLENOID
FILL SOLENOID
VENT SOLENOID
115 VAC POWER
115 VAC POWER
28 VDC POWER
28 VDC POWER
A B C D
E F G H
115 VAC 3ø 400~
115 VAC 60~
28 VDC

EM



SCHEMATIC - "PHASE B" HYDROGEN STORAGE SUBSYSTEM

FIGURE 4.1.1-2


CAPACITANCE READ OUT
A B C D E F G H J K L M N R P
He QUANTITY INDICATOR
A B C D E H F J
PRESS TO TEST
LOX QUANTITY INDICATOR
A B C D E H F J
PRESS TO TEST
115 VAC 400 ~ POWER
INDICATOR POWER 115 VAC 400~
LOWER MOTOR FAN
MANUAL
UPPER MOTOR FAN
UPPER MOTOR FAN
2.2K 5W
SWITCH - UPPER UNIT AUTOMATIC PRESSURIZATION
UPPER HEATER
2.2K 5W
LOWER MOTOR FAN
SWITCH - LOWER UNIT AUTOMATIC PRESSURIZATION
LOWER HEATER
SUPPLY SOLENOID
FILL SOLENOID
VENT SOLENOID
115 VAC POWER
115 VAC POWER
28 VDC POWER
28 VDC POWER
A B C D E F G H I J
E F G H
+ −
28 VDC
115 V AC 60~
A B C D
115 VAC
3Ø 400~

4.1.1.2 Standby

Standby is the period following the filling operation between closing of the fill and vent shutoff valves and the initiation of delivery. During the standby period, the stored fluid pressure increases due to storage tank heat leak. Eventually the saturated liquid pressure of the fluid is reached; following this, the contents of the tank are in a single phase condition. This is the minimum pressure required for the operation of a supercritical system. If fluid is not withdrawn from the storage tank, the fluid pressure will continue to increase until the maximum operation pressure is reached (H_2 - 290 psig, O_2 - 900 psig), at which time fluid will vent from the tank through the system relief valve. Maximum standby is achieved by allowing the pressurization to occur as dictated only by ambient heat leak into the storage tank. If fluid supply is required before the heat leak pressurization has attained minimum operating pressure, the system is equipped with two, electrical heaters which may be energized for the purpose of rapidly pressurizing the cryogen.

The total heat required to pressurize a supercritical pressure vessel is given by the following equation:

$$q = m_f h_f - (f_\ell m_f h_\ell + f_g m_f h_g) - m_f P_f V_f + (f_\ell m_f P_\ell V_\ell + f_g m_f P_g V_g)$$

where:

- q = heat input required to pressurize the system
- m = mass
- h = enthalpy
- P = absolute pressure
- V = specific volume
- f = final pressurized fluid
- g = initial gas in tank
- ℓ = initial liquid in tank
- $f_g = m_g/m_f$ = initial mass fraction of gas
- $f_\ell^g = m_\ell^g/m_f$ = initial mass fraction of liquid.

4.1.1.3 Delivery

Delivery is initiated by opening the delivery solenoid valve. When only a minimum flow is required, the fluid is supplied through the vapor cooling circuit in order to minimize the heat transferred to the stored fluid and avoid pressure buildup in the system. Where higher flow rates are required the fluid is supplied directly from the inner vessel without passing through the vapor cooled

shield. If fluid demand causes the pressure in the system to degrade one internal pressurization heater and motor-fan will be energized by a pressure switch. Redundant heaters, motor-fans and pressure switches were supplied with the system so that system pressure can be maintained should any of these components malfunction. As is shown in the schematic, the system was delivered with the vapor cooling lines plugged and the system plumbed for supplying fluid directly from the inner vessel. For tests requiring the utilization of the vapor cooled shield it was necessary to replumb the system.

The heat required to expell fluid from a supercritical storage tank while maintaining constant pressure is given by the following eqation.

$$dQ/dm = - \rho \, (dh/d\rho)_p$$

where:

dQ/dm = heat required to expell a unit mass of fluid at constant pressure.

ρ = density of the fluid contained in the storage tank

$(dh/d\rho)_p$ = rate of change of enthalpy with density at constant pressure.

At the end of the delivery operation, the temperature of the stored fluid increases until only a small percentage of the original stored mass is still present in the vessel. The temperature eventually reaches a point where it is no longer efficient to heat the gas and the pressure in the tank degrades to the minimum allowable supply pressure, at which time the system is considered to be empty.

4.1.2 System Description

Each system (hydrogen and oxygen) is made up of a high quality insulated storage tank and the necessary valves, sensors, etc. required for operation in the various modes discussed above. This section describes in detail each of the components which make up the system and any special processing techniques used to fabricate those components. Since both the hydrogen and oxygen systems are quite similar, only one system will be described; however, where a significant difference does exist between the two, it will be pointed out and discussed in detail.

4.1.2.1 Storage Vessel Description

A cross section schematic of the storage vessel assembly is shown in Figure 4.1.2-1. Physical characteristics of the oxygen and hydrogen vessel are listed in Tables 4-1 and 4-2 respectively.

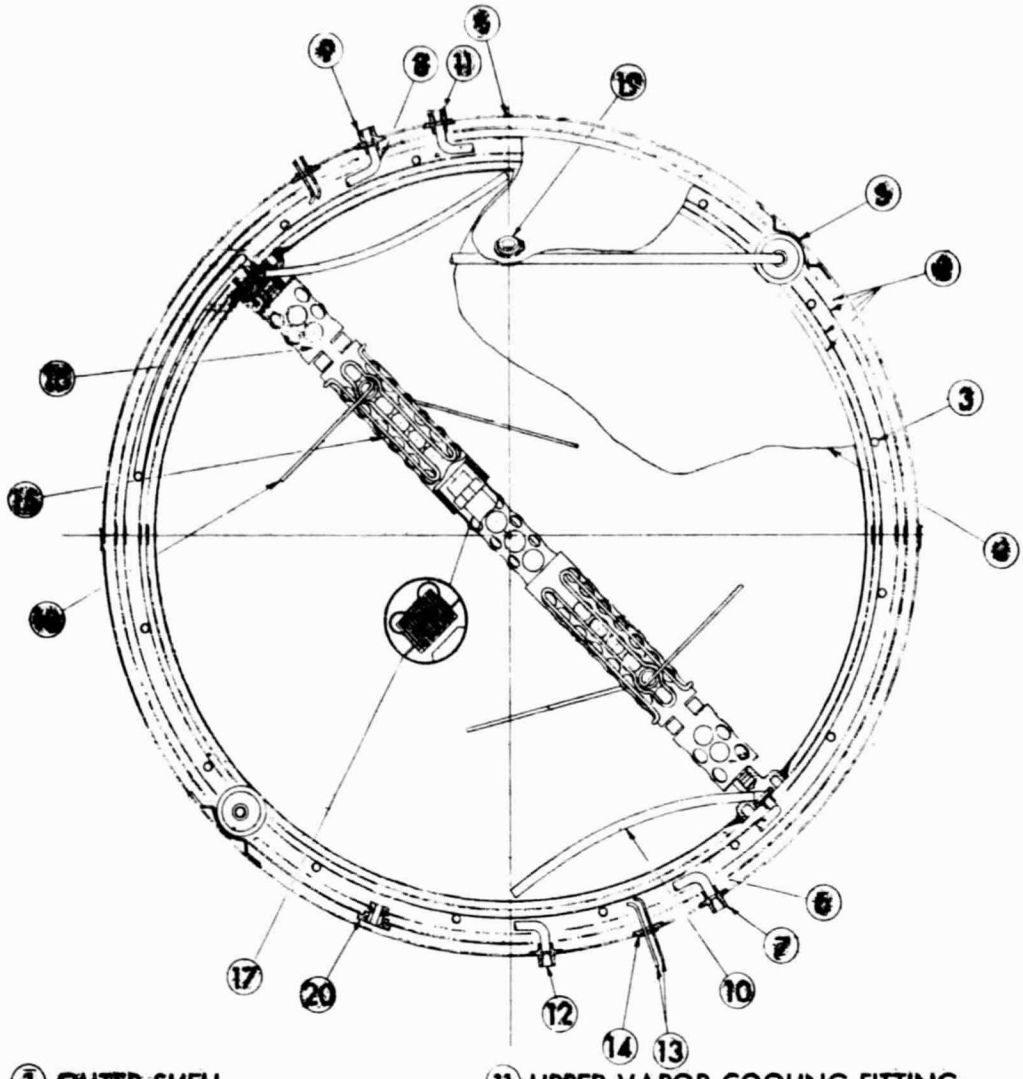
Figure 4.1.2-1 shows that the storage vessel is a double wall (i.e. dewar) constructed tank consisting of an inner tank (4) for fluid storage surrounded by an outer shell (1). The annulus between the storage vessel wall and the outer shell is evacuated to 10^{-6} mm Hg or less to insure the lowest possible amount of thermal gas conduction from the environment to the stored cryogen. Heat leak is minimized further by reducing radiant heat transfer with low emissivity plated surfaces in the vacuum annulus. The outer surface of the storage vessel is electroplated with silver and the inner surface of the outer shell is electroplated with copper. In addition to the highly reflective vessel walls discrete radiation shields (2) are suspended from hangers (19) in the annulus.

The oxygen dewar utilizes two shields located between the fluid tubes (6) & (8) and the inner vessel.

The hydrogen dewar has four shields as shown in Figure 4.1.2-1, two located between the fluid tubes and the inner vessel (4) and two between the fluid tubes and the outer wall (1).

The oxygen dewar has no vapor cooling provision while the hydrogen vessel employs a vapor cooling tube (3) affixed to the second shield. Vapor cooling plumbing permits cooling of both or either shield hemisphere through the use of two separate cooling lines.

Fluid is transferred to and from the inner vessel through the fill tube (6) and vent tube (8). With a two phase fluid (subcritical) in a gravity environment, venting can be accomplished through the vent tube and port (9) and/or through the upper vapor cooled shield hemisphere. When the system is operated in the supercritical condition, fluid may be supplied through any of the lines leaving the inner vessel; vapor cooling of either or both vapor cooled shield hemispheres may be accomplished by routing the supply fluid through either or both of the cooling circuits.



1. OUTER SHELL
2. DISCRETE RADIATION SHIELD
3. VAPOR COOLING TUBE
4. INNER VESSEL
5. RADIAL BUMPER SUPPORT
6. FLUID FILL TUBE
7. FLUID FILL FITTING
8. FLUID VENT TUBE
9. FLUID VENT FITTING
10. FLUID PICK UP TUBE
11. UPPER VAPOR COOLING FITTING
12. LOWER VAPOR COOLING FITTING
13. ELECTRICAL LEADS
14. ELECTRICAL FITTING
15. INTERNAL ELECTRICAL HEATER
16. MOTOR FAN
17. FLUID QUANTITY SENSOR
18. THERMOCOUPLE
19. SHIELD HANGER
20. SHIELD SPACER

SCHEMATIC STORAGE VESSEL ASS'Y

FIGURE 4.12-1

D-3873-67-242

TABLE 4-1

OXYGEN TANK PHYSICAL CHARACTERISTICS

DRY TANK WEIGHT	81.5 lbs w/o external components
OUTER SHELL	
Material	304L Stainless Steel
Thickness	0.033"
Outside Diameter	28.96"
INNER VESSEL	
Material	Cryoformed 301 Stainless Steel
Thickness	0.036"
Outside Diameter	25.176"
Volume	4.8 Cubic Feet
Operating Pressure	900 psia Max.
Proof Pressure	1275 psi
FLUID FILL & VENT TUBING	
Material	304L Stainless Steel
Size	5/16" OD x 0.010" thick
Length	32"
RADIATION SHIELD	
Number	Two
Material	Aluminum 6061-0
Thickness	0.020"
Outside Diameter	25.83", 26.33"
QUANTITY SENSOR	
Type	Interleaf Plate Capacitor
Manufacturer	Bendix - I & LS Div.
Size	.687" x .875" x 5.125" long
Capacitance	
76°F Air	254 Pico Farads
Liquid Oxygen	378 Pico Farads
TEMPERATURE SENSOR	
Type	Thermocouple-Copper Constantan
Manufacturer	American Standard
MOTOR-FAN	
Type	Cryogenic Destratification
Manufacturer	Globe
Input	200 VAC 3 Phase, 900 cps 5.0 Watts Max.
HEATER	
Type	Electrical Resistance
Manufacturer	American Standard

Material	
Element	Nichrome
Insulation	Magnesium Oxide
Sheath	Stainless Steel
Size (element)	65" Long x 0.062" OD
Input	115 VAC - 60 Hz
Power	171.5 Watts
SOLENOID VALVES	
Type	Latching-Manual Override
Manufacturer	Wright Components Inc.
Fittings	1/4" NPT (In & Out)
Input	28 VDC
PRESSURE SWITCHES	
Type	DPDT
Manufacturer	Aero Instrument Co.
Fitting	MS33657-5 Style E
Electrical Connector	To Mate with AN3106-14S-6S
Actuation on Increasing Pressure	815 ± 10 psi
Actuation on Decreasing Pressure	800 ± 10 psig
PRESSURE RELIEF VALVE	
Type	Gage Pressure
Manufacturer	Circle Seal
Fittings	1/2" ANPT - Male Inlet, Female Outlet
Cracking Pressure	900 ± 10 psig
Reseal Pressure	810 ± 10 psig
ION PUMPS	
Manufacturer	Ultek Corp.
Capacity	0.2 LPS
Input	2.9 KVDC

TABLE 4-2

HYDROGEN TANK PHYSICAL CHARACTERISTICS

DRY TANK WEIGHT	114.0 lbs w/o external components
OUTER SHELL	
Material	304L Stainless Steel
Thickness	0.037"
Outside Diameter	32.36"
INNER VESSEL	
Material	Inconel 718 (Aged)
Thickness	0.028"
Outside Diameter	28.180"
Volume	6.7 Cubic Feet
Operating Pressure	290 psia Max.
Proof Pressure	430 psi
FLUID FILL & VENT TUBING	
Material	304L Stainless Steel
Size	5/16" OD x 0.010" thick
Length	35"
RADIATION SHIELD	
Number	Four
Material	Aluminum 6061-0
Thickness	0.020"
Outside Diameters	29.46", 29.96", 31.12", 31.62"
VAPOR COOLING TUBE	
Material	Copper
Size	1/4" OD x 0.030" thickness
Length	47 ft.
QUANTITY SENSOR	
Type	Interleaf Plate Capacitor
Manufacturer	Bendix - I & LS Div.
Size	.687" x .875" x 8.25 long
Capacitance	
76°F Air	404 Pico Farads
Liquid Hydrogen	493 Pico Farads
TEMPERATURE SENSOR	
Type	Thermocouple-Copper Constantan
Manufacturer	American Standard
MOTOR-FAN	
Type	Cryogenic Destratification
Manufacturer	Globe
Input	200 VAC 3 Phase, 900 cps
	5.0 Watts Max.

HEATER	
Type	Electrical Resistance
Manufacturer	American Standard
Material	
Element	Nichrome
Insulation	Magnesium Oxide
Sheath	Stainless Steel
Size (element)	24" long x 0.062" OD
Input	28 VDC
Power	30 Watts
SOLENOID VALVES	
Type	Latching-Manual Override
Manufacturer	Wright Components Inc.
Fittings	1/4" NPT (In & Out)
Input	28 VDC (Momentary)
PRESSURE SWITCHES	
Type	DPDT
Manufacturer	Aero Instruments Co.
Fitting	MS33657-5 Style E
Electrical Connector	To mate with AN3106-14S-6S
Actuation on Increasing Pressure	250 ± 5 psig
Actuation on Decreasing Pressure	235 ± 5 psig
PRESSURE RELIEF VALVE	
Type	Gage Pressure
Manufacturer	Bendix I & LS Div.
Fittings	1/8" ANPT - Male Inlet, Female Outlet
Cracking Pressure	285 ± 5 psig
Reseal Pressure	270 ± 5 psig
ION PUMPS	
Manufacturer	Ultek Corp.
Capacity	0.2 LPS
Input	2.9 KVDC

4.1.2.1.1 Oxygen System Pressure Vessel

The oxygen system pressure vessel was fabricated by cryoforming low silicon 301 stainless steel. This was done by fabricating a composite preform as shown on the left of Figure 4.1.2-2. The composite preform was fabricated by welding roll-formed low silicon 301 stainless steel sheet. The preform was then submerged in liquid nitrogen and pressurized (also with liquid nitrogen) until a predetermined amount of stretching had occurred, at which time the vessel was annealed. By performing a series of stretch-anneal cycles, a spherical pressure vessel as shown on the right of Figure 4.1.2-2 was formed.

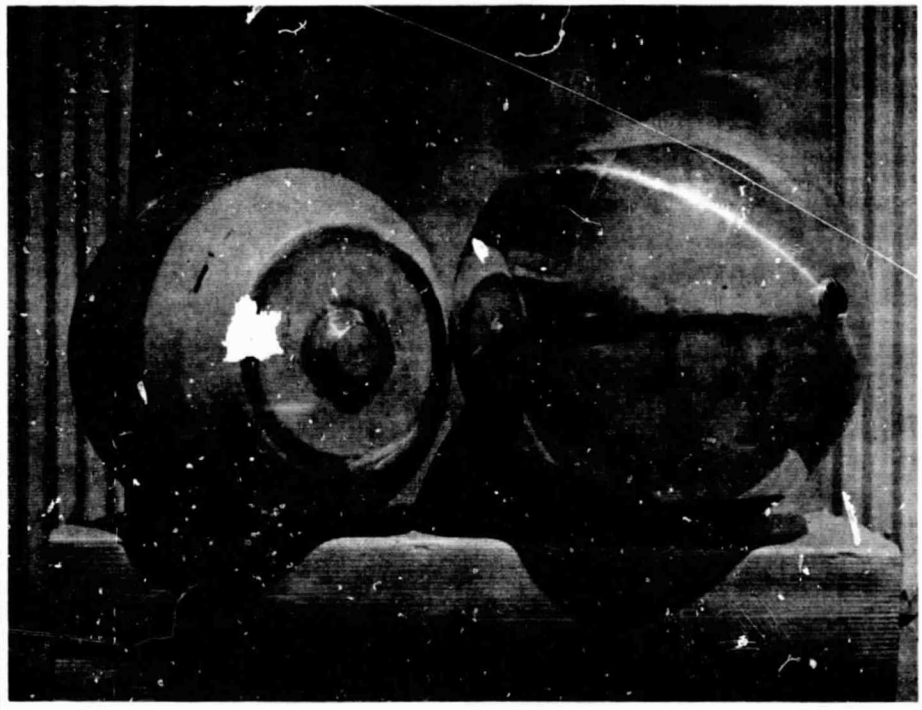


FIGURE 4.1.2-2
COMPOSITE PREFORM AND CRYOFORMED PRESSURE VESSEL

Since the high strength obtained by using this forming technique is caused by the cold-straining of the material during the last stretching cycle, the amount of stretching must be controlled very closely, and the proper vessel size must be obtained. This required considerable planning and accurate measurements during the stretching operations. In addition, no annealing is performed after the final stretch; instead the boss fitting holes are machined in either end and the vessel is aged, pickled and polished.

The final vessel configuration was as shown in Figure 4.1.2-3. As can be seen, the vessel is a sphere of uniform wall thickness except for a boss at each pole. These bosses surround 2.025" holes through which the internal instrumentation package shown in Figure 4.1.2-1 is inserted into the pressure vessel. After insertion of the instrumentation package the fittings at each end of the package were welded into the pressure vessel bosses. The thickened section of the boss allows for the decreased strength of the material in this area after the welding operation due to partial annealing in the heat effected zone.

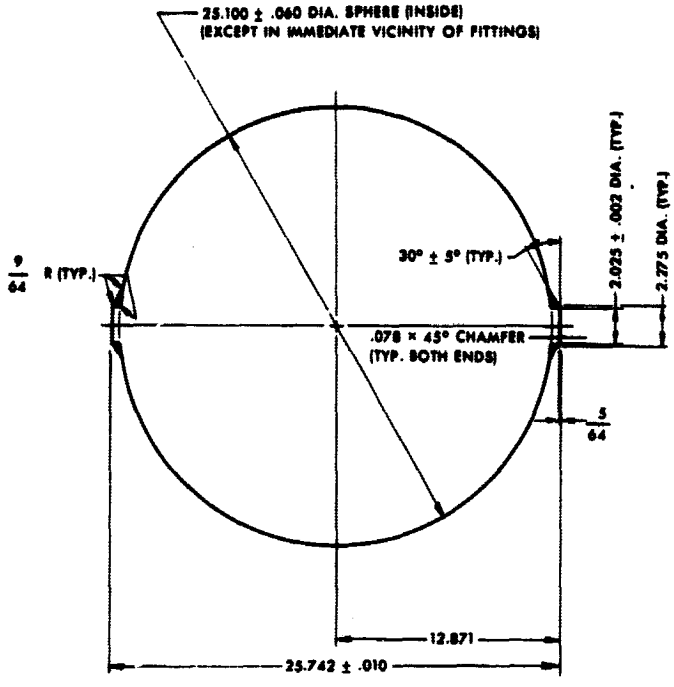


FIGURE 4.1.2-3
SPHERICAL CONTAINER

4.1.2.1.2 Hydrogen System Pressure Vesse

The hydrogen system pressure vessel was intended to be fabricated by the cryoform process, as was the oxygen vessel. However, due to problems encountered during the fabrication of this vessel (which will be discussed in detail later in this report), a backup pressure vessel fabrication technique was utilized to provide a suitable vessel for the hydrogen storage tank.

The pressure vessel was fabricated by welding two Inconel 718 hemispheres at the girth. These hemispheres were formed from flat Inconel sheet by hydraulic bulge forming into a female cavity. A boss fitting similar to that used in the oxygen pressure vessel was welded into each hemisphere at the pole prior to the girth

weld operation. After welding the girth, the vessel was hydrostatically stretched to the desired dimension at room temperature. The stretching operation was required in order to utilize existing bulge forming tooling, hence preventing excessive schedule slippage. Subsequent to the stretching operation the vessel was age hardened in order to provide maximum mechanical properties. The general configuration of the vessel was the same as that shown in Figure 4.1.2-3 for the oxygen pressure vessel except that the dimensions were as given in Table 4-2.

4.1.2.1.3 Quantity Sensor

The quantity sensor mounted within the storage vessel is an interleaf capacitor type sensor, an example of which is shown in Figure 4.1.2-4. This device operates by sensing the dielectric properties of the fluid between two capacitor plates. As can be seen in Figure 4.1.2-1, the sensor is located at the center of the tank and does not run the complete length of the instrumentation tube. Hence the sensor capacitance indicates the quantity of fluid in the tank only when the fluid is in a single phase (supercritical) condition.

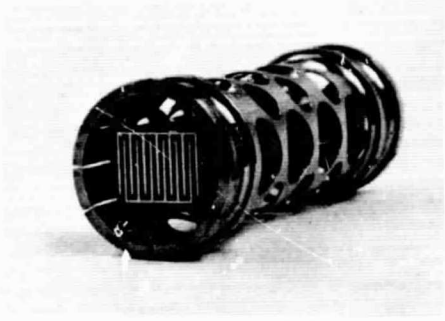


Fig. 4.1.2-4
CAPACITANCE QUANTITY SENSOR

4.1.2.1.4 Electrical Heaters

The storage tank was equipped with two electrical heaters as shown in Figure 4.1.2-1. The heaters are utilized for rapid initial system pressurization and for maintaining operating pressure when fluid is being delivered from the tank. Each heater consists of a resistance wire imbedded in magnesium oxide insulation contained within a metal sheath. The heaters are brazed to the instrumentation support tube which serves as structural support and also provides additional surface area for heat exchange. The heaters can be seen in Figure 4.1.2-5 which shows the complete internal instrumentation package. The characteristics of the heaters provided in the hydrogen and oxygen tanks are given in Tables 4-1 and 4-2.

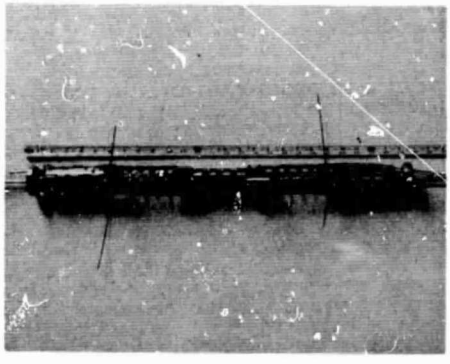


Fig. 4.1.2-5
INTERNAL INSTRUMENTATION PACKAGE

4.1.2.1.5 Motor-Fans

Two motor-fan units are mounted in the internal instrumentation tube as shown in Figures 4.1.2-1 and 4.1.2-5. The fans are so arranged that fluid warmed by the electrical heater is drawn into the fan and expelled outwardly through holes in the support tube. This stirring action eliminates significant thermal stratification of the fluid subsequent to heater operation. As can be seen from the schematic in Figures 4.1.1-1

and 4.1.1-2, each fan-heater set may be operated in either the automatic mode utilizing the pressure switch to maintain system pressure, or the manual mode whereby each heater and motor-fan may be manually energized. The characteristics of the motor-fan units are given in Tables 4-1 and 4-2.

4.1.2.1.6 Temperature Sensor

The hydrogen tank is equipped with a single temperature sensor located near the center of the tank. This sensor is a copper-constantan thermocouple and is utilized to monitor the temperature of the fluid within the tank.

The oxygen tank is equipped with four copper-constantan thermocouples positioned at various locations within the tank. These sensors are shown in Figures 4.1.2-1 and 4.1.2-5.

4.1.2.1.7 Electrical Leads

The electrical leads utilized for power input and sensor signal output consist of conductors surrounded by magnesium oxide insulation and encased in a metallic sheath. The leads pass through holes in the pressure vessel closure fittings and are brazed therein to provide a pressure seal. Similarly, after passing through the evacuated annular space the leads exit from the storage tank through a fitting welded into the outer shell.

4.1.2.1.8 Thermal Radiation Shields

The storage tank contains thermal radiation shields to reduce radiant heat input to the stored cryogen. Each shield consists of two aluminum hemispheres fabricated by the inturgescent (hydraulic-bulge) forming process. This is the same process which was utilized to fabricate the hydrogen tank pressure vessel hemispheres. Both surfaces of each were electroplated with silver to provide the lowest possible emissivity.

The shields are supported by the fill/supply and vent tubes and the electrical lead bundles within the evacuated annulus and are connected thereto with low conductivity attachments. Each set of shield hemispheres is fastened at the equator with small latching devices.

To provide vapor cooling of the hydrogen storage tank, the number two shield (second from the inner vessel) was first electroplated with copper. A copper tube was then soldered to the outer surface of the shield. Subsequent to the attachment of the tube, each hemi-

sphere was electroplated with silver to provide the required low emissivity surfaces. The physical characteristics of the shields for both the oxygen and hydrogen storage tanks are given in Tables 4-1 and 4-2.

4.1.2.1.9 Outer Shell

The outer shell of the storage vessel consisted of two hemispheres welded at the equator. The hemispheres were inturgescently formed from stainless steel sheet. The inner surface of each hemisphere was electroplated with copper to provide a low emissivity surface. The physical characteristics of the outer shells for both the oxygen and hydrogen tanks are given in Tables 4-1 and 4-2.

4.1.2.1.10 Suspension System

The suspension system consists of eight radial bumpers located by the tubulation and electrical leads which lie in two horizontal planes 45° above and 45° below the equator of the pressure vessel. Any loads are thereby transmitted radially from the inner vessel through the bumpers and shell to the mount structure.

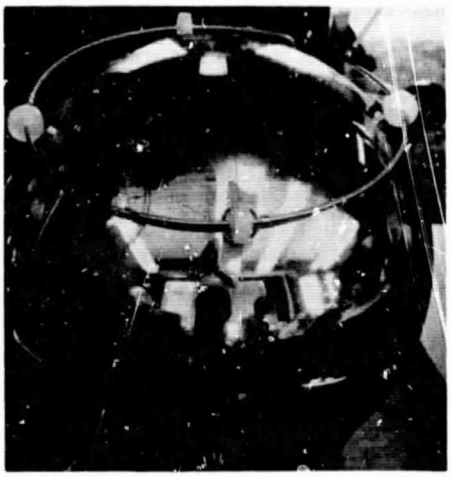


Fig. 4.1.2-6
PRESSURE VESSEL ASSEMBLY

The fill and vent tubes connect to the inner vessel fittings. Each tube then loops through an approximate 180° arc in the horizontal plane of the bumpers before exiting through the outer shell. The electrical leads exiting from within the vessel are located within the vacuum annulus in a similar manner. The tubulation and electrical leads are also utilized for locating and supporting the radiation shields.

The radial bumpers were fabricated from Kel-F. The cylindrical surface of each bumper was contoured to minimize the contact area between the bumper and the inner and outer shells.

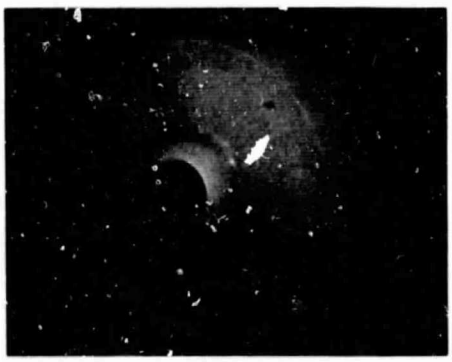


Fig. 4.1.2-7
RADIAL SUPPORT BUMPER

Figure 4.1.2-6 shows a pressure vessel with the tubes, leads and bumpers in place. Figure 4.1.2-7 shows a close up view of a radial support bumper.

4.1.2.1.11 Mount Structure

The storage tank is provided with a magnesium alloy (AZ-31B) cradle type mount carriage. The carriage can be seen in Figures 4.1-1 and 4.1-2. This mount carriage design transmits the pressure vessel loads directly to the subsystem mounting points, thus eliminating stresses in the outer shell which is not an optimum structural member.

4.1.2.2 External Components

Below are described the components which were mounted external to the storage tank. The mounting configuration for these components is clearly seen in Figures 4.1-1 and 4.1-2. It should be pointed out that they are not flight-type components but were chosen to simulate the operation of an actual spacecraft system. The manner in which these components were connected is shown in schematic form in Figures 4.1.1-1 and 4.1.1-2.

4.1.2.2.1 Solenoid Valves

Solenoid valves were utilized for the fill, supply and vent shut-off valves. These valves are latching type valves which require momentary energizing (28 VDC) for both opening and closing. In addition, each valve has a manual override which allows the valve to be opened manually in case of a power failure or malufunction, thus providing a manual means of venting. The characteristics of these valves are given in Tables 4-1 and 4-2. One of the solenoid valves is shown in Figure 4.1.2-8.

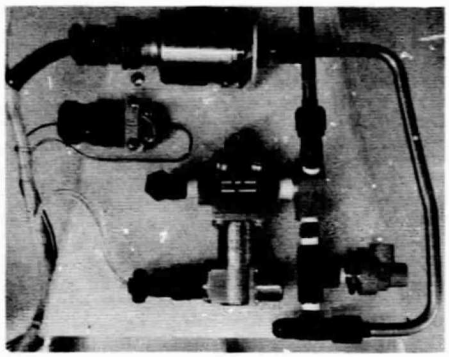


Fig. 4.1.2-8
SOLENOID VALVE, PRESSURE SWITCH, AND RELIEF VALVE

4.1.2.2.2 Pressure Switches

Two pressure switches were provided with the system. As is shown in the schematics in Figure 4.1.1-1 and 4.1.1-2, each pressure switch operates one heater-fan set. Each switch contains two single-pole double - throw snap switches connected for double-pole double - throw service. These switches are actuated by a gage pressure sensing diaphragm. The characteristics of these switches are shown in Tables 4-1 and 4-2. One of the pressure switches is shown in Figure 4.1.2.8.

4.1.2.2.3 Pressure Relief Valve

A pressure relief valve was provided in the vent line of the system to protect the tank against over-pressurization. The relief valve characteristics are given in Tables 4-1 and 4-2. The hydrogen system pressure relief valve is shown in Figure 4.1.2-8. This valve is of Bendix design and manufacture and is utilized on aircraft oxygen converters. It contains a precision metal to metal seal and is designed such that the sealing force increases as system pressure increases to the point of cracking, thus providing an accurate, repeatable cracking pressure and reliable reseating characersitics. The oxygen system relief valve was a

purchased item and is a conventional design utilizing a spring loaded poppet with a Teflon sealing surface seating to a metal seat. Both valves are of the gage pressure type.

4.1.2.2.4 Ion Pumps

The storage tank is equipped with two small (0.2 L/S) ion pumps. These pumps are used to monitor the vacuum space pressure and are capable of removing small amounts of out-gassing. Two pumps were provided for redundancy. The pumps can be seen on the top of the oxygen tank shown in Figure 4.1-2. The current draw of these pumps indicates the pressure within the evacuated annular space. A calibration curve (current versus pressure) is shown in Figure 4.1.2-9.

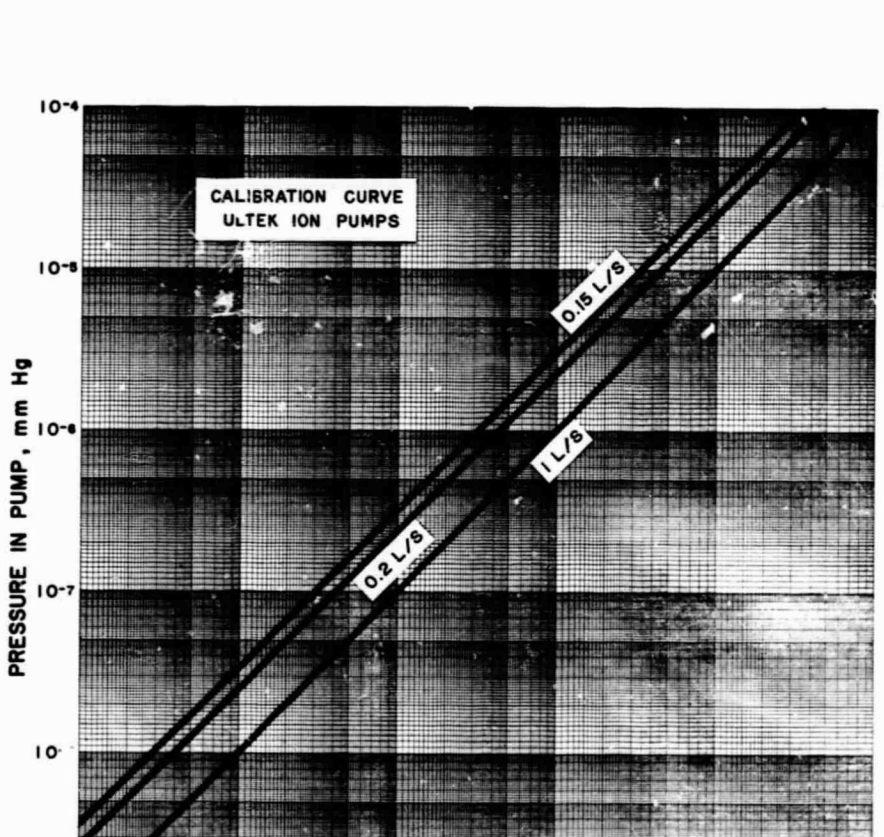


Fig. 4.1.2-9
ION PUMP CALIBRATION CURVE

4.2 Program Description

The scope of the Phase B program included the following major tasks:

1. Design of oxygen and hydrogen supercritical storage systems.

2. Development of techniques required for fabrication.

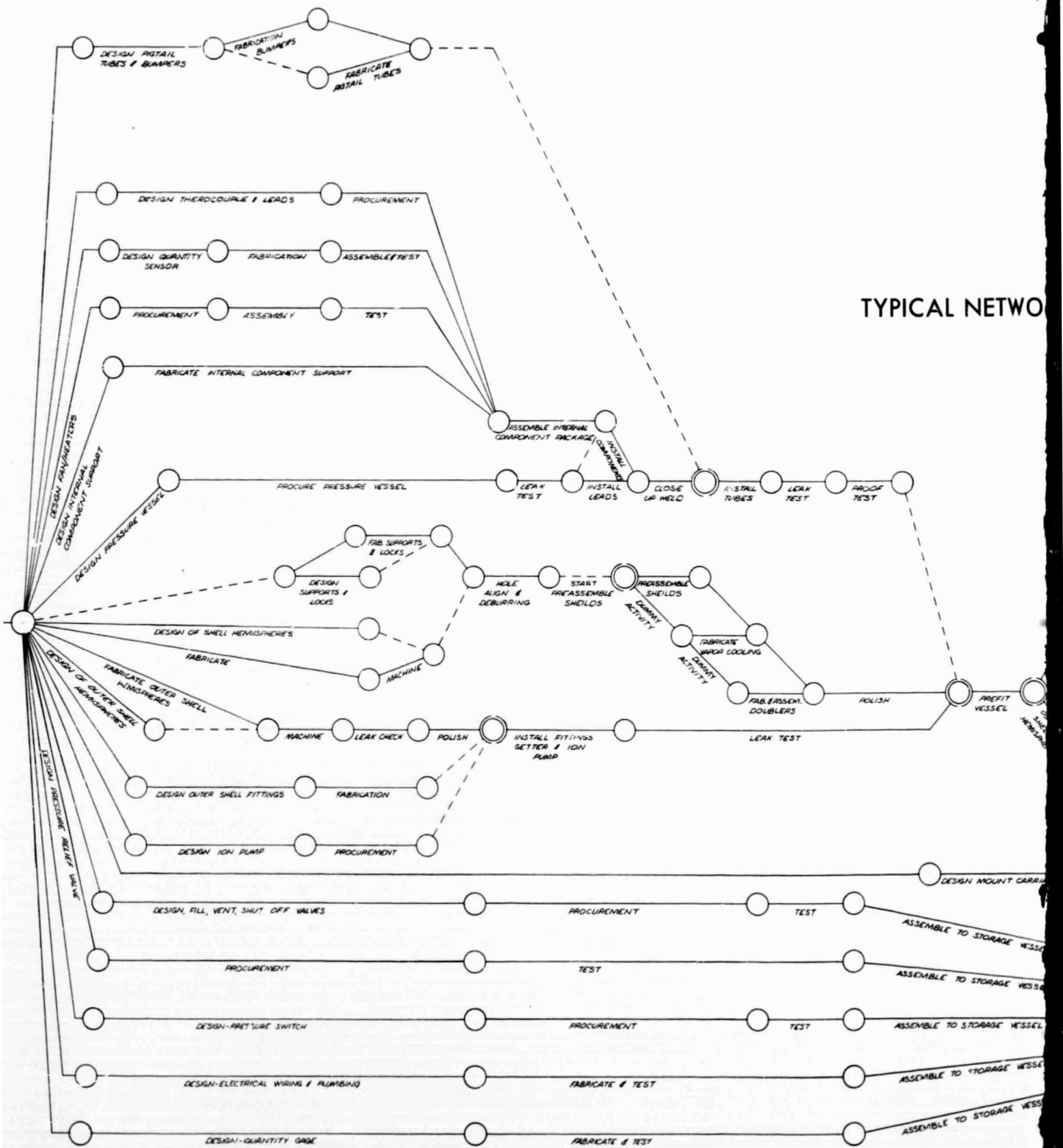
3. Fabrication of one oxygen and one hydrogen prototype system.

4. Testing of the prototype systems and delivery to NASA.

This section will discuss the tasks required to accomplish the program objectives. This will be done by describing the fabrication of the system, the problems encountered during the performance of the program, the solutions which were formulated, and the tests which were conducted to establish the system performance characteristics.

4.2.1 System Fabrication

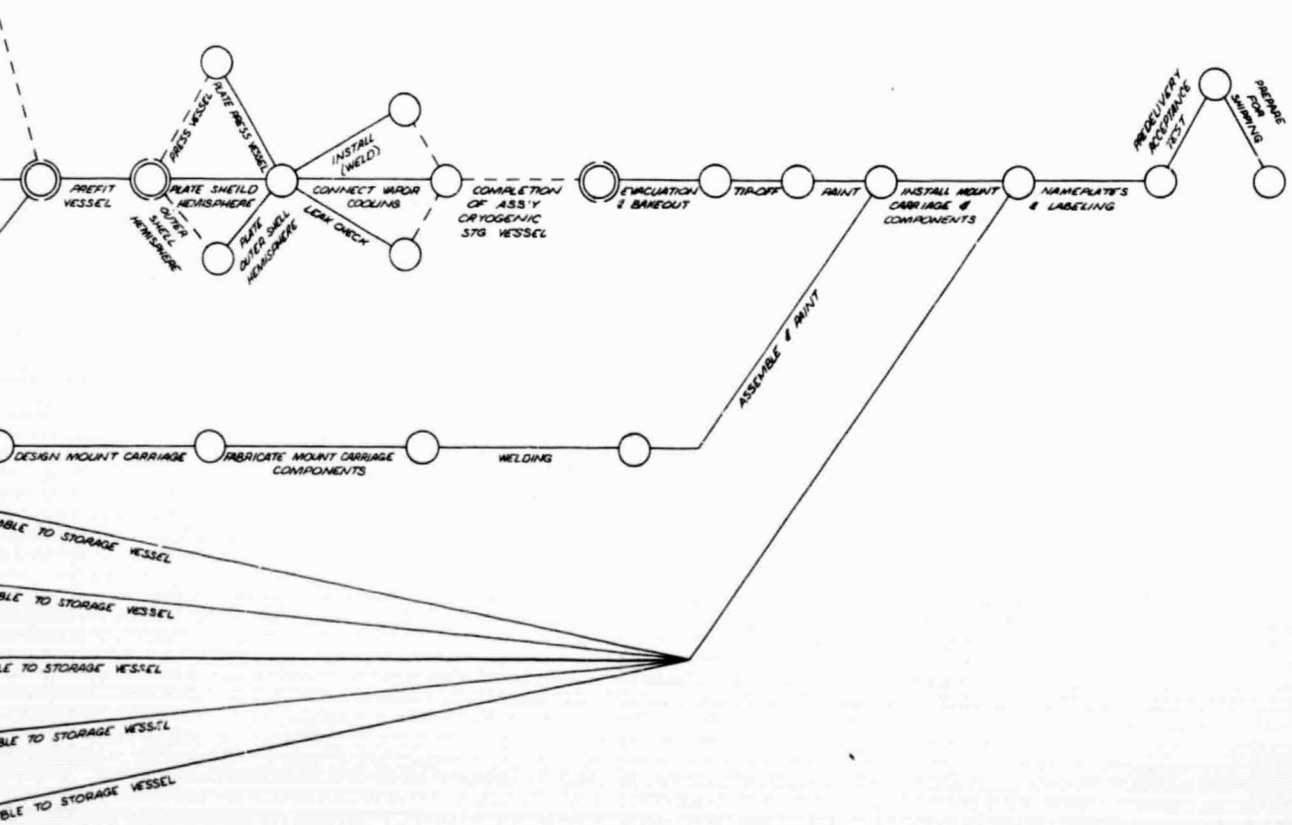
The interrelationships of the various tasks comprising a typical storage system design and fabrication effort are shown in Figure 4.2.1-1. This pert-type chart shows the location of each significant task within the program network and the constraints which the completion of any given task places on the overall program. Since the hydrogen and oxygen subsystems are very similar, the chart can be used to describe the design, fabrication and testing of either system. However, since an alternate pressure vessel fabrication technique was ultimately utilized for the hydrogen pressure vessel fabrication, the pressure vessel circuit would need to be modified to reflect the actual tasks performed in the fabrication of this vessel. This problem area and the solution thereto will be discussed in detail later in this section.



TYPICAL NETWO

FIGURE 4.12-1

AL NETWORK CRYOGENIC STORAGE VESSEL



F-3873-67-230

The following paragraphs describe the major tasks which are required to fabricate and assemble a complete storage system. These descriptions are supplemented by photographs of the various fabrication and assembly tasks and are arranged in chronological order.

4.2.1.1 Assembly of Internal Components

The following components were mounted within the pressure vessel:

1. Capacitance quantity sensor.
2. Electrical pressure-control heaters.
3. Destratification motor-fans.
4. Thermocouple temperature sensors.

The capacitance quantity sensor is shown disassembled in Figure 4.2.1-2. This sensor is of the interleaf type and the plates and plate supports are shown in photograph (a). Figure 4.2.1-3 shows the sensor mounted within the tube which was used to support it within the pressure vessel.

Figures 4.2.1-4 through 4.2.1-6 shows the various parts which were mounted within the pressure vessel. Figure 4.2.1-4 shows the capacitance quantity sensor in the center flanked by the tubes which were used to support the motor-fans heaters and thermocouples. On the right is an additional set of capacitor plates. Figure 4.2.1-5 and 4.2.1-6 show the same parts as Figure 4.2.1-4 with the addition of the closure fittings, vent and fill tubes which extend from the fittings to the top and bottom of the pressure vessel, and a destratification motor-fan.

Figures 4.2.1-7 and 4.2.1-8 show the internal component assembly with the various components installed in their final location. As can be seen in Figure 4.2.1-7, the electrical heaters were brazed to the stainless steel support tube at each end and make multiple axial passes as they proceed around the tube. The thermocouples are mounted in a coil spring fashion such that they could be brought against the support tube for insertion of the tube through the pressure vessel boss fitting and then extend within the pressure vessel to the desired locations. Figure 4.2.1-8 shows the installation and wiring of one of the destratification motor-fan units.

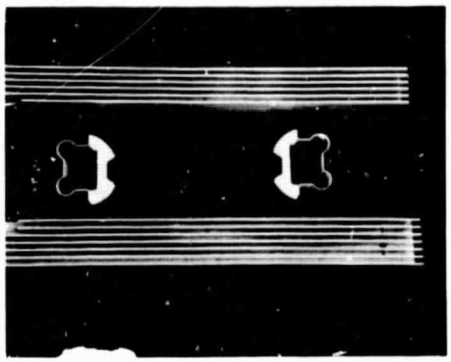


Fig. 4.2.1-2
QUANTITY SENSOR DISASSEMBLED

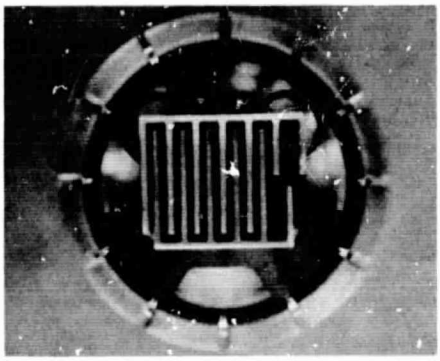


Fig. 4.2.1-3
QUANTITY SENSOR ASSEMBLED AND MOUNTED

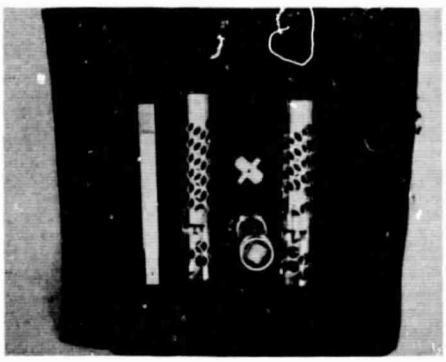


Fig. 4.2.1-4
SUPPORT TUBES

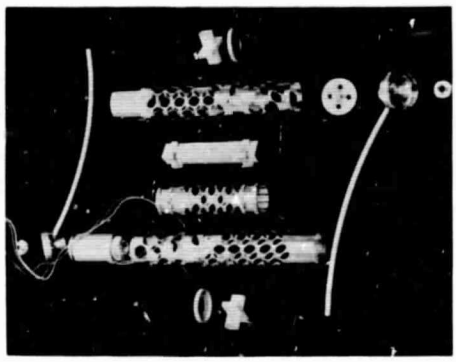


Fig. 4.2.1-5
INTERNAL COMPONENTS WITH FILL & VENT FITTINGS, TUBES

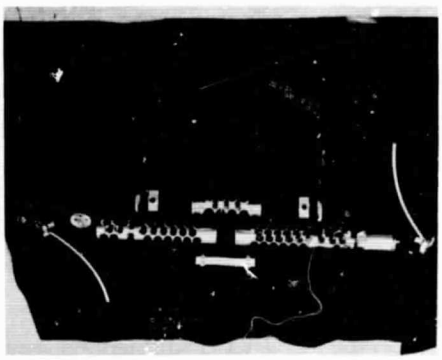


Fig. 4.2.1-6
INTERNAL COMPONENTS WITH FILL & VENT FITTINGS, TUBES

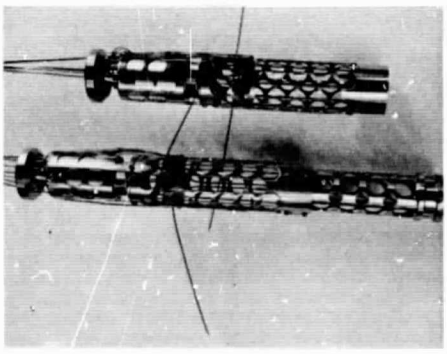


Fig. 4.2.1-7
INTERNAL COMPONENTS

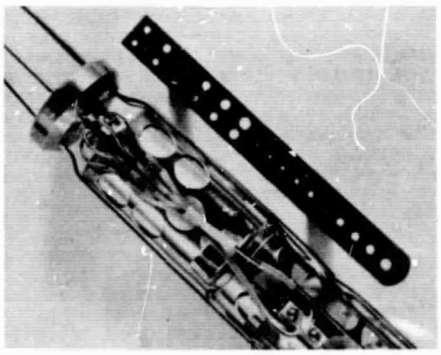


Fig. 4.2.1-8
MOTOR-FAN MOUNTED

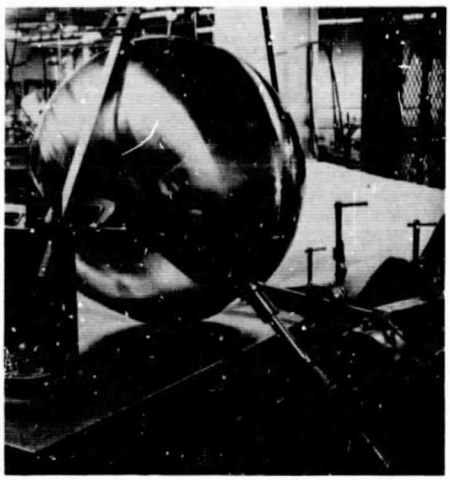


Fig. 4.2.1-9
OXYGEN PRESSURE VESSEL

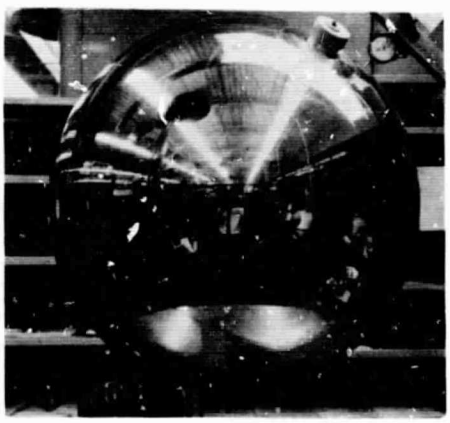


Fig. 4.2.1-10
HYDROGEN PRESSURE VESSEL

4.2.1.2 Pressure Vessel Assembly

The pressure vessel for the oxygen system was fabricated by Arde Inc. using the cryogenic stretch forming process as discussed in Section 4.1.2.1.1. Figure 4.2.1-9 shows the completed pressure vessel undergoing dimensional inspection at Bendix.

The pressure vessel for the hydrogen system was to be formed by cyrogenic stretching. However, due to the unsatisfactory results obtained from attempts to form the vessel by this process, an alternate method was utilized in order to minimize schedule slippage. The problems involved and the method which was ultimately used are discussed later in this report. The hydrogen pressure vessel is shown in Figure 4.2.1-10.

After the pressure vessel was fabricated, the internal component package was inserted as shown in Figures 4.2.1-11 through 4.2.1-13. Figure 4.2.1-11 shows the thermocouples being depressed for passage through the pressure vessel boss fitting and Figure 4.2.1-12 shows the insertion task just prior to completion. Figure 4.2.1-13 shows the pressure vessel after insertion of the internal components and prior to welding the boss closure fittings.

Figures 4.2.1-14 through 4.2.1-17 show the step-wise progression of the closure fitting weld operation. Figure 4.2.1-14 shows the fitting tack welded into position and Figure 4.2.1-15 shows the fitting after the first weld pass was completed. The tube passing through the port carried Argon purge gas. Figure 4.2.1-16 shows the fitting after the final weld pass and Figure 4.2.1-17 shows the tube connection fitting welded in place.

INTERNAL COMPONENT INSTALLATION

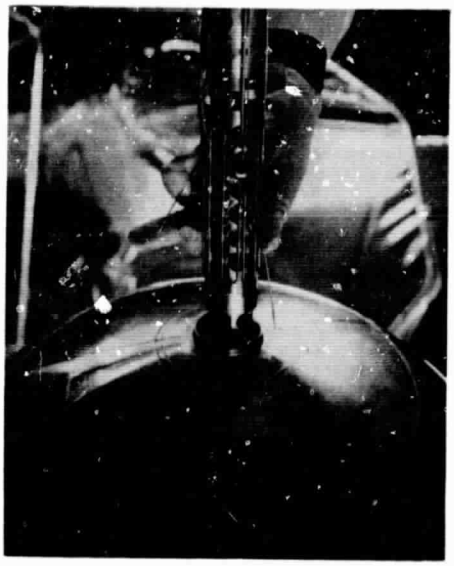


Fig. 4.2.1-11
THERMOCOUPLES DEPRESSED



Fig. 4.2.1-12
PACKAGE PARTIALLY INSTALLED



Fig. 4.2.1-13
PACKAGE INSTALLED

BOSS WELDING OPERATION



Fig. 4.2.1-14
FITTING TACK WELDED

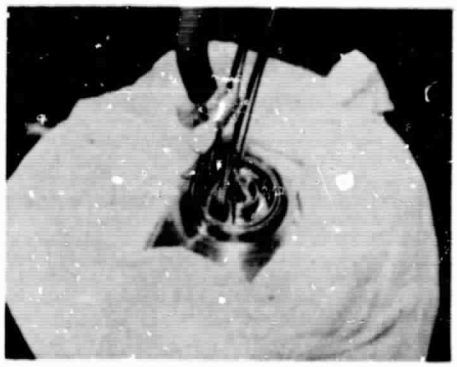


Fig. 4.2.1-15
AFTER FIRST PASS

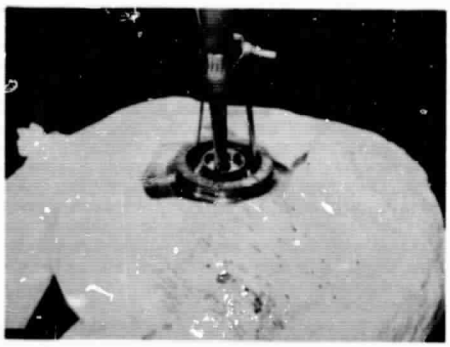


Fig. 4.2.1-16
AFTER FINAL PASS

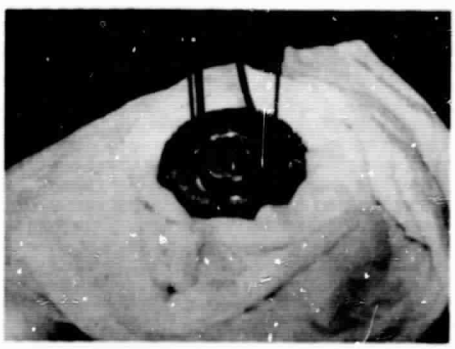


Fig. 4.2.1-17
TUBE CONNECTION FITTING WELDED

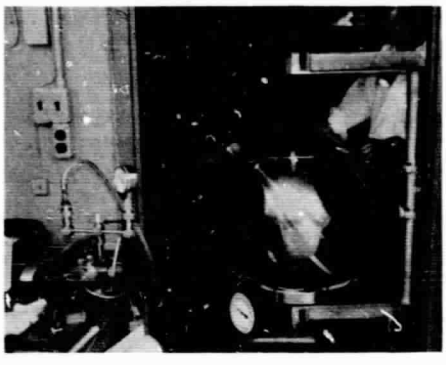


Fig. 4.2.1-18
PROOF PRESSURE TEST

Subsequent to the closure welding operation and installation of the fill and vent tubes, the pressure vessel was proof pressure tested using Freon as the pressurizing medium. Figure 4.2.1-18 shows the proof test in progress. Each completed pressure vessel was pressurized to the respective proof pressures given in Tables 4-1 and 4-2 and held for a minimum of three minutes.

Just prior to final storage tank assembly and evacuation the pressure vessel was electroplated with a thin coat of silver to provide an extremely low radiation emissive surface. Figure 4.2.1-19 shows final cleaning of the vessel prior to plating, Figure 4.2.1-20 shows transfer of the vessel from one plating solution to another, and Figure 4.2.1-21 shows the vessel after plating.

4.2.1.3 Radiation Shield Assembly

The discrete radiation shields are composed of two inturgescently formed aluminum hemispheres attached at the girth or equator as discussed previously in Section 4.1.2.1. Subsequent to forming, each of the shield hemispheres was trimmed and machined to provide the proper attachment and component penetration holes. Figures 4.2.1-22 through 4.2.1-27 show chronologically the installation of a pair of lower shield hemispheres onto a pressure vessel which has already been fitted with radial support bumpers. Subsequent to the installation of the lower shield halves, the pressure vessel was rotated to the upright position and the upper shield halves were installed, as shown in Figures 4.2.1-28A through 4.2.1-33. The pressure vessel shown is a spun aluminum mock-up used for component design and fit-up purposes prior to receipt of the actual pressure vessel.

ELECTROPLATING PROCESS



Fig. 4.2.1-19
CLEANING VESSEL
PRIOR TO SILVER PLATING

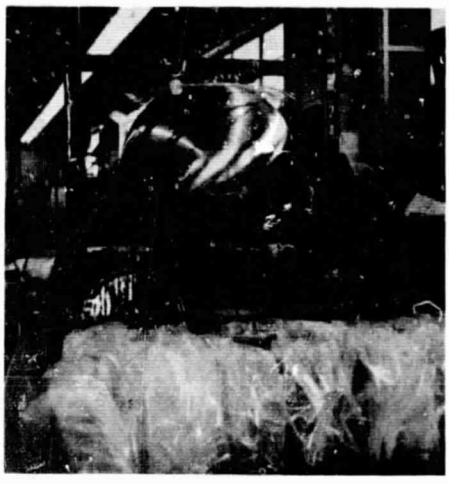


Fig. 4.2.1-20
SILVER PLATING PROCESS

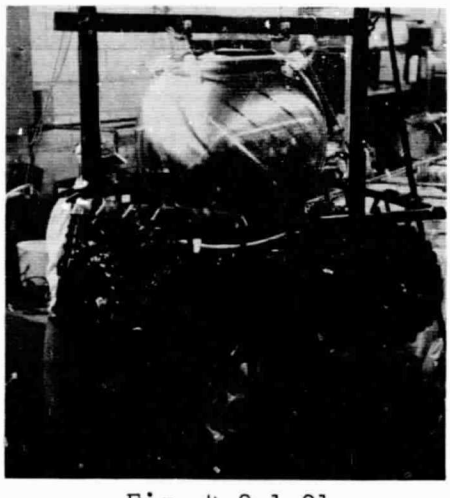


Fig. 4.2.1-21
PRESSURE VESSEL AFTER
SILVER PLATING

LOWER SHIELD ASSEMBLY



Fig. 4.2.1-22
SHIELD UNDER FIRST BUMPER

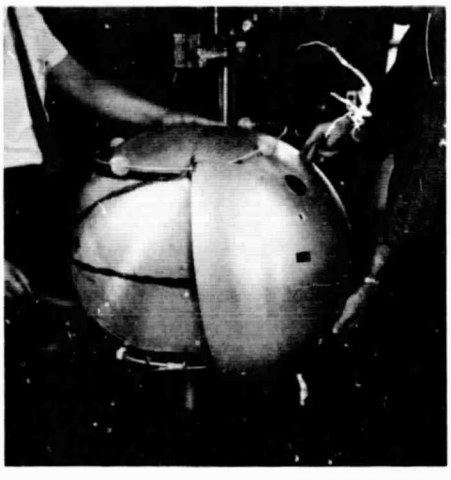


Fig. 4.2.1-23
SHIELD SEPARATING AROUND ELECTRICAL LEAD PIGTAIL



Fig. 4.2.1-24
ELECTRICAL LEADS THROUGH BOSS FITTING CUT-OUT

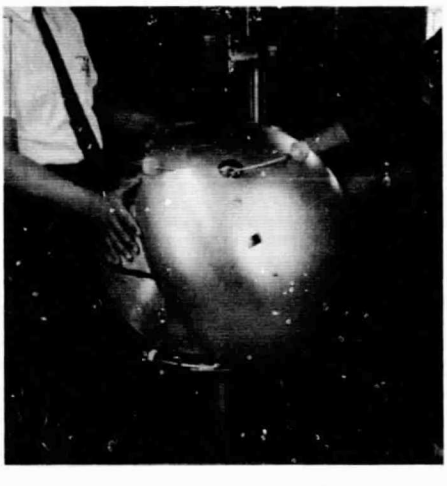


Fig. 4.2.1-25
SHIELD UNDER THIRD BUMPER



Fig. 4.2.1-26
SHIELD UNDER ALL BUMPERS

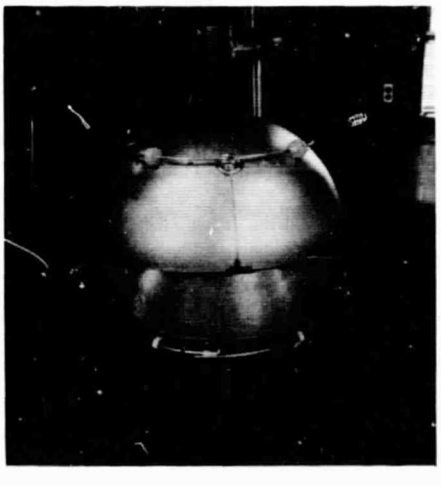


Fig. 4.2.1-27
LOWER SHIELD IN POSITION

UPPER SHIELD ASSEMBLY

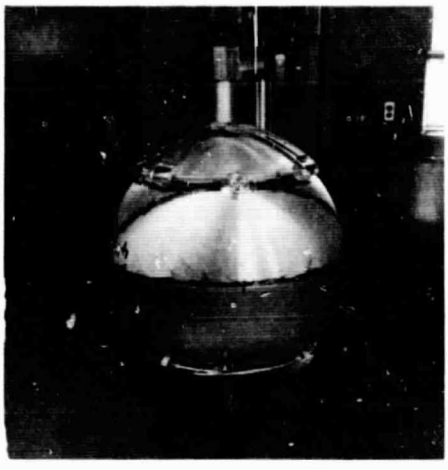


Fig. 4.2.1-28
ASSEMBLY ROTATED

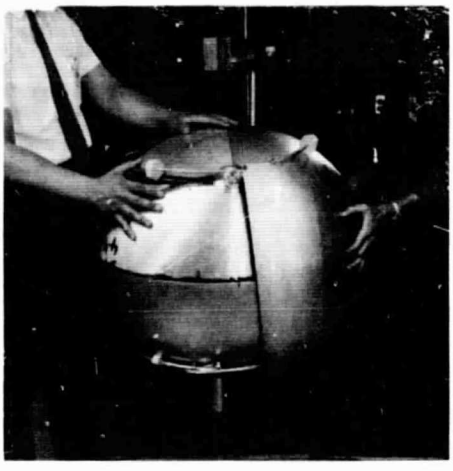


Fig. 4.2.1-29
SHIELD SEPARATING AROUND
VENT PIGTAIL TUBE

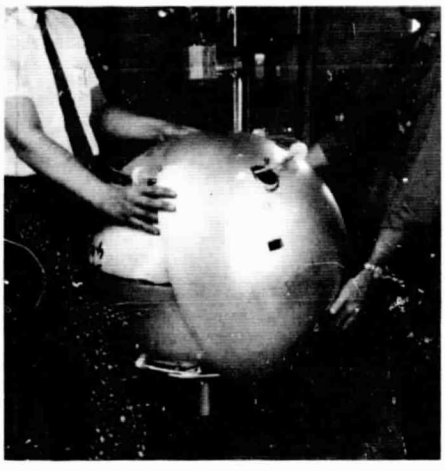


Fig. 4.2.1-30
VENT PIGTAIL TUBE THROUGH
BOSS FITTING CUT-OUT

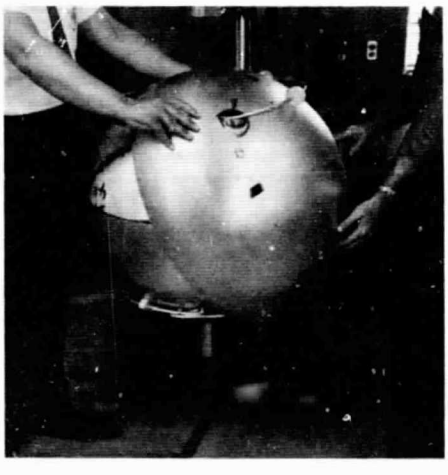


Fig. 4.2.1-31
SHIELD UNDER THIRD BUMPER

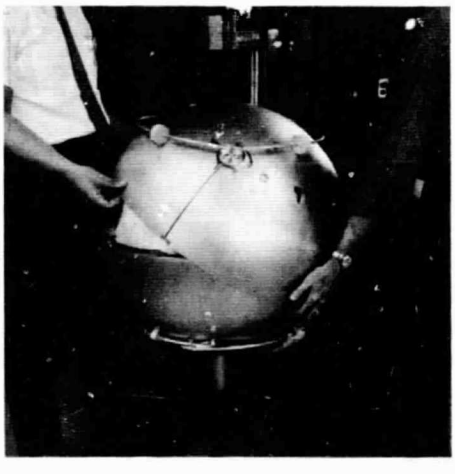


Fig. 4.2.1-32
SHIELD UNDER ALL BUMPERS

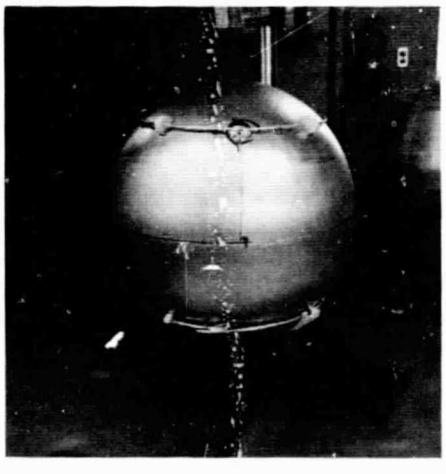


Fig. 4.2.1-33
UPPER AND LOWER SHIELDS
IN POSITION

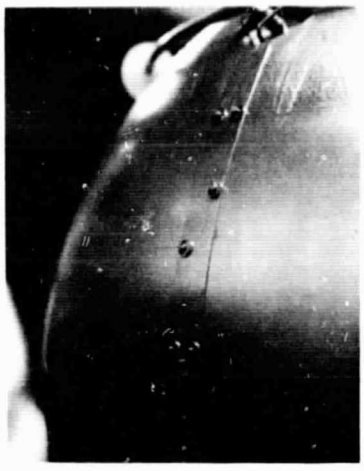


Fig. 4.2.1-34
SHIELD LATCH



Fig. 4.2.1-35
VAPOR-COOLED SHIELD



Fig. 4.2.1-36
ASSEMBLY TENT

The previous eleven figures do not show the shield halves connected at the girth. After shield installation, the shield hemispheres were connected utilizing small latching devices and doubler strips much like the connection shown in Figure 4.2.1-34. The hydrogen storage tank was equipped with a vapor cooled shield. This shield is shown in Figure 4.2.1-35. In this photograph, the tank is shown enclosed in an Argon purged bag subsequent to the shield installation operation. The vapor cooling lines can be seen running horizontally around the shield.

As with the pressure vessel, each shield hemisphere was electroplated with silver just prior to final assembly of the tank. After plating, each part was maintained in an Argon atmosphere and the assembly operation was performed with the tank in an Argon purged assembly tent shown in Figure 4.2.1-36. The maintenance of an inert Argon atmosphere over all plated surfaces and a minimization of the time elapsing between the plating operation and system evacuation greatly reduced the amount of deterioration in the emmissivity quality of the plated surfaces.

4.2.1.4 Outer Shell Assembly

The outer shell is composed of two inturgescently formed stainless steel hemispheres welded at the equator, as discussed in Section 4.1.2.1.9. Figure 4.2.1-37 shows an as-formed outer shell hemisphere undergoing dimensional inspection. Subsequent to forming, each hemisphere was trimmed and machined to provide penetration holes for the various tube and electrical lead fittings. Figure 4.2.1-38 shows an outer shell hemisphere after the trimming and machining operations had been performed. Subsequent to machining, support bumper retainers were welded into each hemisphere and each hemisphere was evacuated to ensure that it would not buckle when subjected to external atmospheric pressure. Figure 4.2.1-39 shows the bumper retainers and 4.2.1-40 shows a hemisphere buckling test.

Figure 4.2.1-41 shows an outer shell hemisphere being helium leak tested subsequent to the buckling test. Just prior to final assembly of the storage tank, the inner surface of each outer shell hemisphere was electroplated with copper to provide a low emissivity surface. Figure 4.2.1-42 shows a set of outer shell hemispheres fitted together on an assembly cart. As can be seen from the photograph,

OUTER SHELL FABRICATION

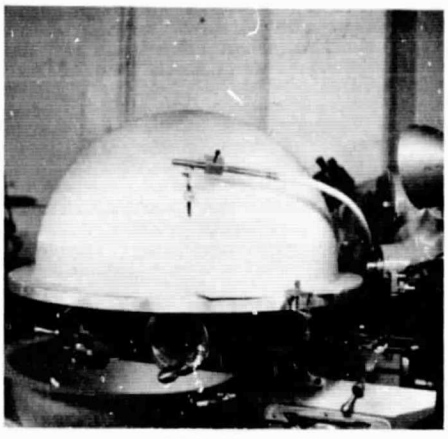


Fig. 4.2.1-37
DIMENSIONAL INSPECTION OF AS-FORMED OUTER SHELL

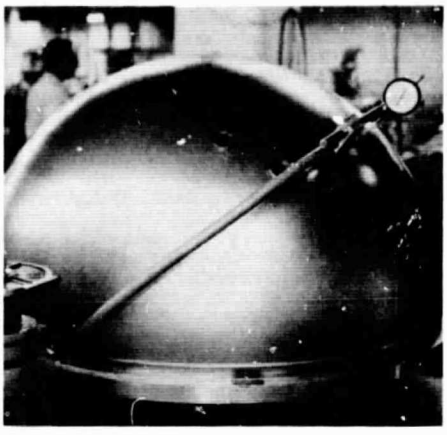


Fig. 4.2.1-38
OUTER SHELL AFTER TRIMMING AND MACHINING

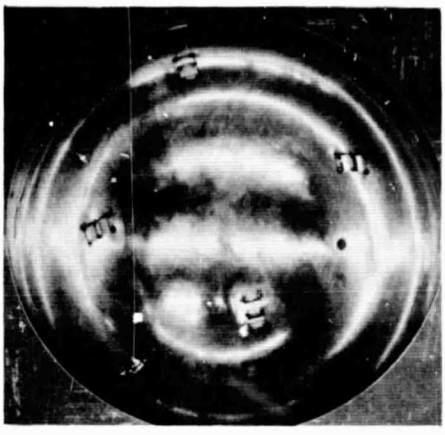


Fig. 4.2.1-39
BUMPER RETAINERS IN OUTER SHELL

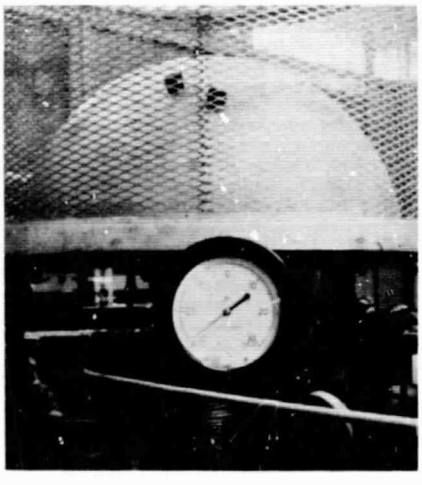


Fig. 4.2.1-40
OUTER SHELL BUCKLING TEST

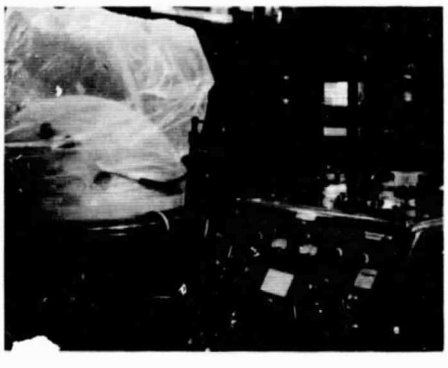


Fig. 4.2.1-41
LEAK CHECK AFTER OUTER SHELL BUCKLING TEST

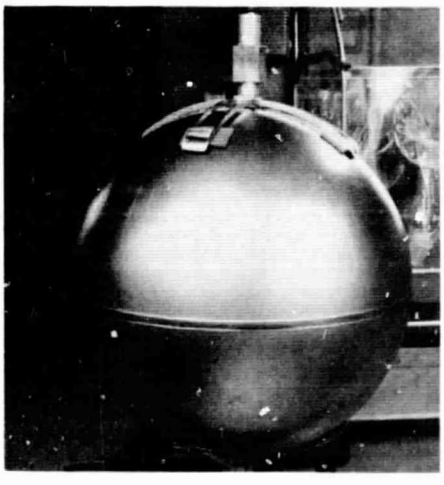


Fig. 4.2.1-42
OUTER SHELLS ASSEMBLED

one hemisphere was flared slightly at the girth such that the other hemisphere edge fits within it when assembled. Since this is a sliding joint, the outer shell hemispheres could be forced together to achieve the desired preloading of the support bumpers prior to welding of the outer shell. Figure 4.2.1-43 shows an assembled tank being helium leak tested, just after welding of the outer shell. This test is performed by evacuating the annular space and surrounding the tank with helium gas. The gas passing through the vacuum pump from the storage tank vacuum space is analyzed for helium content with a mass spectrometer. The presence of helium indicates a leak in the tank outer shell.

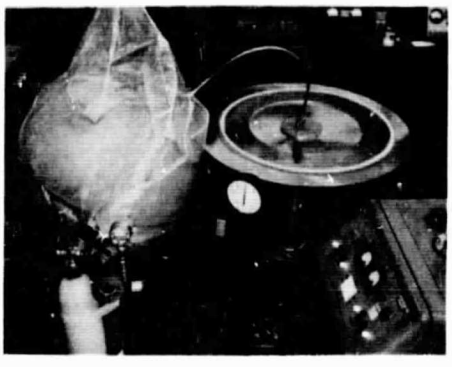


Fig. 4.2.1-43
STORAGE TANK LEAK TEST

4.2.1.5 Evacuation and Bakeout

Subsequent to the storage tank assembly and leak testing operation the tank vacuum jacket was connected to a high vacuum pumping system with a length of 1/2" O.D. oxygen-free copper tubing (tip-off tube). The tank was placed in a circulating hot air oven and evacuated to a pressure of less than 5×10^{-5} mm Hg. After this pressure was obtained, the oven temperature was increased as rapidly as possible while maintaining the pressure below 5×10^{-5} mm Hg. The maximum temperature attained was 300°F due to nonmetallic materials present in the tank. Once this temperature was reached it was maintained until a system pressure of less than 2.5×10^{-6} mm Hg was maintained for a period of at least 24 hours. At this point the vacuum system cold trap was filled with liquid nitrogen, the oven heat was turned off and the inner vessel was purged with gaseous nitrogen. When the tank temperature reached ambient, the tip-off tube was pinched near the tank with a hydraulically operated pinch-off tool, producing a cold welded vacuum space closure.

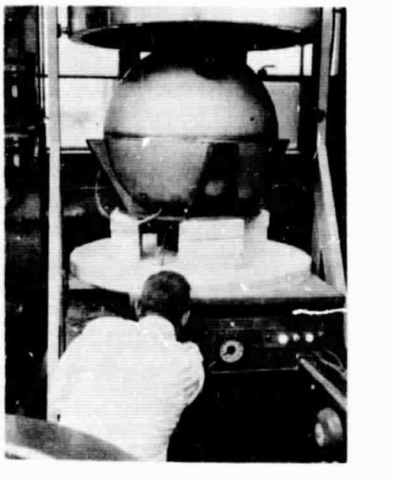


Fig. 4.2.1-44
TANK ON BAKEOUT STAND

Figure 4.2.1-44 shows the tank connected to the vacuum pumping system. The oven enclosure is suspended above the tank by an electric hoist and the pumping system is located below the table on which the tank is supported. Figure 4.2.1-45 shows the oven enclosure in the lowered position. The console at the left houses the oven air heating and circulating equipment.

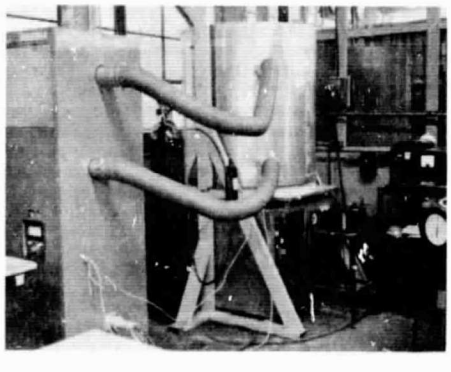


Fig. 4.2.1-45
BAKEOUT OVEN LOWERED

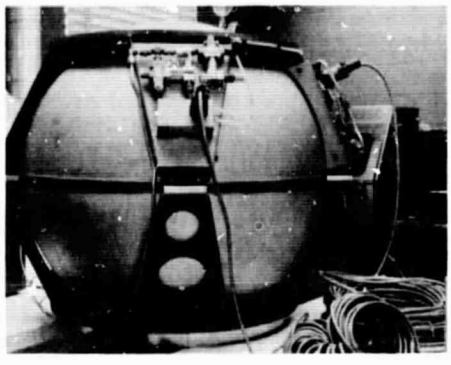


Fig. 4.2.1-46
EXTERNAL COMPONENT ASSEMBLY

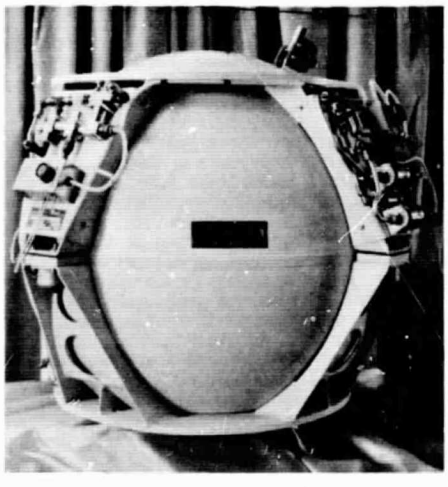


Fig. 4.2.1-47
COMPLETED STORAGE TANK

4.2.1.6 External Component Assembly

Subsequent to the evacuation and bakeout operation, the external mount structure and various external components were installed on the storage tank. Figure 4.2.1-46 shows the tank during the external component assembly operation and prior to painting of the unit. Figure 4.2.1-47 shows the unit after completion of assembly and painting.

4.2.2 System Performance Tests

Throughout the program, testing of the system components was conducted to verify their performance and safety before they were installed. Subsystem assemblies were also tested whenever practicable.

The tank which was fabricated during the Phase A portion of the program was used to provide expected heat leak values and surface emissivity values. The results obtained from tests performed on this tank were used as a guide for the design of the systems during Phase B of the program.

Both the oxygen and hydrogen systems were subjected to tests by Bendix to determine the thermal characteristics of each. In addition, the oxygen system was subjected to a cursory random and sinusoidal vibration test to demonstrate its structural integrity.

4.2.2.1 Oxygen System Tests

4.2.2.1.1 Vented Heat Leak Tests

These tests were performed by filling the tank with cryogenic liquid and measuring the vent rate of the vaporized liquid while the storage tank was vented to atmosphere. In this manner the heat leak through the storage tank insulation was determined from the heat of vaporization of the liquid contained in the tank. The oxygen system was tested with three different fluids and the results are given in Table 4-3. The temperature given with heat leak value is the average environmental temperature at which each test was performed.

TABLE 4-3
PHASE B OXYGEN VENTED HEAT LEAK TESTS

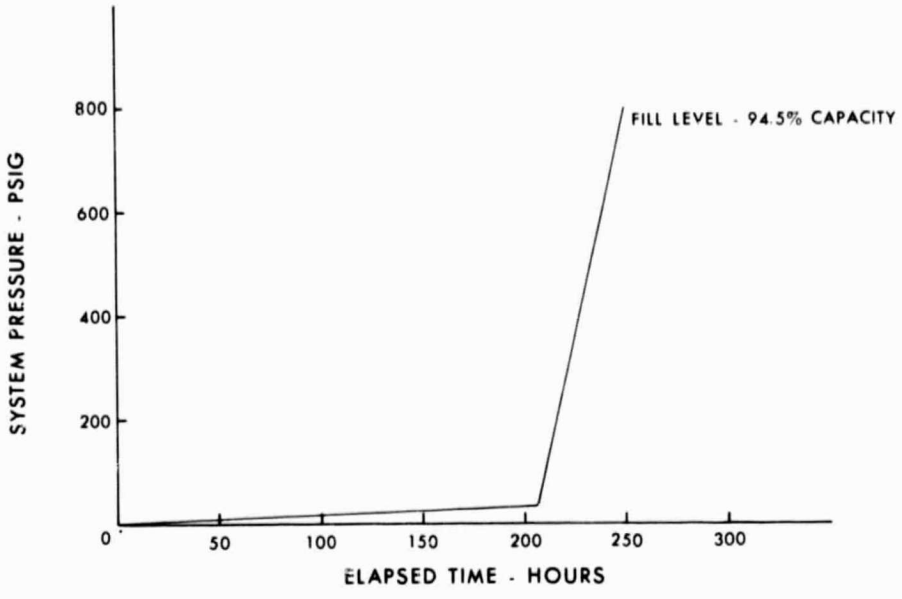
TEST FLUID	HEAT LEAK (BTU/HR)	ENVIRON. TEMP. (°F)
* LO_2	11.7	75
LN_2	10.3	70
LN_2	4.6	-65
LH_2	7.9	70

The changes in storage tank heat leak with different test fluids are attributable to the effects which the changes in contained fluid temperature have upon the insulation system. In a tank utilizing the discrete shield-radial bumper insulation design in which a large proportion of the heat leak is through radiant heat transfer, this decrease in heat leak as the contained fluid temperature decreases must be attributed predominantly to changes in the emissivity characteristics of the various surfaces as their temperatures change.

4.2.2.1.2 Pressure Buildup and Equilibrium Flow Test

This test was performed by first filling the storage tank to approximately 95% of its capacity with liquid oxygen. After allowing the tank to thermally stabilize it was topped off and the vent valve was closed. The system was then allowed to pressurize at the rate dictated by the ambient heat leak of the tank. The rate of pressure build up was monitored and is shown in Figure 4.2.2-1 as a function of elapsed time from the time when the vent was closed. As is shown in the figure, the initial tank fill level at the time of vent closure was 94.5% of its capacity. The quantity of liquid in the container was determined by monitoring the system weight.

* Value determined during NASA test program.

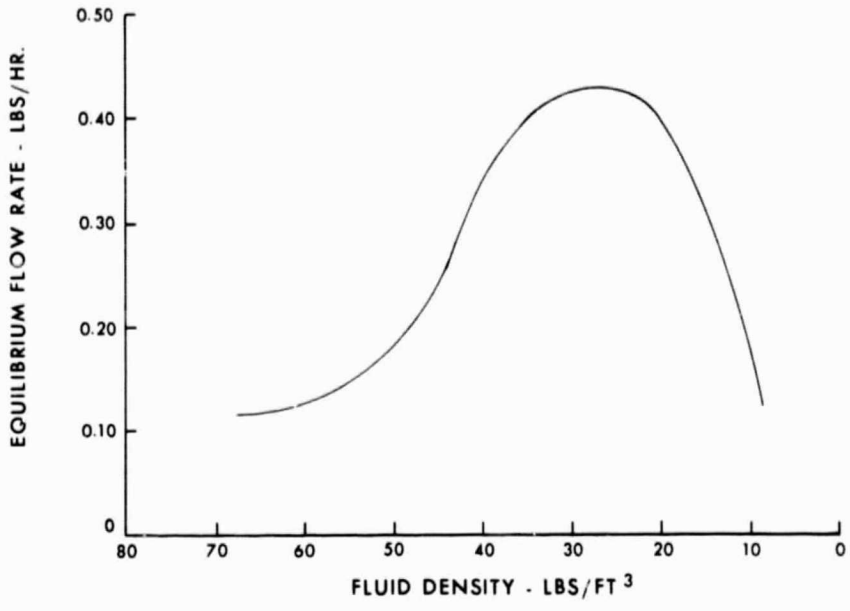


AMBIENT HEAT LEAK PRESSURE BUILDUP

FIGURE 4.2.2-1

A-3873-67-238

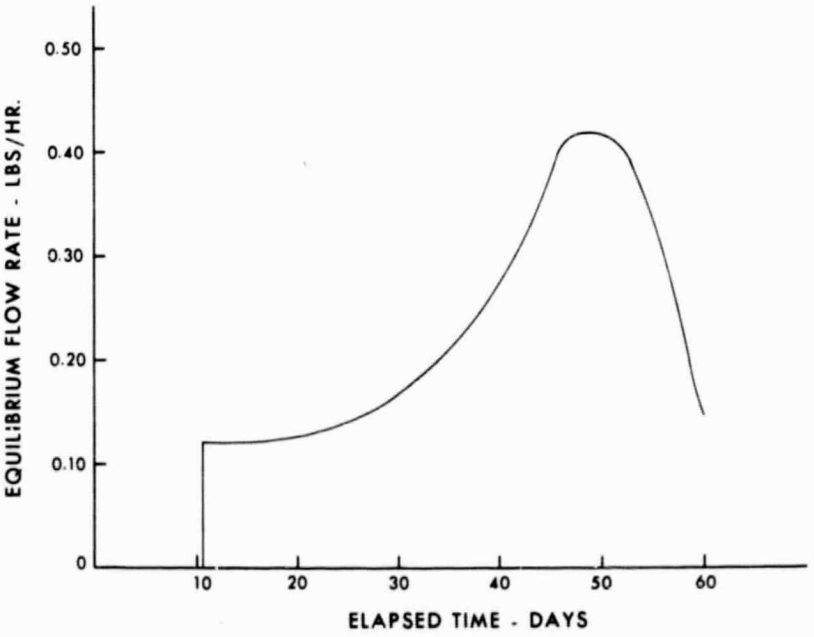
When the system pressure reached 800 psig, it began to vent through a gage pressure type relief valve. The system was allowed to vent at the rate dictated by the ambient heat leak of the storage tank while the system pressure was maintained by the relief valve. This flow rate was determined by monitoring the system weight and is referred to as the system equilibrium flow rate. The equilibrium flow rate as a function of average fluid density is shown in Figure 4.2.2-2 and as a function of elapsed test time from the point of vent closure in Figure 4.2.2-3. The average environmental temperature during this test was 75°F. The variation in flow rate as the tank depleted was due to the combination of two factors. First, the dQ/dm (heat required to expel a unit mass) of the supercritical fluid density, and secondly, the heat leak through the storage tank insulation change as the temperature of the fluid increases throughout the test period.



EQUILIBRIUM FLOW PROFILE (DENSITY)

FIGURE 4.2.2-2

A-3873-67-239



EQUILIBRIUM FLOW PROFILE (ELAPSED TIME)

FIGURE 4.2.2-3

A-3873-67-240

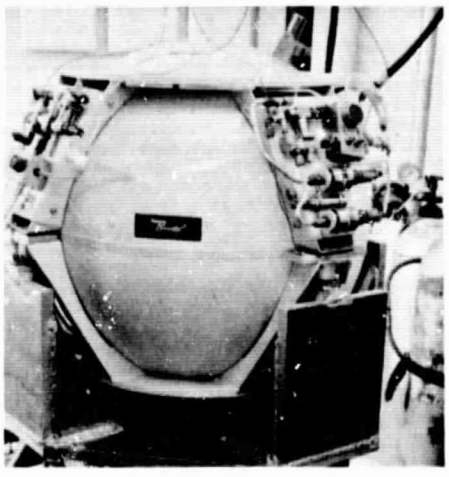


Fig. 4.2.2-4
OXYGEN SYSTEM VIBRATION TEST

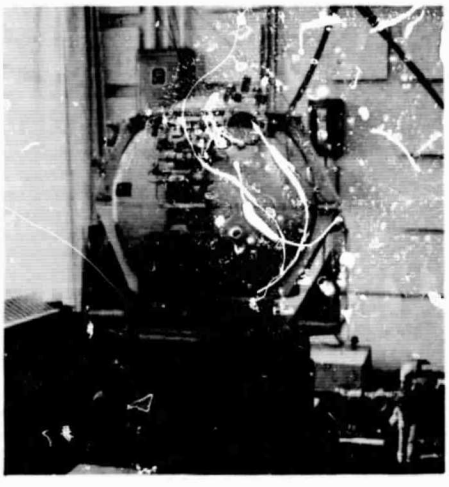
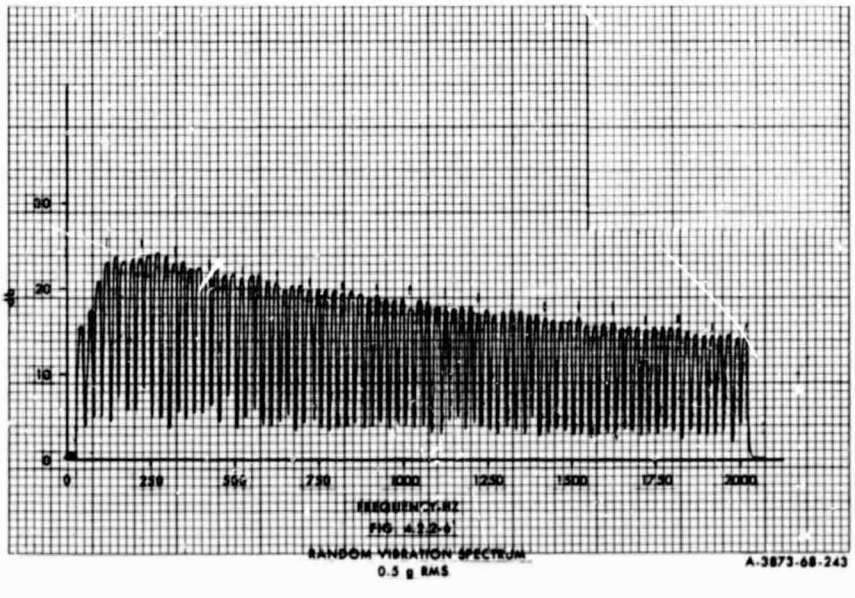


Fig. 4.2.2-5
OXYGEN SYSTEM VIBRATION TEST

4.2.2.1.3 Vibration Tests

The oxygen system was subjected to both sinusoidal and random vibration. Since it was desired to retain the storage tank for further thermal testing, the unit was subjected to reduced vibration levels to observe the behavior of the tank under dynamic loading conditions. Figures 4.2.2-4 and 4.2.2-5 show the unit mounted on the shaker head. A sinusoidal vibration test was performed for a period of 18.8 minutes, sweeping a frequency range of 15-2000 Hz. The unit displayed favorable characteristics under vibration loading throughout the sweep cycle. The only significant storage tank resonance point occurred in the 26-38 Hz range. It was felt that this point could be suppressed by modification of the soft mounts which are attached to the mount frame should it reach destructive magnitudes when the system is vibrated at launch levels. All other resonant points were of a minor nature or occurred in the external components which are not representative of items which would be provided on a flight article. Subsequent to the sinusoidal sweep, the unit was subjected to a random vibration spectrum, as shown in Figure 4.2.2-6, for a period of 12.3 minutes. The unit withstood this loading quite satisfactorily and displayed a resonance point in the same region (26-38 Hz) as in the sinusoidal tests. After the testing was completed the unit was subjected to a vented heat leak test with liquid nitrogen and the results confirmed no degradation of insulation quality.



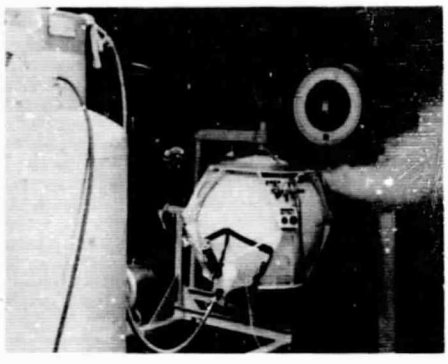


Fig. 4.2.2-7
LHe FILL
PHASE B HYDROGEN SYSTEM

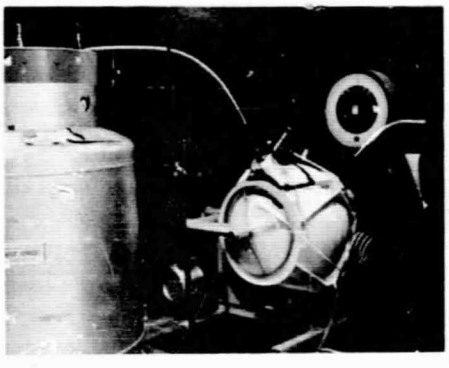


Fig. 4.2.2-8
LHe FILL
PHASE B HYDROGEN SYSTEM

4.2.2.2 Hydrogen System Tests

The hydrogen storage system was subjected to a series of vented heat leak tests in the same manner as was the oxygen system. The results of these tests are presented in Table 4-4.

TABLE 4-4
PHASE B HYDROGEN VENTED HEAT LEAK TESTS

TEST FLUID	HEAT LEAK (Btu/hr)	ENVIRON. TEMP. (°F)
LN_2 (no vapor cooling)	9.1	70
LH_2 (no vapor cooling)	8.0	70
LH_2 (vapor cooling)	2.9	55
LHe (no vapor cooling)	5.3	70
LHe (vapor cooled)	1.7	70

From the above data it can be seen that vapor cooling of the second radiation shield has a significant effect on the heat leak of the tank for hydrogen and helium storage. It should be pointed out that thermodynamic calculations indicate that vapor cooling of the innermost radiation shield would be even more efficient in reducing the heat input to the contained fluid. The figures at the left show the hydrogen system undergoing vented heat leak tests at the Bendix facility. Figure 4.2.2-7 shows a liquid helium filling operation with the tank in the upright position. Figure 4.2.2-8 shows the same operation with the tank in the horizontal position for vapor cooling of both shield hemispheres.

4.2.3 Problem Areas and Solutions

This section discusses the significant engineering problems which were encountered during the course of the program and the solutions which were formulated in order to successfully meet the objectives of the program.

4.2.3.1 Pressure Vessel Procurement

As was discussed in Sections 4.1.2.1.1 and 4.1.2.1.2, the pressure vessels for these storage tanks were intended to be formed by the cryogenic stretch forming technique. The fabrication of these pressure vessels by Arde Inc. of Paramus, New Jersey, was the major cause of schedule slippage during this program. It

should be pointed out, however, that this process is of a developmental nature and therefore has not been well defined, and a great deal of experience does not exist concerning the process.

4.2.3.1.1 Oxygen Pressure Vessels

Twelve sets of composite preform parts were put into process for the fabrication of oxygen pressure vessels for this program. All twelve of these sets were welded into composite preforms and stretched at cryogenic temperatures. Of the twelve, eight failed to yield pressure vessels. Below is a listing of these failures.

1. Three units failed during the third stretching operation.

2. Three units failed during the final stretching operation.

3. One unit completed the stretch forming operation but failed during proof pressure testing at 1280 psig. This tank attained the required cryoformed strength and size but was improperly heat treated.

4. One unit developed the required strength but was undersize.

The four completed pressure vessels were delivered to Bendix for utilization on this program. Although these vessels were not within the drawing tolerances for sphericity, they were found acceptable for the purpose of this program and one vessel was successfully utilized in the oxygen storage tank.

Upon analysis of the failure which occurred during this fabrication program, it was determined that the major cause for these problems was insufficient process control. The very nature of this technique of metal forming requires the preform to be of extremely high quality, both in dimensions and in material properties. For this reason, a stringent nondestructive testing program must be pursued throughout the fabrication of the preform in order to ensure that it will withstand the stretching operation and yield a satisfactory pressure vessel. The necessity of a program of this type is exemplified by the fact that the majority of the failures listed above were traced to areas of insufficient wall thickness which existed in the preform prior to the stretching operation. It is felt that the finished vessel dimensional control problems can be solved by performing a final sizing operation in a closed die.

4.2.3.1.2 Hydrogen Pressure Vessels

The pressure vessels intended for use in the hydrogen storage tank suffered from similar problems which occurred in the forming of the oxygen pressure vessels. Control of preform quality was even more critical for this vessel since the wall thickness was considerably less than that of the oxygen unit.

Due to the fact that the pressure vessels for the hydrogen tank must retain their toughness at -423°F, these vessels had to be formed from material having a special chemical composition. The material used was 301 stainless steel having an extremely low silicon content since it was determined that silicon content above a certain level caused toughness deterioration at temperatures below -320°F. For this reason it was necessary to obtain special heats of material for forming the hydrogen pressure vessels. The first heat of material obtained had to be rejected due to improper chemical composition. The second and third heats were found to contain unacceptably large inclusions and the fourth heat of material was found to be acceptable for the purposes of cryoforming pressure vessels. This delay in obtaining suitable material caused considerable schedule slippage in the program. In future programs it will be necessary to recognize the problems involved in obtaining material of the proper composition and initiate procurement at the earlist possible date. Also, it will be necessary to coordinate closely with the material supplier in order to ensure that the proper quality control procedures are followed, to provide a high probability of obtaining the desired composition from the first heat of material.

Upon receiving an acceptable billet of material, it was formed and welded into six composite preforms for pressure vessels. During the cryoforming operations the following failures occurred.

1. One unit collapsed during quenching following annealing after the third stretching operation. The failure was due to a kinked purge line which caused the pressure within the vessel to decrease during cool-down.

2. Three units burst during the stretching operation.

3. One unit completed the stretch forming operation but failed during proof pressure testing at 450 psig.

Each of the burst failures was traced to preform thin spots, as with the oxygen pressure vessels, again indicating a need for stringent quality control of preforms. This thinning problem occurred predominantly in the conical section of the preform which was spun formed (see Figure 4.1.2-2).

One pressure vessel was successfully formed, heat treated, polished and proof tested to 330 psig. A deviation was granted to proof test at this reduced pressure due to the high probability that the unit contained thin areas similar to those present in vessels which failed. Upon receipt by Bendix, however, this vessel was found to be unacceptable for use in the hydrogen storage tank. The following defects were found upon inspection of the vessel.

1. The surface finish had high and low areas resembling a course orange peel. This was probably the result of heavy scaling that had never been completely removed. Because of this surface condition subsequent polishing touched only the high surface areas, leaving the low areas unpolished. However, even the polished areas were not as bright as the oxygen vessel. It was concluded that the hydrogen tank received a much lighter polish than the oxygen vessel.

2. A crack or tear in the vessel wall adjacent and perpendicular to a girth weld had been repaired by a weld approximately .187 inches long.

3. There was a straight crease in the vessel wall approximately 8 inches long.

4. An area of the surface covering approximately 8 square inches had been severly wrinkled and it appeared that an unsuccessful attempt was made to straighten out the wrinkles.

5. Actual vessel weight was 14.4 lbs. or 20% less than the nominal calculated weight. This indicated vessel wall thickness was considerably less than minimum design requirements.

As the effort to cryoform a pressure vessel for the hydrogen tank progressed at Arde Inc., Bendix initiated a backup program in order to minimize schedule slippage due to the failure of the cryoforming process to yield an acceptable pressure vessel. This backup program was twofold in nature. First, an effort was initiated to form Inconel hemispheres by the hydraulic bulge forming

(inturgescent) process using existing tooling which was somewhat smaller than the desired pressure vessel. The hemispheres were then to be welded together to form a sphere and hydraulically stretched to the desired diameter. The second approach was to initiate the fabrication of the tooling required to inturgescently form Inconel hemispheres to the desired diameter. These hemispheres would then be welded together to form a spherical pressure vessel.

Under this program, a set of 26.53" O.D. Inconel "X750" hemispheres were initially received by Bendix. These hemispheres were fabricated from material which was on hand at the forming facility. After receipt, each hemisphere was inspected and a 5.875" diameter hole was cut in the pole of each to accept a boss fitting similar in configuration to those used in the cryo-formed vessels. Fitting contour from the boss out to the shell wall was designed to stretch with the vessel as it was formed to the desired size. Fitting shape in the stretch area was influenced by stretch tests conducted on three differently shaped fittings subjected to stretching as part of a sphere. These fittings were machined from Inconel "X750" forgings since it was felt that forged material would be best suited for the stretching operation. After the boss fittings were welded into each of the hemispheres, the hemispheres were TIG welded together. Figure 4.2.3-1 shows a boss fitting tack welded into one of the pressure vessel hemispheres. Parallel to the above activities, tensile test specimens were fabricated from Inconel "X750" sheet material and tested to obtain stress-strain curves and fracture point data for use during the stretching operation. After welding, the vessel was submerged in a tank of water and filled with water for pressurization. This action eliminated loads on the shell which would have been induced by supporting the vessel when filled. Water was then pumped into the vessel in order to hydraulically stretch it to size. Dimensional growth of the vessel was monitored and recorded during the entire stretching operation. The vessel ruptured during stretching after having increased in diameter from 26.53" to 28.14". The desired diameter was 28.29. Initial stretching occurred around the girth weld and in the end fittings. Both areas were somewhat thicker than the rest of the vessel; however, because of the heat effected weld zone and the fact that the fittings were annealed, they offered less resistance to movement.

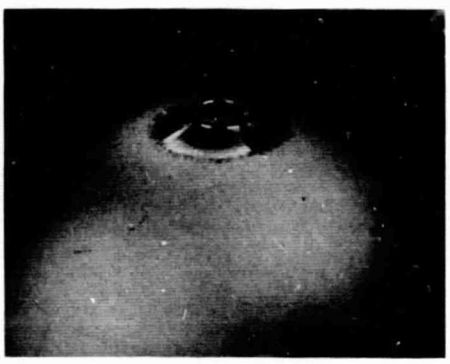


Fig. 4.2.3-1
PRESSURE VESSEL BOSS FITTING

Because of original fitting contour, fitting stretch had little or no effect on pole to pole vessel growth. This coupled with early movement in the girth area produced

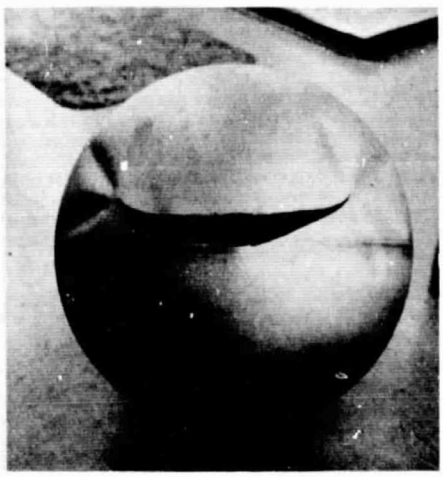


Fig. 4.2.3-2
RUPTURED PRESSURE VESSEL

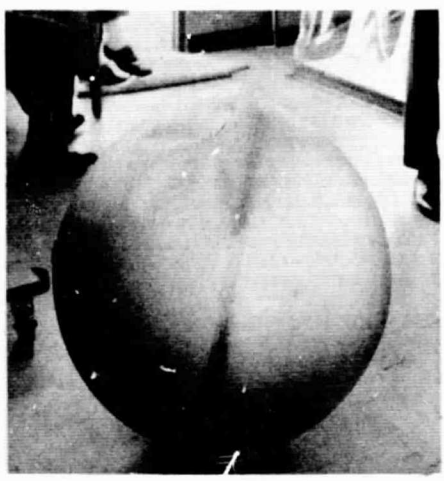


Fig. 4.2.3-3
RUPTURED PRESSURE VESSEL

a pumpkin shaped vessel during initial stretching. As stretching continued this out-of-spherical condition decreased somewhat as less worked areas began to move at a faster rate than previously worked areas.

The failure occurred between 420-430 psi. The bottle was cut into sections suitable for checking wall thickness, mechanical and physical properties and contour. The rupture started parallel to the girth approximately .187" away from the outer edge of the girth weld in the area of greatest movement. Prior to stretching, the location of the failure was closer to the weld and within the heat effected weld zone. The dead annealed condition as a result of welding and the fact that shell hardness ranged from 81 RH_B at the girth to 92 RH_B at the dome contributed to more stretching in the girth than other areas. Hence, wall thickness was reduced to a point below that required for adequate strength at 425 psi. Wall thickness in the area adjacent to the break varied from .028" to .025" and hardness measured 95 on the Rockwell "B" scale. A calculation based on a .028" wall yields a 107,500 psi stress which is close to the 110,000 psi ultimate tensile strength value obtained from uni-axial tensile tests on several coupons of Inconel X750. Figures 4.2.3-2 and 4.2.3-3 shows the pressure vessel after rupturing.

It was concluded that the vessel ruptured in an area that initially was relatively soft and thus stretched more than the rest of the vessel until the wall thickness decreased below that required for adequate strength. Based on experience gained in stretch forming the Inconel X750 vessel, a program was initiated to stretch a second vessel. The hemispheres selected had been in the forming process during the period that the first vessel was being fabricated and stretched. These hemispheres were identical to those used in the first vessel except that they were fabricated from Inconel 718 which was felt to be suitable for a cryogenic pressure vessel application. Since the analysis of the first vessel showed a considerable variation in material hardness at various locations, with failure occurring in a soft region, it was decided to solution anneal both hemispheres after installation of the boss fittings in order to obtain uniform mechanical properties throughout the vessel. After heat treating test coupons of Inconel "718" at various temperatures, it was decided to anneal both hemispheres at 2000°F for 15 minutes to obtain a hardness similar to that which was expected in the girth weld region. After annealing, the hemispheres were welded together and stretched in the same manner as the first vessel

until a stress level was reached which was considerably below the nominal ultimate strength of the material. At this point the vessel was again solution annealed, but due to the slow cool-down rate of the vacuum furnace the material had actually undergone partial age hardening. The vessel was then returned to the heat treat vendor where a second attempt was made to perform a solution anneal, but again the required cooling rate could not be attained. It was then decided to perform the annealing operation in an atmosphere furnace followed by a forced air cooling cycle. The vessel was annealed in an endothermic atmosphere at 1800°F for 15 minutes and air cooled. This produced satisfactory results and the stretch forming was continued until the vessel attained an average diameter of 28.07". At this point it was decided that the unit was suitable for use in the storage tank and that stretching should be discontinued even though calculations indicated that the target diameter of 28.29" could have been attained without overstressing the material. A technical discussion of this stretch forming operation can be found in Appendix E herein.

Subsequent to forming, the pressure vessel was helium leak tested, age hardened, proof pressure tested to 430 psi and polished. The vessel was then assembled into the hydrogen storage tank as described in Section 4.2.1.

4.2.3.2 Solenoid Valves

Upon inspection of the solenoid valves procured from Wright Components Inc., it was found that they were not clean for oxygen service as had been specified. In addition, functional checkout tests showed that the valves would not operate properly at cryogenic temperatures. When cooled to cryogenic temperatures the valve mechanism would seize; it was impossible to operate the valve. The valves were dismantled by Bendix and it was found that a stainless steel poppet had been used within an aluminum housing, thus causing seizing due to differential expansion. Due to limitations of the program schedule, Bendix fabricated new aluminum poppets, cleaned and tested all the valve components per MSFC-SPEC-164 and reassembled them in a clean area. Subsequent testing showed these modifications to be effective. The valves operated satisfactorily at cryogenic temperatures.

4.2.3.3 Ion Pump

Following evacuation-bakeout, the hydrogen storage tank

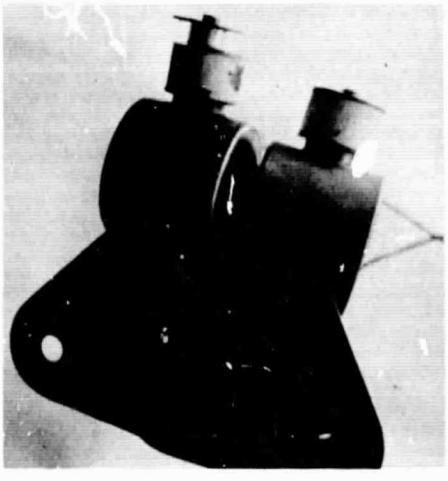


Fig. 4.2.3-4
FAULTY ION PUMP

was subjected to a liquid hydrogen vented heat leak test. During this test, the current draw of the ion pumps was observed to increase. During the 24 hours following this increase in current, the heat leak of the tank also increased. This occurrence lead to the discovery that the ceramic-to-metal seal on the electrical connector of one of the ion pumps had failed and allowed air to leak into the vacuum space of the storage tank. Figure 4.2.3-4 shows the faulty pump (on the left) next to a normal one. As can be seen in this photograph, the electrical connector has separated entirely from the ceramic insulator. When the leak was first discovered the connector had not completely separated from the insulator, however, only a slight amount of force was required to separate them. Visual inspection of the joint surfaces indicated that the braze joint had been improperly formed.

Subsequent to the failure, the faulty pump was replaced with a new one which had been closely inspected for defects and the complete storage tank was helium leak tested to ensure that no other leaks existed in the vacuum space. The tank was then re-evacuated and the test program was resumed.

4.3 Conclusions and Recommendations

4.3.1 Conclusions

The Phase B program successfully fulfilled the basic objectives of demonstrating both the feasibility and desirability of utilizing the radial bumper, discrete shield for the thermal protection of spacecraft sized EPS and ECS cryogenic storage tanks. The following significant conclusions can be drawn from the Phase B program.

1. The radial bumper, discrete shield design displays lower heat leak and hence longer mission capability than other presently available insulations of comparable weight and capacity.

2. Vapor cooling of discrete radiation shields is quite effective for reducing the heat leak of cryogenic hydrogen storage tanks. Since the heat transfer through this type of insulation is predominantly radiant in nature, vapor cooling can be more effectively utilized than in the case of conductive transfer systems.

3. Tests verify that since the heat leak through this type of insulation is predominantly radiant in nature,

the heat leak can be substantially reduced by lowering the outer shell temperature only a few degrees below ambient.

4. Since the annular vacuum space in tanks of this design contain almost no nonmetallic components, this type of insulation displays excellent long term vacuum stability.

5. Inturgescent forming of hemispheres for pressure vessels, radiation shields and outer shells represents a highly reliable, short lead time method of fabricating these components.

4.3.2 Recommendations

In view of the results of Phase B program, the following recommendations are made concerning the direction of future work in the field of spacecraft cryogenic storage systems.

1. Flight configuration storage systems utilizing the radial bumper discrete shield concept should be fabricated and qualified for use in manned spacecraft.

2. Studies should be performed including the fabrication of prototype systems to determine the applicability of this insulation concept with its attendant heat leak advantages to large cryogenic storage systems such as fuel and oxidizer tankage for propulsion systems which must exhibit extended mission duration capabilities.

3. Studies should be performed to determine the effects of lowering the outer shell temperatures by various methods (refrigeration, laminar insulation, shadow shields, etc.) on mission duration capability and system weight. These studies would lead to an optimum combination of discrete shielding and outer shell cooling for various mission requirements.

4. Due to the difficulties and expense involved in electroplating of large hemispheres and particularly complete large pressure vessels, a simpler technique of applying low emissivity coatings such as vacuum vapor plating should be investigated.

APPENDICES

APPENDIX A

HEMISPHERE BUCKLING TESTS

In order to weight optimize cryogenic tanks it is necessary to reduce the wall thickness as much as possible consistent with providing sufficient strength. For pressure vessel design, existing equations and analytical techniques are accurate and can be applied successfully. However, outer shells which are exposed to a pressure of one atmosphere externally and a high vacuum internally present a different problem.

Most references to equations for calculating external buckling pressure on spheres refer to a classical equation known as the Zoelly formula:

$$P = \frac{2\,Et^2}{R^2\,\sqrt{3(1-\gamma^2)}}$$

where P = external buckling pressure
E = modulus of elasticity
t = wall thickness
R = spherical radius
γ = Poisson's ratio

This equation is highly theoretical, however, and covers only a symmetrical buckling case. In addition, it applies only to shells with zero tolerance, i.e., perfect sphericity and no wall thickness variation, conditions which are not possible to attain in actual practice.

Various investigators have attempted to develop a variation to this equation, either analytically by using more practical assumptions or empirically as a result of testing. Unfortunately, in the latter cases most test samples were not accurately measured and reported so that the test results are of marginal value (See Bibliography).

Buckling tests were performed on six hemispheres to obtain usable data for future outer shell design. These hemispheres were manufactured by processes suitable for cryogenic tankage shells and therefore represented shells with sphericity and wall thickness variations expected in practical applications.

The results of these six tests are summarized in Table A-1. All of the four stainless steel hemispheres buckled. Of the two aluminum hemispheres tested, one

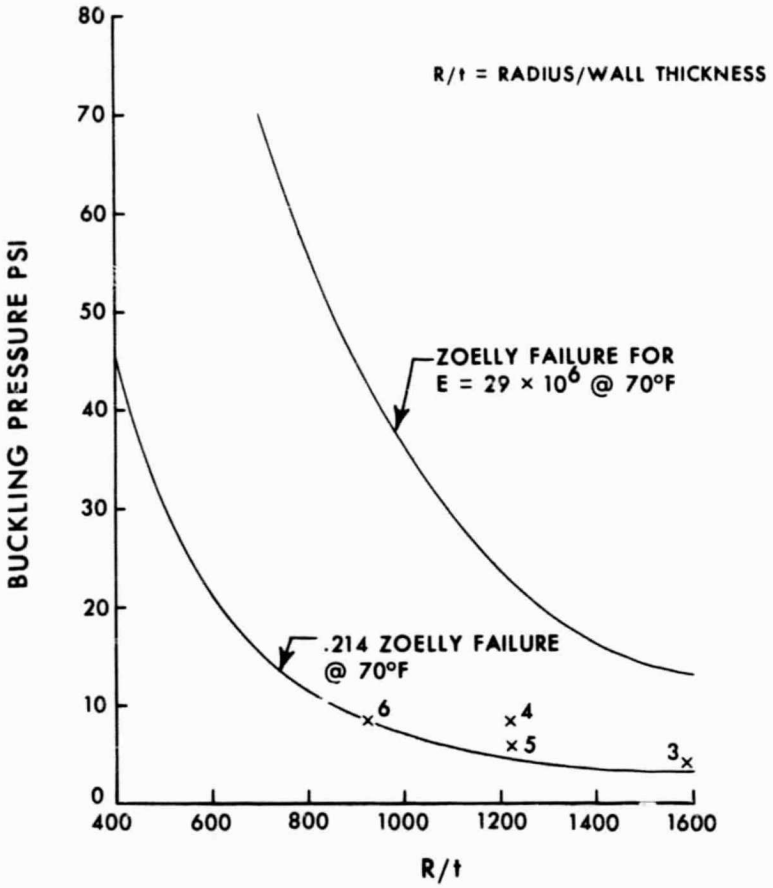
buckled. Cross sectional sketches of each part showing variation in wall thickness are presented in Figure A-2 through A-7.

TABLE A-1

SUMMARY OF HEMISPHERE BUCKLING TEST PROGRAM

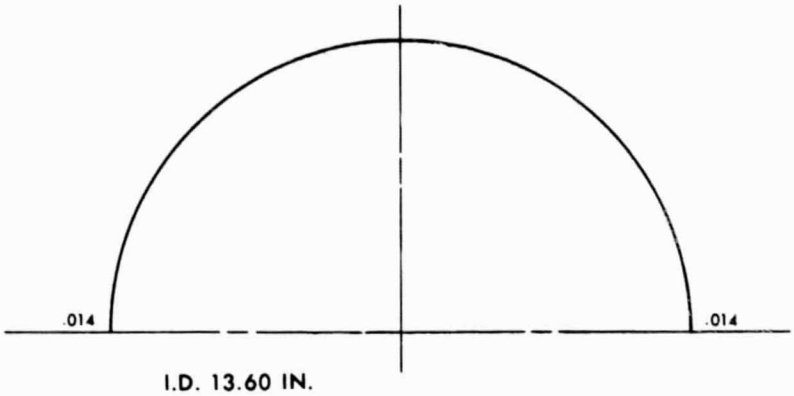
TEST	I.D. IN.	WALL IN.	MATERIAL	PROCESS	FAILURE PRESS. PSID	ZOELLY FAILURE PRESS. PSID	ACTUAL / ZOELLY	R/t RADIUS / THICKNESS	E, PSI
1	13.60	.0140	Alum. 1100	Spun	>14.7	51.4	>.286	485	10×10^6
2	21.00	.0175	Alum. 5052	Hydro-form	14.61	34.00	.43	600	10×10^6
3	18.00	.0057	Stainless AISI 304	Intur-gescent	3.69	14.00	.263	1580	29×10^6
4	22.00	.0099	Stainless AISI 304	Hydro-form	8.60	28.50	.302	1111	29×10^6
5	22.00	.010	Stainless AISI 304	Hydro-form	7.50	29.00	.259	1100	29×10^6
6	22.00	.015	Stainless AISI 304	Hydro-form	13.77	64.50	.214	734	29×10^6

A graph of the radius to wall thickness ratio (R/t) versus buckling pressure for 304L stainless steel is shown in Figure A-1. On this graph the theoretical Zoelly curve of buckling at 70°F is plotted. In addition, the points identified as 3, 4, 5 and 6 represent the actual failures of the respective stainless steel shells. As shown in Table A-1, the ratio of the actual failure to the Zeolly theoretical failure varies from .214 to .302 for stainless steel. Using this lower value (.214), a second curve was plotted in Figure A-1, representing a value of .214 times the Zoelly theoretical pressure. It was concluded that any stainless steel shell ($E = 29 \times 10^6$) was a known R/t ratio will not buckle if the external pressure is not greater than the internal pressure by an amount described by the lower curve. Conversely, for a specified pressure differential, the R/t ratio selected should be no greater than that described by the lower curve.



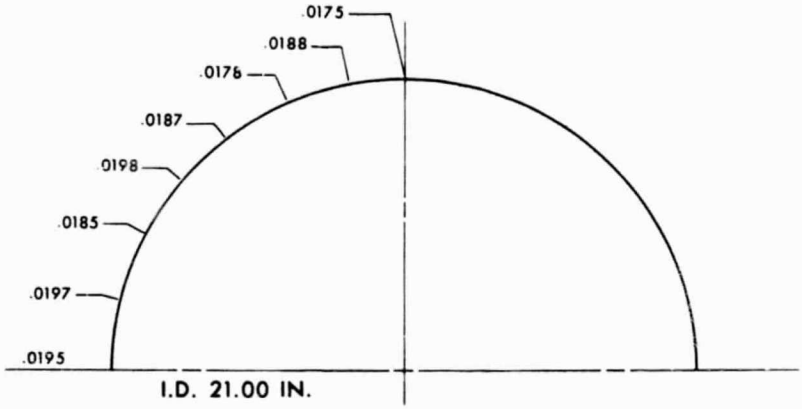
R/t VS. BUCKLING PRESSURE FOR
304 L STAINLESS STEEL

FIG. A-1 A-3873-67-221



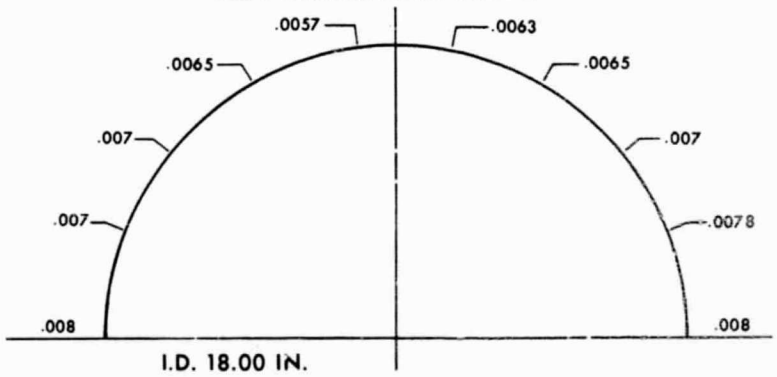
I.D. 13.60 IN.
MATERIAL _____ ALUMINUM 1100
PROCESS _____ SPINNING
FAILURE _____ NO FAILURE AT MAXIMUM PRESSURE OF 14.7 PSI

FIG. A-2 A-3873-67-203
TEST HEMISPHERE NO. 1



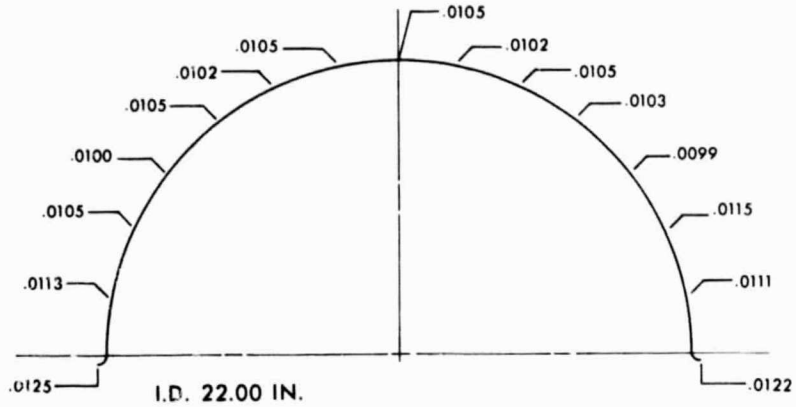
I.D. 21.00 IN.
MATERIAL _____ ALUMINUM 5052
PROCESS _____ HYDROFORM
FAILURE _____ 14.61 PSI

FIG. A-3 A-3873-67-205
TEST HEMISPHERE NO. 2



I.D. 18.00 IN.
MATERIAL _____ STAINLESS AISI 304
PROCESS _____ INTURGESCENT
FAILURE _____ 3.69 PSI

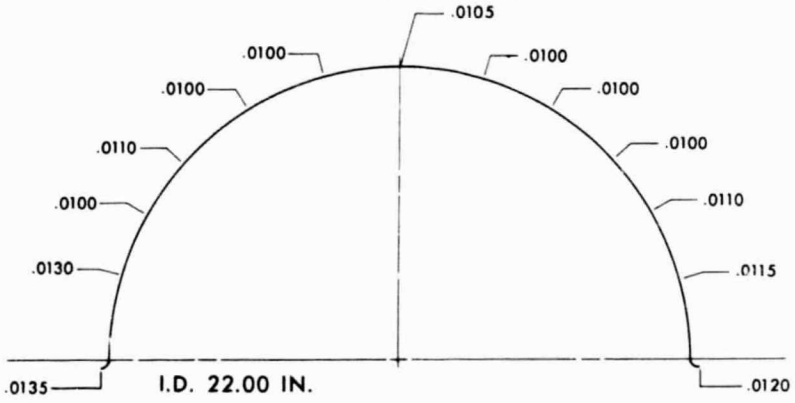
FIG. A-4 A-3873-67-204
TEST HEMISPHERE NO. 3



I.D. 22.00 IN.
MATERIAL _____ STAINLESS AISI 304
PROCESS _____ HYDROFORM
FAILURE _____ 8.60 PSI

FIG. A-5 A-3873-67-206

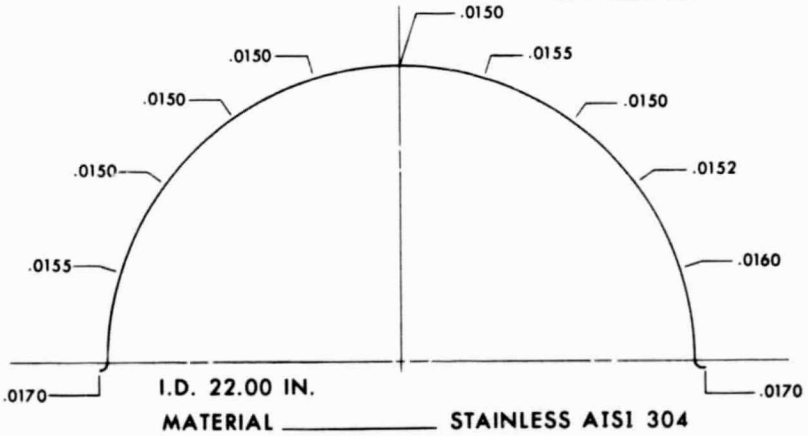
TEST HEMISPHERE NO. 4



I.D. 22.00 IN.
MATERIAL _____ STAINLESS AISI 304
PROCESS _____ HYDROFORM
FAILURE _____ 7.50 PSI

FIG. A-6 A-3873-67-207

TEST HEMISPHERE NO. 5



I.D. 22.00 IN.
MATERIAL _____ STAINLESS AISI 304
PROCESS _____ HYDROFORM
FAILURE _____ 13.77 PSI

FIG. A-7 A-3873-67-208

TEST HEMISPHERE NO. 6

Figure A-8 shows the following:

PHOTO NO.	DESCRIPTION
A	Test set-up showing hemisphere mounted on a flat plate, using rubber gasket for seal. Vacuum pump capable of providing high vacuum within the hemisphere is located under flat plate. Maximum ΔP of 1 atmosphere (approximately 14.7 psi) obtainable.
B	Inside of typical test hemisphere with stiffening ring inserted to assure that test article was round at girth during test.
1.	Test hemisphere #1. Did not fail.
2.	Test hemisphere #2 after failure. Round depression in center is due to hole in flat plate which is entrance to vacuum pump.
2^1.	Test hemisphere #2 after sectioning for wall thickness measurements.
3.	Test hemisphere #3 after failure and sectioning.
4.	Test hemisphere #4 after failure and sectioning.
5.	Test hemisphere #5 after failure and sectioning.
6.	Test hemisphere #6 after failure and sectioning.

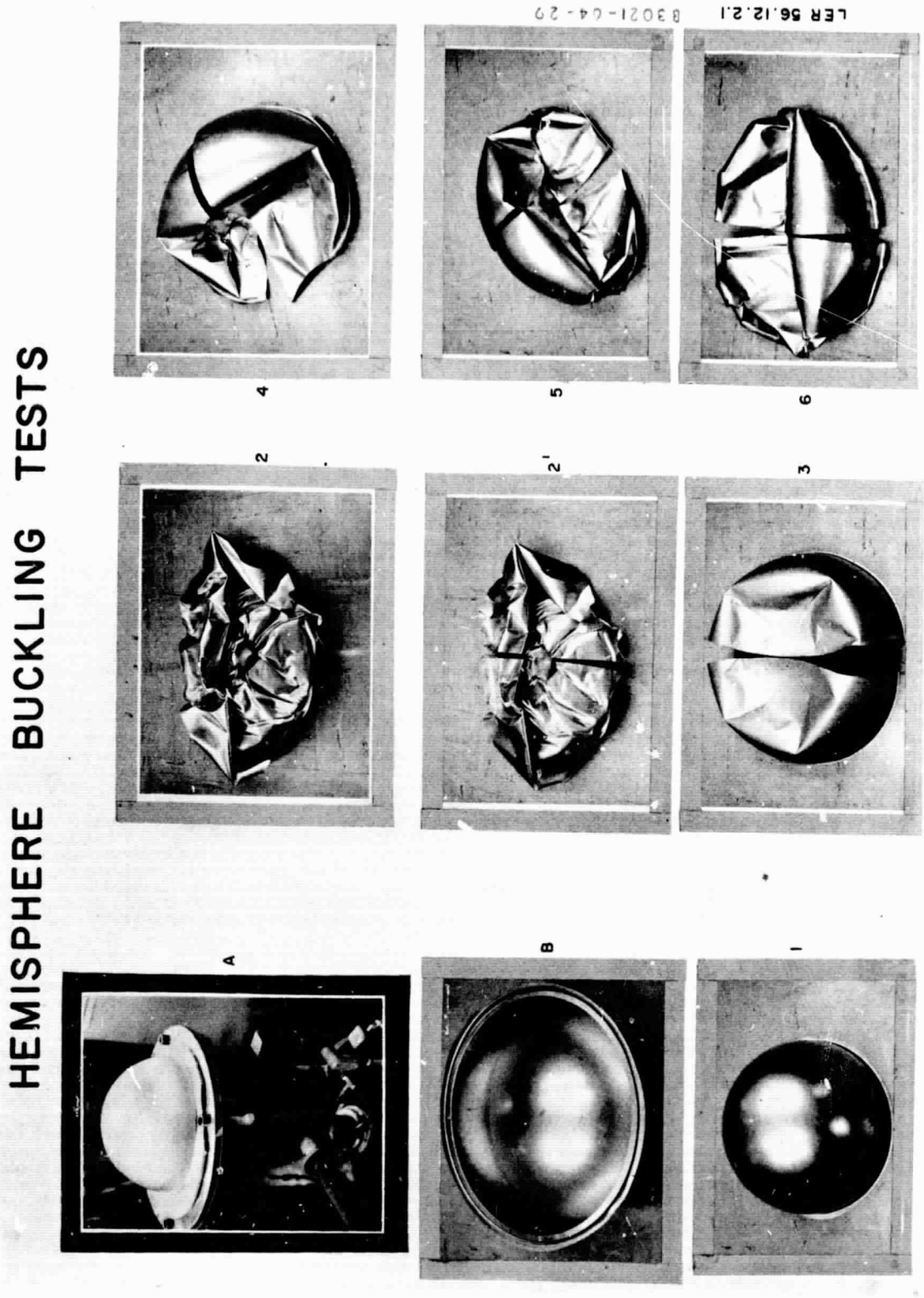

HEMISPHERE BUCKLING TESTS
LER 56.12.2.1
B3021-C4-29
A
B
1
2
2'
3
4
5
6

Fig. A-8

BIBLIOGRAPHY

1. Timoshenko, S., "Theory of Elastic Stability", McGraw-Hill Book Company, Inc., New York (1963).

2. Kloppel, K. and Jungbluth, O., "Bietrag Zum Durchschlags-problem Dunnwandiger Kugelschalen (Versuche and Bemessungs-formeln)", (Contribution to the Durschlag Problem in Thin Walled Spherical Shells (Experiments and Design Formulas). Der Stahlbau, Jahrg. 22, Heft 6, Berlin (1953).

3. Murray, F. J. and Wright, F. W. "The Buckling of Thin Spherical Shells", Journal of the Aerospace Sciences, Volume 28, No. 3 (March 1961).

4. Krenzke, M. A., "Tests of Machined Deep Spherical Shells Under External Hydrostatic Pressure", David Taylor Model Basin, Department of the Navy, Structural Mechanics Laboratory Report 1601 (May 1962) ASTIA No. AD 278075.

APPENDIX B

OUTER SHELL ANALYSES

1. Subject: Analysis of Phase A Outer Shells

Data Source: Roark Table XVI, Example T, page 306

Shell Drawing 1615580

LARGE OUTER END RADIUS

R = 15.47 inches = spherical radius
h = wall thickness
P = 2 x 14.7 psi = external pressure
E = 29×10^6 psi = modulus of elasticity
v = .3 = Poisson's Ratio

$$P = \frac{2 E h^2}{R^2 \sqrt{3(1-v^2)}}$$

$$29.4 = \frac{58 \times 10^6 h^2}{15.47^2 \sqrt{3(1-.3^2)}} = \frac{58 \times 10^6 h^2}{239 \sqrt{2.73}}$$

$$h = \sqrt{\frac{29.4 \times 239 \times 1.65}{58 \times 10^6}} = \sqrt{.0002} = .01414$$

CYLINDRICAL SECTION (BUMPER TUNNEL SECTION)

$$P = .807 \frac{Et^2}{lr} \sqrt[4]{\frac{1}{1 - v^2}\left(\frac{t^2}{v^2}\right)}$$

Data Source: Roark
Example Q31, page 306

E = 29×10^6 psi
t = .030 in. = wall thickness
l = 1.5 in. = length of cylindrical section
r = 8.8 in. = radius of cylindrical section
v = .3

$$P = \frac{.807 \times 29 \times 10^6 \times .03^2}{1.5 \times 8.8} \sqrt[4]{\frac{1}{1 - .3^2}\left(\frac{.03^2}{8.8^2}\right)}$$

$$= 1597 \sqrt[4]{.00001542} = 100 \text{ psi}$$

OUTER SHELL HEMISPHERE

Date Source: Astia Documen: AD 278075
Shell Drawing: 1615520

$$P_1 = 1.21\ E\left(\frac{t}{r}\right)^2 = 1.21 \times 29 \times 10^6\left(\frac{.01414}{15.47}\right)^2$$

$$= 35.1 \times 10^6\ (.00915)^2 = 294 \text{ psi}$$

$$\frac{P_1 R}{2t} = \frac{E\ t}{R\ \sqrt{3(1 - v^2)}}$$

$$P = \frac{2\ Et^2}{R^2\ \sqrt{3(1-v^2)}} = \frac{2}{\sqrt{3(1 - .3^2)}}\ E\left(\frac{t}{R}\right)^2$$

$$P = 1.21\ E\left(\frac{t}{r}\right)^2 = 1.21 \times 29 \times 10^6\left(\frac{.01414}{15.47}\right)^2$$

$$= 35.1 \times 10^6\ (.000915)^2 = 35.1 \times .837 = 29.4 \text{ psi}$$

By use of efficiency factor .6 (same report).

$$\frac{29.4}{.6} = 1.21\ E\left(\frac{t}{15.47}\right)^2$$

Efficiency factor

$$\frac{49 \times 15.47^2}{35.1 \times 10^6} = t^2 = .000333$$

$$t = \sqrt{.000333} = \underline{.0182 \text{ in.}}$$

OUTER SHELL CYLINDRICAL PORTION

Data Source: Roark Table XVI Example R, page 306
Shell Drawing: 1615520

$$P' = \frac{E\left(\frac{t}{r}\right)}{1 + 1/2\left(\frac{r\pi}{n_1}\right)^2}\left\{\frac{1}{n^2\left[1 + \left(\frac{n_1}{r\pi}\right)^2\right]^2} + \right.$$

$$\frac{n^2 t^2}{12r^2(1 - r^2)} \left[1 + \left(\frac{v\pi}{n_i}\right)^2\right]^2 \Bigg\}$$

$E = 29 \times 10^6$ psi
$t = .030$ in.
$r = 8.8$ in.
$\ell = 1.5$ in.
$n = 2$ = no. of lobes formed in buckling
$v = .3$

$$P' = \frac{29 \times 10^6 \left(\frac{.030}{8.8}\right)}{1 + 1/2\left(\frac{8.8\pi}{2 \times 1.5}\right)^2} \Bigg\{ \frac{1}{2^2 \left[1 + \left(\frac{2 \times 1.5}{8.8}\right)^2\right]} +$$

$$\frac{2^2 \times .030^2}{12 \times 8.8^2 (1 - .3^2)} \left[1 + \left(\frac{8.8\pi}{2 \times 1.5}\right)^2\right]^2 \Bigg\}$$

$$= \frac{29 \times 10^6 \times .00341}{1 + 1/2\,(84.9)} \left\{ \frac{1}{4\,[1 + .01177]^2} + \right.$$

$$\left. \frac{.0009}{3 \times 77.5\,(.91)} \left[1 + 84.9\right]^2 \right\}$$

$$= 2275 \left\{.244 + .0314\right\} = \underline{626 \text{ psi}}$$

2. Subject: Analysis of Phase A Outer Shell Safety Factor
Shell Example Part Number 1615520.
Spherical Sections only.

$$\sigma_{cr} = \frac{E\,h}{a\,\sqrt{3\,(1 - \mu^2)}} \quad \text{(buckling)} \qquad (1)$$

a = radius
h = wall thickness
E = elastic modulus
μ = Poisson's ratio
* = Theory of Elastic Stability by Timoshenko, Pages 512-519.

$$\sigma_{cr} = \frac{(29)\,10^6\,h}{\sqrt{2.73\,a}}$$

$$\sigma_{cr} = (17.5)\ (10^6)\ h/a$$

$$\sigma_e = \frac{(14.69)\ (a)}{2\ h}$$

$$\frac{\sigma_{cr}}{\sigma_e} = \frac{(17.5)(10^6)\ h/a \cdot h/a}{(\frac{14.69}{2})\ a/h \cdot h/a} = (2.38)\ 10\left(\frac{h}{a}\right)^2$$

CASE I $\quad h = (30)\ 10^{-3} \quad a = 11$

$$\frac{\sigma_{cr}}{\sigma_e} = (2.38)(10^6)(\frac{900}{121})\ 10^{-6} = 17.5$$

CASE II $\quad h = (30)(10^{-3}) \quad a = 15.47$

$$\frac{\sigma_{cr}}{\sigma_e} = (2.38)(10^6)\ (\frac{900}{240})\ 10^{-6} = 8.87$$

CASE III $\quad h = (20)(10^{-3}) \quad a = 11$

$$\frac{\sigma_{cr}}{\sigma_e} = (2.38)(10^6)(\frac{400}{121})\ \ 10^{-6} = 7.85$$

CASE IV $\quad h = (20)(10^{-3}) \quad a = 15.47$

$$\frac{\sigma_{cr}}{\sigma_e} = (2.38)\ \frac{(10^6)(400)\ 10^{-6}}{240} = 3.95$$

Safety factors based on buckling are:

Case	S.F.
I	17.50
II	8.87
III	7.85
IV	3.95

The safety factor based on yield is:

$$S.F. = \frac{(30000)}{(qa/2h)} = \frac{(60000)}{14.69}\left(\frac{h}{a}\right)$$

The minimum h/a occurs for Case IV, hence

$$S.F. = \frac{(4060)(20)\ 10^{-3}}{15.47} = 5.25$$

BIBLIOGRAPHY

Roark, Raymond J., "Formulas for Stress and Strain", McGraw-Hill Book Company, Inc., New York (1943).

APPENDIX C

PHASE A POST-CONTRACT EFFORT

1. External Insulation-Vapor Cooling

Following the contract test effort, the Phase A dewar was externally insulated and the outer shell vapor-cooled according to the following procedure:

1. Wrapped dewar outer shell with two layers aluminum foil.

2. Mechanically attached copper refrigeration tubing around dewar on top of aluminum foil in a total of nine wraps with 4" spacing between wraps.

3. Attached thermocouples on and between tubing.

4. Wrapped two layers aluminum foil over tubing and dewar.

5. Poured Urethane Foam around dewar, using stainless steel hemispheres as mold and protective skin.

6. Attached vent port of dewar to inlet of refrigerating tubing such that dewar can be vented through external vapor-cooling tubing or directly to atmosphere.

Figure C-1 is a cross-sectional drawing of the dewar showing the foam insulation, external vapor-cooling tubing configuration and the plumbing hookup. Listed in Table C-1 are physical characteristics relating to the modifications.

TABLE C-1

PHYSICAL CHARACTERISTICS - PHASE A EXTERNAL INSULATION

VAPOR-COOLING TUBING

Material	Copper
Outer Diameter	.250 in.
Wall Thickness	.030 in.
Total Length	50 ft.

EXTERNAL INSULATION

Type	CPR Series 314 Rigid Urethane Foam
Manufacturer	The Upjohn Company CPR Division

TABLE C-1 (Cont.)

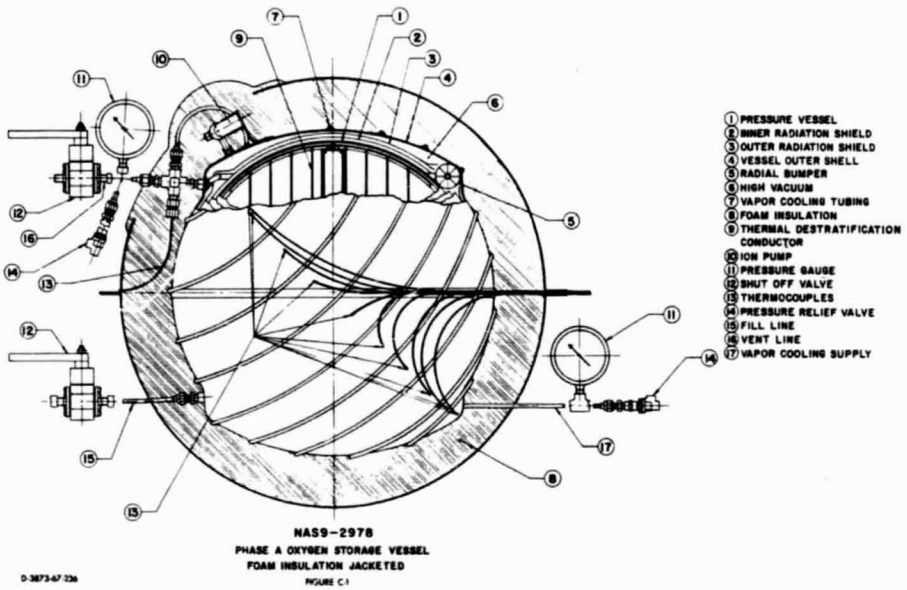
Advertised Thermal Conductivity	0.14-0.17 Btu/ft^2-hr-°F/in @ 74°F
Thickness	3.5 inches

EXTERNAL INSULATION OUTER SHELL

Material	Stainless Steel 304L
Outer Diameter	29.06 in.
Wall Thickness	0.035 in.

THERMOCOUPLES
(FOR MONITORING SYSTEM PERFORMANCE)

Type	Copper-Constantan



NAS9-2978
PHASE A OXYGEN STORAGE VESSEL
FOAM INSULATION JACKETED
FIGURE C-1

D-3873-67-226

Liquid oxygen and liquid hydrogen vented heat leak tests were performed on the unit. Listed in Table C-2 are results obtained from these tests. Included are the average heat leak values for the same fluids before the Phase A tank was modified.

TABLE C-2

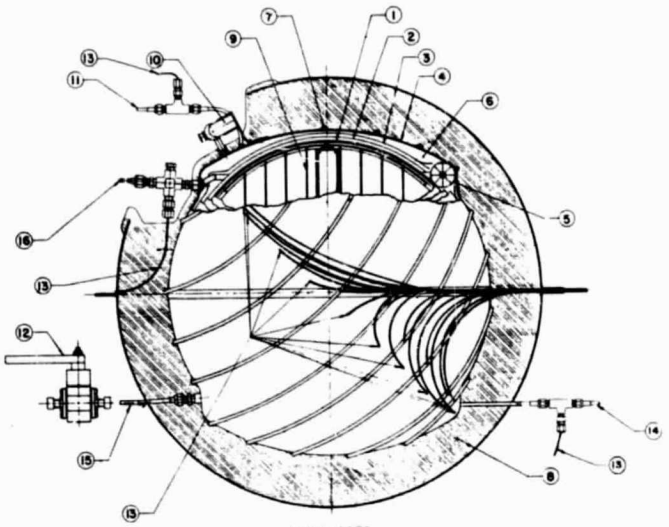
VENTED HEAT LEAK TEST RESULTS
PHASE A TANK
70-80°F ENVIRONMENTAL TEMPERATURE

FLUID	VENTED HEAT LEAK BTU/HR	RATIO OF HEAT LEAK TO INNER VESSEL SURFACE AREA BTU/HR-FT^2	TEST CONDITION
LO_2	7.25	0.777	Non-Insulated
LO_2	6.7	0.718	Insulated, Non V-C
LO_2	6.7	0.718	Insulated, V.C.
LH_2	5.1	0.547	Non-Insulated
LH_2	3.9	0.418	Insulated, Non V.C.
LH_2	3.3	0.354	Insulated, V.C.

The results of this limited test program showed definite thermal advantages obtained from the external insulation alone. No external vapor-cooling thermal advantages were observed from the liquid oxygen vented tests. However, a definite decrease in vented heat leak was obtained when the external vapor-cooling function was employed in the liquid hydrogen test series.

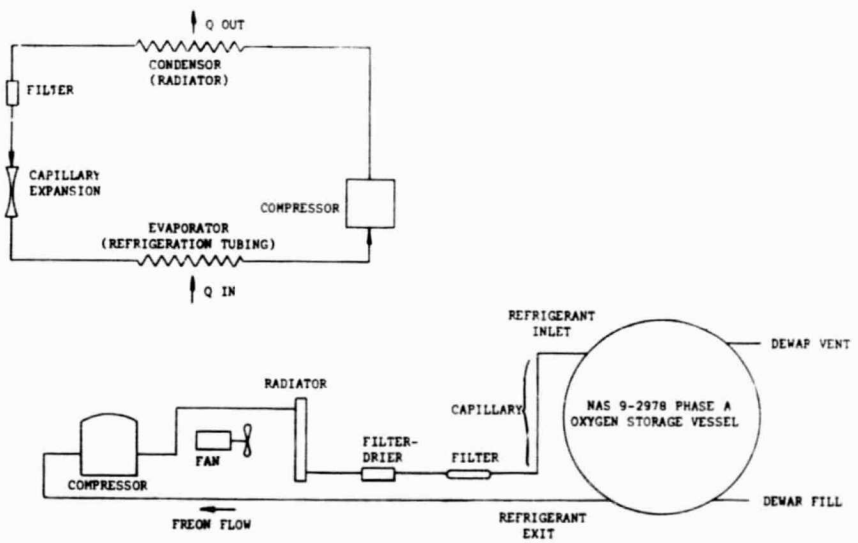
2. External Refrigeration

The copper tubing wrapped on the outer shell for use as vapor-cooling tubing was subsequently utilized as the evaporation coil for a small refrigeration system used to cool the dewar outer shell. Figure C-2 is a cross-sectional drawing showing the plumbing modifications made to accommodate the external refrigeration function. Figure C-3 shows schematically the external refrigeration circuitry and components. The capillary-tube expansion device outlet was attached to the upper end of the refrigeration (previously vapor-cooling) tubing, thus providing the refrigerant inlet to the evaporation coil. The lower end of the refrigeration tubing, being the refrigerant exit from the evaporation coil, was plumbed to the inlet of the system compressor. Refrigerant inlet and refrigerant exit temperatures were measured with copper constantan thermocouples, in addition to the temperatures on the dewar outer shell. Listed in Table C-3 are physical characteristics of the external refrigeration components.



NAS9-2978
PHASE A OXYGEN STORAGE VESSEL
FOAM INSULATION JACKETED
WITH EXTERNAL REFRIGERATION CIRCUIT
FIGURE C-2

D-3873-67-237



SCHEMATIC - NAS 9-2978 PHASE A OXYGEN STORAGE VESSEL WITH EXTERNAL REFRIGERATION CIRCUIT COOLING VESSEL VACUUM JACKET

FIGURE C-3

A-3873-67-241

TABLE C-3

PHYSICAL CHARACTERISTICS
PHASE A EXTERNAL REFRIGERATION

CONDENSING UNIT

Manufacturer	Copeland Refrigeration Corporation
Model No.	KCAH-0013-SAA
Power Requirements	115 V, 60 hz, single-phase
Compressor Power	1/8 HP
Compressor Displacement	34.3 ft^3/hr (1.075" bore, 0.625" stroke)
Weight	38 lb.

REFRIGERANT

Type	Freon-12 (R-12)

EXPANSION DEVICE

Type	Capillary Tube (with moisture removal)
Manufacturer	Parker-Hannifen Corporation
Model	KKIL .250 KMP

FILTER-DRYING DEVICE

Type	Silica Gel-Molecular Sieve
Manufacturer	Alco Valve Company
Model NO.	ADK-052

Limited testing with atmosphere-vented LN_2 was performed to determine the refrigeration capacity available and the effect of lowering the outer shell temperature on dewar heat leak. Due to ice build-up on the expansion and exhaust tubes, a wet test meter rather than a recording scale was used to determine the LN_2 evaporation rate. A small portion of the foam insulation was removed in the area of the dewar vent fitting and ion pump, as shown in Figure C-2. This appeared to be partially responsible for the fact that a temperature gradient existed on the dewar outer shell when the refrigeration system was in operation. The lowest temperatures obtainable during operation were in the -22 to -25°F range, near the bottom outer surface of the dewar. The overall average temperature of the dewar outer surface was approximately -20°F.

Following is a brief summary of the limited test program performed on the system.

SUMMARY OF TESTING
PERFORMED ON NAS 9-2978 PHASE A OXYGEN STORAGE VESSEL
WITH EXTERNAL INSULATION AND REFRIGERATION OF
DEWAR OUTER SHELL

1. Average vented LN_2 heat leak of system, no refrigeration = 6.7 Btu/hr.

   Average ambient temperature = 75°F = temperature of outer surface of insulation.

2. Observed average temperature on dewar vacuum jacket during non-refrigerated vented LN_2 heat leak testing = 55°F = temperature of inner surface of insulation.

3. Determination of thermal conductivity of foam insulation (CPR 314 Series Rigid Polyurethane Foam):

$$Q = \frac{4\pi K r_1 r_2 (T_1 - T_2)}{r_1 - r_2}$$ = heat loss through concentric spherical super insulation

where

Q = heat loss, Btu/Hr
K = thermal conductivity of insulation, Btu/ft^2-hr-°F/in.
r_1 = outer spherical radius, ft = outer skin radius
r_2 = inner spherical radius, ft = dewar vacuum jacket radius
T_1 = outer surface temperature, °F
T_2 = inner surface temperature, °F

Therefore

$$K = \frac{Q (r_1 - r_2)}{4\pi r_1 r_2 (T_1 - T_2)}$$

From experimental data given in 1 and 2:

$$K = \frac{(6.7)(14.53 - 11.05)}{(4)(\pi)\frac{(14.53)(11.05)}{144}(75 - 55)} = 0.084$$

4. Average vented LN_2 heat leak of system, when refrigerated = 4.5 Btu/Hr.

   Average ambient temperature = 75°F = temperature of outer surface of insulation.

5. Observed average temperature on dewar vacuum jacket during refrigerated vented LN_2 heat leak testing = -20°F = temperature of inner surface of insulation.

6. Heat transferred across insulation:

$$Q = \frac{4 \pi K r_1 r_2 (T_1 - T_2)}{r_1 - r_2}$$

$$Q = \frac{(4)(\pi)(0.084)\frac{(14.53)(11.05)}{144}(75 + 20)}{(14.53 - 11.05)} = 32 \text{ Btu/hr}$$

7. Heat transferred to cryogen is 4.5 Btu/hr, from 4. above.

Therefore, heat removed by refrigeration system is:

$32 - 4.5 = 27.5$ Btu/hr

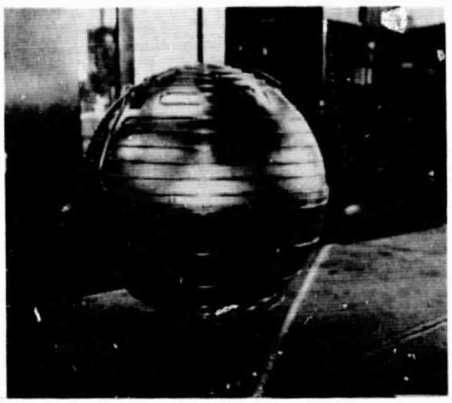


Fig. D-1
VAPOR-COOLED
RADIATION SHIELD

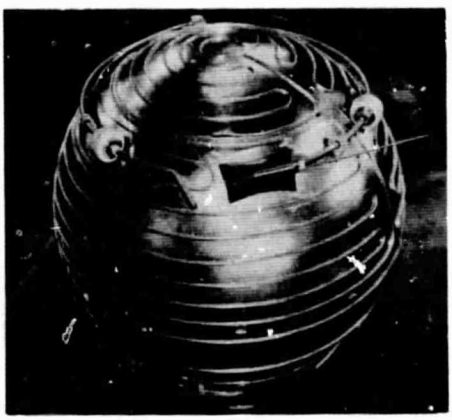


Fig. D-2
VAPOR-COOLED
RADIATION SHIELD

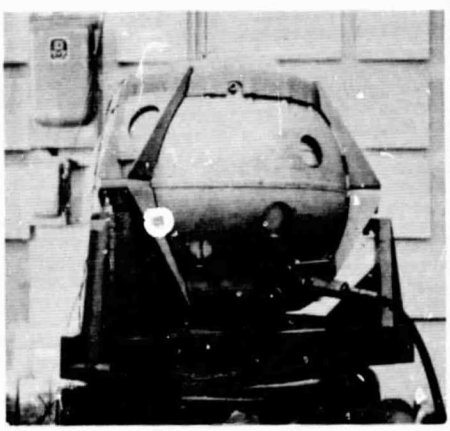


Fig. D-3
VIBRATION TEST
VAPOR-COOLED UNIT

APPENDIX D

PHASE A VAPOR COOLED UNIT VIBRATION TESTING

1.0 Unit Description

At the conclusion of the NAS 9-2978 Phase A fabrication program, the spare parts were modified by Bendix funding for fabrication of a single vapor-cooled shield tank. The inner pressure vessel and outer vacuum jacket were the same as used on the Phase A tank. Figure D-1 shows the single vapor-cooled discrete shield. Copper tubing (0.125 in. OD) was soldered to the copper-plated aluminum hemispheres. The complete assembly was then silver plated for low emissivity. Figure D-2 shows the single vapor cooled shield assembled to the inner pressure vessel and bumper assembly. No internal components are located within the inner vessel, and therefore there are no electrical leads passing through the annular region. The only other difference between the vapor-cooled unit and the contract-Phase A tank was that the segmented bumpers were fabricated from Kel-F instead of 25% glass-filled teflon.

The Phase A vapor-cooled unit was subjected to several vibration tests, utilizing the Phase A mount carriage and vibration fixture described in Section III of this report. Visual inspection of the unit's various subassemblies during vibration was possible through seven 2-1/2 inch holes cut in the outer shell. These holes were located in such a manner that the upper and lower bumpers and shield hangers, fill and vent lines, and the shield itself were plainly visible. In addition, these holes permitted the attachment of accelerometers to the shield during sinusoidal vibrations. A valve was placed on the fill port and a pressure gage on the vent port to permit partial filling of the inner vessel with water and pressurization of the system during the vibration testing. Figure D-3 shows the unit mounted on the vibration stand. The total weight of the empty tankage and its mount carriage was 66.6 pounds. The weight of the vibration fixture on which the unit was mounted was 59.3 pounds.

2.0 Vibration Tests

The vibration tests performed on the Phase "A" vapor-cooled unit involved both random and sinusoidal vibration in two planes, horizontal and vertical. The tests were performed with the unit both soft and hard mounted, and by using varying amounts of water and pressures in the inner vessel.

The specifications to which the unit was vibrated included both the LEM Specification ASP 13-9151, and the Apollo Block II at 9 db above the design proof level. In testing to the LEM Specification, only the launch and boost spectrum was used since this appeared considerably more severe than the translunar or lunar descent spectrums. In the case of the Apollo-Block II Specifications, the combined atmospheric and space flight spectrum was used.

For each of these sets of specifications, a computer program (Source Program No. 1037 JTB) was run to obtain db readings at intervals of 25 H_z and to determine the RMS and peak g values in each region of the individual spectrum.

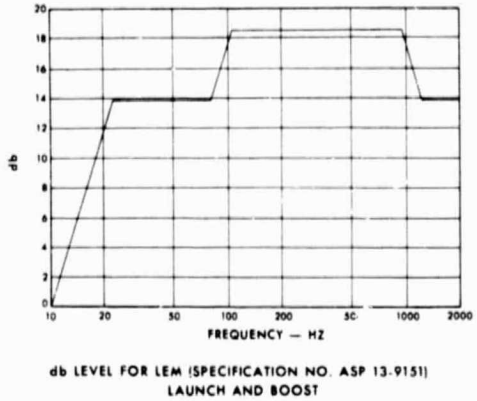
2.1 Random Vibration

2.1.1 Random Vibration Test Description

The first vibration tests were performed to the LEM Specification referred to previously. The specific vibration used was the input from the exterior primary structure which had a root mean square g loading of 7.5976. Table D-1 represents that portion of the specification. Figures D-4 and D-5 respectively show the db level profile and the acceleration density spectrum for this specification as plotted from the previously mentioned computer program.

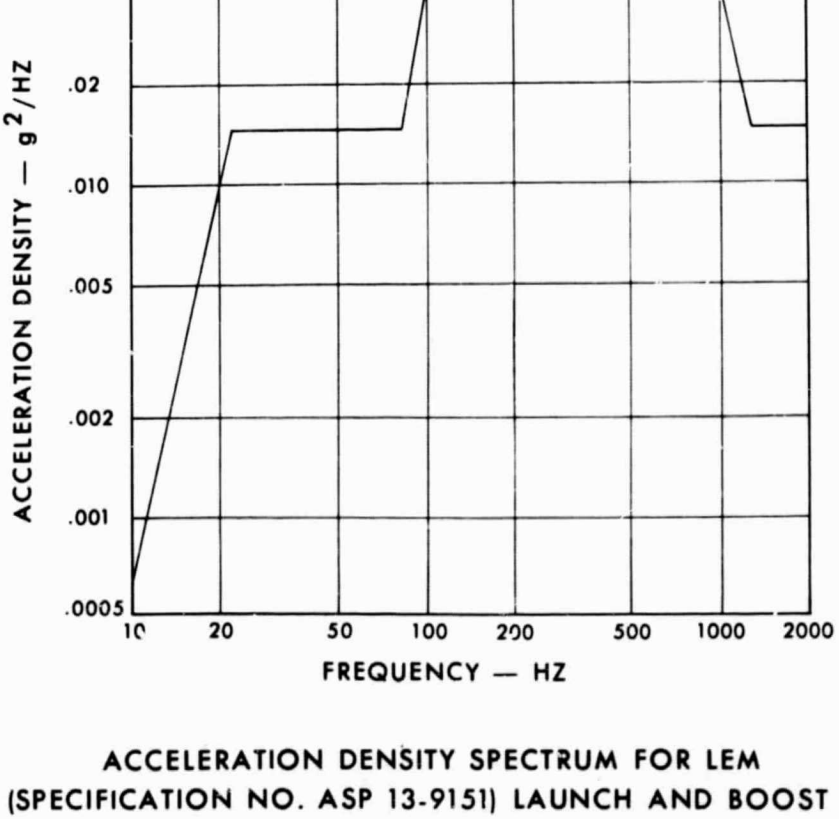
TABLE D-1
LEM RANDOM VIBRATION SPECIFICATION NO. ASP 13-9151 - LAUNCH AND BOOST INPUT FROM EXTERIOR PRIMARY STRUTURE

10 to 23 Hz	12 db/octave rise to
23 to 80 Hz	0.0148 g^2/Hz
80 to 105 Hz	12 db/octave rise to
105 to 950 Hz	0.044 g^2/Hz
950 to 1250 Hz	12 db/octave decrease to
1250 to 2000 Hz	0.0148 g^2/Hz



db LEVEL FOR LEM (SPECIFICATION NO. ASP 13-9151) LAUNCH AND BOOST

FIG. D-4 A-3873-67-226



ACCELERATION DENSITY SPECTRUM FOR LEM (SPECIFICATION NO. ASP 13-9151) LAUNCH AND BOOST

FIG. D-5 A-3873-67-22

Table D-2 represents the portion of the Apollo Block II Specification used in testing. Figures D-6 and D-7 respectively show the db level profile and the acceleration density spectrum for this specification, as plotted from the computer program output.

TABLE D-2

APOLLO BLOCK II RANDOM VIBRATION SPECIFICATION
+ 9 db ABOVE THE DESIGN PROOF LEVEL
ATMOSPHERIC AND SPACE FLIGHT ENVELOPE

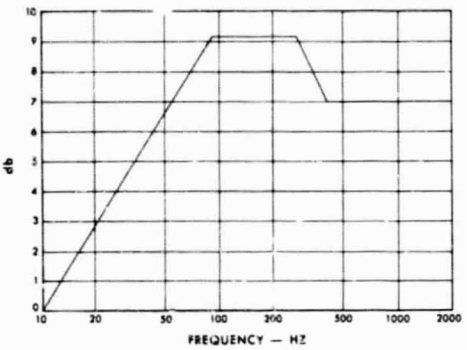
10 Hz	.003 g^2/Hz
10 to 90 Hz	3 db/octave increase to
90 to 250 Hz	.025 g^2/Hz
250 to 400 Hz	3 db/octave decrease to
400 to 2000 Hz	.015 g^2/Hz

Since this was a test program of an experimental search nature, the initial vibrations were not to the full 7.6 g rms level specified by the acceleration density profile. Instead, the procedure used was to begin at 2 g's rms and to proceed from there to 4, 6 and 7.6 g's rms. As a result, the first three individual tests were not to the specification, but were at less severe vibration levels than those set forth in the specification. This procedure was followed to allow observation of the vibration intensity which would cause failure in some part of the system should it occur. Also, at these levels the actual cause of any resulting damage could be more readily determined.

2.1.2 Observations and Results

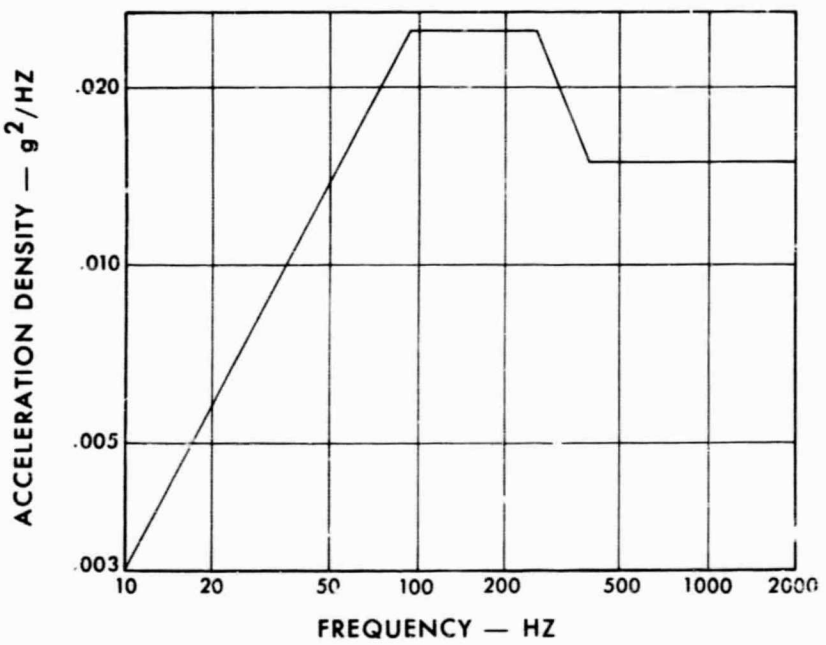
The Phase "A" vapor-cooled unit was subjected to 2 hours, 2 minutes and 39 seconds of random vibration. This time represents actual test time, and does not include the time spent setting up or checking the unit. Included in the actual test time was 9 minutes and 40 seconds during which the unit was tested at the full rated output of 7.6 g's rms as specified for the Apollo Block II. These tests were conducted with the vessel filled with water and pressurized to 100 psi, and without shock mounts between the vibration fixture and mounting carriage.

A total of 6 tests were run to the full 7.6 g's RMS of the LEM Specification. These tests included vibrations with the vessel both full and half-full of water, pressurized and non-pressurized, and with and without shock mounts while in both the horizontal (Z) and



db LEVEL FOR APOLLO-BLOCK II ATMOSPHERIC AND SPACE FLIGHT ENVELOPE SPECTRUM

FIG. D-6 A-3873-67-225



ACCLERATION DENSITY SPECTRUM FOR APOLLO-BLOCK II ATMOSPHERIC AND SPACE FLIGHT ENVELOPE

FIG. D-7 A-3873-67-228

vertical (X) planes. These six tests involved a total time duration of 26 minutes and 15 seconds.

The remainder of the tests involved those tests conducted at lower acceleration densities.

Apparent resonances were encountered in the area of 900 Hz in many of the tests. Other than in this one particular area, the random vibration tests were relatively trouble free. No other peaks were encountered.

2.2 Sinusoidal Vibrations

2.2.1 Sinusoidal Vibration Test Description

Originally, it was planned to employ the LEM Launch and Boost Specifications (ASP 13-9151) for the sinusoidal vibrations. However, it was found that the vibration equipment available at the Bendix Corporation's Instrument and Life Support Division was not capable of vibrating the vessel to these specifications. This was caused by the weight of the system overdriving the head, which resulted in the displacements of the head becoming too large for the equipment to handle and automatically shutting off the vibration system. The combined weight of the system which included the vibration fixture, vessel and water was 294.5 lbs.

The specific sinusoidal vibrations to which the vessel was subjected are discussed below.

As with the random vibrations, the system was vibrated in both the horizontal (Z) and vertical (X) planes, pressurized and unpressurized, full and half-full of water, and with and without shock mounts.

Table D-3 summarizes the actual sinusoidal vibration tests performed and gives the duration of each individual test.

During the sinusoidal tests three calibrated accelerometers were used. One, the input sensor, was mounted on the vibration fixture. The remaining two were placed at other points of interest, such as on the mount carriage, shield and outer shell. The outputs of these accelerometers were plotted by the monitoring equipment to provide a series of frequency versus "g" loading graphs at the points where the pickups were attached.

TABLE D-3

SINUSOIDAL VIBRATION TESTS

Unit filled with water, pressurized

Test No.	Test Description	Time	Total Time
	X plane - shock mounted		25:03
1	50 to 2000 Hz @ 3 g's peak	6:23	
2	50 to 15 Hz @ 0.050" D.A.	1:49	
3	59 to 19 Hz @ 0.010" D.A.	2:35	
4	5 to 26 Hz @ 0.020" D.A.	4:55	
5	100 to 24 Hz @ 2.7 g's peak	3:35	
6	25 to 5 Hz @ 0.030" D.A.	5:46	
	X plane - solid mounts		17:35
7	50 to 2000 Hz @ 2.7 g's peak	6:00	
8	50 to 20 Hz @ 2.7 g's peak	2:00	
9	30 to 5 Hz @ 0.030" D.A.	7:00	
10	30 to 21 Hz @ 0.050" D.A.	2:35	
	Z plane - solid mounts pressurized		11:13
11	50 to 2000 Hz @ 2.7 g's peak	6:13	
12	Dwelling at frequencies listed 20, 300, 450, 900, 1500, & 1800	5:00	
	Unit half-filled with water, unpressurized		
	X axis - solid mounts		25:13
13	50 to 2000 Hz @ 2.7 g's peak	7:30	
14	1100 to 700 Hz @ 2.7 g's peak	5:45	
15	300 to 180 Hz @ 2.7 g's peak	3:30	
16	50 to 30 Hz @ 2.7 g's peak	3:03	
17	30 to 5 Hz @ 0.030" D.A.	4:25	
18	30 to 24 Hz @ 0.050" D.A.	1:00	

2.2.2 Observations and Discussion of Results

The first series of sinusoidal tests were performed in the vertical (X) plane and required a total of 25 minutes and 3 seconds operating time (exclusive of set-up and check-out). The system was shock mounted, the vessel was filled with water and pressurized to 100 psi. The system weight was approximately 294.5 pounds.

In Test #1 (50 to 2000 Hz @ 3 g's peak), several resonance points appeared. The most important of these occurred at about 920 Hz where the outer shell entered a region of apparent resonance. The accelerometer sensing this resonance was located at the top of the vessel about 1 inch from the boundary of a hole cut in the outer shell for the shield accelerometer pickup. An acceleration of about 58 g's was experienced by the outer shell. It appears that this large vibratory level provided a feedback to the shields through the mounting system, producing a shield acceleration (top center) of about 17 g's. As noted in Section 2.1.2, this frequency range presented problems during the random vibrations. It should be noted, however, that the hole in the outer shell, adjacent to where the outer shell accelerometer was located, could have weakened the shell and permitted it to "flutter" under vibration. This could possibly explain the high "g" level experienced.

Above this frequency (920 Hz), the outer shell experienced two other resonant points. One was at slightly over 1200 Hz (19 g's) and the other was at 1500 Hz (21 g's). The shield acceleration at both of these points was quite low, being in the area of 4 g's.

Between the frequencies of 920 Hz and 50 Hz, the shield vibratory level was very low, being considerably less than the input level. At several points, the outer shell experienced increased "g" levels, but these were of considerably lower magnitudes. At about 305 Hz, mounting fixture resonance occurred giving 27 g's. This, as may be expected, resulted in higher g levels being experienced by both the shield and the outer shell. There appeared to be a considerable amount of vibration damping, however, since the outer shell and shield were at 15 and 6 g's, respectively.

At about 135 Hz, the three components again were at higher "g" levels (fixture - 5 g's, outer shell - 15 g's and shield - 3 g's). This region cannot be attributed to either the fixture or outer shell since

it occurred at lower harmonics of both the shell and fixture resonance frequencies.

The second test (50 to 16 hz at .050 inch double amplitude - vessel water filled and pressurized) demonstrated that the outer shell was at a considerably higher vibration level than either the shield or fixture. At 50 Hz the shell was at 13 g's, tapering down to about 4 g's at 22 Hz, and then increasing to 9 g's at 16 Hz. The shield vibrations followed this same general trend but at a considerably lower level.

The third test (5 - 19 Hz @ .010 inch double amplitude) was clear of any resonance points as was test #4 (5 - 26 Hz @ .020 inch double amplitude). In the latter test, however, there was a relatively small but readable vibratory level between 19 and 26 Hz.

The fifth test (100 - 24 Hz @ 2.7 g's) showed a nearly constant increase in the vibratory level from about 4 g's at 100 Hz to 11 g's at 24 Hz for the outer shell The shield followed the same pattern going from 1 g to 4 g's in this same range.

The final test in this series was test #6 (25 - 5 Hz at 0.030 inch double amplitude). During this test all three accelerometers showed a very low vibratory level up to about 16 Hz, and then a sharp increase to 6, 4 and 1 g's for the outer shell, shield and fixture, respectively. This was followed by a fairly constant decrease up to 25 Hz, which was apparently caused by the outer shell vibrations being fed back to the shield through the shield mounting system. This opinion is based upon the fact that the outer shell appeared to begin vibrating at a higher level, and somewhat before the shield vibratory level increased.

The second series of sinusoidal vibration tests was also in the vertical (X) plane with the unit filled with water and pressurized to 100 psi. However, in this case, no shock mounts were used, the unit being rigidly attached to the vibration fixture. The accelerometers were located in the same positions as in the previous tests.

Test #7 involved going from 50 to 2000 Hz at 2.7 g's peak. From 50 to 150 Hz, with a peak level of 2.7 g's being maintained, the outer shell maintained about the same level of vibration (2.7 g's) as the fixture while the shield remained nearly motionless. At 150 Hz the level began to increase until reaching a maximum of 8.5 g's for the fixture and shield, and 30 g's for the

outer shell. Both the shield and fixture returned to a very low level at 250 Hz, but the shell vibrations remained high until 300 Hz was reached. At 450 Hz the shell vibratory level again began an irregular increase to a maximum of 43 g's at 950 Hz. Again, the shield appeared to be excited by the shell, reaching 12 g's at 950 Hz. The fixture itself remained at a low level (3 - 4 g's). The outer shell resonated again at 1200 Hz (12 g's), 1550 Hz (16 g's) and at about 1700 Hz (11 g's). In the latter two cases, the shield was again excited to 11 g's and 7 g's respectively. The fixture did not appear to have any serious resonance points in this range.

The eighth test (50 to 30 Hz at 2.7 g's peak) showed that the shield and outer shell maintained nearly constant "g" levels in this range at 3 g's and 5 g's, respectively. No resonance was encountered.

In test #9 (30 - 5 Hz @ .020 inch double amplitude) the "g" levels began, at 30 Hz, at about the same levels as in test #8. They remained constant to about 19.5 Hz where they began decreasing. At 19 Hz and below, they were of negligible magnitudes.

In test #10, the final test in this series (30 - 21 Hz @ .050 inch double amplitude), no resonance was encountered. All three accelerometers monitored nearly constant "g" levels (shield - 4 g's, fixture - 3.5 g's and outer shell - 6 g's) except for the outer shell which began to realize slightly increasing "g" levels below 23 Hz.

The third series of sinusoidal vibrations was conducted in the horizontal (Z) plane with the vessel filled with water and pressurized to 100 psi. The accelerometers were located at the girth on the outer shell, on the top band of the mount carriage and on the vibration fixture (input). The purpose of this series of sinusoidal vibration tests (no. 11 and 12) was to attempt to find the reason for the 900 Hz peak in the random tests.

The first test (no. 11) of this series involved sweeping from 50 to 2000 Hz at 2.7 g's peak. The three accelerometers remained at relatively low vibratory levels (fixture-5 g's, outer shell - 8 g's and mount carriage - 11 g's). At 300 Hz some vibration fixture resonance was encountered, but this had little or no effect on the other two pickups. At 500 Hz there was a slight resonance of the mount carriage. Beginning at 900 Hz and continuing to

2000 Hz, there was an irregular but rapid increase in vibratory levels as sensed by all three accelerometers. The peak accelerations sensed in this region occurred at about 1810 Hz, where at the girth on the outer shell about 50 g's were indicated. The mount carriage was subjected to 43 g's and the vibration fixture to 24 g's. The data available does not indicate that this was due to resonance in any particular element of the system and resulting feedback to the other components.

The second and final test (No. 12) in this series did not involve a sweep of all frequencies in a specific range. Throughout both the random and sinusoidal tests, resonance of some component has been encountered at around 900 Hz. This resonance may have been in the fixture, outer shell or other component with the probable exception of the shield. There had been some indication that this was not an instantaneous occurrence when 900 Hz was reached, but was a "buildup" phenomena with the vibratory level increasing slowly to a peak. In an attempt to validate this interpretation, certain frequencies which are harmonics of 300 Hz were chosen. The system was vibrated at each of these frequencies for several seconds. Most of these dwell tests produced negative results. At 300 Hz there was a definite resonance of the fixture (16 g's) but this had little or no effect on the outer shell or mount carriage. There was no resonance of the system at 900 Hz as had been expected. At 1500 Hz, all three accelerometers sensed increased vibration levels (fixture - 16 g's, mount carriage - 13 g's outer shell - 4.5 g's). At 1650 Hz there appeared to be a definite mount carriage resonance point (32 g's). However, there was no indication of "build up" resonance.

The final series of sinusoidal tests involved vibration in the vertical (X) axis with the unit half-full of water and unpressurized. No shock mounts were used.

Test #13 was a sweep from 50 to 2000 Hz at 2.7 g's peak. As in the previous tests, the major problems encountered involved the outer shell which resonated at 200, 800, 1000 and 1600 Hz, and in each case appeared to increase the "g" level of both the shield and fixture due to feedback.

These same frequencies created problems in tests #14 (1100 to 700 Hz @ 2.7 g's peak) and #15 (300 to 180 Hz @ 2.7 g's peak). The vibratory level at each of the points in question (1000, 800 and 200 Hz) was in the area of 36 - 40 g's for the outer shell. The feedback

to the shield and vibration fixture at two higher frequencies was relatively small (5 g's or less). At the lower frequency, however, (200 Hz) the vibration fixture was exposed to somewhat more than 10 g's and the shield to approximately 7 g's.

In neither of the next two tests, #16 (50 to 30 Hz @ 2.7 g's) and #17 (30 to 10 Hz @ .030 inch double amplitude) did any problems arise. In the first case, the vibratory level of all three sensors was nearly constant (shield - 4 g's, outer shell - 6 g's, fixture - 4 g's) throughout the range. In the latter, the levels were uniform (at below 3 g's for the three sensors) down to about 20 Hz where measurable vibratory levels ceased.

In the final test, #18, (30 to 24 Hz @ .050 inch double amplitude) low levels were recorded down to 25 Hz where they increased sharply to about 17 g's for the shield and outer shell and 7 g's for the fixture.

3.0 Vibration Test Summary

The Phase A vapor-cooled unit was subjected to a total of 3 hours, 24 minutes and 43 seconds in recorded vibration. Of this, 2 hours, 5 minutes and 39 seconds were random and 1 hour 19 minutes and 4 seconds were sinusoidal.

The cutouts in the outer shell permitted qualitative visual observation of the motion of several internal system components during vibration. The bumpers, both top and bottom, were observed to rotate at relatively low rates. This occurred during vibration in both planes and with both random and sinusoidal inputs. In addition, rotation occurred only in specific frequency ranges.

During the more severe vibrations, the vapor-cooled shield was observed to rotate slightly back and forth around a vertical axis. This is permitted by the mounting of the shield to the fill and vent tubes which lie in horizontal planes.

Both the shield and outer shell underwent sizeable deflections during severe vibrations. These two effects did not appear to be inter-related since they did not occur simultaneously.

From a more quantitative standpoint, the random vibrations indicated resonance of some portion of the system at about 900 Hz. The sinusoidal tests indicated that this was caused by resonance of the outer shell, though

this was not definitely established. The other high "g" levels appearing in the sinusoidal tests in general appeared in a harmonic series, with 900 Hz being a member of this series.

It appeared quite obvious that the shield mounting system acts as a shock absorbing system, which in effect, isolates the shield from both the inner vessel and outer shell. This opinion is borne out by the generally lower vibratory level of the shield as compared to both the input and the outer shell, and also by the small observable vibrations of the shield as compared to the outer shell. This is especially true of higher frequencies above 200 Hz.

Subsequent to all testing described herein, there was no visible damage to the tank. In addition the system was pressurized and leak checked and found to be leak tight.

APPENDIX E

PHASE B HYDROGEN PRESSURE VESSEL STRETCH FORMING

INTRODUCTION:

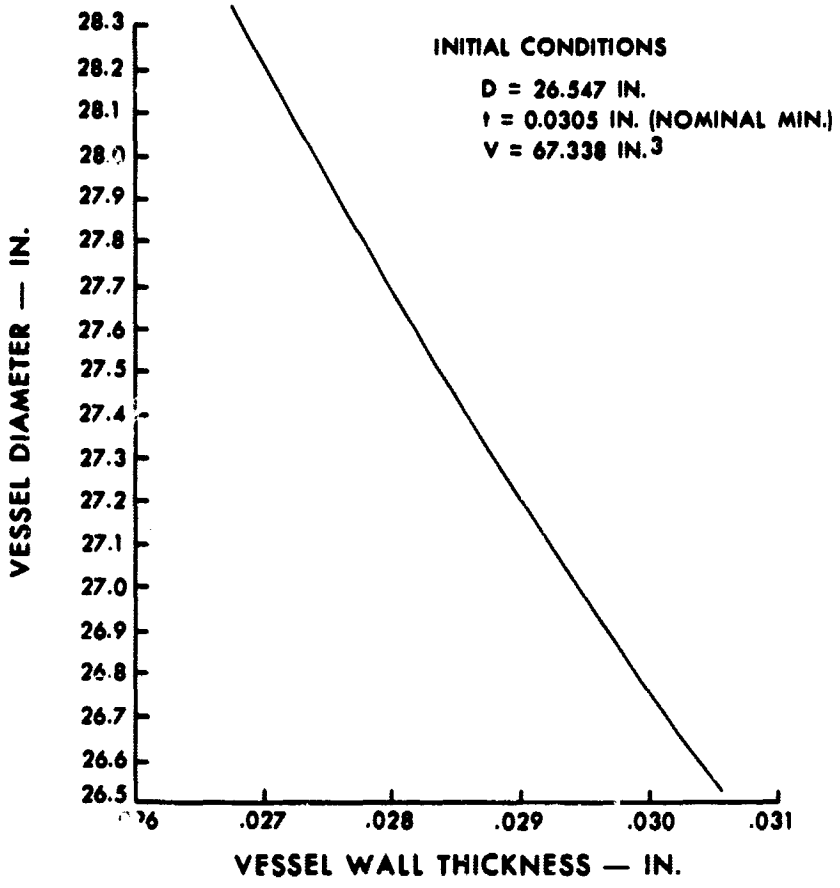
During the Phase B Hydrogen dewar program, the pressure vessel subcontractor failed to provide the pressure vessel as scheduled. As a result, a program was initiated to fabricate the required vessel. The program consisted of hydrostatically stretch forming an undersized spherical vessel to the required final diameter. The undersized vessel was fabricated by welding together two Inconel 718 inturgescently formed hemispheres which each had prewelded transition fittings at the apex to accommodate the apex access hole. Contained herein is the theoretical-experimental procedure used to monitor the nominal effective stress-strain states in the pressure vessel during the hydrostatic stretch forming operation and the results of that endeavor.

PROCEDURE:

The procedure used to monitor the vessel consisted of a two step approach: (1) the development of curves based upon constant material volume and effective stress and effective strain relations and (2) the use of the above curves during the stretch forming operation. A detailed description of these two steps follows.

Technical Approach

Based upon the undersized vessel nominal spherical diameter and shell thickness, the volume of vessel material was calculated. Diameters and corresponding thicknesses for the constant material volume were determined for the span from initial diameter to desired final diameter. From this data Figure E-1 (Vessel Diameter vs Wall Thickness) was constructed.



VESSEL DIAMETER VS. WALL THICKNESS FOR SPHERE OF CONSTANT MATERIAL VOLUME

FIGURE E-1 **A3873A-68-63**

With this information, the next step was to determine the relationship between effective stress and vessel diameter. The effective stress is the resultant stress in a multi-dimensional stress state which is analogous to the stress from a uniaxial tension test. The relationship used for the effective stress of a multi-dimensional stress state in spherical coordinates is as follows.

$$\sigma_{EFF} = \frac{1}{\sqrt{2}} \sqrt{(\sigma_\theta - \sigma_\phi)^2 + (\sigma_\theta - \sigma_r)^2 + (\sigma_\phi - \sigma_r)^2} \quad (1)$$

where:

σ_{EFF} = Effective stress analogous to uniaxial tensile test

σ_θ = Hoop stress in great circle

σ_ϕ = Hoop stress in great circle normal to above circle

σ_r = Radial stress in shell

Now, it can be shown that for a thin walled spherical vessel

$$\sigma_\theta = \sigma_\phi \, , \; \sigma_r \approx 0$$

Substitution into (1) gives

$$\sigma_{EFF} = \frac{1}{\sqrt{2}} \sqrt{2 \, \sigma_\theta^2} \qquad (2)$$

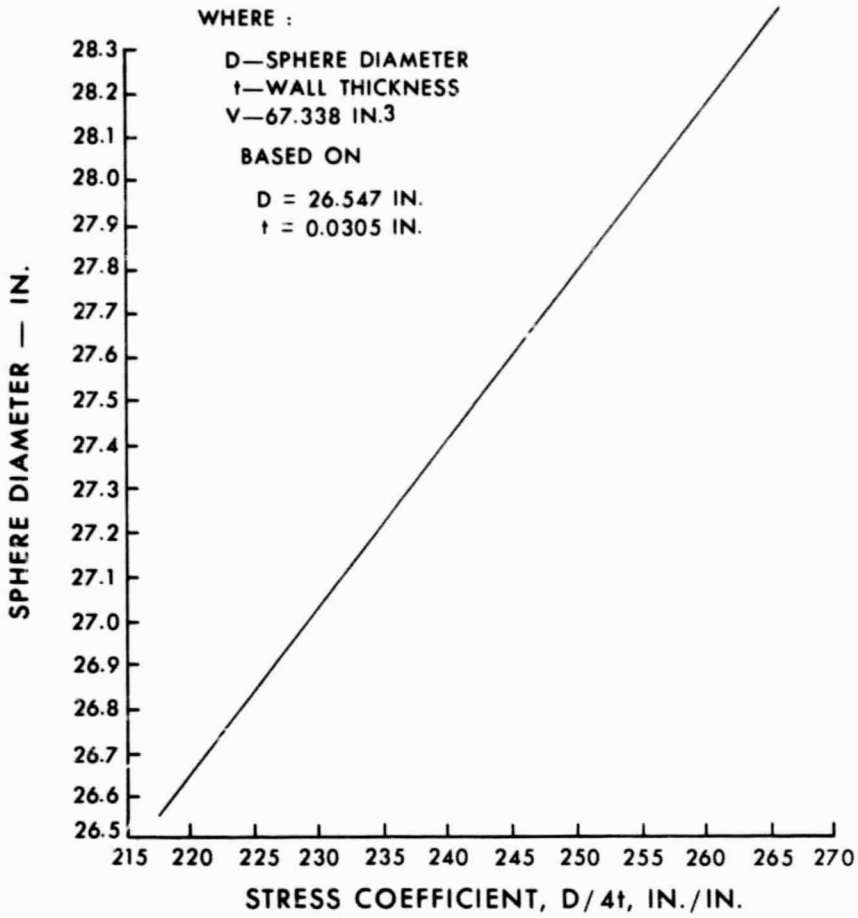
which becomes

$$\sigma_{EFF} = \frac{PD}{4t}$$

where:

P = Internal Pressure
D = Vessel Diameter
t = Wall Thickness

when the relationship for σ_θ is sutstituted. Equation 2 and the diameter-thickness combinations were then used to generate Figure E-2 (Vessel Diameter vs Stress Coefficient, D/4t). With the relationship for nominal effective stress and vessel diameter determined, the next step was to establish effective strain as function of vessel diameter.



SPHERE DIAMETER VS. D/4t FOR SPHERE OF CONSTANT MATERIAL VOLUME

FIGURE E-2 A3837A-68-64

The expression used for the nominal effective strain, analogous to that for effective stress, is as follows.

$$\varepsilon_{EFF} = \frac{\sqrt{2}}{3}\sqrt{(\varepsilon_\theta - \varepsilon_\phi)^2 + (\varepsilon_\theta - \varepsilon_r)^2 + (\varepsilon_\phi - \varepsilon_r)^2} \quad (3)$$

where:

ε_{EFF} = Effective strain in multi-dimensional stress state

ε_θ = Nominal hoop strain

ε_ϕ = Nominal meridional strain

ε_r = Radial strain

As with stress $\varepsilon_\theta = \varepsilon_\phi$, hence the effective strain becomes

$$\varepsilon_{EFF} = 2/3\ (\varepsilon_\theta - \varepsilon_r) \qquad (4)$$

Now from definition

$$\varepsilon_\theta = \frac{\Delta D}{D_o}$$

$$\varepsilon_r = \frac{\Delta t}{t_o}$$

where the subscript refers to the initial dimensions. Substitution into (4) then yields

$$\varepsilon_{EFF} = 2/3\ \left(\frac{\Delta D}{D_o} + \frac{\Delta t}{t_o} \right) \qquad (5)$$

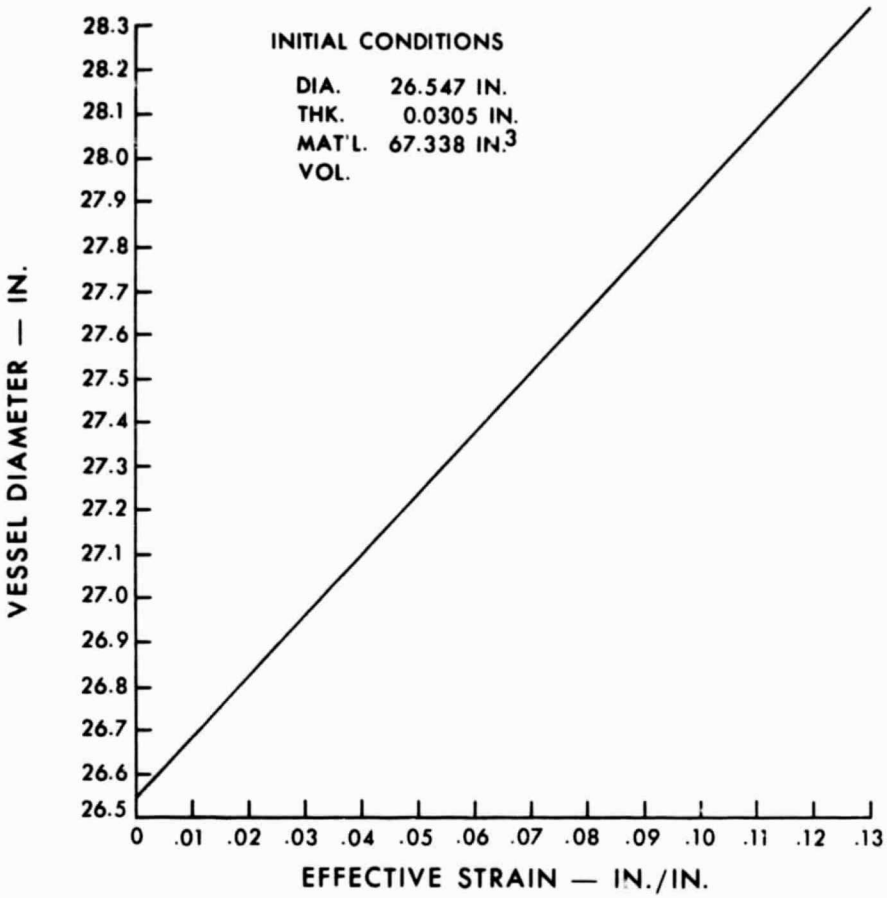
Now $\Delta D/Do$ is determined from the constant material consideration, which for the hydrogen vessel is 478 as determined from Figure E-1. Substitution of this ratio and the original vessel dimensions into (5) gives

$$\varepsilon_{EFF} = 0.07095\ \Delta D \qquad (6)$$

This relationship was then used to generate Figure E-3. With these so-generated curves, the nominal effective stress-strain state in the pressure vessel can be determined at any stage during the pressure stretch operation.

Experimental Procedure

During the hydrostatic pressure vessel stretch operation for the hydrogen vessel, a π-tape was used to obtain the vessel diameter at a given applied internal pressure. The nominal effective stress and strain state in the vessel wall was then determined at a given applied internal pressure by applying the diameter and internal pressure to Figures E-2 and E-3. At the measured vessel diameter, the effective strain was read directly from Figure E-2. The effective stress was obtained from Figure E-2 by multiplying the internal pressure by the value of D/4t corresponding to the vessel diameter. In this manner the stress-strain curve for the vessel, analogous to that of a uniaxial tensile test, was plotted during the stretch operation to monitor the state of the material.



VESSEL DIAMETER VS. EFFECTIVE STRAIN FOR SPHERE OF CONSTANT MATERIAL VOLUME

FIGURE E-3 A3837A-68-65

RESULTS:

Figure E-4 represents the nominal effective stress-strain curves that were generated by this monitoring technique. Region I represents the stress-strain curve generated during the first stretch cycle. Since the effective stress is analogous to the stress obtained from a uniaxial tension test, during the monitoring procedure it was used to determine when the stretch limit of the vessel was reached. This limit is the design value which incorporates a factor of safety and hence is below the tensile strength. As noted from the monitoring curve, the vessel would not be able to be stretched to size without being heat treat annealed after a partial stretch. In addition to achieving the desired vessel size, a high strength level had

TRUE EFFECTIVE STRESS VS TRUE EFFECTIVE STRAIN FOR STRETCH FORMED SPHERICAL PRESSURE VESSEL MAT'L - INCONEL-718

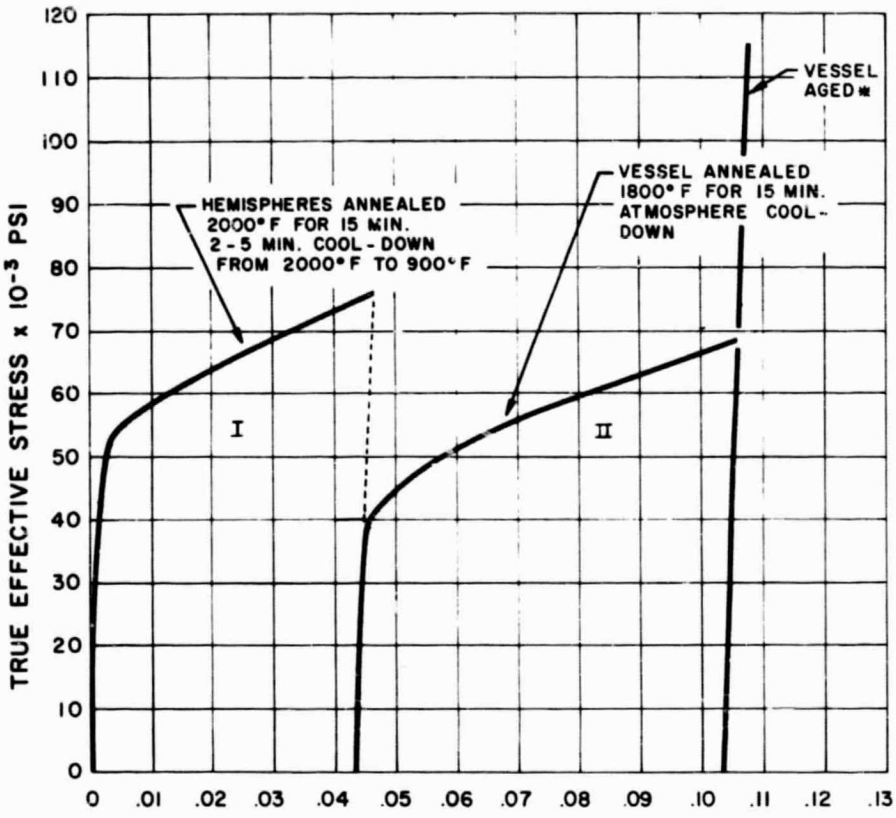


FIGURE E-4

*1325°F FOR 8 HRS. COOLED TO 1150°F AND MAINTAINED FOR 10 HRS.

A3873A-68-66

to be attained. Hence from projected stress-strain curves that would occur after an anneal cycle, it was decided that the vessel should be heat treat annealed when an effective stress value of 76,000 psi was generated. Stress relieving at this state of deformation would enable the vessel to achieve size and also have maximum cold worked strength properties after the second stretch. Region II of Figure E-4 respresents the stress-strain curve generated after the heat treat anneal operation.

Since maximum strength properties were desired, the pressure vessel was heat treat aged after the final stretching operation. The stress-strain curve plotted by the monitoring technique is also shown in Figure E-4 during the hydrostatic proof pressure test of the vessel.

Contained in Table I is a listing of the diameters, pressure calculated stresses and strains recorded during the stretch forming and proof test operations.

CONCLUSIONS:

For the Phase B Hydrogen pressure vessel stretch forming endeavor, the theoretical-experimental monitoring procedure proved to be very valuable in attaining the desired vessel. As previously noted, this technique enables the nominal stress-strain state to be known at any phase of stretch forming. It therefore can be used to determine the number of required heat treat anneal cycles and the stress state when the anneal is required to achieve the desired size and attain the maximum vessel strength. Although this technique was quite satisfactory for the immediate stretch forming, its value is dependent upon (1) the pressure vessel material and (2) the preform design. The first of these factors becomes apparent when a vessel is stretched. If the vessel is made from a material with low strain hardening characteristics, it is possible that during the stretch forming the strain hardening will not compensate for local neck down. If this occurs, a local deformation will continue till vessel failure. Since the technique considers only uniform nominal deformation, that which occurs when the strain hardening compensates for local neck down causing total deformation to proceed by successive regional deformations, the procedure cannot be used with materials of low strain hardening rate. Factor (2) presents a similar situation which is associated with the preform design. The preform must be such that there are no built-in factors such as abrupt thickness changes, holes, and poor welds that can contribute to localized failure instead of uniform growth. Thus, concentrating upon the preform design and employing a high strain hardening material not only permits the monitoring technique to be used with high assurance but also presents the greatest assurance that the preform can be stretch formed to the desired size and strength.

TABLE I

PRESSURE VESSEL STRETCH FORMING

PRESSURE psig	DIAMETER in.	NOMINAL STRAIN in./in.	NOMINAL STRESS psi
0	26.554	0	0
100	26.559	.0005	21,750
150	26.564	.0008	32,600
195	26.571	.0015	42,500
222	26.577	.0020	48,500
244	26.593	.0035	53,400
247	26.608	.0040	54,100
250	26.612	.0044	54,700
252	26.620	.0051	55,300
254	26.630	.0060	55,800
258	26.639	.0067	56,700
260	26.645	.0070	57,200
262	26.654	.0080	57,600
262	26.665	.0086	57,800
264	26.680	.0095	58,200
266	26.708	.0118	58,800
266	26.712	.0120	58,900
0	26.688	.0100	0
272	26.714	.0125	60,400
275	26.724	.0130	61,000
275	26.740	.0141	61,200
278	26.764	.0160	62,400
282	26.787	.0176	63,000
283	26.803	.0190	63,400
285	26.816	.0200	63,900
286	26.820	.0201	64,300
288	26.833	.0212	64,750
291	26.845	.0220	65,400
292	26.855	.0228	65,800
293	26.871	.0240	66,200
295	26.888	.0252	66,750
297	26.901	.0262	67,400
0 empty	26.864	.0235	0
300	26.915	.0273	68,200
301	26.928	.0282	68,400
302	26.940	.0291	68,750
303	26.954	.0302	69,000
304	26.965	.0310	69,400
305	26.975	.0318	69,700
307	26.986	.0325	70,200
308	26.995	.0330	70,550
309	27.005	.0340	70,800
310	27.016	.0348	71,100

PRESSURE VESSEL STRETCH FORMING

PRESSURE psig	DIAMETER in.	NOMINAL STRAIN in./in.	NOMINAL STRESS psi
311	27.025	.0355	71,400
312.5	27.034	.0361	71,800
313.5	27.045	.0370	72,200
315	27.055	.0375	72,600
316	27.063	.0381	72,900
316.5	27.073	.039	73,150
317	27.084	.0400	73,400
318	27.094	.0405	73,650
319	27.104	.0413	74,000
320	27.115	.0420	74,350
321	27.127	.0430	76,650
322.5	27.137	.0437	75,000
323	27.148	.0445	75,350
324	27.160	.0452	75,600
324.5	27.170	.0460	75,800
325	27.180	.0468	76,000
0 empty	27.131	.0430	0
Vessel annealed at 2000° F in vacuum and quenched in nitrogen atmosphere.			
0	27.120	.0424	0
150	27.135	.0435	34,900
175	27.137	.0436	40,750
200	27.140	.0438	46,600
220	27.142	.0440	51,400
230	27.145	.0442	53,550
242	27.147	.04435	56,400
250	27.149	.04455	58,200
259	27.149	.0448	58,400
272	27.150	.0449	63,400
280	27.152	.04495	65,250
290	27.153	.04500	67,600
300	27.155	.04505	70,000
310	27.1555	.04507	72,300
322	27.1560	.04508	75,100
332	27.1570	.04510	77,000
0	27.120	.0424	0
Vessel taken to obtain anneal.			
0	27.120	.0424	0
100	27.131	.0432	23,260
150	27.139	.0438	34,900
200	27.145	.0442	46,600
250	27.151	.0444	63,400

PRESSURE VESSEL STRETCH FORMINA

PRESSURE psig	DIAMETER in.	NOMINAL STRAIN in./in.	NOMINAL STRESS psi
275	27.153	.0450	64,100
298	27.158	.0452	69,500
330	27.163	.0455	77,100
340	27.165	.0458	79,400

Vessel exhibited no yield (not annealed), hence was taken to Tri-City Heat Treat for anneal.

0	27.135	.0435	0
50	27.138	.0438	11,640
100	27.142	.0440	23,280
150	27.148	.0443	34,950
172	27.159	.0452	39,900
175	27.163	.0454	40,950
180	27.180	.0466	42,100
181	27.183	.0470	42,350
182	27.188	.0473	42,550
182.5	27.190	.0475	42,750
186	27.198	.0481	43,550
189	27.210	.0490	44,350
190	27.218	.0496	44,550
192	27.225	.0500	45,150
192.5	27.229	.0510	45,250
193	27.232	.0506	45,450
195	27.239	.0510	45,800
198	27.250	.0518	46,550
200	27.265	.0529	47,200
201	27.272	.0534	47,250
0	27.244	.0514	0

Small hole detected in forged fitting; hole drilled out, welded and ground.

0	27.246	.0515	0
200	27.268	.0530	47,350
205	27.272	.0534	48,400
206	27.289	.0546	48,750
206.5	27.296	.0550	48,900
207	27.304	.0557	49,150
209	27.309	.0560	49,550
210	27.318	.0566	49,800
212	27.330	.0575	50,400
0 Small Hole			
210	27.330	.0575	49,850
220	27.363	.0600	52,500
221	27.403	.0628	52,900

PRESSURE VESSEL STRETCH FORMING

PRESSURE psig	DIAMETER in.	NOMINAL STRAIN in./in.	NOMINAL STRESS psi
225	27.425	.0643	54,100
230	27.435	.0650	55,350
234	27.452	.0662	56,400
0	27.419	.0638	0
Gauge Malfunction.			
277	27.453	.0663	54,700
228	27.473	.0678	55,500
230	27.497	.0694	55,650
232	27.511	.0705	56,350
234-6	27.540	.0725	57,200
235-7	27.562	.0740	57,500
Repaired small "hole".			
0	27.502	.0698	0
227	27.553	.0734	55,300
237	27.559	.0738	57,650
238	27.596	.0765	58,200
240	27.602	.0770	58,750
241	27.624	.0786	59,100
242	27.639	.0769	59,550
244	27.664	.0813	60,150
247	27.682	.0826	61,000
248	27.703	.0841	61,350
249	27.725	.0857	61,750
249.5	27.746	.0870	62,000
251	27.757	.0878	62,500
Dropped pressure to 100 psi over night.			
251.5	27.766	.0884	62,550
253	27.781	.0894	63,100
254	27.791	.0901	63,400
255	27.811	.0916	63,800
256	27.833	.0930	64,250
257	27.844	.0936	64,550
258	27.872	.0958	65,100
259	27.888	.0968	65,400
260	27.900	.0976	65,550
261	27.913	.0985	65,900
261.5	27.947	.1007	66,400
262.5	27.954	.1012	66,800
264	27.968	.1021	67,200
265	27.983	.1032	67,500

PRESSURE VESSEL STRETCH FORMING

PRESSURE psig	DIAMETER in.	NOMINAL STRAIN in./in.	NOMINAL STRESS psi
266.5	27.997	.1040	68,000
268	28.017	.1054	68,500
269	28.029	.1060	68,900
269.5	28.036	.1068	69,100
270	28.044	.1073	69,250
270.5	28.047	.1074	69,450
270.8	28.051	.1079	69,550
0	28.003		0

PRESSURE VESSEL PROOF TEST

PRESSURE psig	DIAMETER in.	NOMINAL STRAIN in./in.	STRAIN INCREMENT in./in.	NOMINAL STRESS psi
0	27.989	.1034	.0000	
100	27.995	.1040	.0006	25,530
200	22.008	.1047	.0013	51,100
250	28.014	.1052	.0018	63,900
275	28.018	.1055	.0021	70,400
300	28.021	.1058	.0024	76,800
325	28.027	.1060	.0026	83,300
350	28.031	.1064	.0030	89,600
375	28.035	.1067	.0033	96,100
400	28.039	.1069	.0035	102,700
419	28.041	.1071	.0037	107,700